AN INVESTIGATION INTO THE FLOTATION RESPONSE OF SPERRYLITE ($PtAs_2$) BY COMPARATIVE EVALUATION OF CRYSTAL STRUCTURE AND BONDING ATOMS.

By

SEBIA PIKININI

2022

A thesis submitted to the University of Cape Town as a fulfilment of the requirement for the degree of Doctor of Philosophy in Chemical Engineering.

CENTRE FOR MINERALS RESEARCH

Department of Chemical Engineering

Faculty of Engineering and the Built Environment

Plagiarism Declaration

I hereby declare that this thesis is my personal work in design and execution and has not been submitted for any degree at any academic institution. I understand the meaning of plagiarism and all the work in this thesis is my own work, except for the material contained herein that has been duly acknowledged.

Signature: Signed by candidate

Date: 8 July 2022

Acknowledgements

I would like to thank the almighty God for His grace and ability that has helped me this far in this journey. I was indeed marvellously helped by the Lord. I would also like to thank my man of God Pastor Chris Oyakhilome for the word and prayers and for investing so much in our lives in the Love World nation. Thank you for raising great Pastors that have taught me the word: Pastor Lawal, Pastor Amaechi, Pastor Ose, Pastor Gert, Pastor Percy, Pastor Karen and Pastor Felicity. Listening to them and the Love World singers sustained me, I was too surrounded to surrender.

I would like to also thank my supervisors, A/Prof Belinda McFadzean and Prof Cyril O'Connor for their guidance throughout this work. Their wisdom, excellence and commitment has been amazing indeed.

I would like to thank all the CMR Staff: A/Prof Kirsten and fellow post graduate students: Dandre, Lucia, Avuyile, Everjoice and Michael for their help and support throughout my research. My gratitude to Kenneth, Shireen, Ngqobile, Refilwe for all the technical support. I would like to thank Kathija for loaning us the natural sperrylite electrode.

I would like to also thank the catalysis department for allowing me to use their equipment, especially Portia and Dr Pieter Levecque.

I would like to thank Dr Natalie Shackleton for her advice during mineral synthesis.

I would also like to thank MINTEK management and Dr Jestos Taguta for sponsoring my surface analysis test work.

I would also like to thank my husband, Ignatius for his support throughout my studies. I would also like to thank my father-in-law for his prayers and encouragement to enrol for PhD studies. I would like to especially thank the following people for all their support: our boys, Nigel and Jesse, my mother-Rosemary Dumbura, Mr and Mrs Rungwave, Nosizi, Albert, Morris, Calistus, Blessing, Mduduzi, Ruth, Sekuru Farai, Sekuru Nkosi, Victor for all their support throughout my studies. Also, I would like to thank family friends for their support: Dr and Mrs Masukume, Mr and Mrs Mahachi, Deaconess Rejoice, Deaconess Fide, Br Hughes, Gov Luckson, Mr and Mrs Nyabadza, Mr and Mrs Macheza, Theophilus, Thamsanqa, Alouise, and Mufaro.

List of Publications and Conferences

The interactions of butyl thiol collectors with sperrylite ($PtAs_2$) at different pulp chemistries. Proceedings of the International Mineral Processing Congress (IMPC 2020), 18-22 October 2020, Cape Town, South Africa. Pikinini, S., McFadzean, B., & O'Connor, C. T.

Investigating the floatability of sperrylite ($PtAs_2$) and its interactions with selected standard and novel collectors, IMPC Asia-Pacific 2022, Paper accepted. Pikinini, S., McFadzean, B., O'Connor, C. T., & Zhang, X.

Flotation behaviour of platinum group of minerals (PGM) species- A Review (Draft Paper)

Abstract

The Bushveld Complex in South Africa is the biggest platinum group elements reserve in the world. One of the major platinum group mineral (PGM) components in this ore is sperrylite ($PtAs_2$), which has been found to be slow floating compared to the other PGMs and often reports to the tailings stream. Sperrylite comprises about ~21% of the platinum groups minerals (PGMs) in the Platreef ore hence, improving its recovery will be of great economic value to the South African PGM industry. The flotation of PGM ores aims to recover at least five minerals using the same reagent suite. These minerals have different physical and chemical properties and only a few studies so far have investigated the floatability of individual PGM minerals.

The reasons for the poor floatability of sperrylite are not yet clear although some studies suggest that poor collector adsorption or poor collector choice might be the major cause. Molecular modelling computations have indicated that the platinum atoms on sperrylite working surfaces are not well exposed, posing some steric hindrances to the approaching collector ligands. In addition, adsorption studies, using molecular modelling computations, indicated that the OH^- ions had higher binding energy compared to SEX, suggesting that increasing pH may have a detrimental effect on collector adsorption. This study sought to establish the reasons why xanthate collectors, which are used as the main collector used in industry in the flotation of PGM ores, appear not to promote the flotation of sperrylite. Also, novel collectors were suggested based on the donor-acceptor theory with the aim of improving the floatability of sperrylite. It was hypothesized that increasing the electron density around the collector coordinating atoms will result in stronger bonds with sperrylite. The suggested novel collectors were screened using molecular modelling computations carried out by researchers at the University of Limpopo. Collectors that gave higher binding energies were then synthesized at BGRIMM Technology, in China.

Tests were carried out to compare the floatability and related phenomena of sperrylite, pyrite (FeS_2), arsenopyrite (FeAsS) and cooperite (PtS). These minerals were chosen due to their having either similar crystal structures and/or binding ligands (S, As) on the mineral surface and to ascertain how their floatability compares to that of sperrylite. Pyrite was selected as a cheap proxy for sperrylite since they have the same isometric crystal structure. Also, the effect of its S bonding ligand as opposed to As in sperrylite was investigated. Arsenopyrite was also selected to investigate the effect of a monoclinic crystal structure and the effect of the As and S ligands. Lastly, cooperite was also selected as a standard sulphide PGM mineral with a tetragonal crystal structure that is known to have a good flotation response. These minerals were included in this study in order to investigate how their floatability differs from that of sperrylite based on their crystal structures and bonding atoms.

In addition, experiments were carried out to determine the energy and extent of collector adsorption on the minerals and electrochemical interactions between the minerals and standard collectors. XPS and TOF-SIMS analyses were also carried out to determine the surface products formed on sperrylite and arsenopyrite in the presence of synthetic plant water with and without collectors. Novel collectors were tested to establish the molar energy of interaction with sperrylite using isothermal titration calorimetry and this was compared to those determined by molecular modelling computations.

The results indicated that the crystal structure and the binding ligands played a key role in the floatability of the selected minerals. Minerals with the isometric crystal structure had poor collectorless recoveries, viz. FeS_2 (12.3%) < $PtAs_2$ (14.5%) < FeAsS (85.4%) < PtS (94.7%) and different collector-induced flotation recoveries. However, the recovery of FeS_2 (94%) improved to a greater extent when PNBX was used as a collector compared to $PtAs_2$ (26%). Sperrylite and pyrite had poor natural floatabilities under both alkaline and acidic conditions, indicating that their floatability is strongly dependent on their interaction with collectors. The poor recovery of this relatively hydrophilic mineral is due to poor collector adsorption of the collectors at pH 9 which is the usual pH in operating plants. Rest potential tests revealed that sperrylite had the least extent of interaction with the standard collectors compared to the other minerals. Furthermore, sperrylite rest potentials remained unchanged with a change in pH, indicating its resistance to surface alteration. The minerals rest potentials at pH 9.5 followed the order FeS_2 (282) > PtS (254) > $PtAs_2$ (233) > FeAsS (177) mV, while there was a great increase for all the minerals except sperrylite at pH 3.5, with the order PtS (523) > FeS_2 (407) > FeAsS (333) > $PtAs_2$ (243) mV. Surface alteration is key in the flotation of different minerals as it either determines the natural floatability of the minerals or aids or hinders collector adsorption.

Furthermore, XPS results indicated that the collectors were not chemisorbed onto sperrylite, since the chemisorption process requires concurrent oxidation of the collector and the mineral surface. It was further revealed that metal oxides were formed on the sperrylite surface when conditioned in plant water at pH 9. Plant water ions were also found to be detrimental to the recovery of sperrylite. The recovery of sperrylite with PNBX in deionised water (51%) was double that with synthetic plant water at pH 9 (26%), even though the adsorption tests which were carried out in deionised water indicated that only 5.7% of the dosed PNBX was adsorbed onto the mineral surface. Sperrylite might be also very sensitive to any pulp chemical changes. This was shown by the reduced recoveries after adding copper sulphate and after raising the pulp Eh using sodium hypochlorite. Also, the higher recoveries in distilled water can be a pointer that surface contamination could be one of the reasons for the poor recoveries of sperrylite.

This study has also indicated that the reactivity of the arsenic bonding atom was dependent on the metal bonded to it (Pt or Fe). The reactivity of arsenopyrite when conditioned in synthetic plant water resulted in the formation of a hydrophobic surface layer that led to its high natural floatability and poor interaction with collectors. In the case of an unreactive surface of sperrylite, the arsenic bonding atom, which can also act as an electron acceptor could be the major reason for the poor collector adsorption at pH 9. This leads to an increase in the number of bonding sites that the sulphur ligands are attracted to (Pt, As) as opposed to pyrite (Fe), thereby reducing the overall collector binding energy with the mineral. Molecular modelling computations, in collaboration with the University of Limpopo, also showed that the sulphur ligand had the ability of bonding with both platinum and arsenic on the sperrylite mineral surface. Nevertheless, pH seemed to play a role in the poor collector adsorption and flotation recoveries of sperrylite at pH 9, however, the moderate recoveries at pH 4, in synthetic plant water, were a sign that this is not the major cause for the poor floatability of sperrylite. Moreover, recovery using PNBX remained unchanged at pH 4 despite the indication by the adsorption test results that 93% of the collector was adsorbed on the mineral surface under acidic conditions. In addition, the isothermal titration calorimetry tests indicated that the binding energy of the hydroxide ions in a high pH solution with sperrylite was lower than that with PNBX and SNDBDTC collectors. This indicates that collectors have the ability to displace the hydroxide ions which could be preferentially adsorbed on the mineral surface at high pH during the conditioning period. This is in contradiction with the molecular modelling computation findings.

Ultimately this work has shown that sperrylite is a relatively hydrophilic mineral under both acidic and alkaline conditions and requires the action of collector reagents to effectively recover it. This study also corroborates the suggestion that poor collector adsorption is the major cause for the poor floatability of sperrylite. It is also important to note that all the adsorption tests were carried out in deionised water and that all the adsorbed collectors were only physisorbed onto the mineral. Chemisorption of collectors on minerals is generally key to effectively recover the valuable minerals and a degree of oxidation is also a requirement on the mineral to catalyse the oxidation of collectors. However, this study has shown that sperrylite is resistant to surface alteration, making it difficult to recover it. Even though the mineral has more binding sites as opposed to pyrite, the mineral has proved to be sensitive to any form of contamination in the form of ions present in plant water or any activator ions, such as copper ions, that could be found in the pulp. Hence, the hypothesis which proposed that a ligand with a greater inter-atomic distance between the two chelating atoms compared to that of typical thiol collectors will have a better crystal structure compatibility with $PtAs_2$ as well as the hypothesis which proposed that linking atoms that are less electronegative (S, N), or electron-donating would be superior options were not sustained in the case of sperrylite.

However, the hypotheses were sustained in the case of pyrite which is fairly reactive and also consists of a sulphur bonding ligand.

Since the collectors were adsorbed to a greater extent under acidic conditions, it is recommended that collectors that have higher binding energies with sperrylite, which are stable under acidic conditions should be designed to improve the recoveries of sperrylite. Moreover, sperrylite was found to be relatively inert under conditions of increasing pH, it is suggested that a complete mapping of floatability as a function Eh and pH be made to determine floatability domains, as is common for base metal sulphide minerals.

Table of Contents

List of Illustrations

List of Figures

List of Tables

Nomenclature

ΔH	Enthalpy of adsorption
pKa	negative logarithm of the acid dissociation constant

Greek Letters

μ	micron (10^{-6}m)

Abbreviations

$PtAs_2$	Sperrylite
FeS_2	Pyrite
FeAsS	Arsenopyrite
PtS	Cooperite
SEX	Sodiun Ethyl Xanthate
SIBX	Sodium Isobutyl Xanthate
PNBX	Potassium Normal Butyl Xanthate
SNBDTC	Sodium Normal Butly Dithiocarbamate
SNDBDTP	Sodium Normal Di-Butyl Dithiophosphate
SNDEDTP	Sodium Normal Di-Ethyl Dithiophosphate
SDTDBAT	2,6-dithio-4-di-butylamino-1,3,4-triazine
SDTBAT	2,6-dithio-4-butylamino-1,3,4-triazine
SDCDTDBAT	2,6-dicarbonodithioate-4-di-butylamino-1,3,5-triazine
SDCDTBAT	2,6-dicarbonodithioate-4-butylamino-1,3,5-triazine
$CuSO_4$	Copper Sulphate
XRD	X-Ray Diffraction
EDS	Energy Dispersive Spectroscopy
BSE	Back Scattered Electron
BE	Binding Energy
XPS	X-Ray Photoelectron Spectroscopy
TOF-SIMS	Time of Flight Secondary Ion Mass Spectroscopy
SIMS	Secondary Ion Mass Spectroscopy

UV-VIS	Ultraviolet-Visible Spectroscopy
BET	Brunauer-Emmet-Teller
PGMs	Platinum Group Minerals
PGE	Platinum Group Elements
wt%	weight percent
rpm	revolutions per minute
ppm	parts per million
X_2	Dixanthogen
X^-	Xanthate anion
UCT	University of Cape Town
CSIR	Council for Scientific and Industrial Research

1. INTRODUCTION AND LITERATURE REVIEW

1.1. INTRODUCTION

The recovery of valuable minerals using the froth flotation process is complex and the flotation of PGMs is more complicated since it seeks to recover at least six platinum group minerals containing, respectively, platinum, palladium, rhodium, ruthenium, iridium and osmium, with the same reagent suite. Xanthate collectors are generally employed as the main collector with the dithiophosphate collectors often used as the co-collector and they are added at a ratio of about 3:1 respectively. These thiol collectors, xanthate and dithiophosphate, originally used for the recovery of sulphide minerals have been found to be poor collectors of sperrylite (Shackleton et al., 2007. This arsenide PGM has been found to be relatively slow floating as opposed to the other PGM minerals. Sperrylite ($PtAs_2$) comprises about 21% of the platinum group minerals (PGMs) in the Platreef ore and regularly reports to the tailings due to its poor floatability. Hence, improving its recovery will be of great economic value to the South African PGM industry. The reasons for its poor floatability are not yet clear and only a few studies have been carried out to date on the floatability of individual PGMs. This is mostly due to their extremely low concentrations in PGM ores, making a study of their flotation characteristics difficult.

Froth flotation is a physico-chemical concentration method that is used for the selective separation of mineral species from the slurry, which consists of both valuable and gangue minerals (Gorain et al., 2000). The separation is achieved by exploiting the difference between induced surface properties on the valuable and gangue minerals respectively. The overall flotation process consists of several sub-processes including the creation of the hydrophobic mineral surface, the formation of air bubbles, the attachment of hydrophobic minerals to air bubbles, the transfer of the bubble-particle aggregates to the froth phase, and the collection of these bubble-particle aggregates (Bradshaw, 1996).

Sperrylite, a PGM mineral present in the Platreef and Great Dyke ores, is recovered with the other PGM minerals by the froth flotation process. Thiol collectors, that were mainly designed for the flotation of sulphide ores have been used during the flotation of PGM ores because of the latter's association with base metal sulphides. Therefore, it has been assumed that these PGM minerals will behave in the same way as the sulphide minerals during the flotation process. However, as new ore deposits are exploited, there has been a change in the type and association of the PGM ores. For example, Platreef ore generally contains platinum and palladium tellurides (20%-45%), alloys (26%), arsenides (21%) and sulfides (19%) (O'Connor & Shackleton, 2013). In addition, many of these platinum group minerals in the feed and tailings are well liberated and not associated with base metal sulfides. Of particular importance to the present study are the reports in the literature which have shown that sperrylite (platinum arsenide) is slow floating and poorly recovered in the treatment of Platreef ore (Shamaila, 2007).

Considering the substantial quantity of sperrylite (21%) in the Platreef deposit, it will be of great economic advantage to improve its recovery.

The present study is aimed at gaining a better understanding of the interactions occurring between $PtAs_2$ and the selected standard collectors, viz. potassium n-butyl xanthate (PNBX), sodium di-(n-butyl) dithiophosphate (SNBDTP) and sodium (n-butyl) dithiocarbamate (SNBDTC) with a view to establishing the reasons for its poor floatability as reported above. Due to the difficulty in obtaining the natural PGM minerals, in this first phase of the study, pyrite was also used as a test mineral since it has a similar crystal structure to sperrylite. Furthermore, the floatabilities of pyrite, arsenopyrite and cooperite will be studied and compared to sperrylite, taking into consideration their crystal structures and bonding ligands (S, As). The microflotation tests were carried out as a measure of the hydrophobicity of sperrylite under different pulp conditions and other minerals. In addition, electrochemical, isothermal titration, adsorption and surface analysis studies were carried out to contribute to an understanding of the nature of the interactions between the mineral and different reagents. The ultimate aim was to identify possible new candidate collectors which may increase the floatability of sperrylite.

1.2. THE MINERALOGY OF PGM ORES

The mineralogy of the different PGM ore reserves found in South Africa is given in the following sections:

1.2.1. The Bushveld Complex

The Bushveld Complex contains the largest reserves of platinum group elements (PGE) in the world and it is comprised of the Merensky Reef, the Upper Group 2 (UG2) Reef and the Platreef. It is made up of layered igneous intrusions which were made up of rocks that were slowly cooled from molten magma. The gradual cooling of molten magma results in the crystallisation and concentration of different minerals that take place at different temperatures. This cycle of magma intrusions results in the formations of layers of different rocks and they determine the distribution of the different ore deposits. The PGM ores in the Bushveld complex are usually associated with the less frequent intrusion that results in the formation of the mafic rocks. The layer is rich in sulphides of base metals (Fe, Ni, Cu), arsenides, tellurides and PGE alloys (Cawthorn, 1999).

The PGE elements: platinum, ruthenium, rhodium, palladium, osmium, and iridium are of great importance in various sectors of industry and this has resulted in their increased demand throughout the world.

Their application in various sectors takes advantage of their intrinsic properties, viz. inertness with excellent corrosion and oxidation resistance, biocompatibility, high melting temperature, good conductivity and electronic and catalytic properties.

They are used in catalytic converters in the automobile industry, electronic industry, medical industry in the treatment of cancer and the jewellery industry.

The beneficiation of different types of ores is the key primary stage for the recovery of these precious metals: PGM ores, which are exploited primarily for PGEs, while other metals like copper, nickel and cobalt are produced as co-products. In addition, the copper-nickel dominant ores are mainly exploited for copper and nickel and the platinum group elements are produced as co-products. The Bushveld complex has ore reserves containing about 939 million ounces of platinum and 711 million ounces of palladium that make up around 75% and 50% of the world's platinum and palladium, respectively (Schouwstra & Kinloch, 2000; Cawthorn, 1999). Table 1.1 gives the inferred platinum and palladium reserves from the Bushveld Complex in South Africa (Cawthorn, 1999).

Table 1.1 Inferred Pt and Pd reserves in the Bushveld Complex (Cawthorn, 1999)

Region	**Pt 10^6 oz**	**Pd 10^6 oz**
Platreef	136	136
Merensky Reef	400	221
UG2 Chromite	403	354
Total	939	711

The Merensky reef was discovered in 1920 and for several years it was the major source of platinum in the world (Cole & Ferron 2002-3). It consists of base metal sulphides: pyrrhotite (~40%), pentlandite (~30%), and chalcopyrite (~15%) which could be exploited economically to produce copper and nickel as by-products. Other sulphide minerals that are found in lower concentrations are millerite (NiS), troilite (FeS), pyrite (FeS_2) and cubanite (Cu_5FeS_4) (Schouwstra & Kinlonch, 2000). The major PGMs in the Merensky reef are cooperite (PtS), braggite ((Pt, Pd, Ni)S), sperrylite ($PtAs_2$), and PGE alloys.

They occur as fine inclusions within the base metal sulphide (BMS) and silicate gangue mineral surfaces (Schouwstra & Kinlonch, 2000; Cole & Ferron 2002-3). Also, laurite (RuS_2) has been found in substantial amounts in some parts of the reef. The reef consists of 57% Pt, 25% Pd, 4% Au, 1% Ir, 8% Ru, 1%Os and 4% Ru (Hochreiter et al., 1985). The Merensky Reef concentrators have good PGE metal recoveries, ranging from 80-90%, because of their high association with base metal sulphides (Rule, 2011).

The UG2 is mainly a chromite reef and it was exploited since the 1970s. The mineralogy of the UG2 reef consists of mainly chromite (55-65% by mass) and contains smaller amounts of pyroxene (25-35%) and plagioclase (1-10%) (Schouwstra & Kinloch, 2000). The PGMs within the UG2 ore consist mainly of sulphides. These include laurite ((Ru, Os, Ir)S_2), cooperite (PtS) and braggite ((Pt, Pd, Ni)S).

The remainder of the PGMs are made up of malanite ((Pt,Rh,Ir)$_2$ CuS_4), vysotskite ((Pd,Ni)S) Pt-Fe alloy, sperrylite ($PtAs_2$) and Pt and Pd tellurides. These minerals can be found as single grains along the chromite grain boundaries or as inclusions within the chromite or other silicate gangue minerals (Cabri, 1981). Laurite, in the UG2 ore, was found to be predominantly associated with the chromite grains (Schouwstra & Kinloch, 2000). The feed at Waterval UG2 Concentrator has a relatively constant head grade and mineralogy (Rule et al., 2008). Mineralogical analysis showed that 70-75% of the PGMs in the final tail occur as locked or middling particles with gangue association (Nichol, 2006, Van Staden, 2006, Van Staden, 2007). Poor recoveries were noted in the UG2 concentrators where the feed had a higher degree of association with the silicate minerals resulting in increased losses to the tailings, caused by insufficient liberation of the PGMs (Rule, 2011).

1.2.2. The Platreef

The Platreef, which was initially exploited in the 1990s, is a pyroxenite silicate reef that has been hydrothermally altered and has variable gangue mineralogy. The bulk mineralogy of the Platreef is complex, predominantly comprised of pyroxene (40-60% by mass). There are relatively large concentrations of alteration minerals (10-20%), which cause rheological problems during processing (Shabalala et al, 2011). The PGM mineralisation is variable but consists mostly of platinum and palladium tellurides (20%-45%), alloys (26%), arsenides (21%) and sulfides (19%) (O'Connor & Shackleton, 2013). The serpentinite rocks have been found to be rich in $PtAs_2$, whereas the upper pyroxenite rocks are rich in PGM sulphides and alloys (Schouwstra & Kinloch, 2000). The Platreef ore has a low percentage of its PGMs that are associated with the base metal sulphides and mostly PGMs associated with silicates which are often very fine-grained, hence it is difficult to achieve high metal recoveries (Rule et al., 2008). Mineralogical investigations revealed that 55–65% of the PGMs occurred as locked or middlings associated with gangue minerals (Clark-Mostert, 2006, Nichol, 2006, Schalkwyk, 2007). Hence, the installation of IsaMills resulted in improved liberation and increased PGE flotation recovery of the Mogalakwena C Section by 7% (Rule, 2011).

Table 1.2 shows some of the common PGMs found in the deposits around the world with their respective crystal structures, hardness and specific gravity (https://www.mindat.org/min-1123.html).

Table 1.2 Crystal structures, hardness and specific gravity of common PGMs found in deposits around the world (https://www.mindat.org/min-1123.html).

Mineral	Formula	General Appearance in deposits around the World (Cabri, 2002)	Crystal Structure	Mohs Hardness	Specific Gravity
Cooperite	PtS	Euhedral to anhedral micrometer to 1.5mm grains	Tetragonal	4-5	9.5
Pallado arsenide	Pd_2As	Long and irregular grains	Monoclinic	5	10.42
Sperrylite	$PtAs_2$	Micrometer to centimetre size crystals and rounded grains	Isometric	6-7	10.58
Vysotskite	(Pd, Ni) S	As intergrowths and lensoid inclusions in other sulphides	Tetragonal	-	6.71
Laurite	RuS_2	Grains and crystals from 0.0001 to a few mm	Isometric	7-7.5	6.43
Merenskyite	$PdTe_2$	As minute grains, intimately intergrown with other PGM or as single-phase inclusions	Trigonal	3.5-4	8.5
Moncheite	$PtTe_2$	Crystals up to 1mm and minute grains	Trigonal	3.5	9.88
Braggite	(Pt, Pd, Ni) S	Fractured grains up to 8mm long	Tetragonal	5	10
Platarsite	PtAsS	-	Isometric	7.5	8.0
Malanite	$Cu(Pt, Ir) S_4$	-	Isometric-Hexoctahedral	5	7.92
Maslovite	PtBiTe	Grains up to 0.12mm in size	Isometric	4.5-5	11.23
Michenerite	PdBiTe	Grains from 0.0001 to 2mm	Isometric	4-4.5	9.81

These properties can give us information about the possible behaviour of the different minerals, especially the ones that belong to the same crystal groups, for example, pyrite and sperrylite, cooperite and braggite.

These properties further give insight into the possible recovery methods that can be exploited taking into consideration the differences in physical properties. It is important to note that the PGM minerals in the Platreef deposit are fine grained and have an average diameter (d_{50}) of 5µm.

1.2.3. Crystal Structures and Working Surfaces of Selected Minerals in the Study

The crystal structures and properties of sperrylite, pyrite, cooperite and arsenopyrite will be discussed in the following sections. Understanding the properties of these minerals will further shed light on the behaviour of the targeted mineral, sperrylite. The roles of their crystal structures and bonding atoms will be analysed in this study.

1.2.3.1. Sperrylite

Sperrylite has the pyrite (FeS_2) group structure (Figure 1.1), and it is crystallized as cubes and cubo-octahedrons. Its Moh's hardness is between 6 to 7, and it has a high specific gravity (calculated) of 10.8 (Xiao & Laplante, 2004).

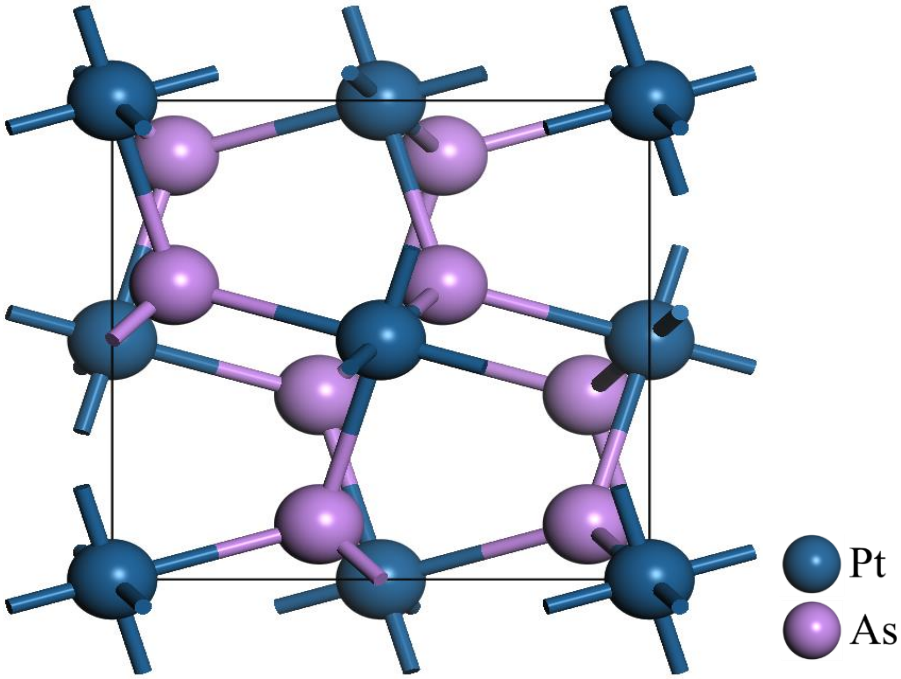

Figure 1.1 Crystal structure of sperrylite (Mkhonto, 2018)

It has a chemical composition of 56.6% Pt, and 43.4% As. The formal oxidation state of Pt in sperrylite is (+4) and that of As is (-2) (Bai et al., 2017). However, Mwase (2016) cited a controversy that surrounds the oxidation states of Pt and As in the mineral and that there is no conclusive information available in literature. Sperrylite crystallizes in Pa_3 space group, with a lattice parameter a = 5.9681 (Szymaitski, 1979).

It has the (100), (111), and (110) cleavage planes, however, the (100) plane is the most stable dominant surface expressed by the morphology of $PtAs_2$ crystal. Figure 1.2 shows the working surface of sperrylite and the surface coordination of Pt and As on the (100) plane are 5 and 3 respectively (Mkhonto, 2018).

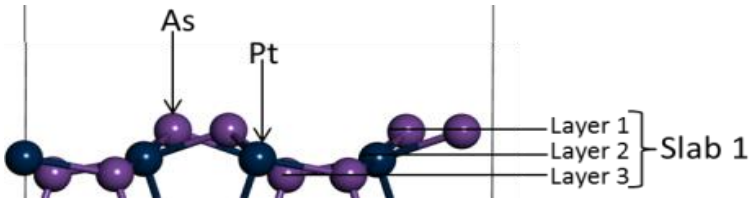

Figure 1.2 Working surface of sperrylite showing the exposed sulphur atoms (Mkhonto et al., 2018)

1.2.3.2. Cooperite

Cooperite is a sulphide PGM mineral, which is mostly S-deficient. It crystallizes into a tetragonal crystal system shown in Figure 1.3. The working surface of cooperite is also shown in Figure 1.4.

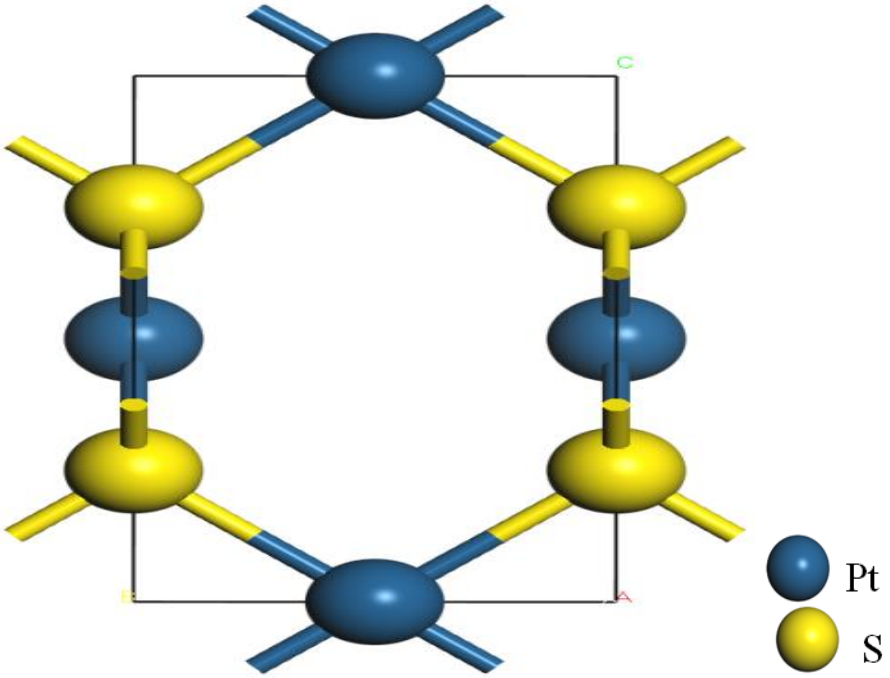

Figure 1.3 Crystal structure of cooperite (Hicks et al., 2021)

It has a Moh's hardness of 4 - 5 and a specific gravity of 9.5. Cooperite belongs to the braggite group of minerals. The oxidation of the sulphide ion on Pt has been found to produce a hydrophobic surface (Tolun & Kitchener, 1963-64).

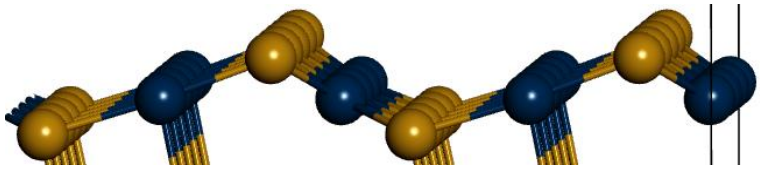

Figure 1.4 The working surface of cooperite, Pt-navy blue, S-brown (Mkonto, personal communication)

1.2.3.3. Pyrite

Pyrite is a common sulphide mineral and is mainly found in igneous, metamorphic and sedimentary rocks. It is a brassy-yellow mineral that crystallizes in an isometric crystal structure (Figure 1.5) and is a member of the pyrite group. It has the Mohs hardness of 6 - 6.5 and a specific gravity of 4.8-5. The unit cell is made up of a Fe-face-centred cubic sub-lattice with S_2 ions. The Fe atoms are bonded to six S atoms to give a distorted octahedron.

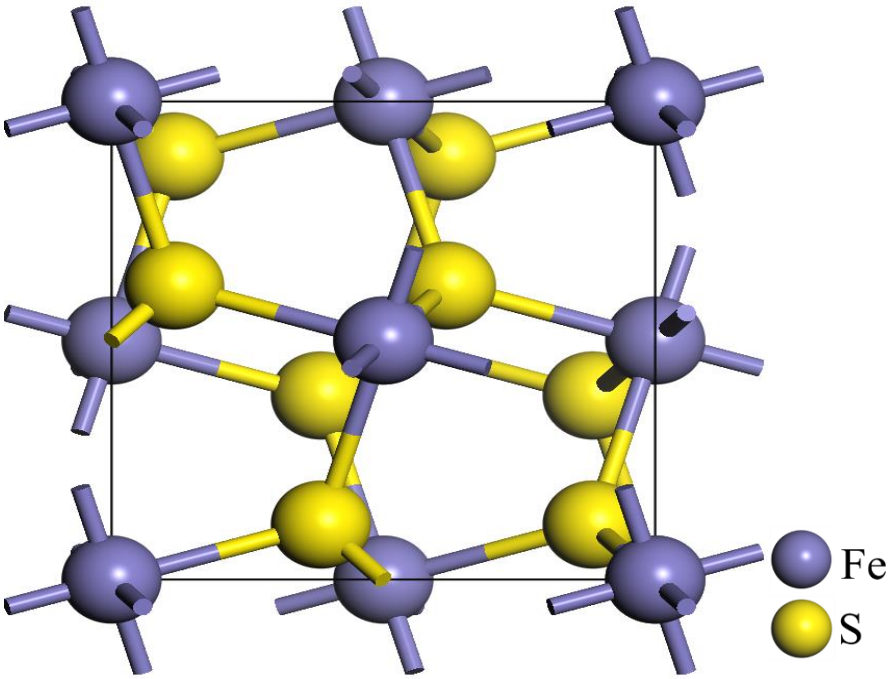

Figure 1.5 Crystal structure of pyrite (Mkhonto et al., 2018)

Figure 1.6 shows the working surface of pyrite and the orientation of the iron and sulphur atoms on the mineral surface.

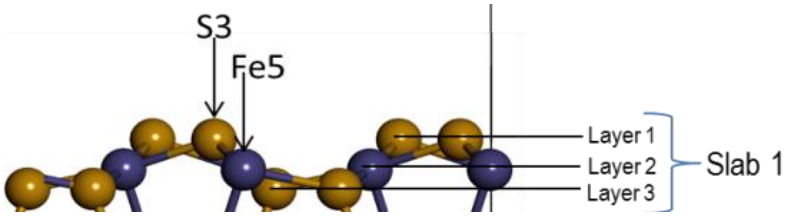

Figure 1.6 Working surface of pyrite showing the exposed sulphur atoms (Mkhonto et al., 2018)

Pyrite is fairly unstable and reacts with water to give:

$$2FeS_2(s) + 7O_2 + 2H_2O\ (l) \rightarrow 2Fe^{2+}\ (aq) + 4SO_4^{2-}\ (aq) + 4H^{+}\ (aq)$$

This reaction results in the formation of acid and the problems associated with acid mine drainage.

1.2.3.4. Arsenopyrite

Arsenopyrite is a sulphur-arsenide mineral that crystallizes to form a monoclinic crystal system (Figure 1.7) where each Fe centre is connected to three As and three S atoms. It has the Mohs hardness of 5.5 – 6 and a specific gravity of 5.9 – 6.2.

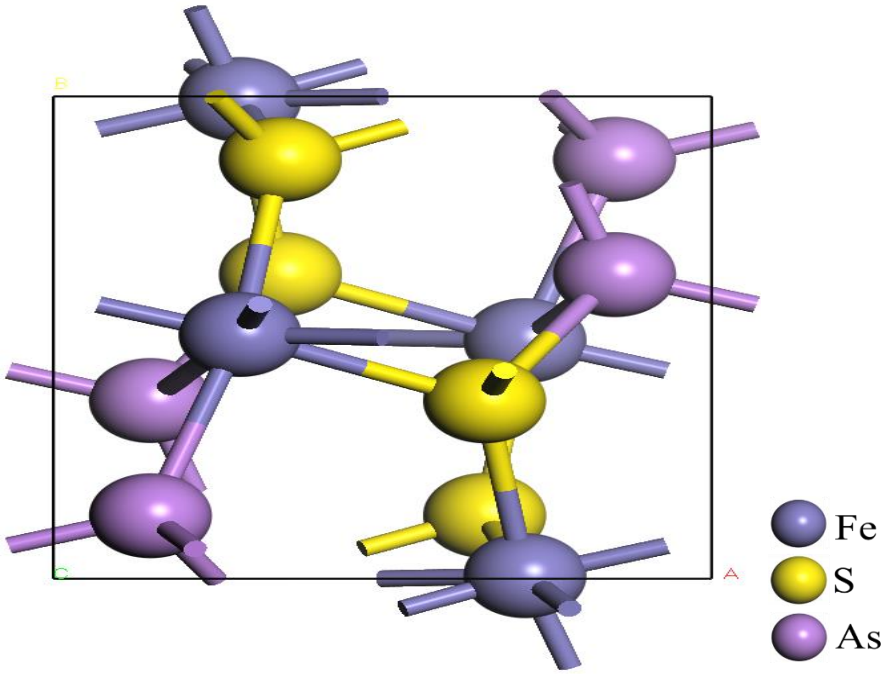

Figure 1.7 Crystal structure of arsenopyrite (Mkonto, personal communication, 2022)

Figure 1.8 shows the working surface of arsenopyrite which has alternating sulphur and arsenic atoms exposed to the surface.

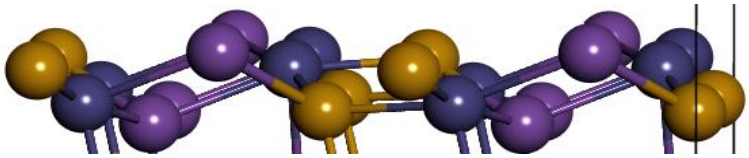

Figure 1.8 Working surface of arsenopyrite with exposed alternating arsenic (purple) and sulphur (brown) atoms (Mkonto, personal communication, 2022)

The mineral slowly converts into iron arsenates ($FeAsO_4$) when exposed to the atmosphere. Unlike pyrite which is acid-forming, arsenopyrite is acid-consuming.

Arsenopyrite is mainly associated with the gold-bearing ores, which are usually refractory making the gold difficult to leach with cyanide from the mineral matrix.

1.3. FROTH FLOTATION PROCESS

Froth flotation is the primary commercial method applied in the separation of the PGMs from the gangue minerals in the slurry. During the flotation process, the slurry is conditioned using different flotation reagents such as collectors, frother, depressants, and activators, to impart the desired surface properties to the minerals that allow good separation between the valuable and gangue minerals (Wills & Napier-Munn, 2006). The valuable, targeted minerals are rendered hydrophobic by reagents called collectors when they selectively adsorb on the targeted mineral. The hydrophobic particles get attached to air bubbles in a continuously agitated slurry and the particles are recovered in the froth phase. A typical flotation cell is shown in Figure 1.9. The valuable, floatable minerals as well as some particles which are entrained are then collected into the concentrate launder while the non-floatable and gangue minerals are collected into the tailings stream. This processing stage may result in significant losses of valuable minerals such as sperrylite, which is a platinum arsenide.

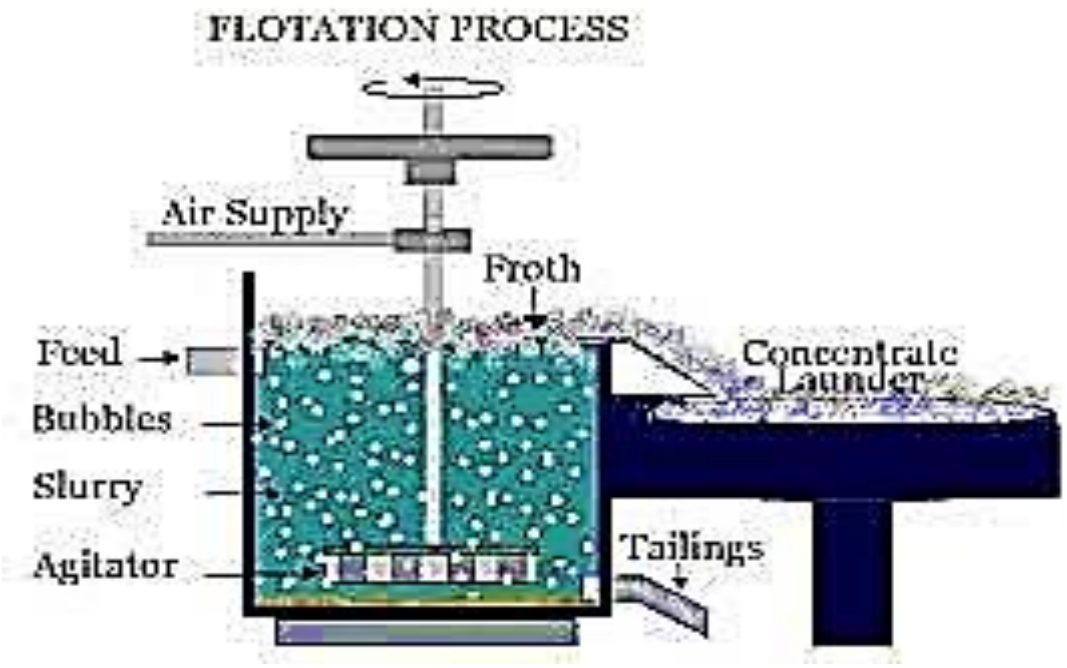

Figure 1.9 Typical flotation cell that shows the pulp and the froth phases in the cell (911 Metallurgist)

The processing of PGM ores is complex, taking into consideration the presence of different mineral species with their different physical properties and mineral associations. Moreover, the behaviour of all these individual mineral species in the pulp phase is not well understood. South African concentrators generally make use of the mill float-mill float flotation circuits (MF2) to minimize overgrinding, which in turn helps to minimize the loss of valuable minerals.

In the MF2 circuits, primary milling is carried out to just sufficiently liberate the coarser-grained sulphide minerals, especially pentlandite which is prone to over-grinding (Cole & Ferron, 2002-3). The first rougher bank tailings are taken for secondary milling to further liberate the locked small-grained PGMs.

Fine grinding is necessary for the liberation of the PGMs since their average grain size is about 10 µm. However, a study by Penberthy et al. (2000) indicated that the milling in general, reduced the particle size of the minerals in the UG2 ore, resulting in an increase of finer particles of size classes 0-2 µm and 2-4 µm, which were difficult to recover during the batch flotation tests. Therefore, the very fine grinding required to liberate these fine grains creates a new set of downstream problems that are associated with the recovery of fine particles (bubble-particle collision efficiency decreases; pulp viscosity increases; entrainment increases). Plant operations tried to strike a balance between liberation and overgrinding, and it was also noted that some PGMs, associated with silicates, were lost to the tailings as middling or locked particles in the UG2 and Platreef concentrators. However, the use of Mainstream inert regrind (MIG) technology has been employed and it resulted in improved final tail grind (Rule, 2010). The use of IsaMills in concentrators minimizes the production of super fines (< 5µm), due to the low mill residence time and improved attrition grinding action (Rule et al., 2008; Rule, 2010). In addition, the use of inert ceramic grinding media, as opposed to steel grinding media, is beneficial in offsetting the detrimental effects of hydroxide coatings on the fine mineral particles that occur when grinding with steel media (Rule, 2010).

To date, thiol collectors, are mainly used for the flotation of sulphide ores during the flotation of PGM ores because of their high association with base metal sulphides (BMS). Therefore, it has been assumed that the PGM species behave in the same way as the base metal sulphide minerals during the flotation process. However, due to a decrease in base metal sulphide association of PGMs in the Platreef and UG2 reef compared to the Merensky reef that was initially exploited, the use of thiol collectors has, in some cases, yielded unsatisfactory flotation recoveries. The type of reagent suite has a great influence on the floatability of PGM ores, as seen in the study carried out on the Merensky Reef ore (Wiese et al., 2005) which showed that the ores responded in a similar manner to the three reagent suites tested and differences relating to specific mineralogy were also observed.

There is little information on the relative floatability of the various PGMs. Such studies are difficult due to the problem of obtaining relatively pure samples because of the low mineral concentrations within the ore and their occurrence as discrete phases with most of the grains that are generally less than 10µm. The PGM-bearing ores have been mineralogically characterized based on the PGM species, size distribution, degree of liberation, gangue and base metal sulphide associations (Penberthy et al., 2000; Chetty et al., 2009; Becker et al., 2008; Becker et al., 2014) in order to understand their floatability under different milling and flotation conditions. Mineralogical characterization gives information on the ore variability in the Bushveld Complex and how it affects the recovery of different PGMs.

1.3.1. Flotation Studies of PGM Minerals

The flotation and mineralogical studies on the PGM ores have helped in giving an insight into the flotation behaviour of different PGM minerals.

However, these studies have been limited mostly to PGMs associated with base metal sulphides, and very little information was made available on the individual minerals. Two mineralogical studies on UG2 ores explained their findings based mainly on the BMS association, degree of liberation and particle size. Batch flotation tests carried out on UG2 ore by Penberthy et al., (2000) recovered fast, medium and slow-floating concentrate after 1, 2 and 20 minutes respectively. The study showed that the PGMs associated with liberated base-metal sulphides (BMS) were mainly found in concentrates while those associated with gangue minerals were found in the tailings stream. Also, depending on the degree of liberation, most of the PGMs locked in gangue or associated with locked base metal sulphides either reported to the slower-floating concentrate or tailings. Moreover, particle size was found to play a role in the recovery of these PGMs, with larger particles (~8µm) being recovered into the fast-floating concentrate whereas medium-sized (~4µm) and smaller particles (~2µm) were recovered into the medium-floating and slow-floating concentrates. Flotation rates of PGMs followed the order: braggite > cooperite > malanite > ferro platinum and other non-sulphide platinum-group mineral phases > laurite (Penberthy et al., 2000). In this study, the number of liberated PGM grains found in the tailings was too small to calculate the grain-size distribution and no data was provided on the unrecovered PGMs.

Chetty et al., (2009) carried out a PGM analysis on the primary rougher flotation bank, which consisted of 10 cells, from a South African concentrator treating UG2 ore from the Western limb of the Bushveld Complex. Around 60% of the PGMs were recovered in the first 2 cells and the remaining 10% was recovered in the subsequent cells. The palladium minerals were found to be fast floating as opposed to the platinum minerals, and their larger proportion was recovered in the first cell compared to the second cell (Chetty et al., 2009). These fast-floating particles were mostly comprised of the liberated PGMs (>3µm) as opposed to the liberated PGM particles associated with BMS. Mineral particles larger than 3 µm were recovered at a fast rate while those smaller than 3µm were recovered down the bank (Chetty et al., 2009). The rougher bank tails were comprised of the slow-floating and non-floating particles and PGMs locked in silicate or oxide gangue particles (Chetty et al., 2009).

According to grouped mineral species data, in a study carried out by Bushell (2011), it was shown that laurite (RuS_2) and arsenides had the highest proportion of non-recoverable PGMs compared to the sulphides and alloys.

The amount of tellurides present, from the mineralogical data, was inadequate to reasonably quantify the recovered and the telluride minerals that reported to the tailings (Bushell, 2011).

Another study by Taguta & Ross (2021) investigated the possibility of replacing the thiol collectors with a Tecflote S11, a nitrile-based collector or using it as a co-collector in the flotation of Platreef ores. Unlike thiol collectors, nitrile collectors' bond with the nitrogen atom and they are adsorbed on the air-water interface, as they improve film thinning which results in improved recoveries (Lewis and Lima, 2018). The batch flotation tests showed that the highest recovery was achieved with PAX at a dosage of 160 g/t and as a co-collector with the S11 Tecflote collector at the dosage of 80 g/t each.

The collector combination resulted in increased recovery of fully liberated PGMs and minerals associated with BMS. The mineralogical analysis of tailings indicated that greater losses were realised in tellurides and arsenides which were below the 15µm size fraction. On the other hand, the use of the S11 Tecflote collector alone, at a dosage of 160 g/t, resulted in losses of fully liberated PGMs and those associated with base metal sulphides. Also, the Tecflote tailings had a lesser amount of PGMs that were locked in or attached to the silicate or oxide gangue compared to the Tecflote and PAX tailings. The study concluded that there was a need to combine the S11 Tecflote collector with a long chain xanthate collector to achieve optimum recoveries. However, the combination does not seem to offer any improved recoveries on the telluride and arsenide PGMs.

1.3.1.1. Flotation of Synthetic and individual PGM Minerals

Only two studies have been carried out to date on the floatability of individual PGM species (Shackleton et al., 2007; Shamaila et al., 2008). Shackleton et al., (2007), carried out a study on the floatability of different synthetic PGMs, which were ideally pure, fully liberated minerals. Microflotation tests were carried out using the -106+38µm size fraction, SIBX collector, and synthetic plant water at pH 9. The cumulative recoveries obtained under different test conditions are shown in Table 1.3. Most PGM minerals showed remarkably high flotation recoveries after adding the SIBX collector. With the exception of sperrylite which had the lowest recovery of 1.9%, all samples had recoveries above 94%, with the two telluride samples being above 99%. The recoveries of the bismuth telluride samples are consistent with the recovery obtained by Vermaak et al., (2005) using the same mineral size fraction.

The difference in the recoveries of the two sperrylite samples shown in Table 1.3 was attributed to the distribution of platinum blebs as shown in the micrographs in Figure 1.10. The study showed that SIBX adsorbed more readily on unreacted platinum (sample 1) than sperrylite (sample 2) $PtAs_2$ particles. The sperrylite sample with more unreacted platinum blebs, gave a higher recovery of 74% as opposed to a sample with few platinum blebs (1.9%), suggesting that SIBX adsorbed more readily on Pt as compared to $PtAs_2$.

Table 1.3 Recoveries of synthesized PGM group of minerals using SIBX dosage of 5 x10^{-5} M (Shackleton, 2007)

			-106+38 µm Recovery (%)		
PGM Mineral	**Formula**	**Crystal Structure**	**No Reagent**	**SIBX**	**SIBX & $CuSO_4$**
Cooperite	PtS	Tetragonal	94	94	88
Vysotskite	PdS	Tetragonal	64	95	99
Pallado Arsenide	Pd_2As	Monoclinic	27	96	67
Moncheite (1)	$PtPd(BiTe)_2$	Trigonal	18	>99	48.5
Moncheite (2)	$PtTe_2$		49	>99	41.3
Merenskyite (1)	$PdPt(BiTe)_2$	Trigonal	75	>99	87
Merenskyite (2)	$PdTe_2$		63	>99	96
Sperrylite (1)	$PtAs_2$	Isometric	7.14	74	69
Sperrylite (2)	$PtAs_2$		0.9	1.9	8.5

This was confirmed by molecular modelling computations carried out by Waterson et al., (2016), which showed that ethyl xanthate had higher binding energy with pure platinum compared to sperrylite. Surface analysis using TOF-SIMS also confirmed that SIBX was adsorbed in greater quantities in sample 1 compared to sample 2. This study revealed that a homogenous sample, that is free from platinum blebs is key to understanding the behaviour of the mineral.

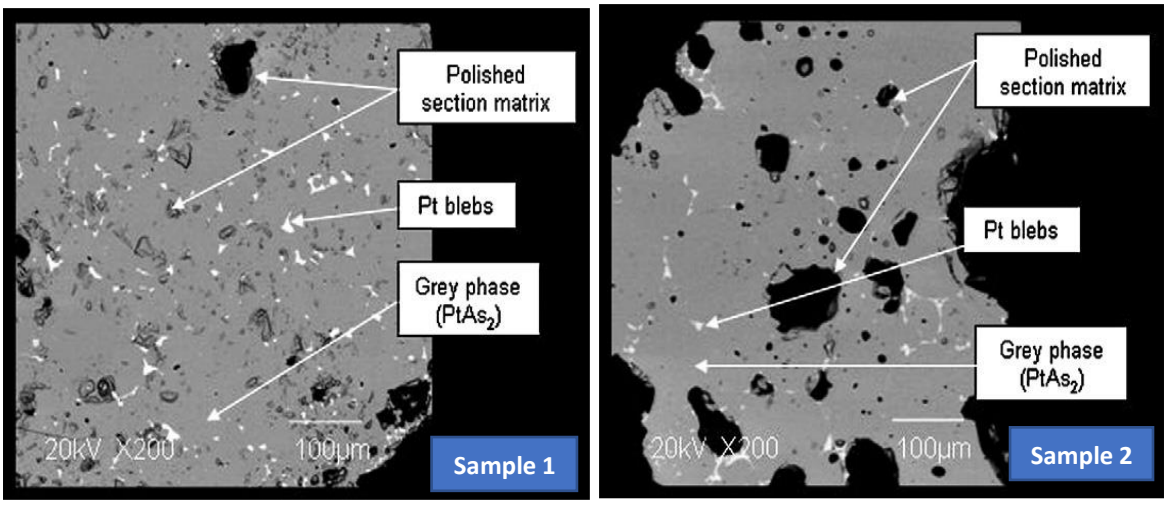

Figure 1.10 Micrographs of sperrylite samples 1 & 2 (Shackleton et al., 2007)

Merenskyite and cooperite samples showed a high degree of natural floatability compared to the other minerals. However, the study did not explain the reasons behind the high natural floatability of this mineral. Moreover, the study also revealed that the addition of the copper sulphate activator generally resulted in the reduced recoveries of the PGM minerals except for sperrylite sample 2, whose recovery was slightly improved.

In addition, the study by Shackleton (2007) investigated the effect of pH on the recovery of sperrylite. It was found that $PtAs_2$ recoveries decreased with an increase in pH. At pH values of 6, 9, and 10, the recoveries of sperrylite were 15%, 8.5% and 0.59%, respectively (Shackleton, 2007). Molecular modelling computations carried out by Waterson et al. (2016) indicate that the binding energy of the OH^- (-473.8 kJ mol^{-1}) ions on sperrylite was found to be more negative than that of ethyl xanthate (-371.3 kJ mol^{-1}), making it difficult for the collector ligands to displace the OH^- ions that preferentially get adsorbed on the mineral surface at high pH. The presence of metal hydroxide species may thus be forming hydrophilic coatings that adversely affect the floatability of minerals (Rao, 2004).

In the study by Shackleton (2007) all the minerals were considered to be fully liberated since they were synthesized as pure samples, and a uniform PSD (which excludes very fine particles) was used during the microflotation tests. This eliminates particle size and mineral liberation effects as the major possible causes for the poor floatability of $PtAs_2$. Therefore, the study concluded that the surface properties of $PtAs_2$ were responsible for poor collector adsorption, which in turn resulted in its poor floatability. It was found that SIBX adsorbed to a much greater extent on $PtAs_2$ sample 1 and the other PGM minerals compared to sample 2. TOF-SIMS and XPS results indicated that dixanthogen was responsible for the flotation of these PGM minerals as it was observed on all the surfaces of the minerals tested, except for $PtAs_2$ sample 2 (Shackleton, 2007).

Shamaila et al. (2008), also investigated the floatability of PGE tellurides and PGE arsenides using Platreef ore. The studies were carried out using a Flexi-float mini-pilot plant with a particle size distribution of 80% passing 75µm, an SIBX collector, and synthetic plant water at natural pH of the ore (~pH 9). It was found that the tellurides yielded better recoveries, higher flotation rate constants and upgrade ratios compared to the arsenides. The flotation recoveries of tellurides ranged from 82.6% to 89.9% while those of arsenides ranged from 45% to 52.8% (Shamaila, 2007). Mineral Liberation Analysis (MLA) indicated that the PGE arsenides had a higher proportion of fully liberated particles (74.3%) in the feed as opposed to the tellurides (67.2%) and yet showed poor floatability (Shamaila, 2007). The unliberated arsenides (25.7%) were associated with silicates whereas the unliberated tellurides (32.8%) had a higher association with the base metal sulphides (Shamaila, 2007). This study provided the clearest indication yet that the floatability of PGE arsenides is poor in comparison to the PGE tellurides. Furthermore, the study also investigated the behaviour of synthetic sperrylite and moncheite. The synthetic minerals were found to behave the same way as natural minerals as indicated by the trend in the grade concentrates at different spiking levels. The floatability of the sperrylite was also found to be lower than that of moncheite even when the minerals were spiked on barren feldspathic pyroxenite, which had a gangue mineralogy that was similar to that of the natural Platreef ore (Shamaila et al., 2008). Their recoveries were 88.1% and 95.3% respectively.

1.3.1.2. Flotation of Pyrite

Pyrite is one of the abundant sulphide minerals that is usually found in the ore deposits that are associated with base metal sulphides, coal, and gold (Wang, 1995; Bulut et al., 2014). This mineral is generally unwanted in the differential flotation of base metals as it leads to a decreased concentrate grade, consequently reducing the values of the concentrate (Wang & Forssberg, 1991). Also, the combustion of the pyrite bearing coal emits sulphur dioxide (SO_2) which results in acid rain.

Xanthate collectors are usually used in the flotation of base metal sulphides. Dixanthogen is formed on the mineral surface when its mixed potential is greater than the X^-/X_2 equilibrium potential value (Allison et al., 1972). Even though pyrite is considered to be an unwanted gangue mineral, studies have concluded that the formation of dixanthogen on the mineral surface is responsible for the hydrophobicity of the mineral (Fuerstenau et al., 1968). Moreover, the cyclic voltammetric studies revealed that dixanthogen was the major species found on the pyrite surface after adding the xanthate collector (Janetski et al., 1977). Figure 1.11 indicated that the recovery of pyrite increased with an increase in collector concentration and much higher concentrations led to the elimination of the two peaks that were observed at lower concentrations.

Speciation diagrams by Wang and Forssberg (1991) have attributed the poor floatability of pyrite within the pH range of 5 to 8, to the presence of the ferric hydroxy xanthate ($Fe(OH)_2X^+$ as the predominant species. Thus, the depletion of free xanthate results in poor pyrite recoveries.

The formation of ferric xanthate has also been found to contribute to the floatability of pyrite (Taggart et al., 1930; Wang & Forssberg, 1991).

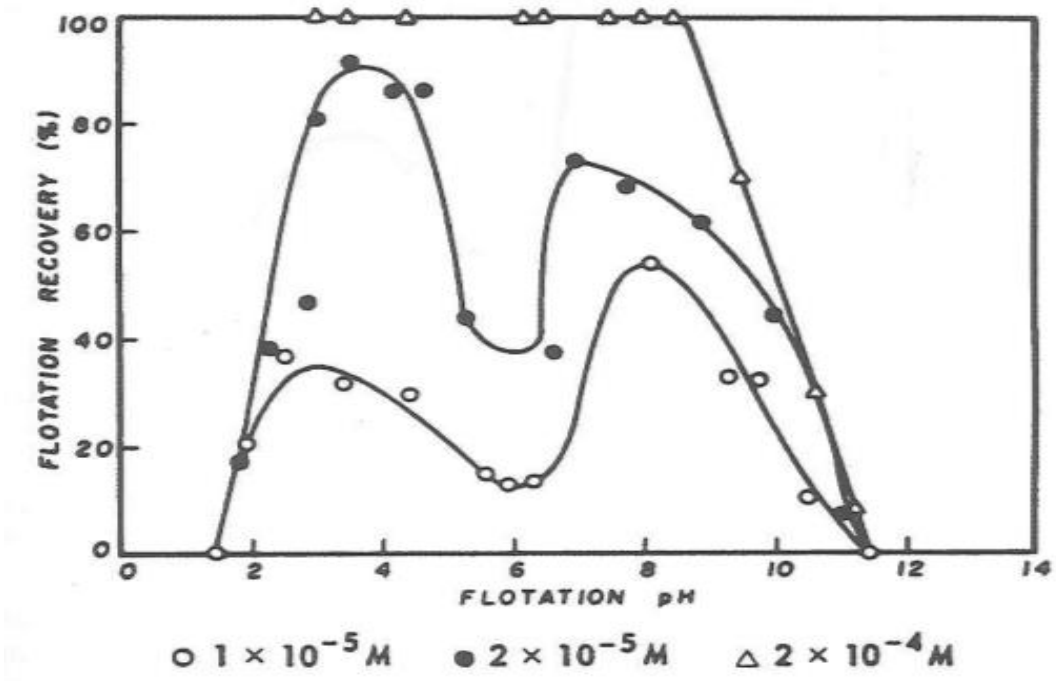

Figure 1.11 Flotation recovery of pyrite with potassium amyl xanthate (Fuerstenau et al., 1968)

The high recoveries observed at pH 4 have been attributed to the formation of sulphur-rich products and dixanthogen (Wang & Forssberg, 1991; Leppinen, 1990). The depression of pyrite below pH 2 and above pH 11 was attributed to the decomposition of xanthate and the thermodynamic instability of dixanthogen giving way to the formation of ferric hydroxides on the mineral surfaces respectively (Leppinen, 1990; Fuerstenau et al., 2007). Hence, the pH changes can be manipulated to form the desirable species that could either float or depress pyrite (He et al., 2005). Under alkaline conditions pyrite can be activated by metal ions such as Cu^{2+} and Pb^{2+} or any contaminants in process plant water have been found to activate the pyrite surfaces thereby making the depression of the mineral difficult (Owusu et al., 2014; Barker et al., 2014).

1.3.1.2.1. Flotation of Nickel Arsenide and Arsenopyrite

The flotation of arsenide minerals has been found to be similar to those of sulphide minerals and they also demonstrate an appreciable amount of electrochemical activity. This is caused by the reactivity of the arsenic bonding atom that has variable oxidation states like sulphur. Nickel arsenide (NiAs) has a low rest potential of -70 mV in air as opposed to pyrrhotite which has the rest potential of 40 mV under the same conditions (Nakazawa & Iwasaki, 1986). Hence, nickel arsenide is expected to be readily oxidised compared to pyrrhotite. The zeta potential tests indicated that the xanthate collector was adsorbed on the mineral surface as indicated by the decrease in the zeta potential after adding the collector.

The high recoveries were realised between the pH range of 4 to 8. The recovery of nickel arsenide was adversely affected by the formation of nickel hydroxide.

Arsenopyrite consists of the S and As donor atoms and its behaviour as opposed to pyrite is of great interest in this study. Arsenopyrite has good floatability, and this is of great benefit in the flotation of gold-bearing ores that are associated with the mineral, as it results in high recoveries of gold. On the other hand, when associated with base metal sulphides, there is a need to depress arsenopyrite as it reduces the grade of the concentrate and attracts smelter penalties. When xanthate collectors are added, dixanthogen is formed on the mineral surface, which is responsible for the high floatation response of the mineral which can catalyse the oxidation of the collector (Allison et al., 1972; Lopez Valdivieso et al., 2003). Dixanthogen has been found to be very stable at pH ranges of 4 to 5.

The depression of arsenopyrite can be carried out at high pH in the presence of oxidizing agents like hydrogen peroxide. This results in the formation of surface ferric hydroxides and arsenate species (Monte et al., 2002; Beattie and Poling, 1987). Adjusting pulp Eh to a value that is below the oxidation potential of the xanthate collector was proposed to also result in the depression of arsenopyrite (Lopez Valdivieso et al., 2006). A study by Lopez Valdivieso et al. (2006) indicated that at low pH, dixanthogen forms at low concentrations of the xanthate collector whereas at high pH, higher concentrations of xanthate are required. The study proposed that the formation of ferric oxy-hydroxide species can act as cathodic sites for the oxidation of the xanthate ions. It was also shown that lower collector amounts of longer-chain xanthates were more effective in floating arsenopyrite as opposed to the shorter chain lengths xanthates (Gonzalez Chavez & Bessiere, 1989; O'Connor et al., 1990).

1.3.2. Surface Oxidation of PGM and Sulfide Minerals

Surface oxidation of the mineral surfaces could hinder collector adsorption leading to reduced recoveries. According to the study by Shackleton (2007), the XPS and TOF-SIMS results showed no evidence of surface oxidation on sperrylite surfaces throughout the conditioning process. On the contrary, palladium minerals like PdS, $PdPt(BiTe)_2$, $PdTe_2$ and Pd_2As were heavily oxidized by synthetic plant water whereas the platinum minerals were lightly oxidized (Shackleton, 2007). However, the palladium minerals still gave higher flotation recoveries compared to platinum minerals after adding SIBX, an indication that the surface oxidation could have enhanced their floatability. The plant water ions were not strongly adsorbed onto the heavily oxidised minerals.

There was no oxidation of arsenic or platinum observed in sperrylite. Also, the light oxidation of cooperite could be due to the presence of plant water ions as Mg^{2+} ions were adsorbed on the mineral surface. Also, the oxidation tests, where samples were placed under oxidizing conditions, showed that the bismuth-containing samples were susceptible to surface oxidation while the telluride samples were not affected.

The study by Vermaak et al., (2007), indicated that some oxidation of $PtAs_2$ occurred in the absence of xanthate, at potentials more positive than 300mV vs SHE. At pH 9, the natural Eh of the Merensky ore pulp was between 100mV and 200mV vs SHE (Chimonyo et al., 2017).

Sperrylite is, therefore, expected to remain unoxidized throughout the flotation process of PGM minerals, thus surface alteration can probably be eliminated as a possible cause for lower recoveries for sperrylite. It is of interest to note that surface oxidation has also been reported during the flotation of nickel arsenides resulting in reduced recoveries (Iwasaki et al., 1988).

Particle size has also been found to affect the extent of surface oxidation of sulphide minerals. Oxidized, fine sulphide minerals, have been found to have similar surface chemistry properties like metal hydroxide precipitates when they are fully covered by the hydroxide layer (Smart et al., 1998). Oxidation of different mineral particles has been found to differ and that has been attributed mainly to the difference in surface area and other factors (Smart et al., 1996). This could be another reason why fine sulphide mineral particles are usually lost to the tailings, showing low collector coverage compared to particles recovered in concentrates (Chryssoulis et al., 1995). As a result, different mineral particles exhibit different collector surface coverages of adsorbed xanthates, with more xanthates adsorbed on surfaces with lower levels of surface oxidation.

1.3.3. Natural Floatability of Minerals

Selective separation of valuable minerals during froth flotation is dependent on surface properties of minerals, and the surface characteristics are mainly determined by the crystal structure of minerals (Rao, 2003). These surface properties reflect the internal features of the minerals, however, the chemical environment in the pulp phase can alter them to a certain degree (Rao, 2003). Natural floatability of has been linked to the crystal structures and their cleavage surfaces of minerals like molybdenite or realgar (Rao, 2004). Flotation studies have also shown that the flotation response of minerals in the presence of a collector varies in different minerals and very few studies have explained the difference in relation to crystal structures of the minerals. Molecular modelling studies have been helpful in revealing the stable working surfaces of different minerals and the orientation of both the metal and ligand ions on the mineral surface (Waterson et al., 2017; Nemutudi et al., 2020).

In this study, it has been proposed that the surface energy of the different minerals is responsible for their natural floatabilities. The study by Hu et al. (2012) states that surface broken bond density determines the surface energy and that lower surface energy results in a more hydrophobic surface. A study by Taguta et al. (2018) corroborates this as indicated by the energy of immersion results between selected mineral surfaces and water interactions. The surface energy of minerals given in Table 1.4 gave an indication that the surface energy of minerals is inversely proportional to their hydrophobicity (lower surface energy = more hydrophobic surface).

Table 1.4 The surface energy components and surface energies of different minerals.

Mineral	Hs^{LW}	Hs^{+}	Hs^{-}	Hs^{AB}	Hs^{T}
Talc	29.5	48.6	9.6	21.6	51.0
Realgar	41.8	107.5	0.016	1.3	43.2
Galena	265.5	4.3	95.4	20.3	285.9
Albite	84.9	19.8	432.8	92.6	177.6
Mica	125.9	21.6	742.1	126.5	252.4
Wollastonite	551.4	17573.0	2344.8	6419.1	6970.4

Different sulphide minerals have different natural-induced flotation recoveries that can be attributed to the difference in the types of oxide layers formed during conditioning. If substantial hydrophilic, oxidized material is formed on the mineral surface, it tends to overcome the natural-induced floatability of the mineral and also reduce the effectiveness of the collector in rendering the mineral hydrophobic (Shannon & Trahar, 1986).

1.4. INTERACTIONS OF MINERALS WITH COLLECTORS

The following section will discuss the interactions of minerals with different collectors using molecular modelling computations and electrochemical interactions with minerals. The role of different donor atoms in collector molecules and donor atoms on the mineral surfaces will also be discussed.

1.4.1. Molecular Modelling Computations

Molecular modelling computations, based on the density functional theorem (DFT) provides an opportunity to make a detailed study of the mineral crystal structures, cleavage surfaces, and the effect of different ligands bonded to minerals. They also reveal the interaction of various mineral surfaces with collector ligands (Waterson et al., 2016; Nemutudi et al., 2020; Yekeler & Yekeler, 2005; 2006; Chen et al., 2013; Yuan et al., 2012; Liu et al., 2008; 2010; 2012; 2013). The computed binding energy between a mineral and a collector indicates the structure-property relationship of a given collector with a selected mineral; however, the given total energy of interaction does not provide information on the energy contribution of the functional groups (Liu et al., 2017).

Molecular modelling computations can also be useful in explaining the collector adsorption mechanisms on the mineral surfaces and this knowledge can be applied in designing new flotation collectors.

Molecular modelling studies carried out by Waterson et al., (2016) revealed that the Pt atoms on the $PtAs_2$ working surfaces are not accessible to collector binding ligands. It was seen that the surface topography played a major role as indicated by the higher binding energies (Table 1.5) of all ligands on the pure platinum surface since it offers no steric hindrances to the approaching ligands.

Table 1.5 Binding energies of different ligands on sperrylite and pure platinum surface (Waterson et al., 2016)

Ligand BE (kJ/mol)	**Ethyl Xanthate**	**OH^-**	**H_2O**
$PtAs_2$	-371.3	-473.8	-21.5
Pt	-503.7	-568.3	-32.1

Furthermore, this study revealed that the arsenic atoms, each having a projected lone pair of electrons, could have induced some repulsive forces towards the approaching bonding atoms, as shown in Figure 1.12.

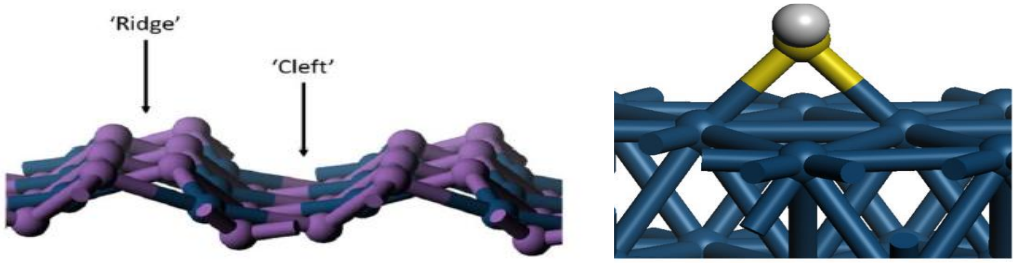

Figure 1.12 Working surfaces of sperrylite and pure platinum (Waterson et al., 2016)

In addition, binding energies of other ligands that were tested, such as H_2O and OH^- ions, were stronger on the platinum surface compared to the sperrylite surface. These results strongly indicate that surface topography plays a major role when it comes to the binding energy between minerals and collector ligands.

Another molecular modelling computational study of PNBX with the sperrylite surface revealed that the sulphur ligand of the xanthate could bond with both the Pt and As atoms on the mineral surface. The highest binding energy of -270.92 kJ mol^{-1} was achieved upon bridging the sulphur ligand on Pt and As atoms (Nemutudi et al., 2020). Bridging on the 2 As atoms gave a similar binding energy of -270.38 kJ mol^{-1}, whereas forming a bridge on the 2 Pt atoms gave the lowest binding energy of -249.46 kJ mol^{-1} (Nemutudi et al., 2020). Figure 1.13 also shows the interactions of the sperrylite 100 surface with the bonding sites Pt and As atoms on the mineral surface.

It was also revealed that nitrogen can also bond with arsenic on the mineral surface. Sulphur ligands have to pass over the arsenic atoms that are projected above the Pt atoms in order to form the Pt-Pt bonds, which gave the lowest binding energy.

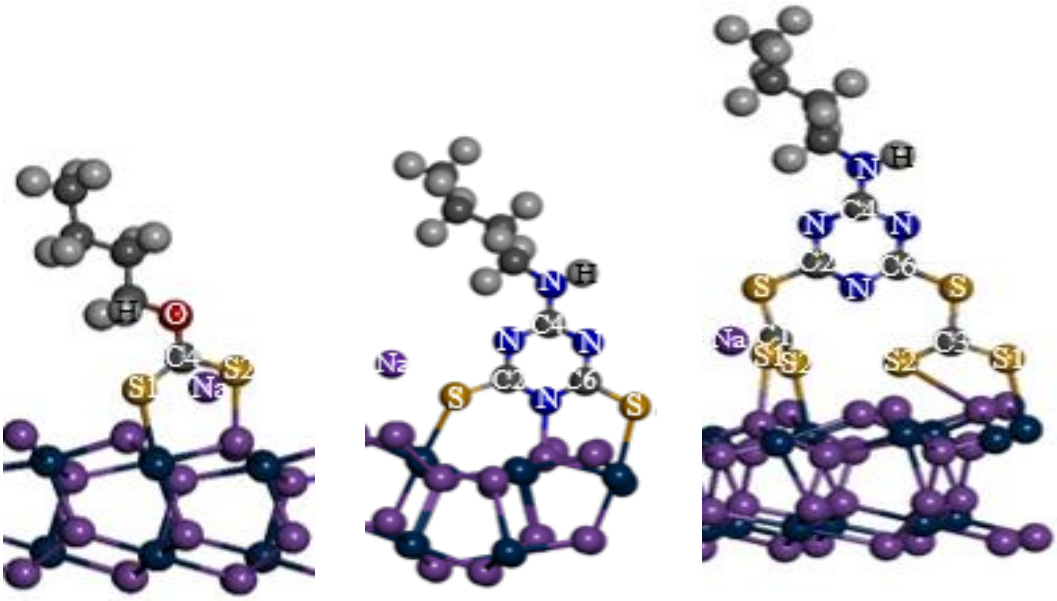

Figure 1.13 Sperrylite bonding sites (Pt and As) interactions with different collectors on (100) surfaces with SNBX, SDTBAT and SDCDTBAT (Nemutudi et al., 2022)

Lastly, molecular modelling computations were carried out by Mkonto et al., (2018) with heterocyclic collectors on the pyrite surface. The study revealed that the exocyclic S and N atoms bonded with the Fe ion on the mineral surface using 2-mercaptobenzothiazole (MBT), 2-mercaptobenzoxazole (MBO) and 2-mercaptobenzimidazole (MBI) collectors. Also, the $-CS_2$ group in the modified 2-mercaptobenzothiazole (MMBT) collector bonded with the Fe atoms.

This study revealed that the S donor atom on the pyrite surface did not participate in the bonding with any of the collectors. Also, the oxygen atom in MBO did not take part in the bonding with pyrite.

1.4.2. Electrochemistry Studies

Rest potential measurements of minerals have been found to be useful in determining the surface properties and the interaction of minerals with different collectors. Electrochemical studies by Tadie et al., (2015) determined the rest potentials of Pt, Pd, PtS, PdS, $PtTe_2$ and $PdTe_2$ before and after adding sodium ethyl xanthate collector (SEX). The pure metals (Pt, Pd) had relatively high rest potentials compared to the respective minerals. The final rest potentials predicted the possible formation of dixanthogen for PtS and $PdTe_2$ at a much slower rate compared to the pure metals (Tadie et al., 2015). On the other hand, the final rest potentials of PdS and $PtTe_2$ at pH 9.2 were below the dixanthogen equilibrium potential line, suggesting the formation of the metal thiolate on the minerals' surfaces. Dixanthogen is said to be more hydrophobic than the metal thiolate.

However, there are conflicting views on the role of the chemisorbed species on the hydrophobicity they impart to the mineral surface and it is thus not possible to conclude that the electrochemical results suggest that the dithiolate promotes the recovery of the minerals (Nagaraj and Ravishanker, 2007).

At a pH of 4.2 the study revealed that dixanthogen was formed on the metal and all the mineral surfaces and the extent of interaction with SEX collector was higher as opposed to that at pH of 9.2 (Tadie et al., 2015). The decrease in potential after adding SEX and SEDTP was greater for the telluride minerals compared to the sulphide minerals. The results conform with the results from the study by Shackleton et al., (2007) where the recoveries of telluride minerals were greater than PtS after adding the SIBX collector. The results predicted by the rest potential measurements in this study were found to be in agreement with those predicted by the cyclic voltammetry tests under the same conditions. Moreover, the study also confirmed the inhibiting effect of the OH^- ions on the adsorption of collectors, which was pointed out in other studies (Shackleton 2007; Waterson et al., 2016).

Electrochemical and in situ Raman spectroscopic studies carried out by Vermaak et al., (2007) indicated that the hydrophobicity of sperrylite, one of the slow floating PGMs, increased with an increase in potential. The potential controlled contact angle measurements, in the presence of ethyl xanthate, gave the highest contact angle of 54º at a potential of 400 mV (vs SHE). The surfaces of sperrylite were found to be hydrophilic at low potentials, with contact angles of 0º at potentials of 200 mV and below. In situ Raman spectroscopy results demonstrated that the high anodic currents found on sperrylite, when anodically polarized at 300 mV (vs SHE), reflected the oxidation of ethyl xanthate to dixanthogen.

The formation of dixanthogen was rapid on the surface of $PtAs_2$ as reflected by the formation of strong dixanthogen bands after 2 minutes of polarisation (Vermaak et al., 2007). Unlike the case of Pd-Bi-Te, no molecular xanthate was detected on the sperrylite surface using the Surface-enhanced Raman Spectroscopy (SERS). Xanthate chemisorption was not completely ruled out in this study and the failure to detect the dixanthogen bands at this point was attributed to the possibility of poor enhancement of the Raman signal. The mixed potential of the system was more positive than the dimerization potential of the collector and hence this predicted the formation of dixanthogen on the mineral surface. This study suggested that an increase in pulp potential could increase the floatability of sperrylite. However, no flotation tests were carried out at high pulp potentials.

Another electrochemical study was carried out by Vermaak et al., (2005) to understand the surface properties of another poorly recovered mineral, viz. Pd-Bi-Te. After polarizing the mineral at 300 mV (vs SHE), the chemisorbed molecular xanthate was identified on the surface of Pd-Bi-Te after 120s had lapsed. Dixanthogen was identified on the mineral surface after 1600s, indicating that the formation of the dithiolate was much slower on Pd-Bi-Te as opposed to the $PtAs_2$ electrode. The potential controlled contact angle measurements, in the presence of ethyl xanthate, gave the highest contact angle of 63º at 200 mV. The contact angles at potentials below 115 mV were found to be 0º and just like sperrylite, the mineral was found to be hydrophobic as the potential increased.

Microflotation tests with Pd-Bi-Te, using the size fraction to -106µm+38µm, at pH 9 with a 5 x 10^{-5}M SIBX collector gave a fairly high recovery of 97% (Vermaak, 2005). The authors concluded that the presence of xanthate and dixanthogen on the Pd-Bi-Te and $PtAs_2$ mineral surfaces was an indication that the minerals are hydrophobic. The study ruled out mineral collector interaction as the cause for poor flotation recoveries but cited poor flotation response of small, liberated mineral particles, usually less than 4 µm in size (Vermaak et al., (2005, 2007)). Mineralogical studies showed that about 70% of liberated Pt-Pd-Bi-Te, with a size fraction of less than 4µm, were found in the tailings stream of the Mimosa mine in Zimbabwe (Vermaak, 2005). Mineralogical studies by Bushell (2011) revealed that the loss of PGMs to the tailings, that were classified as too small to float (< 3µm) (Pernberthy et al, 2000), was around 8%. Sizing in mineralogical studies were done by the analytical software and were not physically sized. When it comes to liberated PGM species, the individual minerals' flotation response could also be a contributing factor, other than particle size alone.

However, no flotation tests were carried out on sperrylite, and the authors failed to take into account that PGM plants do not operate at such high potentials, with pulp potentials generally ranging from 100-200 mV (vs SHE). Studies have indicated that the flotation response of sperrylite is poor even with size fractions greater than 38µm (Shackleton et al., 2007; Pikinini et al., 2020).

1.5. COLLECTOR DESIGN BASED ON DONORS AND ACCEPTORS

The interaction of collector molecules with minerals is mainly based on the interaction of the bonding ligands with the metal atoms on the targeted mineral surface. The common ligands that are found in collectors, that bond directly with the metal cations on minerals, are S, O and N. Phosphorous is one of the ligands found in the dithiophosphate collectors and it forms part of the functional group. Phosphorous does not directly bond with the metal atoms on the mineral surface in the aqueous phase, but readily complexes with metals in the organometallic compounds. Because these ligands possess a lone pair of electrons which they donate to effect a bond with the metal cations on the mineral surface, like Pt, and Ni, they are called donors. Also, the metal cations in minerals that accept electrons from the ligands to effect a bond are called acceptors (Nagaraj & Ravishankar, 2007). In collector design, the natural occurrence of minerals serves as a pointer to show the affinity of these donors to certain elements that form the minerals (Nagaraj & Ravishankar, 2007). Transition metals like Cu, Au, Ag, and the platinum group elements have been found to show a high affinity for S (Nagaraj & Ravishankar, 2007). This could be the reason why thiol collectors are used in the flotation of the PGMs. The high PGE concentration of arsenides and sulfarsenide minerals in the Platreef deposit is an indication that the PGE elements have a higher affinity for arsenic than sulphur (Bai et al., 2017).

To aid the design of reagents, elements that act as electron acceptors have been classified based on their affinity towards the important donors: S, O and N (Nagaraj & Ravishankar, 2007).

1. Those that show strong affinity for O and N: Most elements in the periodic table show a very strong affinity for O because it is highly electronegative.

2. Those that show strong affinity for S: Transition metals like Cu, Ni, Au, Ag, and the platinum group elements show high affinity for S.

3. Elements in the intermediate region show an affinity for both O and S.

The mineral of interest, sperrylite consists of As donor atom. However, because it has empty d-orbitals just like Pt, it can also act as an acceptor to electrons from the collector ligands. Platinum has a high affinity for S and can also bond with N. Arsenic on the sperrylite surface has a high affinity for S and O and has an ability to also bond with N.

1.5.1. Properties of Donor Atoms

The basic characteristics of O, N, S and P play an important role in the behaviour of flotation reagents (Nagaraj & Ravishankar, 2007). A summary of the properties of the four donor atoms and the bonds that they form with acceptors is given in Table 1.6.

Table 1.6 Properties of major donor atoms and the bonds that they form with metals. [He] and [Ne] represents the Helium and Neon electronic configurations (Somasundaran & Nagaraj, 1984)

	O	**N**	**S**	**P**
Configuration	[He] $1s^2 2s^2 2p^2$	[He] $1s^2 2s^2 2p^3$	[Ne] $3s^2 3p^4 3d^0$	[Ne] $3s^2 3p^3 3d^0$
Electronegativity	3.5	3.07	2.44	2.06
Valence electrons	2	5	2	5
Normal valency	2	3	2	3
Number of orbitals	4	4	4 + d	4 + d
Number of bonds (valency expansion)	3	4	2–6	3–6
Lone pairs	2	1	1	1
pπ-pπ	Strong	Strong	Poor	None
dπ-pπ (back-bonding)	None	None	Strong	Strong
Polarizability	Nil	Good	Strong	Good
Hydrogen bonds	Strong	Strong	Very weak	None
Bonds	More ionic	More ionic	Covalent	Covalent
Steric Accessibility	Low	Low	High	High

1.5.1.1. Oxygen and Nitrogen

Oxygen has high electronegativity; hence it has the ability to bond with most elements in the periodic table, with the exclusion of noble gases. Thus, chelating agents which contain the O-O donors have been found to form chelates with a greater number of metals.

These chelates are less selective compared to collectors that contain sulphur because S is less electronegative (Somasundaran & Nagaraj, 1984). Both ligands can form multiple bonds and readily form pπ-pπ bonds using their outer 2p orbitals.

Moreover, they also form strong hydrogen bonds while the rest show very little to no tendency to form hydrogen bonds (Somasundaran & Nagaraj, 1984).

1.5.1.2. Sulphur and Phosphorus

P and S are less electronegative and they have a bigger atomic radius with vacant d-orbitals and their valencies are not restricted to 3 and 2. Their property of additional bond formation- valency expansion, that arises when paired 3s or 3p electrons are promoted to empty d-orbitals to enable the formation of multiple bonds (Somasundaran & Nagaraj, 1984). Hence, they readily form strong dπ-dπ bonds with transition metals that have partly filled d-orbitals (Somasundaran & Nagaraj, 1984). In addition, they have the ability to back-bond forming dπ-pπ bonds since they can accommodate electrons from metals into their empty d-orbitals. Unlike O and N which have smaller p-orbitals, P and S have larger d-orbitals which are more sterically accessible for bond formation (Somasundaran & Nagaraj, 1984).

1.5.1.3. Arsenic

Arsenic is a bonding ligand on the mineral surface of sperrylite, the mineral of interest in this study. This element exists in two solid forms: yellow arsenic and grey or metallic arsenic. Yellow and gaseous arsenic both consist of tetrahedral As_4 molecules. Yellow arsenic transforms into a more stable metallic arsenic when exposed to light. At room temperature, metallic arsenic has a structure that consists of puckered hexagonal layers and each arsenic atom is coordinated to the three nearest neighbouring atoms (Weller et al., 2014).

Arsenic usually exhibits the +3 and +5 oxidation states, just like the other elements in group 5. It has the Pauling electronegativity of 2.20. It forms the AsX_3 compounds (X= halogen, alkyl or aryl), and it has empty d orbitals of fairly low energy (Cotton et. al., 1999). When As donates electrons to an atom that has electrons in orbitals of the same symmetry as the empty d orbitals, back-donation takes place which results in overall multiple bonds. This property greatly contributes to the formation of stable complexes with the transition elements where the dπ-dπ overlap contributes substantially to the bonding, resulting in higher bond strengths (Cotton et. al., 1999).

The donor ability of the group 5 elements decreases in this order P > As > Sb > Bi. The arsenic compounds are generally similar to their phosphorous analogues.

Unlike phosphorus-based ligands that display strong σ-donor and π-acceptor abilities, arsenic ligands are known to be moderate σ-donors and π-acceptors. As a result, many arsenic ligands display lower reactivity when compared to similar phosphorus-based ligands (Christopher et al., 2004).

It must be noted, based on the above information, that arsenic acts as a soft base when it bonds with transition metal ions.

1.5.2. Chelating Agents and Their Requirements to act as Collectors

The ability of chelating agents to form strong and multiple bonds makes them more desirable for the formation of collectors. For chelating agents to function as collectors, they should meet the following requirements:

- Molecules that form functional groups should also consist of a reasonably long hydrocarbon chain to render the mineral hydrophobic when the collector is adsorbed on the mineral.
- The functional groups should be positioned such that they allow a ring to be formed by the chelate with metal on the mineral surface as the closing member.
- The chelates should be neutral complexes; neutral complexes are usually insoluble in water and therefore promote hydrophobicity.
- The chelate formed should bond strongly with the mineral and not scale off easily (Somasundaran & Nagaraj, 1984).

Almost all the chelating functional groups can form complexes with all metals, hence selectivity is based on donor combinations that can be chosen taking into consideration the properties of a specific acceptor (Somasundaran & Nagaraj, 1984).

The stability constant, K, of the complexes formed gives a relationship between metal cations and ligands and is linked to the selectivity of the collector. Their magnitude gives a qualitative measure of the relative stability and selectivity of one ligand over another (Rao, 2004). The stability constants in minerals do not usually correspond to the flotation response of the minerals and the information from the thermodynamic stability constants does not provide information on the kinetics of the reaction (Somasundaran & Nagaraj, 1984).

Therefore, it has been concluded that the formation of complexes on the mineral surfaces must be dependent on the correct orientation of the mineral lattice ion orbitals. Also, during bond formation, the steric hindrances between the ligands must be minimized.

Thus, coordination is dependent on surface topography and composition of the mineral surface (Somasundaran & Nagaraj, 1984). This has already been discussed in the context of the projection of the lone pair of electrons on the arsenic atoms hindering ligand adsorption.

1.5.3. Typical Collector Structure and Modifications to Promote Binding

A collector is an organic compound that selectively binds with the mineral resulting in the formation of a hydrophobic layer, which causes the mineral to attach to a bubble and hence to float from the flotation pulp (Bulatovic, 2007). It consists of a nonpolar (hydrophobic) group, linking atom, bonding atoms, and a charge balancing metal cation. During the adsorption process of a collector onto the mineral surface, the non-polar group of the collector is oriented towards the water phase and the polar parts towards the mineral surface (Bulatovic, 2007). Figure 1.14 shows a typical collector structure, and the possible structural modifications will be discussed with reference to it.

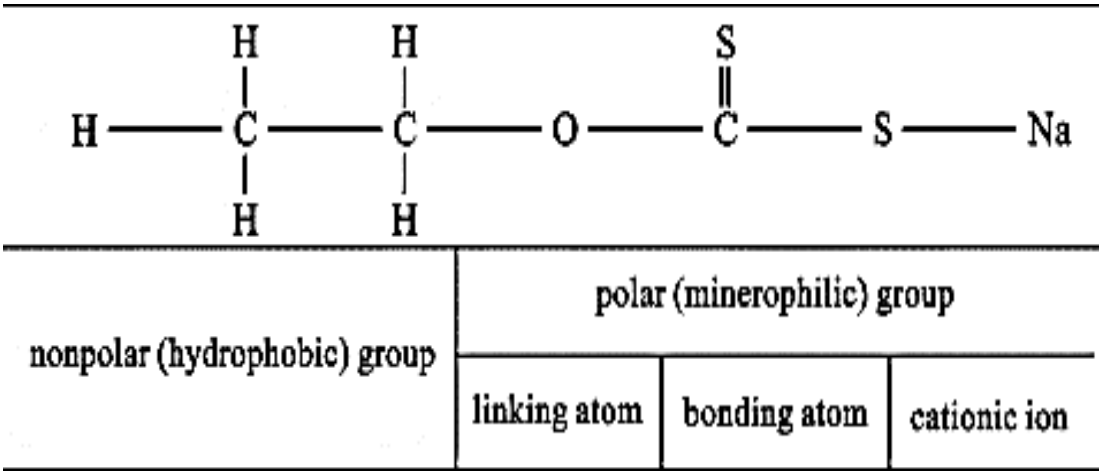

Figure 1.14 Typical xanthate collector structure and its respective components (Somasundaran and Wang, 2006)

- **The functional group:** The functional group consists of the linking atoms and the donor atoms that directly bond with metal cations. Changing the functional group, although complex, affects the selectivity and the strength of the collector. The selectivity of the collector decreases with the increase in the electronegativity of the coordinating or linking atoms (Somasundaran & Nagaraj, 1984).

- **The substituents attached to the functional group:** Making changes to the linking atom increases or decreases the pKa of the collector. This change can lead to a decrease or increase in the electron densities of the bonding donor atoms (Somasundaran & Nagaraj, 1984). When an electron-withdrawing substituent is added, the pKa of the collector is reduced and the collector molecule becomes more acidic. Also, this reduces the stability constant of the metal complex and the pH range in which it can form stable complexes. Furthermore, the bond strength of the collector with the metal cations is reduced. A collector with a low pKa or high value of Ka has a high degree of dissociation of the chelating agent producing ligands in ionic form (Rao, 2004).

  The pKa also indicates the conditions under which the metal ion replaces the proton on the chelating agent. The higher the pKa ($-\log_{10}Ka$), the greater the ability of the collector to donate electrons to the mineral surface.

- **Hydrophobic chain length:** The hydrophobicity of the mineral surface is a function of the collector carbon chain length. Increasing the carbon chain length of xanthate collectors results in increased recoveries of chalcopyrite, pyrite and pyrrhotite (Taguta et al., 2017). The heat of adsorption values also indicated stronger mineral-collector interactions as the carbon chain length increased, which resulted in increased hydrophobicity. The pKa values of the xanthate collectors slightly increased with the increase in the hydrocarbon chain length; indicating that changing the hydrocarbon chain length altered the pKa to a lesser extent than changing the linking atoms (Taguta et al., 2017).

1.6. ADSORPTION MECHANISM OF THIOL COLLECTORS ON SULPHIDE MINERALS

Thiol collectors can be adsorbed on the mineral surfaces by either chemisorption or physical adsorption or both. In chemisorption, there is an exchange of electrons involved between the collector and the acceptor on the mineral surface, resulting in the formation of chemical bonds. Chemisorption is limited to one monolayer surface coverage; however, collector molecules can still diffuse through the layer and further electron exchange takes place, resulting in the formation of reaction products that get co-adsorbed on the initial layer by physical adsorption (Rao, 2004). Localized chemisorption can take place on active sites of heterogeneous mineral surfaces such as emerging dislocations, lattice defects, and kinks. The adsorption on such surfaces is usually associated with high energy which can break bonds and distort the crystal structure. Dissolution also takes place due to multiple dipole-dipole interactions of water molecules that have the ability to break stronger individual ionic bonds in solids (Rao, 2004). This is enabled by the increase in the number of bonds per unit area of solids.

In the case of sulphide minerals, they are rendered floatable after adding the thiol collectors due to the formation of dithiolates or metal thiolates. For example, the adsorption of xanthate is believed to be an electrochemical process, where a charge transfer takes place to form dixanthogen or the metal thiolate. The process or proposed mechanism is represented by the anodic reactions in equations (1-3) (Ralston, 1991; Miller et al., 2002):

Equation (1) is the adsorption of xanthate as it donates an electron to the metal acceptor

$$X \rightarrow X_{ads} + e- \quad (1)$$

Formation of dixanthogen results from the oxidation of xanthate in equation (2)

$$2X^{-} \leftrightarrow X_2 + 2e- \quad (2)$$

Formation of a metal thiolate as the metal sulphide reacts with the xanthate ions in equation (3)

$$MS + 2X^{-} \rightarrow MX_2 + S + 2e- \quad (3)$$

The above anodic oxidation reactions are coupled with the cathodic reduction of oxygen given in equation (4) (Miller et al., 2002; Guo et al., 2014).

$½O_2 + H_2O + 2e- \rightarrow 2OH^-$ (4)

1.7. SUMMARY AND GAP ANALYSIS

The individual PGM minerals have different crystal structures, physical, and chemical properties. All the minerals had different natural floatation responses, and fairly high collector induced flotation floatabilities. Plant studies revealed that the fully liberated PGM sulphides were fast floating as opposed to the arsenides which were recovered down the flotation bank. Also, the telluride PGE minerals had higher rate constants and flotation recoveries as opposed to the PGE arsenides. These studies that made use of natural PGM ores showed that poor mineral liberation and mineral associations were the major reasons for the poor recoveries of the PGM mineral. However, fully liberated sperrylite particles were still found in the PGM plants tailing streams, giving an indication that liberation was not the cause of the mineral's poor recoveries. Another study by Shackleton on the synthetic PGE minerals showed that sperrylite had poor flotation recoveries as opposed to the rest of the minerals. The natural floatability of these minerals also ranged from very poor ($PtAs_2$) to very good (PtS). It is worth noting, that the microflotation tests carried out by Shackleton et al. (2007), used synthetic minerals, which were considered to be fully liberated, in the floatable size range and with no competing activator ions present and yet the recovery of $PtAs_2$ was still poor.

Surface analysis results, that revealed the absence of dixanthogen on sperrylite, pointed to poor collector adsorption as one of the major reasons for the poor floatability of sperrylite. Also, a study by Waterson revealed that the platinum atoms on sperrylite are not readily accessible to the approaching sulphur ligands in thiol collectors. Moreover, it cited that the high concentration of the OH^- ions could be the cause for poor collector adsorption as the molecular modelling results showed that the binding energy of the OH^- ions was higher than that of ethyl xanthate.

The flotation process of the PGM minerals is carried out at pH 9, and there is still a need to establish whether preferential adsorption of OH^- could be the major reason for the poor flotation response of $PtAs_2$. A study by Vermaak et al. (2007) showed that dixanthogen formed rapidly on the sperrylite surface when it was anodically polarized at 300 mV and revealed that the mineral contact angles increased with an increase in Eh.

Unlike sperrylite, Pd-Bi-Te when anodically polarized at 200 mV had a contact angle of 60º and molecular xanthate was found on the mineral surface which resulted in high flotation recoveries of the mineral. The above also agrees with literature findings that surface oxidation can have opposing effects on collector adsorption, depending on the degree of oxidation. The natural pulp potential of the PGM ores ranges from 100 mV to 200 mV and no tests have been carried out at high Eh so far.

Molecular modelling computations revealed that the binding energy of the PNBX collector on pyrite, which was used as a cheap proxy for sperrylite, was higher than that with sperrylite (Nemutudi et al., 2020). The sulphur ligands on the collector could only bridge with the two Fe atoms in pyrite. On the other hand, the ligands were found to have the ability to bridge with either two Pt atoms or two As atoms or with Pt and As on sperrylite. This also agrees with literature that suggested that As has the ability to back-bond with sulphur and hence it can also act as an electron acceptor on the sperrylite mineral surface.

The literature review summary shows that very few studies have been carried out on the floatability of sperrylite and the reasons for its poor floatability are still not clear. Therefore, this study seeks to establish the reasons for the poor floatability of sperrylite with the aim of improving its recovery. The floatability and interactions of sperrylite with different collectors will be compared to that of pyrite, arsenopyrite and cooperite due to similarities in their crystal structures and/or bonding ligands (S, As).

1.8. DESIGN OF NOVEL COLLECTORS

From the knowledge gained from reviewed literature that adding electron-donating linking atoms (S, N) would result in the increased binding energy of the collector ligand to the mineral surface; novel collectors were proposed that could possibly improve the floatability of sperrylite. The first three collector structures are given in Figure 1.15. These sought to increase the binding energy of the sulphur and nitrogen ligands by substituting the oxygen linking atom on the xanthate collector with S and N.

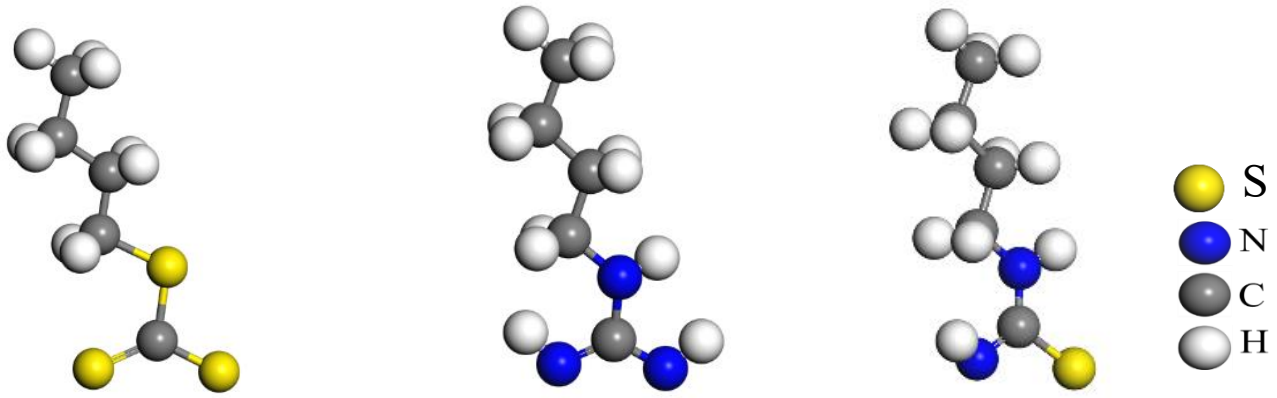

Figure 1.15 Suggested collector structures, based on hypothesis 3, where electron donating linking atoms (S and N) would increase the binding energy of the S and N bonding ligands

The next three sets of collectors (Figure 1.16) sought to increase the interatomic distance between the bonding atoms in order to reduce steric hindrances posed by the sperrylite surface to the approaching S and N ligands. Straight chain collectors were preferred as opposed to ring collectors to reduce the steric hindrances, however, most of the suggested collector structures had a tendency to form rings and as a result, mostly ring collectors that had nitrogen linking atoms were synthesized.

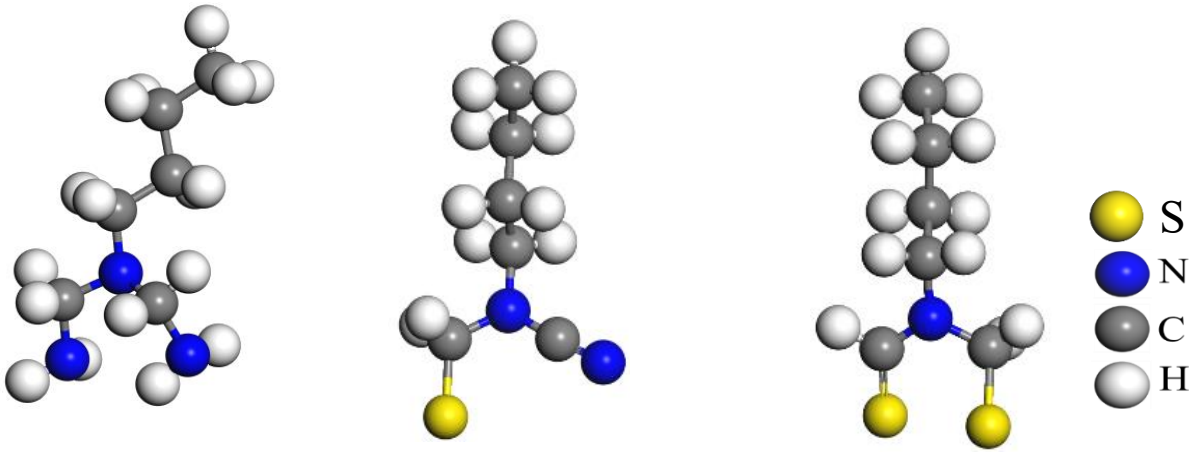

Figure 1.16 Suggested collector structures, based on hypothesis 2, that increasing the inter atomic distance between the S and N bonding ligand would reduce the steric hindrances posed by the sperrylite surface to the approaching ligands.

The suggested collectors were then screened and modified during the molecular modelling computations in collaboration with colleagues at the University of Limpopo. The collectors that gave the higher binding energies with the sperrylite surface and were considered fairly easy to synthesize were identified. These collectors were then synthesized by BGRIMM Technology Group in Beijing, China. Suggestions for the improvement on the existing collectors were made to increase the binding energy with sperrylite and the collector ligands which should ultimately result in improved recoveries. The factors that were taken into consideration are discussed in detail in the hypothesis for the selection and design of collectors.

- Replacing the oxygen linking atoms with nitrogen atoms that are electron-donating would lead to increased binding energy on the collector bonding ligands (Figure 1.17).

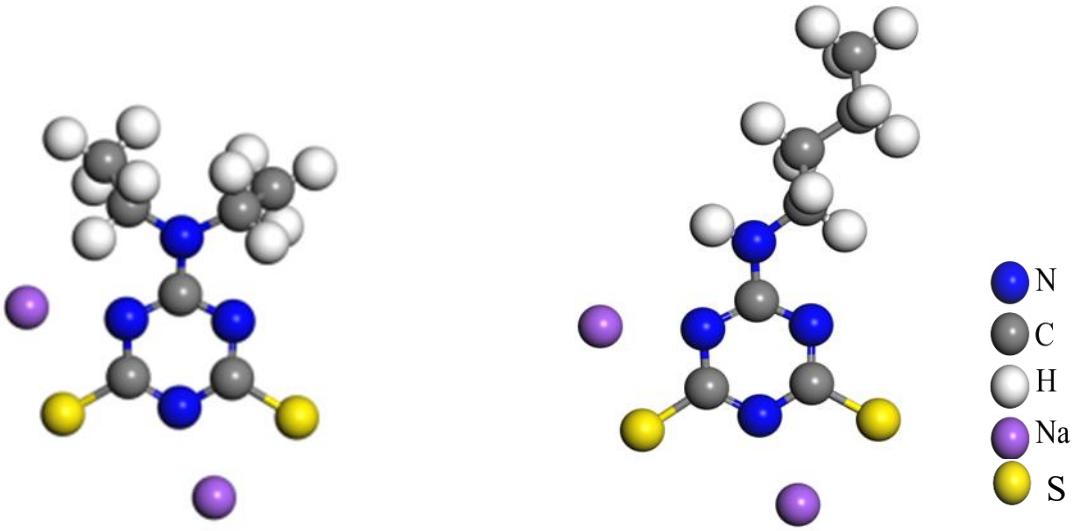

SDTDBAT SDTBAT

Figure 1.17 Modified structures of suggested novel collectors, based on hypothesis 3, aiming at increasing the binding energy of the bonding ligands

- The increase in the interatomic distance between the bonding ligands was suggested in order to reduce the steric hindrances between the bonding atoms and the mineral acceptors (Figure 1.18).

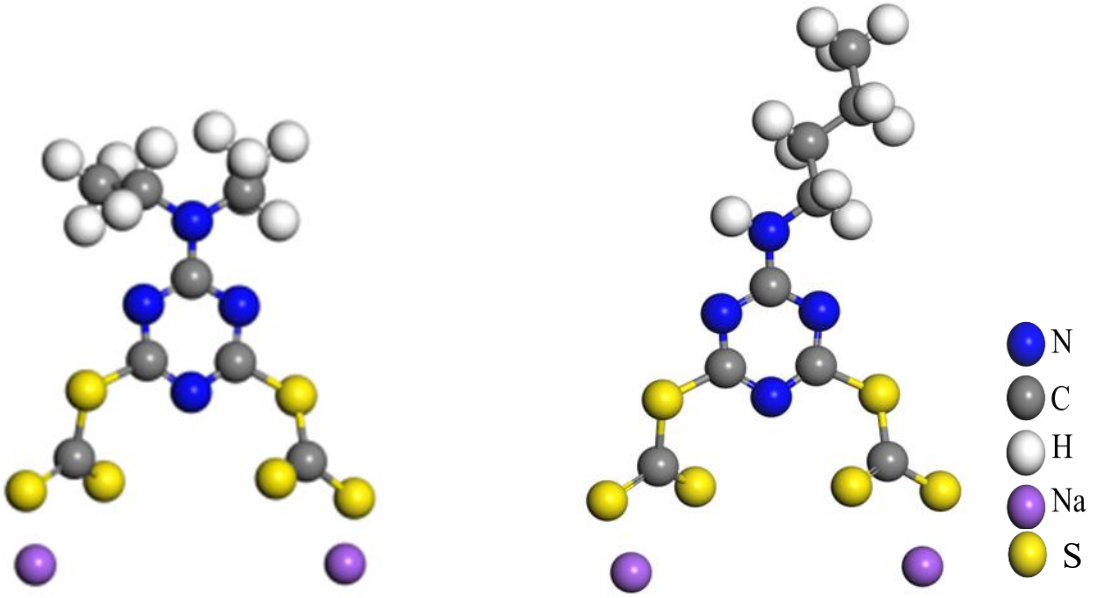

SDCDTDBAT SDCDTBAT

Figure 1.18 Modified structures of suggested novel collectors, based on hypothesis 2, aiming at reducing the steric hindrances posed by the sperrylite surface to the approaching ligands.

The names and acryonyms given to the synthesized collectors are 2,6-dithio-4-di-butylamino-1,3,4-triazine (SDTDBAT), 2,6-dithio-4-butylamino-1,3,4-triazine (SDTBAT), 2,6-dicarbonodithioate-4-di-butylamino-1,3,5-triazine (SDCDTDBAT), and 2,6-dicarbonodithioate-4-butylamino-1,3,5-triazine (SDCDTBAT) and their structures are given in Figure 1.17 and Figure 1.18.

1.9. HYPOTHESES

The following hypotheses will be investigated in this study.

1. Based on the structure of a typical collector shown in Figure 1.14, it is hypothesized that S and N bonding atoms in S and N-based collectors will bond strongly with:

    i. Pt^{4+} in sperrylite, which is a soft acid.

    ii. As^{2-} on sperrylite mineral surface, which is a soft base and has the ability to back-bond with the other soft bases.

2. A ligand with a longer inter-atomic distance between the two chelating atoms compared to that of typical thiol collectors will have a better crystal structure compatibility with $PtAs_2$ because the Pt atoms are not well exposed, and the lone pair of electrons projected by arsenic atoms make it difficult for the bridging sulfur ligands to interact with two Pt atoms in different clefts simultaneously.

3. In selecting candidate collectors, linking atoms (Figure 1.14) that are less electronegative, or electron donating should be selected since this will increase the electron density around coordinating atoms and that, consequently, stronger bonds will be formed between the mineral and collector.

4. The crystal structure and the donor atoms (As, S) on the minerals' surfaces will have a great influence on the floatability of the minerals because they also have an ability to act as electron acceptors.

2. RESEARCH OBJECTIVES

2.1. THESIS OBJECTIVES

This study seeks to understand the interactions of sperrylite with the selected thiol and novel collectors with the aim of improving its flotation recovery. Sperrylite has been found to be slow floating compared to the other PGM minerals and most of the fully liberated particles have been found in the tailings stream. It would be beneficial to improve the recovery of this precious mineral as it constitutes about 21% of the PGMs in the Platreef ore.

2.1.1. Research Objectives

This work will seek to determine the reasons for poor sperrylite floatability by addressing the following objectives:

- Compare the floatability of $PtAs_2$ to that of pyrite (FeS_2) using various collectors to establish if there is any relationship between mineral crystal structure and its floatability since these minerals have similar crystal structures.
- Determine the effect of (As, S) bonding atoms on the surfaces of $PtAs_2$, FeS_2, FeAsS and PtS and the effect of crystal structures on their floatability
- Apply the donor-acceptor model to suggest collectors that have a strong affinity for sperrylite for molecular modelling screening in collaboration with the University of Limpopo.
- Compare the molecular modelling computational values of individual collectors with the isothermal titration calorimetry results and highlight the limitations of each technique in the screening of potential collectors.
- Compare the rest potentials of the selected minerals under alkaline and acidic conditions and infer from those results the surface characteristics of each mineral under these conditions.

2.2. KEY QUESTIONS

- Why is the current reagent suite in the floatation of PGM minerals, which has xanthates as the main collector selective against sperrylite as opposed to the other PGM minerals?
- What is the effect of donor atoms (As, S) on the mineral surfaces and crystal structures on the floatability of the $PtAs_2$ and how do they relate to the floatability of FeS_2, FeAsS and PtS?
- What are the adsorption densities and binding energies of collectors with different linking atoms on $PtAs_2$ and the other selected minerals and how do they affect the flotation performance?

- How is the hydrophobicity of $PtAs_2$ and FeS_2 affected by the presence of varying concentrations of OH^- ions?
- What is the effect of pulp potential on the floatability of sperrylite?
- Which functional groups or ligand atoms will most likely improve the floatability of $PtAs_2$ by coordinating with the Pt^{4+} ion or As^{2-} anion or both?
- What is the effect of adding substituents such as S and N in designing the novel collectors, that increase the electron density around the coordinating atoms of collectors, to the floatability of sperrylite?

2.3. RESEARCH APPROACH

The reasons for the poor floatation response of sperrylite are still not clear and in order to understand the interactions of sperrylite with different collectors the following research approach was implemented:

2.3.1. Minerals Selection and Experimental Techniques

The following minerals were selected based on their crystal structures and donor atoms to clearly understand the floatation response of sperrylite.

1. **Sperrylite:** The main slow floating mineral in the study
2. **Pyrite:** Was selected as a cheap proxy for sperrylite because they have the same isometric crystal structure. Also, the influence of the S bonding atoms on the mineral surface will be studied as opposed to As atoms in sperrylite.
3. **Arsenopyrite:** The mineral was selected to investigate the presence of the As atom and the monoclinic crystal structure. The response will be compared to that of pyrite. This will further shed light on the effect of the As donor atom and also the influence of crystal structure in sperrylite.
4. **Cooperite:** The mineral was selected as a standard PGM mineral that is known to have good floatability. The influence of the tetragonal crystal structure and the influence of one S donor atom as opposed to two S donor atoms in pyrite.

The following experimental techniques were selected to understand the interactions of the minerals with different collectors and how these shed light on the reasons for the floatability of sperrylite.

1. **Microflotation Tests:** To measure the hydrophobicity of the minerals before and after adding the collectors at different pulp conditions.

2. **Adsorption Test:** To determine the amount of collectors adsorbed on the mineral surface and how it relates to the floatability of the minerals.

3. **Rest Potential Measurements:** To determine the rest potentials of the minerals before and after adding the collectors. They will also give the extent of interaction of minerals and help predict the possible surface products that are likely to form on the mineral surface.

4. **Isothermal Titration Calorimetry:** The tests will be carried out to determine the heats of adsorption of the collectors onto the different minerals. They will further shed light on the minerals' interaction with collectors and how it relates to their floatability.

5. **Surface analysis tests:** XPS and TOF-SIMS tests will be carried out to determine the surface products on sperrylite and arsenopyrite after conditioning the minerals with synthetic plant water and with PNBX and SNBDTC collectors.

3. EXPERIMENTAL METHODS

3.1. INTRODUCTION

This study aimed at determining the reasons for the poor floatability of sperrylite with the aim of improving its flotation recoveries. The proposed hypotheses and the corresponding experimental work undertaken to investigate the hypotheses are shown in Table 3.1.

Table 3.1 Proposed hypotheses and the corresponding experimental methods

Research Objectives	**Key Questions**	**Hypothesis**	**Experimental Methods**
Apply the donor-acceptor model to suggest and identify collectors that have a strong affinity for sperrylite for molecular modelling screening in collaboration with the University of Limpopo.	Which functional groups or ligand atoms will most likely improve the floatability of $PtAs_2$ by coordinating with the Pt^{4+} ion or As^{2-} anion or both?	S and N bonding atoms in S and N-based collectors will bond strongly with: Pt^{4+} in sperrylite, which is a soft acid. As^{2-} on sperrylite mineral surface, which is a soft base and has the ability to back-bond with the other soft bases.	Molecular modelling computations were carried out on sperrylite and pyrite, in collaboration with the University of Limpopo, using selected standard collectors and collector molecules suggested by UCT.
Determine reasons for poor sperrylite floatability.	What is the effect of donor atoms (As, S) on the mineral surfaces and crystal structures on the floatability of the $PtAs_2$ and is it possible to infer the role of these atoms by investigating the behaviour of FeS_2, FeAsS and PtS?	A ligand with a greater inter-atomic distance between the two chelating atoms compared to that of standard thiol collectors will have a better crystal structure compatibility with $PtAs_2$ because the Pt atoms are not well exposed, and the lone pair of electrons projected by arsenic atoms make it difficult for the bridging sulfur ligands to interact with two Pt atoms in different clefts simultaneously (sperrylite and pyrite).	Microflotation tests on sperrylite and pyrite using the novel collectors: SDCDTDBAT and SDCDTBAT. ITC tests on sperrylite using the same novel collectors.

To compare the rest potentials of the selected minerals under alkaline and acidic conditions and to infer the surface characteristics of each mineral under these conditions.	How do the crystal structures and the donor atoms (As, S) on the minerals' surfaces influence their floatabilities?	The crystal structure and the donor atoms (As, S) on the minerals' surfaces have a great influence on the floatability of the minerals sperrylite, pyrite, cooperite and arsenopyrite.	Microflotation, rest potential and adsorption tests of the selected minerals under alkaline and acidic conditions. Rest potential tests and adsorption tests on the minerals with collectors under alkaline and acidic conditions. Isothermal titration calorimetry tests using the selected minerals with standard collectors.
To compare the floatability of the selected minerals under alkaline and acidic conditions and to determine the surface characteristics of each mineral under these conditions.	How is the hydrophobicity of $PtAs_2$ and FeS_2 affected by the presence of varying concentrations of OH^- ions?	The OH^- ions can act as a ligand and have the ability to form strong bonds with the sperrylite mineral under the PGM plant operating conditions thus resulting in reduced collector adsorption which ultimately results in low recoveries.	Microflotation, rest potential and adsorption tests of minerals under alkaline and acidic conditions with selected standard and novel collectors.
Determine reasons for poor sperrylite floatability and the other selected minerals.	What is the effect of donor atoms (As, S) on the mineral surfaces and crystal structures on the natural floatability of the $PtAs_2$ and how do they relate to the floatability of FeS_2, FeAsS and PtS?	The surface energy of minerals determines the natural hydrophobicity of minerals. The lower the surface energy the greater the natural hydrophobicity of the mineral.	Analysis of minerals surface energy data and the microflotation results of minerals in the absence of a collector

Tests were carried out to determine the interactions of sperrylite with different collectors under different pulp conditions. Three other minerals, viz.: pyrite, arsenopyrite and cooperite, as outlined in Section 2.3.1, were selected to further shed light on the behaviour of sperrylite with different collectors based on the similarity of their crystal structures and in the case of the latter two the bonding atoms As and S.

3.2. MINERAL SYNTHESIS AND CHARACTERISATION

Mineral synthesis was carried out in this study because the platinum group minerals are finely disseminated at extremely low concentrations in the PGM ores and hence it is essentially impossible to access sufficient quantities required to carry out microflotation tests. Sperrylite and cooperite were synthesized using the methods that were developed by Shackleton et al. (2007).

3.2.1. The Platinum-Arsenic System

The phase diagram of sperrylite is given in Figure 3.1. The reagents used in the synthesis are sponge platinum, which has a melting temperature of 1769ºC, and arsenic which sublimes at 614ºC under the pressure of 1 atmosphere (Okamoto, 1990). Due to the high vapour pressure of arsenic which makes up about 43.4 wt% of the mineral, sperrylite also sublimes at the temperature of 1475ºC. The phase diagram shows the eutectic point (indicated by a red arrow) which occurs at a temperature of 597ºC and Pt composition of 72 wt%.

At this point, a transformation of molten sperrylite takes place to form sperrylite and platinum as given by equation (6):

$$L_{\text{molten sperrylite}} \leftrightarrow PtAs_2 + Pt \qquad (6)$$

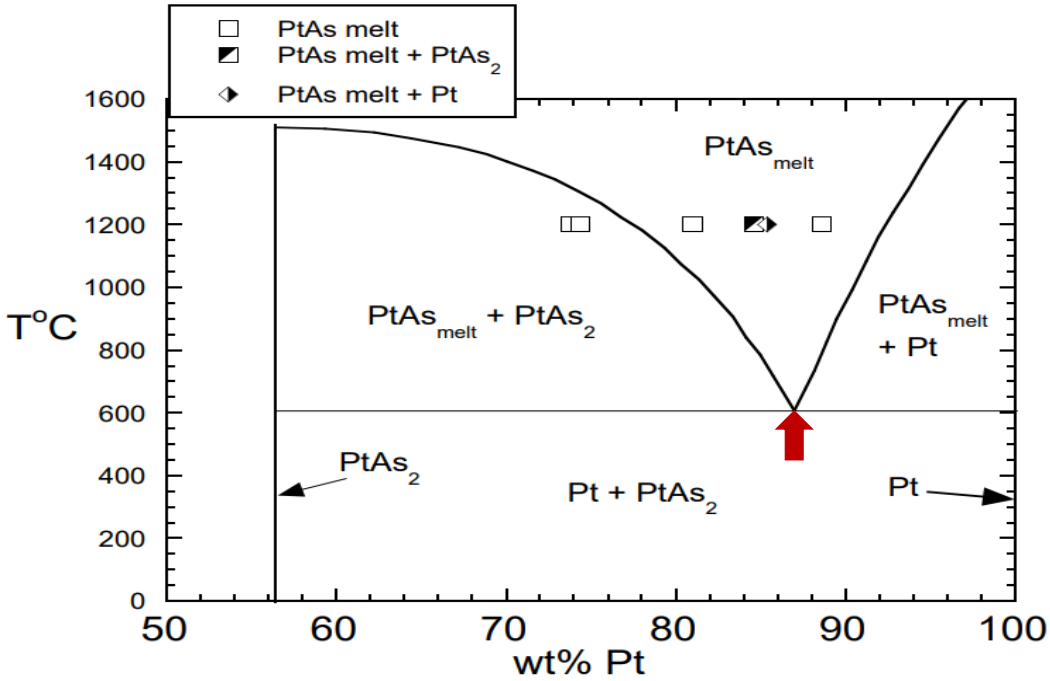

Figure 3.1 The Platinum-Arsenic (Pt-As) system (Canali et al., 2017; Okamoto, 1990)

Pure sperrylite is formed when the melt with the composition of 56.6% Pt and 43.4% As is cooled below the eutectic temperature. However, the process employed in this study is the low-temperature sintering that allows the mineral to form by diffusion of the arsenic vapour into the platinum particles. Metal particles also sinter when heated to temperatures that are greater than a third of their melting temperatures. Hence, it is also important to note that the platinum particles will also start to sinter once the temperature of 531ºC is exceeded. Hence the need to regrind and resinter the sample to ensure that the sample is free from unreacted platinum.

From the Pt-As system diagram, it can be seen that the liquidus temperature increases from the Pt eutectic composition of 72% to 56.6% Pt composition, which increases the solubility of arsenic.

Therefore, the most ideal operating temperatures should be in the range of 1000ºC to 1200ºC which allows the increased solubility of the arsenic into the mixture, even though complete fusion will still not be attained. However, the operating temperature is solely dependent on the type of material used for the ampoule. The quartz ampoules can withstand higher temperatures (~1200C) compared to the silica ampoules (~900ºC to 1000ºC). Quartz is also more expensive than silica and it is also fairly difficult to seal. Moreover, the content of volatile matter also plays a role in the operating temperature. For example, cooperite could be synthesized at 1000ºC using the silica ampoule because the S content was around 14.1%.

3.2.2. Mineral Synthesis Equipment

The synthesis equipment given in Figure 3.2 consists of a vertical tube furnace and a temperature controller that can enable a maximum temperature of 1200ºC. Care was taken to purge the furnace with an inert gas throughout the runs in case an ampoule should crack due to high pressure built up. The gas was then directed to a gas scrubbing unit containing NaOH and water.

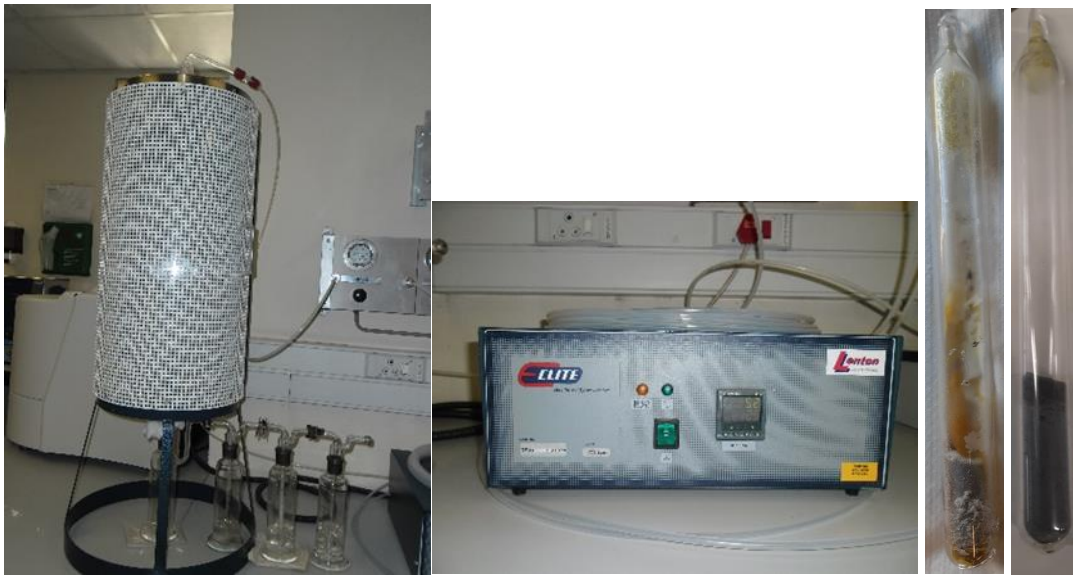

Figure 3.2 Vertical tube furnace and furnace controller. The sealed silica tubes contain synthesized sperrylite and cooperite minerals.

Due to the volatile nature of arsenic and the pressure build-up that takes place during the synthesis process, the maximum operating temperature was 800ºC. No other safer laboratory equipment that could allow complete fusion of the materials during the synthesis of these minerals was available.

3.2.3. Sperrylite Synthesis

The stoichiometric amounts of sponge Pt, purity of 99.95%, and As were weighed and placed into the silica ampoule. The tube was evacuated for 24 hours and the tube was then sealed by heating with an oxy-propane gas flame. The sealed tube was then placed into a vertical tube furnace and sintered according to the following program. The sample was:

- Heated to 800ºC at a rate of 2.5ºC/minute
- Held at 800ºC for 84 hours
- Slowly cooled to 400ºC at a rate of 0.5ºC/minute
- Held at 400ºC for 24 hours
- Cooled to room temperature at a rate of 0.4ºC/minute

The mineral samples were ground and sintered for the second time to avoid the presence of free platinum since the maximum sample weight of 60g was synthesized in each experiment. The minerals were cooled at a slightly lower rate compared to the recommended cooling rate to avoid the formation of yellow arsenic.

An attempt was made to synthesise platarsite (PtAsS), which was one of the minerals proposed in this study to investigate the effect of the S and As bonding atoms. 15.0394g cooperite (PtS) was used as the starting material to synthesize 20g of platarsite. The stoichiometric amount of As was added to the sample and the thermal treatment for that was applied to produce a cooperite sample was run twice. The XRD analysis of the mineral produced showed that $PtAs_2$, PtS and PtS_2 were formed instead of PtAsS. This indicated that the pressure in the ampoule was not sufficiently high enough to form the sulphur-arsenide mineral. The formation of sperrylite also indicated that arsenic has a high affinity for arsenic as opposed to sulphur.

3.2.4. Cooperite Synthesis

To make a 40g sample of cooperite, stoichiometric masses of Pt and S were weighed into the silica ampoule, evacuated under vacuum for 24 hours and then sealed using the oxy-propane gas flame. The sealed tube was then placed into the vertical tube furnace and sintered according to the following method. The sample was:

- Heated to 1000ºC at a rate of 5ºC/minute
- Held at 1000ºC for 96 hours
- Then cooled to room temperature at a rate of 5ºC/minute

The sample was taken out, reground, and sintered for the second time.

3.3. MINERAL CHARACTERISATION

The sintered cooperite and sperrylite samples were then characterised using both X-Ray Diffraction (XRD) and EDS analysis to confirm the phases present and their compositions. The natural minerals, pyrite and arsenopyrite were also characterized by XRD analysis to confirm the presence of the required crystal structures. The pyrite sample was supplied by Ward's Natural Science Establishment NY while the arsenopyrite sample was supplied by Pert Industrials (PTY) LTD, Johannesburg.

3.3.1. X-Ray Diffraction (XRD) Analysis

X-ray diffraction (XRD) analysis using Rietveld refinement was carried out by an external, accredited laboratory on both natural and synthetic minerals to identify and quantify the mineral phases present in the minerals. This also served to confirm the presence of the required crystal structures in the synthetic minerals and the success of the synthesis process. The XRD samples were prepared using a micronizer to reduce the particle sizes of the minerals while maintaining their crystal structures. A micronizer utilizes a particle-to-particle collision mechanism that takes place under air turbulence to produce a narrow distribution product.

3.3.2. Energy Dispersive Spectroscopy (EDS) Analysis

The energy dispersive spectroscopy (EDS) analysis was used to identify and quantify the elemental composition of the phases that were present in the synthetic mineral particles and the synthetic electrodes that were used in this study. The phases present in the mineral particles were shown by the back scattered electron (BSE) micrographs. The identification of phases helped to evaluate the success of the synthesis methods. The natural sperrylite electrode was also characterised by EDS analysis and a single-phase was also identified by the BSE micrographs

3.3.3. BET Analysis Test Results

The surface area of the minerals was determined using the Brunauer-Emmett-Teller (BET) method for the minerals -106+38µm and -38µm size fractions. The mineral surface areas (Table 3.2) were used to calculate the collector dosage for the 1 pseudo-monolayer coverage for the microflotation, adsorption and isothermal titration calorimetry tests.

Table 3.2 BET analysis results of the minerals for the -106+38µm and -38µm size fractions and the respective purity for each mineral determined by XRD analysis.

Mineral	Formula	Size Fraction (µm)	Density (g/cm^3)	BET Results (m^2/g)	Purity (%)
Synthetic Sperrylite	$PtAs_2$	-106+38	10.58	0.1495	87
		-38		0.4280	
Pyrite	FeS_2	-106+38	5.0	0.2329	89
		-38		0.5412	
Arsenopyrite	FeAsS	-106+38	6.07	0.0762	74.2
		-38		0.3401	
Synthetic Cooperite	PtS	-106+38	9.5	0.0961	97
		-38		0.2436	

The head of the thiol collector molecules was assumed to have a cross-sectional area of 28.8Aº (Grano et al., 1997). It was assumed that all the minerals' samples were pure minerals to simplify the calculations.

3.4. SAMPLE PREPARATION AND REAGENTS

The sample preparation of the minerals and the reagents used in this study have been outlined in the following sections. Several reagents were used during the selected tests: collectors, frothers, regulators and buffers.

3.4.1. Sample Preparation

The dry synthetic minerals were ground using the agate mortar and pestle and screened into -106+38µm and -38µm size fractions. Dry synthetic sperrylite and arsenopyrite were fairly harder and they were hand pulverised in a ring pulveriser using a puck before screening to avoid overgrinding the minerals as much as possible. The dry pyrite mineral chunks were hammered and then pulverised for 10 seconds and then screened into -106+38µm and -38µm size fractions. All the materials were split using a rotary splitter and stored under nitrogen in a freezer to minimize the oxidation of the samples. In addition, dry grinding minimized the oxidation of all the minerals and all the samples were sonicated for 5 minutes before running the flotation tests in order to clean the mineral surfaces.

3.4.2. Collectors

The collectors that were selected for this study are listed in Table 3.3. The selection criteria for the standard collectors were based on the fact that they are widely used in the flotation of PGMs in industry and the butyl chain length (normal or iso-) was used as the standard. Studies have revealed that longer chain lengths in collectors resulted in higher flotation recoveries (Taguta et al., 2015). A SIBX collector which is currently used in most PGM plants was tested to investigate the effect of the branched butyl chain and also to act as a standard in the flotation of sperrylite and cooperite.

The novel collectors were tested on sperrylite and pyrite in order to test hypotheses 2 and 3 stated in Section 1.9. The novel collectors were screened by molecular modelling computations in collaboration with the University of Limpopo and the collectors that gave the higher binding energies with the sperrylite surface were then synthesized by BGRIMM Technology in China.

Table 3.3 Collectors and collector abbreviations used throughout this study

Collector Group	Collector Name	Collector Abbreviations	Molecular Mass (g)	Purity (%)
Standard Collectors	Potassium Normal Butyl Xanthate	PNBX	188.36	96.8
	Sodium Isobutyl Xanthate	SIBX	172.198	100
	Sodium Normal Butyl Dithiocarbamate	SNBDTC	171.14	35.7
	Sodium Normal Di-Butyl Dithiophosphate	SNDBDTP	265.25	48.4
Novel Collectors	2,6-dithio-4-di-butylamino-1,3,4-triazine	SDTDBAT	216.37	100
	2,6-dithio-4-butylamino-1,3,4-triazine	SDTBAT	216.37	100
	2,6-dicarbonodithioate-4-di-butylamino-1,3,5-triazine	SDCDTDBAT	368.67	100
	2,6-dicarbonodithioate-4-butylamino-1,3,5-triazine	SDCDTBAT	368.67	100
Other Tested Collectors	Sodium Normal Di-Ethyl Dithiophosphate	SNDEDTP	208.178	46.6
	Flotigam 7100		201.234	100

3.4.3. Frothers

The MIBC frother was used throughout this study and it was dosed at 20ppm, which is above the critical coalescence concentration (Cho & Laskowski, 2002). Also, the Dow 200 frother, dosed at 15ppm, was used to investigate the effect of different frothers in combination with SIBX and ethyl DTP collectors.

3.4.4. Synthetic Plant Water

Synthetic plant water was used in this study to mimic the ions that are generally found in the PGM flotation plants and how they affect the recoveries. The composition of the synthetic plant water with ionic strength of 4.84E-2 M is given in Table 3.4.

This ionic strength, which is twice the ionic strength of the standard plant water (labelled as 2 SPW which indicates an ionic strength of twice that of the standard Synthetic Plant Water) was selected in this study because the ionic strength of the process water of many flotation plants is usually greater than 2.42E-2 M.

Table 3.4 Synthetic plant water (2SPW) composition with the ionic strength of 2.42E-2 M

Chemical	Chemical Formula	Molecular Mass (g/mol)	Purity (%)	2SPW Mass (g/L)	Solubility at 20°C (g/L)
Magnesium Sulphate	$MgSO_4.7H_2O$	246.48	99	1.23	246.48
Magnesium Nitrate	$Mg(NO_3)_2.6H_2O$	256.41	99	0.214	420
Calcium Nitrate	$Ca(NO_3)_2.4H_2O$	236.15	99	0.472	1.293
Calcium Chloride	$CaCl_2.2H_2O$	147.01	99.99	0.294	147
Sodium Chloride	NaCl	58.44	99.5	0.712	358
Sodium Carbonate	Na_2CO_3	105.99	99.5	0.06	217

3.4.5. pH and Eh Modifiers

Hydrochloric acid (HCl) and sodium hydroxide (NaOH) were used as pH modifiers throughout the tests to adjust the pulp pH to the required pH. 10% sodium hypochlorite (NaClO) was mainly used as a pulp Eh modifier at pH 9. However, sodium hypochlorite is also a strong oxidizing agent that was found to depress the readily floating arsenopyrite (Lopez Valdivieso et al., 2006) and might also affect the flotation behaviour of sperrylite.

3.4.6. Buffer Solution Reagents

Buffer solutions used during the rest potential tests and the collector oxidation tests gave the pHs of 9.5 and pH 3.5. The buffer solution of pH 9.5 was made up of 0.05M sodium tetraborate ($Na_2B_4O_4$) in a solution of 0.1M sodium sulphate ($NaSO_4$) which was added as an electrolyte. Potassium hydrogen tartrate ($KHC_4H_4O_6$), with a purity of 97.5%, was used to make the pH 3.5 buffer solution. All the buffer solutions used for the rest potential tests were made using deionized water.

3.5. MICROFLOTATION TESTS

Microflotation tests were carried out as a measure of hydrophobicity for sperrylite at pH 9 and pH 4. Further tests were carried out with pyrite, arsenopyrite and cooperite in order to compare their floatabilities with sperrylite based on their crystal structures and bonding atoms (S, As), as explained previously in Section 2.3.1.

The flotation tests of minerals were also carried out without adding a collector to determine the natural hydrophobicity of the minerals and to compare the recoveries with the effect of adding different collectors on the flotation recoveries of the minerals. The natural hydrophobicity of sperrylite and pyrite was determined at pH 9 and pH 4 to determine the effect of pH on the natural hydrophobicity of the minerals. It has been hypothesized that the hydroxide particles can also act as a ligand on the mineral surfaces resulting in poor collector adsorption and reduced mineral flotation recoveries.

3.5.1. Microflotation Cell and Equipment

A schematic of the UCT microflotation system is given in Figure 3.3. It consists of a microflotation cell, peristaltic pump, and the pump used to supply air at a steady airflow rate.

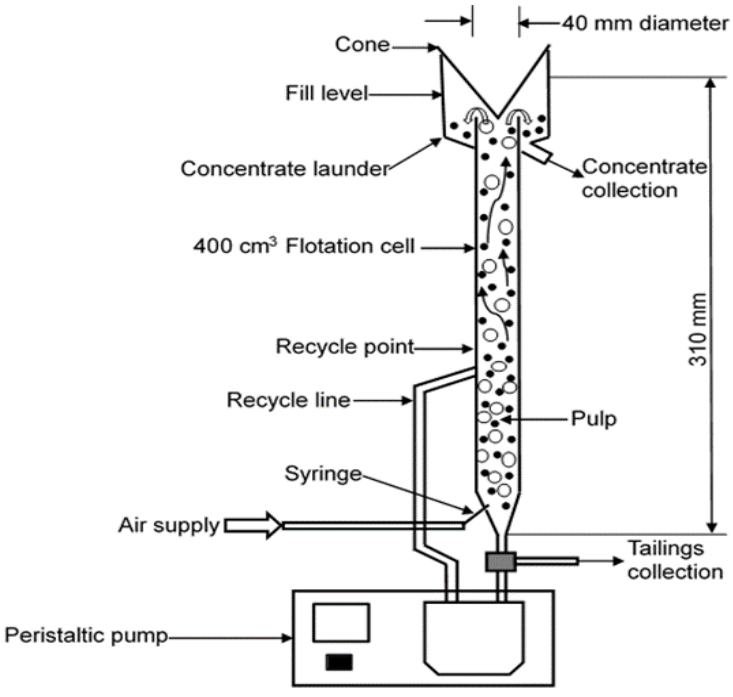

Figure 3.3 Schematic diagram of the microflotation cell

The mineral particles that form the slurry are kept in suspension by recirculating the slurry utilizing the peristaltic pump that is run at a constant speed. A constant airflow is also introduced using a selected micro-litre syringe through the air supply inlet as indicated in the diagram.

When air is introduced, the rising air bubbles get attached to hydrophobic particles which get carried upwards and are collected in the concentrate launder when the loaded bubbles hit the cone, releasing the attached particles. The concentrate and the mineral tailings are collected, filtered, dried and analysed to compute the recoveries for each run.

3.5.2. Microflotation Procedure

The UCT microflotation rig (Figure 3.4) was used to determine the hydrophobicity of the selected minerals. A 2g mineral sample of size fraction of -106+38µm particles was used to carry out each microflotation test. This size fraction was chosen as the objective was to measure changes induced by different collectors on recovery by true flotation. There was an attempt to exclude recovery by entrainment since particles above 38 µm are not expected to be recovered by entrainment in the microflotation cell. The upper limit was chosen as 106 µm since this is where detachment of the bubble-particle aggregate becomes a problem.

Figure 3.4 UCT microflotation rig with the pump used to supply a steady airflow at a rate of 8 ml/minute

Another pump was also used to supply air at a constant airflow rate of 8 ml/minute. A 2g mineral sample was placed in a beaker with 50 ml of plant water or distilled water and sonicated for 5 minutes to fully disperse all the particles in the sample. The calculated collector dosage, based on the BET analysis results, was added and the slurry was then conditioned for 10 minutes while stirring at a constant rate using a magnetic stirrer. The pH was constantly adjusted to the required pH during the conditioning period as the pH drop was noted with all the minerals. The mineral slurry with the adjusted pH of 9 or pH 4 was poured into the 410 cm^3 microflotation cell and a peristaltic pump was used the circulate the slurry and to keep the particles in suspension at a pump speed of 65 rpm.

Top-up water, adjusted to the required pH was then added to the mark. Airflow was introduced using a micro syringe and the concentrates were collected at timed intervals of 2, 6, 12 and 20-minute intervals.

Few tests with prolonged runs were also carried out where concentrates were collected at 2, 6, 12, 20, and 30 minutes intervals. The concentrates were dried at 40^0C because some of our minerals contained arsenic. The mineral recoveries were calculated from the dried masses of the collected concentrates and tailings. All the tests with pyrite and arsenopyrite were carried out in duplicate and the average values were reported.

Bubble size also plays a very important role in the flotation of minerals and care was taken to make sure it remains constant during the study. The same micro syringe was used throughout the tests and the same pump was used at the same speed to maintain the same bubble size and distribution. The flow of bubbles was checked to ensure that there were no blockages before each run.

3.5.2.1. Flotation of Sperrylite at Elevated Eh

The same method outlined in Section 3.5.2 was used during the experiment. In addition, the Eh of the pulp was also measured by a multimeter and adjusted by the dropwise addition of 1% sodium hypochlorite (NaClO). The top-up water used during the test was also adjusted to the Eh of 660 mV and pH 9. There were no variations of pH during the Eh adjustments that occurred.

3.5.3. Reproducibility of Microflotation Test Results

Reproducibility tests were carried out using the UCT microflotation rig to test the reliability of the equipment and the reproducibility of the experimental method. Collectorless runs were carried out to determine the natural hydrophobicity of sperrylite and the results are given in Figure 3.5.

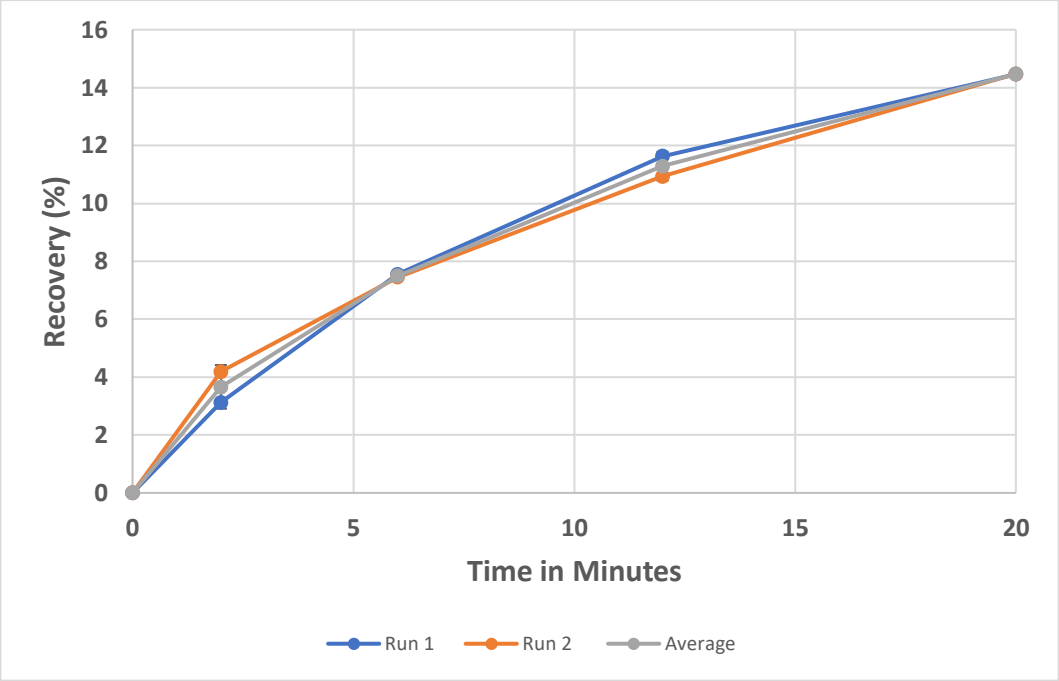

Figure 3.5 The reproducibility investigation of the UCT microflotation equipment using sperrylite collectorless tests runs at pH 9 in synthetic plant water, I = 4.84E-2 and 20 ppm MIBC frother.

Concentrates were collected after 2, 6, 12 and 20 minutes from the start of the test and the recoveries, standard deviations, standard errors and relative standard errors are given in Table 3.5. The results show that the UCT microflotation equipment and test procedures produced adequately reproducible results as indicated by the relative standard errors for the concentrates that were below 5% except for the first concentrate that had a relative standard error of 14.5%. The relative standard error of the first concentrate was higher since it is more difficult to obtain small relative standard errors when the recovered sample masses are so small.

Table 3.5 Collectorless recovery of sperrylite at pH 9 and the standard deviations, standard errors and relative standard errors

	Recovery (%)					
Time (Minutes)	**Run 1**	**Run 2**	**Average Recovery (%)**	**Standard Deviation (%)**	**Standard Error (%)**	**Relative Standard Error (%)**
0	0	0	0	0	0	0
2	3.1	4.2	3.7	0.75	0.53	14.52
6	7.5	7.5	7.5	0.07	0.05	0.63
12	11.6	10.9	11.3	0.50	0.35	3.11
20	14.5	14.5	14.5	0.01	0.01	0.06

Similar tests were carried out in duplicate using pyrite and arsenopyrite and the results also showed that the relative standard errors were less than 5% for the 6, 12 and 20-minute concentrates and the highest relative standard error for the 1st concentrates was 21.1% as given in Table 3.6.

Table 3.6 SNBDTC recovery of arsenopyrite at pH 9 and the standard deviations and standard errors

Time (Minutes)	**Run 1 (%)**	**Run 2 (%)**	**Average Recovery (%)**	**Standard Deviation (%)**	**Standard Error (%)**	**Relative Standard Error (%)**
0	0.0	0.0	0.0	0.00	0.00	0.00
2	25.3	38.8	32.1	9.56	6.76	21.07
6	65.4	68.5	67.0	2.19	1.55	2.31
12	83.9	85.7	84.8	1.23	0.87	1.03
20	87.2	93.1	90.2	4.21	2.98	3.30

Tests using synthetic sperrylite and cooperite were only carried out in duplicate for one condition to determine the reproducibility of the results. The rest of the microflotation tests could not be carried out in duplicates due to limited amounts and the high cost of the samples.

3.6. REST POTENTIAL MEASUREMENTS

The rest potential measurements were carried out with synthetic and natural sperrylite to determine their rest potentials before adding the standard collectors and the extent of interaction of the collectors with the minerals. These tests served as an indicator of how the synthetic sperrylite correlated in its behaviour compared to the natural sperrylite and thus to evaluate the validity of the synthesis process. Furthermore, the rest potentials of pyrite, arsenopyrite and cooperite were determined and compared to those of sperrylite. Their extent of interaction with the standard collectors was also evaluated and compared to those of sperrylite.

3.6.1. Rest Potential Measurements Procedures

The working electrode preparation is the critical stage prior to running the rest potential tests to ensure that accurate and reproducible potentials are measured. The details for the manufacture of electrodes are given by Tadie (2015). Wet grinding of the working electrode was carried out using 1200 grit silica carbide paper. A stagewise polishing using a cloth disk with aluminium powders, supplied by IMP Scientific and Precision (Pty) Ltd, of 1µm, 0.3 µm and 0.05µm sizes was carried out to give a smooth shiny surface. The polished electrode was washed with deionised water and then dried.

The rest/open circuit potentials of the minerals were measured using a Gamry Instruments Reference 600^{TM} Potentiostat/Galvanostat/Zero Resistance Ammeter (G) (Figure 3.6).

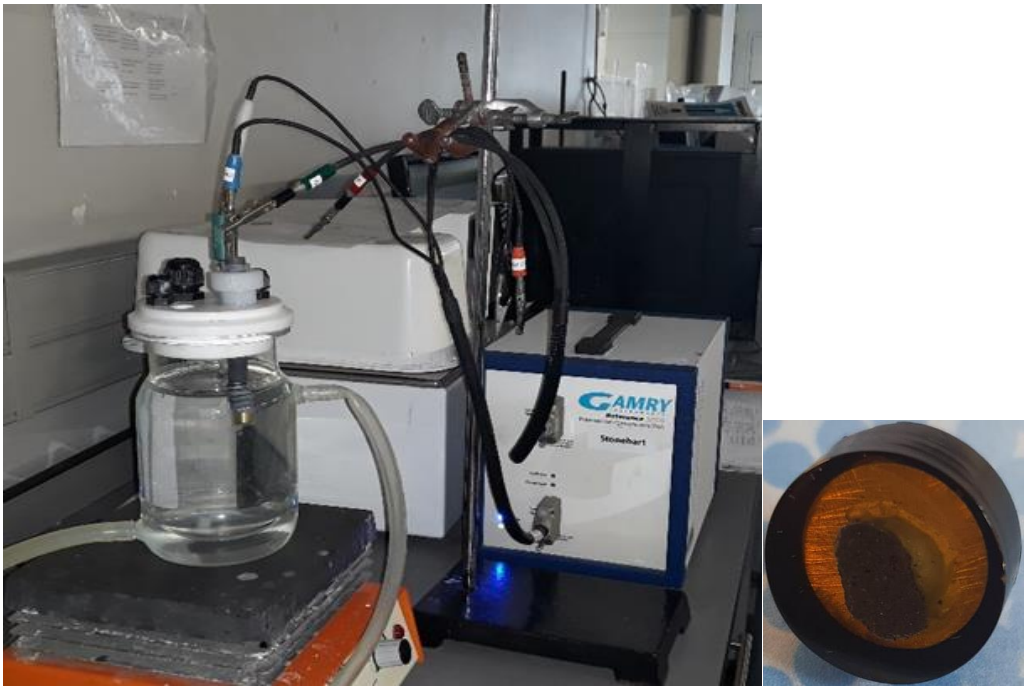

Figure 3.6 Electrochemistry equipment used for the rest potential measurements and a cooperite electrode

A detailed explanation for the electrochemistry equipment set-up used for the rest potential measurements is given by Tadie (2015) and Dzinza (2018).

The silver/silver chloride (Ag/AgCl) reference electrode and the working electrode, where a prepared mineral block is mounted were immersed into 450 ml of the buffer solution contained in a reaction vessel. The solution was stirred continually during the runs using a magnetic stirrer bar. Also, the temperature of the buffer solution was maintained at 25 ± 1ºC by continuously circulating water from a water bath around the outer jacket of the reaction vessel. The respective cables were connected to the electrodes and the Module PHE^{TM} 200 was run under open circuit for 600 seconds before adding the collector and another 600 seconds after adding the collector. The potential reading at 600 seconds is the rest potential of the minerals, while the reading at 1200 seconds is the final rest potential of the mineral that results from the interaction of the mineral with the collector. The collector dosage of 6.24 x 10^{-4} M was maintained throughout all the runs.

The oxidation potentials of the standard collectors were determined at pH 9.5 and pH 3.5 using the three-electrode system, where the Ag/AgCl electrode was used as the reference electrode while the two other platinum electrodes were used as a counter electrode and working electrode respectively. The collector at a dosage of 6.24 x 10^{-4} M was added to the 450 ml buffer solution, in the reaction vessel. The respective cables were connected to the electrodes and the Module PHE^{TM} 200 was run under open circuit for 1200 seconds and the final potential reading at 1200 seconds was recorded as the oxidation potential of the collector.

3.6.2. Reproducibility of Rest Potential Test Results

The rest potential tests were carried out in duplicate and the average values were plotted for each run that is reported in the results section. Figure 3.7 shows the rest potential profiles of pyrite before and after adding the PNBX collector. The results show that the difference between the two potential readings for run 1 and run 2 for the pyrite and PNBX was less than 10 mV. Also, the difference between the reported average potentials of each mineral, at zero seconds, ranged from 10 mV to 40 mV indicating that the potentials of the mineral surfaces were fairly consistent for each run. The highest starting potential deviation of 40 mV was recorded during the run with the synthetic sperrylite with the SNBDTC collector. Moreover, the difference between the average rest potential measurements of the minerals before adding the collectors was much smaller and ranged from 10 mV to 25 mV. The difference between the measured potentials for all repeats was always less than 50 mV, showing that the results were adequately reproducible.

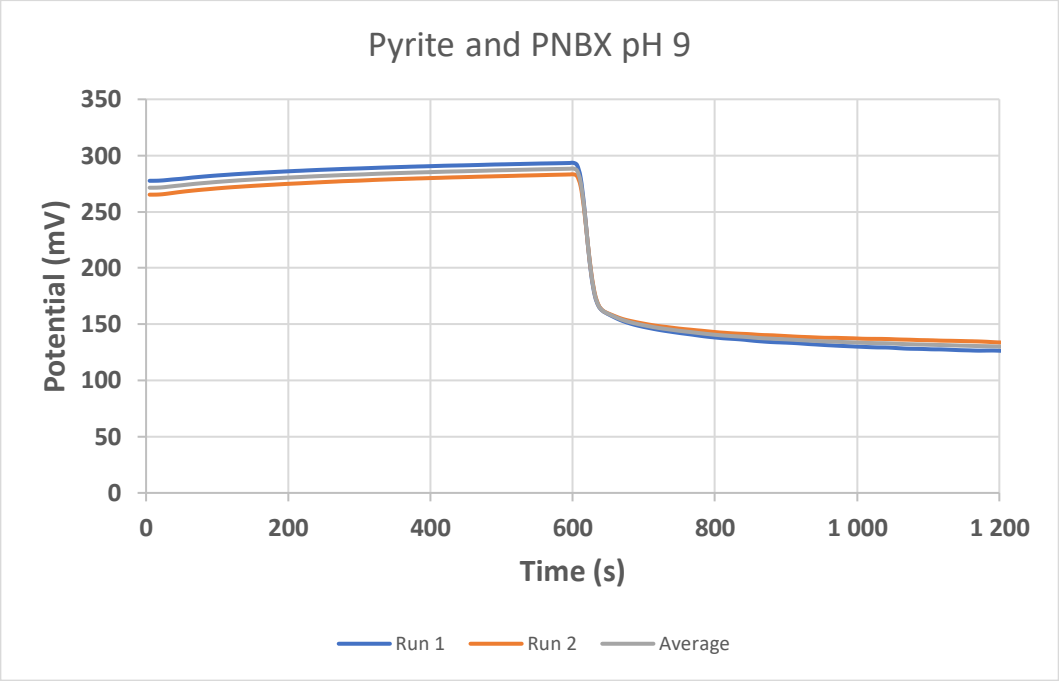

Figure 3.7 The reproducibility of the rest potential test results using pyrite electrode before and after adding the PNBX collector, at 600 seconds, at pH 9.5.

3.6.3. Reproducibility of Minerals Rest Potentials

The standard deviations of the minerals' rest potentials were also calculated from the average rest potentials determined for each collector run and it was indicated that the rest potentials were quite reproducible (Table 3.7). The standard deviations ranged from ±1.07 mV to ±26.67 mV. The highest deviation realised was for arsenopyrite at pH 9.5.

Table 3.7 Average rest potentials for the standard collectors for the minerals and their standard deviations, standard errors and relative standard errors.

	Average Rest Potentials (mV)						
	PNBX	**DTP**	**DTC**	**Average Rest Potential (mV)**	**Standard Deviation (mV)**	**Standard Error (mV)**	**Relative Standard Error (%)**
Sperrylite pH 9.5	241.5	232.2	227.3	233.7	7.21	4.16	1.78
Sperrylite pH 3.5	250.5	249.7	231.6	243.9	10.69	6.17	2.53
Pyrite pH 9.5	288.4	281.2	283.0	284.2	3.75	2.16	0.76
Pyrite pH 3.5	412.5	411.8	410.4	411.6	1.07	0.62	0.15
Arsenopyrite pH 9.5	226.6	179.2	181.7	195.8	26.67	15.40	7.86
Cooperite pH 9.5	264.2	259.9	244.5	256.2	10.36	5.98	2.33
Cooperite pH 3.5	512.8	529	512.3	518.0	9.50	5.49	1.06
Synthetic Sperrylite pH 9.5	207.8	201.4	204.8	204.7	3.20	1.85	0.90
Synthetic Sperrylite pH 3.5	261.6		263.5	262.6	1.34	0.95	0.36

3.7. ADSORPTION TESTS

Adsorption tests were carried out to determine the adsorption density of standard and the novel collectors on sperrylite. The results were compared to those obtained in the case of pyrite, arsenopyrite and cooperite, to determine the possible influence of the minerals' crystal structures and bonding atoms on adsorption behaviour.

3.7.1. Adsorption Test Procedure

The difference between the absorbance spectra of the collectors in 50 ml of distilled water before and after adding the mineral was used to calculate the amount of collector adsorbed on the mineral surface. A collector, with a dosage equivalent to that required to achieve 1 pseudo-monolayer coverage was added into a 100 ml beaker and stirred for five minutes with a magnetic stirrer bar to ensure that the solution is well mixed. The absorbance spectrum was recorded for each collector. Then 1g of the mineral of -38µm size fraction was then added into the solution and conditioned for 10 minutes while stirring with the magnetic stirrer bar. The pH of the pulp was adjusted to either pH 9 or pH 4 as required throughout the conditioning period. The pulp was subsequently filtered using the syringe filters of pore size 0.45µm and the absorbance reading was taken.

In a separate experiment, 1g of the mineral was placed in a beaker with 50 ml of deionised water, conditioned for 10 minutes and then filtered to obtain a profile for the blank mineral. The blank profile was used as a reference to determine whether the collectors were fully adsorbed or not. At pH 4, the spectra for the SNBDTC, SDTBAT, and SDCDTDBAT were different from the spectra at pH 9. Also, it was noted that the whole spectrum appeared to have changed after contact with the sperrylite. This method is only useful when the spectrum remains completely unchanged and is just reduced after contact with the mineral. Deionized water was used for all the adsorption tests because the plant water ions products also introduced their effect on the minerals spectra making it difficult to interpret the data. Hence the adsorption data obtained does not take into account the effect of plant water ions that could also get adsorbed onto the mineral surface.

3.7.2. Reproducibility of Adsorption Test Results

Reproducibility tests were carried out to test the reproducibility of the readings that are obtained from the UV-Vis spectrophotometer. Two separate runs were carried out to determine the absorbance of the SDCDTDBAT collector, at equal concentrations, in the absence of a mineral. The absorbance spectra are given in Figure 3.8. The absorbance curves overlay one another and show that both the experimental technique and the absorption spectra are reproducible.

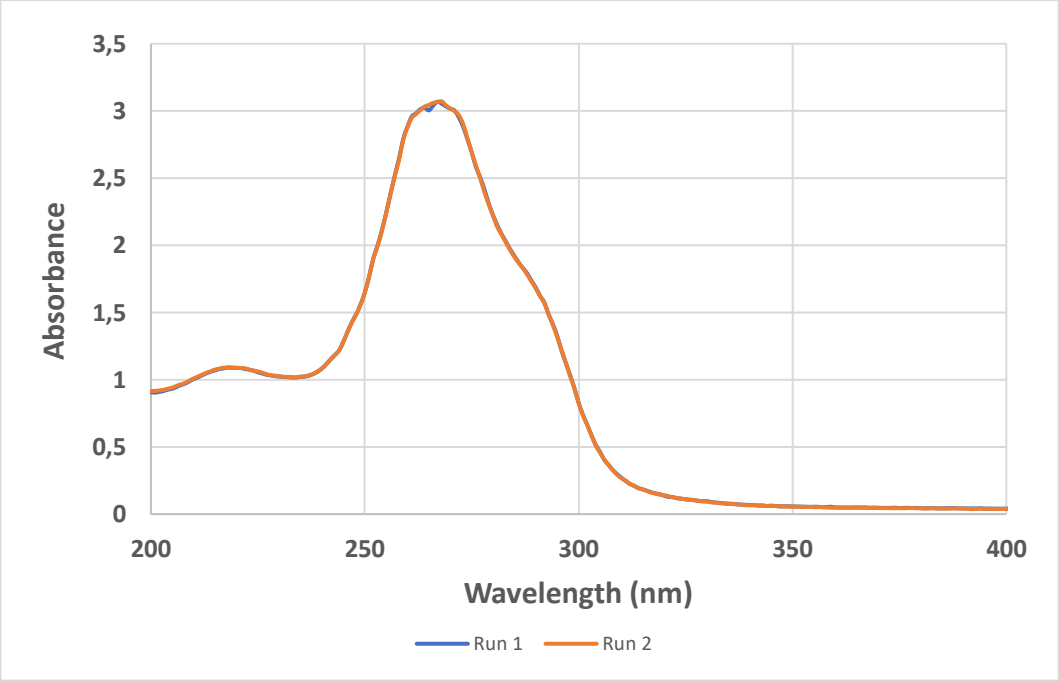

Figure 3.8 The reproducibility test results for the UV-Vis Spectrophotometer showing the absorbance of SDCDTDBAT collector at pH 9 before adding pyrite

3.8. ISOTHERMAL TITRATION CALORIMETRY

The isothermal titration calorimetry tests were carried out on sperrylite with the standard and the novel collectors. These tests sought to establish the link between the heats of adsorption obtained using the isothermal titration calorimetry tests and the molecular modelling computational values that were used to screen the novel collectors. Also, the isothermal titration heats of adsorption were compared to those of pyrite, arsenopyrite and cooperite.

3.8.1. Isothermal Titration Calorimetry Test Procedure

Isothermal titration calorimetry tests were carried out to measure the adsorption enthalpies at 25ºC using the TAM III isothermal titration microcalorimeter. Figure 3.9 shows the equipment used during the isothermal titration calorimetry tests. This technique measures the heat consumed or released during a reaction of the minerals with a given ligand. The change in enthalpy measured is given by the Gibbs energy value (equation 7):

$$\Delta G = \Delta H - TS \qquad (7)$$

Where:

ΔG = change in Gibbs Free Energy

ΔH = change in enthalpy

ΔS = change in enthropy

T = temperature in Kelvin

And when ΔS approaches zero then $\Delta G \approx \Delta H$

The mineral sample of mass 0.2 ± 0.0005g was weighed into a stainless steel ampoule and 0.7 ml of distilled water was added into each ampoule and sonicated for 3 minutes to disperse the slurry. It was not possible to control and adjust the pH of the slurry after loading the ampoules into the titration channel, hence all the tests were carried out at the natural pH of the slurry. When all the minerals tested were placed in water, a pH drop was noted and the change was found to be different for each mineral. The ampoules were loaded into the calorimeter and the titration syringe was loaded with the collector solution. Time was given for the machine to stabilize and full calibration of the machine against a known power input was carried out before each run. The machine was then programmed to run and to add 2 µL of the collector every hour once the selected conditions were met. The 2 µL collector solution was precalculated based on the BET results to cover approximately 0.25 pseudo-monolayers of the mineral surface. Ten titrations that amount to 2.5 pseudo-monolayers collector coverage were carried out for each run.

Figure 3.9 TAM III Isothermal Titration Microcalorimeter machine with the loaded shaft and the sample ampoule

The area under the peaks that result from the mineral-collector interactions was integrated to obtain the specific enthalpies of adsorption per injection. Heats of dilution per injection of a collector were also carried out for each collector and subtracted from the mineral-collector heats of adsorption. In this study, data from 4 titrations that amount to 1 pseudo-monolayer collector coverage heats of adsorption were calculated and reported.

The validation test was also carried out for the dilution of 10% propanol, where 2µl of 10% propanol was titrated into 0.7 ml distilled water, to ensure that the machine gave accurate readings. The ΔH_{dil} of 3.01 ± 0.03 mJ was obtained during the test, which is in the range of values reported by Wadso and Goldberg (2001), viz. ΔH_{dil} of 2.57 ± 0.03 mJ. A more detailed methodology and information on the isothermal titration calorimetry tests have been extensively described by Taguta (2015).

3.8.2. Reproducibility of Isothermal Titration Calorimetry Test Results

Reproducibility tests were carried out using PNBX and pyrite. Figure 3.10 shows the results obtained from 2 tests and their averages.

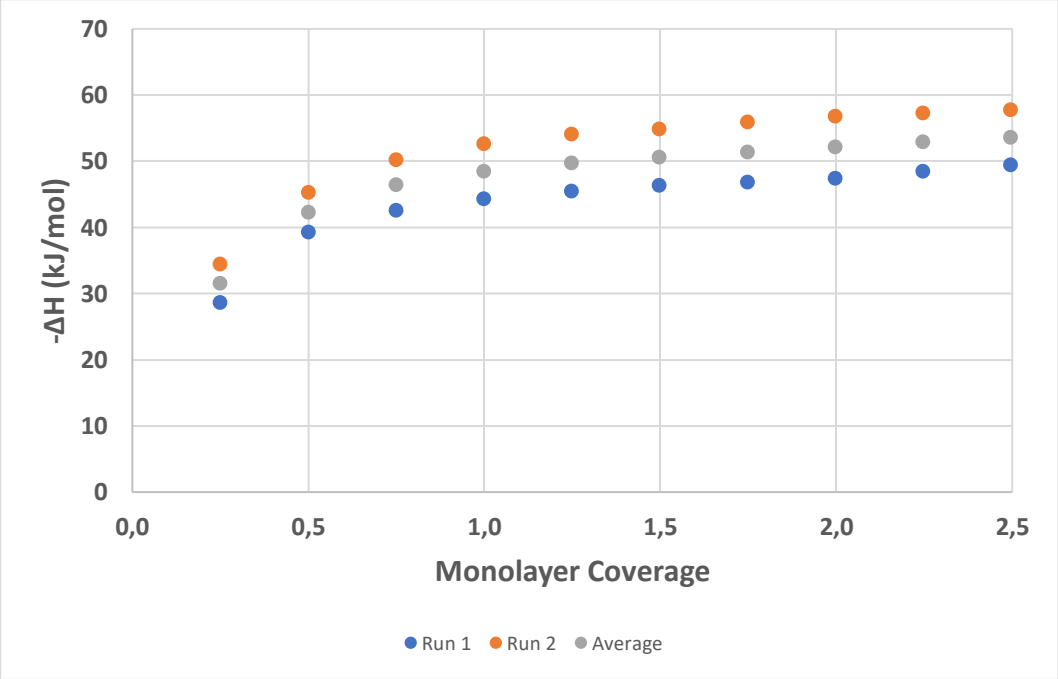

Figure 3.10 Reproducibility test results carried out in microcalorimetry tests for a pyrite-PNBX system at natural pH of 2.8

The calculated heats of adsorption and their standard deviations, standard errors and relative standard errors are given in Table 3.8. The results obtained show that the relative standard error is less than 10%.

Table 3.8 Heats of adsorption for pyrite and PNBX at natural pH with their standard deviations and standard errors

	Heats of Adsorption (-kJ/mol)					
Monolayer Coverage	**Run 1**	**Run 2**	**Average**	**Standard Deviation (-kJ/mol)**	**Standard Error (-kJ/mol)**	**Relative Standard Error (%)**
0.25	28.6	34.4	31.5	4.09	2.89	9.18
0.50	39.3	45.2	42.2	4.22	2.99	7.07
0.75	42.6	50.2	46.4	5.40	3.82	8.22
1.00	44.3	52.6	48.5	5.94	4.20	8.66
1.25	45.4	54.0	49.7	6.10	4.31	8.68
1.50	46.3	54.8	50.6	6.02	4.25	8.41
1.75	46.8	55.9	51.4	6.42	4.54	8.85
2.00	47.4	56.8	52.1	6.61	4.67	8.97
2.25	48.5	57.3	52.9	6.24	4.41	8.35
2.50	49.4	57.7	53.5	5.89	4.17	7.78

3.9. SURFACE ANALYSIS

The aim was to determine the surface products that form when these minerals react with the selected collectors and when conditioned with synthetic plant water the composition of which has been described previously. The techniques selected for analysis are X-Ray Photoelectron Spectroscopy (XPS) and Time-of-Flight Secondary Ion Mass Spectrometry (TOF-SIMS). The sample preparation for sperrylite and arsenopyrite minerals for analysis samples involved conditioning of the minerals with 5 x 10^{-3}M PNBX and SNBDTC collectors in synthetic plant water at pH 9 for 10 minutes. Both minerals were also conditioned for 10 minutes in synthetic plant water at pH 9, to investigate the natural surface composition of the minerals under flotation conditions. Dry, untreated minerals samples were also tested, to act as standards. The prepared samples were analysed using XPS and TOF-SIMS at the Council for Scientific and Industrial Research (CSIR).

3.9.1. X-Ray Photoelectron Spectroscopy (XPS)

X-ray Photoelectron Spectroscopy (XPS) analysis was used to determine the surface products of sperrylite and arsenopyrite. It is a surface sensitive technique, that is based on the photoelectron effect and is useful for analysing the depth of the samples that range from 5µm to 10µm, the top few atoms that can be formed as a result of collector adsorption or corrosion. During the test, low energy X-rays are bombarded onto a surface material to eject photoelectrons. The ejected photoelectrons' kinetic energy is given by equation (8).

$$\mathrm{KE} = hv - (BE + \mathrm{WF}) \qquad (8)$$

where:

hv – X-Ray energy applied, where h is the Plank's constant and v is the frequency of the incident radiation

BE – Binding energy of the photoelectron

WF – Spectrometer work function of the material or sample

The XPS spectrum generated is a plot that shows the number of electrons detected at a specific binding energy. This makes it possible to identify and quantify all elements on the surface of a material with the exception of hydrogen. Table 3.11 shows the experimental setup details for the given parameters.

Figure 3.11 XPS experimental setup parameters

Parameter	**Value**
Instrument Brand	Thermo
Model	ESCAlab 250Xi
X-Ray	Monochromatic Al kα (1486.7 eV)
X-Ray Power	300 W
X-Ray Spot Size	900 µm
Pass Energy (Survey)	100 eV
Pass Energy (Hi-res)	20 eV
Pressure	$< 10^{-8}$ mBar

Each element has its distinct peak which corresponds to an electron configuration of electrons in a given atom. Also, the number of detected electrons in each peak is directly related to the amount of the detected element in the sample.

3.9.2. Time-of-Flight Secondary Ion Mass Spectrometry (TOF-SIMS)

Time-of-Flight secondary ion mass spectrometry (TOF-SIMS) is a very sensitive surface analysis technique and is a combination of the SIMS (Secondary Ion Mass Spectrometry) analytical technique with Time-of-Flight mass analysis (TOF). It provides detailed elemental and molecular composition of surface layers from one to two monolayers. Primary ions with some keV energy are used to bombard a surface and the transferred primary ion energy targets atoms via atomic collisions to generate a collision cascade. Part of the energy that is transferred back to the surface allows the emission of atoms and molecular compounds when they overcome the surface binding energy.

This method is based on the fact that ions with the same energy but different masses travel at different velocities. The generated ions are accelerated to a common energy and then travel over a drift path to the detector. This allows the lighter ions to travel at a higher velocity, as a result, they arrive at the detector before the heavier ions. The mass of each ion is then determined by measuring the flight time of each ion. The experimental setup parameters for the tests are given in Table 3.12.

Figure 3.12 TOF-SIMS experimental setup parameters

Parameter	**Value**
Instrument Brand	Ion TOF
Model	TOF-SIMS 5
Primary Beam Species	Bi
Primary Beam Energy	25 keV
Primary Beam Current	~1 pA
Mass Resolution	< 10000
Pressure	$< 10^{-8}$ mBar

4. RESULTS

4.1. INTRODUCTION

This chapter outlines the results obtained from the microflotation, adsorption, rest potential and isothermal titration calorimetry tests of the minerals selected in this study. The minerals were characterized using X-Ray Diffraction (XRD) and Scanning Electron Microscope (SEM), and the results are given in Section 4.2. These tests were carried out to enhance the understanding of sperrylite interactions with selected standard collectors under various pulp conditions. Consequently, the acquired knowledge will in turn be useful in improving the overall recovery of the mineral in the South African PGM industry.

4.2. MINERAL CHARACTERISATION

The sperrylite and cooperite mineral samples were characterised by X-Ray Diffraction (XRD) and Scanning Electron Microscope (SEM) to confirm the structure and to determine the composition of phases present in synthetic minerals. The natural minerals, pyrite and arsenopyrite were only characterised using the XRD technique to confirm the presence of the required crystal structure and composition of the minerals.

4.2.1. X-Ray Diffraction (XRD) Results

XRD analysis on both the synthetic and natural samples was carried out to determine the mineral crystal structures and how they compare with those formed naturally. All the XRD spectra for the minerals are given in Appendix A.

4.2.1.1. Rietveld Refinement for Sperrylite

Table 4.1 shows the Rietveld refinement results for synthetic sperrylite. The Rietveld refinement for synthetic sperrylite showed that 87% sperrylite was formed with 12% arsenolite and 1% platinum. The sample consists mostly of the expected phase, viz. sperrylite.

Table 4.1 Rietveld refinement results for synthetic sperrylite

Mineral	Expected Phase	Identified Phases	Chemical Formula	Rietveld Quantification (%)
Synthetic Sperrylite	Sperrylite	Sperrylite	$PtAs_2$	87
		Arsenolite	AsO_3	12
		Platinum	Pt	1

4.2.1.2. Rietveld Refinement for Cooperite

The Rietveld refinement for synthetic cooperite in Table 4.2 showed that 97% cooperite was formed with 2% mackinawite and 1% ulvospinel. According to the crystal database, the cooperite matched the typical Bushveld PtS sample. Even though the sample was not pure, it consists mostly of the required phase.

Table 4.2 The Rietveld refinement results for synthetic cooperite

Mineral	Expected Phase	Identified Phases	Chemical Formula	Rietveld Quantification (%)
Synthetic Cooperite	Cooperite	Cooperite	PtS	97
		Mackinawite	$(Fe, Ni)_{1+X}S$	2
		Ulvospinel	$TiFe_2O_4$	1

4.2.1.3. Rietveld Refinement for Pyrite

Natural pyrite Rietveld refinement results given in Table 4.3 indicated that the sample was comprised of 89% pyrite, 7.6% jarosite and 3.4% pseudobrookite. Pyrite, the required phase made up the greater part of the sample.

Table 4.3 The Rietveld refinement for pyrite

Mineral	Expected Phase	Identified Phases	Chemical Formula	Rietveld Quantification (%)
Pyrite	Pyrite	Pyrite	FeS_2	89
		Jarosite	$Fe_2H_{6.65}Na_{0.35}O_{14}S_2$	7.6
		Pseudobrookite	MgO_5Ti_2	3.4

4.2.1.4. Rietveld Refinement for Arsenopyrite

Natural arsenopyrite Rietveld refinement results indicated that the sample was comprised of 74.2% arsenopyrite, 16.52% pyrite and other minor phases shown in Table 4.4.

The results indicate that arsenopyrite, the required phase makes up the greater part of the sample. However, the presence of pyrite might also influence the behaviour of the sample.

Table 4.4 The Rietveld refinement results for arsenopyrite

Mineral	Expected Phase	Identified Phases	Chemical Formula	Rietveld Quantification (%)
Arsenopyrite	Arsenopyrite	Arsenopyrite	FeAsS	74.2
		Pyrite	FeS_2	16.52
		Galena	PbS	0.65
		Siderite	FeO_3	3.99
		Lollingite	$FeAs_2$	2.46
		Quartz	SiO_2	2.17

4.2.2. Scanning electron microscope (SEM) Results

Energy Dispersive Spectroscopy was further used to characterise the synthetic sperrylite and cooperite to confirm the composition of the mineral phases formed during the synthesis process. Also, the SEM analysis was carried out on the natural sperrylite electrode to confirm the composition of the phases present.

4.2.2.1. Natural Sperrylite Electrode

The natural sperrylite electrode was provided by the UCT Hydrometallurgy Research group and the mineral was sourced from the nickel ore deposit of the Sudbury Basin in Ontario Canada. Figure 4.1 shows the Back Scattered Electron (BSE) micrograph of the electrode and the respective spectra. The Energy Dispersive Spectroscopy (EDS) results (Table 4.5) for the natural sperrylite electrode show that it consists mainly of sperrylite in spectra 1 and 2. Spectrum 3 shows a crack between the 2 sperrylite mineral pieces that were mounted on the electrode, hence it does not contain any Pt and As. The expected Pt to As ratio in sperrylite was calculated based on the individual atomic masses of the elements according to their stoichiometric quantities, as given by the empirical formula. If the sample were completely homogenous then the expected ratio of platinum to arsenic would be 1.3, as shown in Table 4.5.

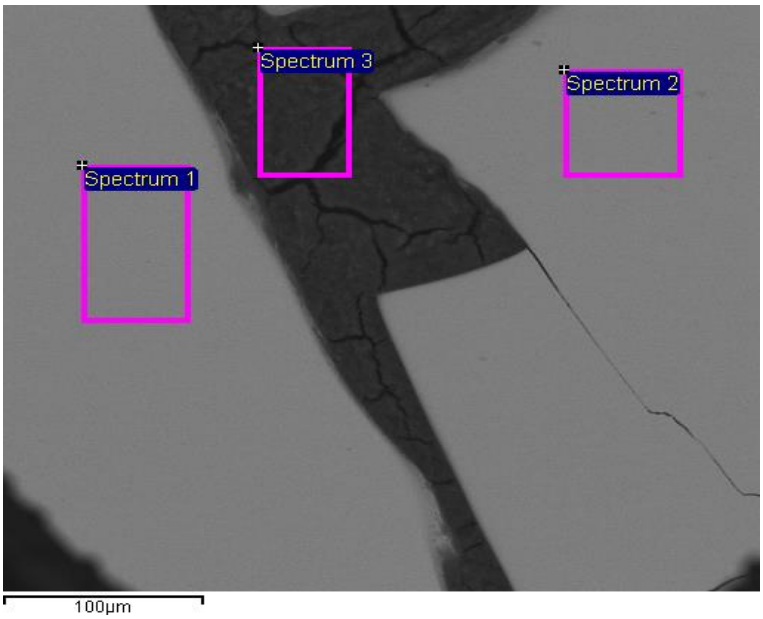

Figure 4.1 BSE micrograph of the natural sperrylite electrode

The average Pt:As ratio from the electro probe analysis was 1.33, which is very close to the calculated value and it could be concluded that the sperrylite sample was almost completely pure.

Table 4.5 EDS results of the natural sperrylite electrode

Spectrum	C (wt%)	O (wt%)	Al (wt%)	As (wt%)	Pt (wt%)	Pt/As Ratio from SEM	Pt/As Expected Ratio
Spectrum 1				42.17	57.83	1.37	1.3
Spectrum 2				43.91	56.09	1.28	1.3
Spectrum 3	5.64	54.56	39.8				

4.2.2.2. Synthetic Sperrylite Electrode

Figure 4.2 shows the Back Scattered Electron (BSE) micrograph of the synthetic sperrylite electrode and its respective spectra. The Energy Dispersive Spectroscopy (EDS) results given in Table 4.6 show that the electrode is made up of mainly the sperrylite phase. A few white specks of free platinum which are less than 10µm can also be seen as a minor phase in the electrode. In the case of spectrum 5, a third of the oxygen wt% was subtracted from the total arsenic wt% which contributes to the formation of arsenolite and the remainder was used to determine the sperrylite ratio present.

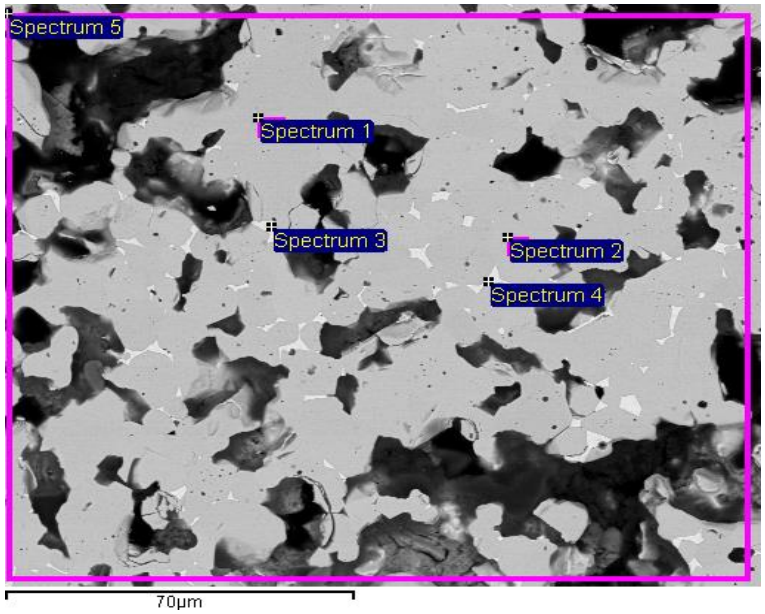

Figure 4.2 BSE micrograph of the synthetic sperrylite electrode

Table 4.6 EDS results of the synthetic sperrylite electrode

Spectrum	O (wt%)	As (wt%)	Pt (wt%)	Pt/As Ratio from SEM	Pt/As Expected Ratio
Spectrum 1		43.00	57.00	1.33	1.3
Spectrum 2		42.73	57.27	1.34	1.3
Spectrum 3		0.89	99.11	111.16	1.3
Spectrum 4		39.46	60.52	1.53	1.3
Spectrum 5	18.30	37.60	44.11	1.4	1.3

4.2.2.3. Cooperite Synthetic Electrode

The cooperite synthetic electrode was supplied by the UCT Centre for Minerals Research (CMR) and Figure 4.3 shows the Back Scattered Electron (BSE) micrograph of the electrode and its respective spectra. The Energy Dispersive Spectroscopy (EDS) results given in Table 4.7 indicate that the electrode is mainly made up of the cooperite phase. The elemental compositions indicate there is a variation in the sulphur content as shown by the calculated ratios.

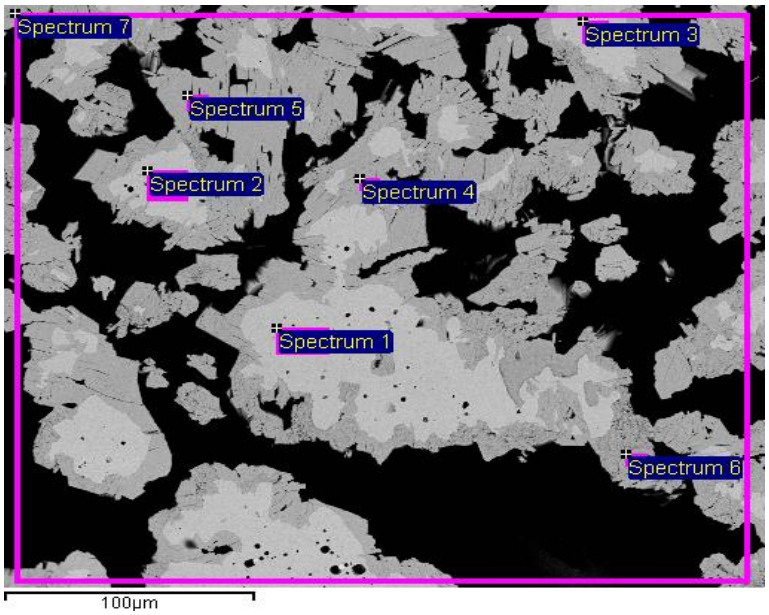

Figure 4.3 BSE micrograph of a synthetic cooperite electrode

Table 4.7 EDS results for the synthetic cooperite electrode

Spectrum	S (wt%)	Pt (wt%)	Pt/As Ratio from SEM	Pt/As Expected Ratio
Spectrum 1	15.25	84.75	5.56	6.08
Spectrum 2	14.78	85.22	5.76	6.08
Spectrum 3	15.10	84.90	5.62	6.08
Spectrum 4	26.23	73.77	2.81	6.08
Spectrum 5	26.26	73.74	2.81	6.08
Spectrum 6	25.90	74.10	2.86	6.08
Spectrum 7	18.49	81.51	4.41	6.08

The outer parts of the electrode (spectra 4, 5 and 6) had higher sulphur contents as opposed to the core (spectra 1, 2 and 3). Also, the EDS results in Appendix A, show the presence of free platinum, estimated to range from 10 to 35µm.

4.2.2.4. Sperrylite

Figure 4.4 shows the Back Scattered Electron (BSE) micrograph of the -106+38µm synthetic sperrylite sample and its respective spectra. The Energy Dispersive Spectroscopy (EDS) results given in Table 4.8 confirms that the sample consists mostly of sperrylite, which is the required phase. The elemental compositions indicate that there are small amounts of free platinum mostly locked within the larger sperrylite particles. Smaller particles in the micrograph do not contain any free platinum.

Table 4.8 EDS results for synthetic sperrylite of size fraction, -106+38µm

Spectrum (-106+38µm)	As (wt%)	Pt (wt%)	Pt/As Ratio from SEM	Pt/As Expected Ratio
Spectrum 1	42.38	57.62	1.36	1.3
Spectrum 2	42.81	57.19	1.34	1.3
Spectrum 3	43.08	56.92	1.32	1.3
Spectrum 4	42.83	57.17	1.33	1.3
Spectrum 5 to 8		98.34		1.3

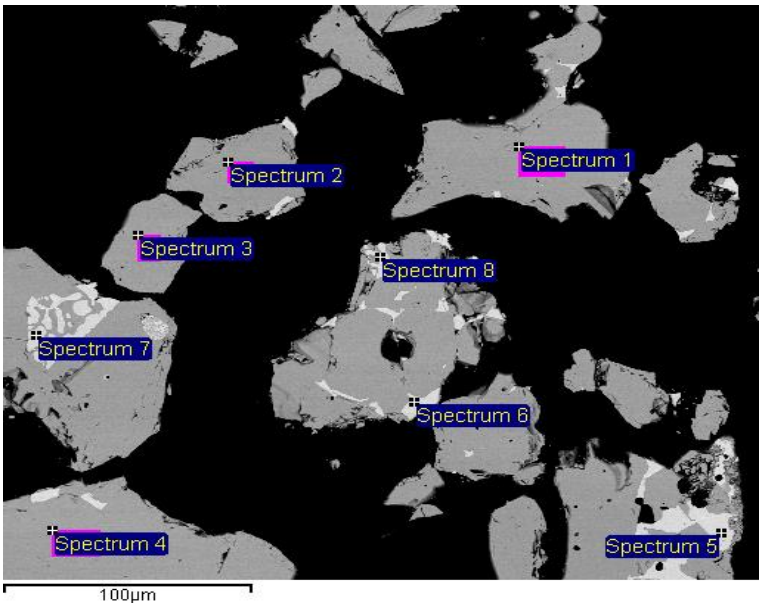

Figure 4.4 BSE micrograph of synthetic sperrylite of size fraction, -106+38µm

The Back Scattered Electron (BSE) micrograph of the -38µm synthetic sperrylite sample is given in Figure 4.5. The Energy Dispersive Spectroscopy (EDS) results indicate that sperrylite is the main phase present in the sample (Table 4.9). The elemental compositions indicate that there is the presence of free platinum (less than 5µm) in spectrum 5. Also, the EDS results in Appendix A show some spectra with oxygen and excess arsenic which can be an indication of the arsenolite particles that were noted in the XRD data.

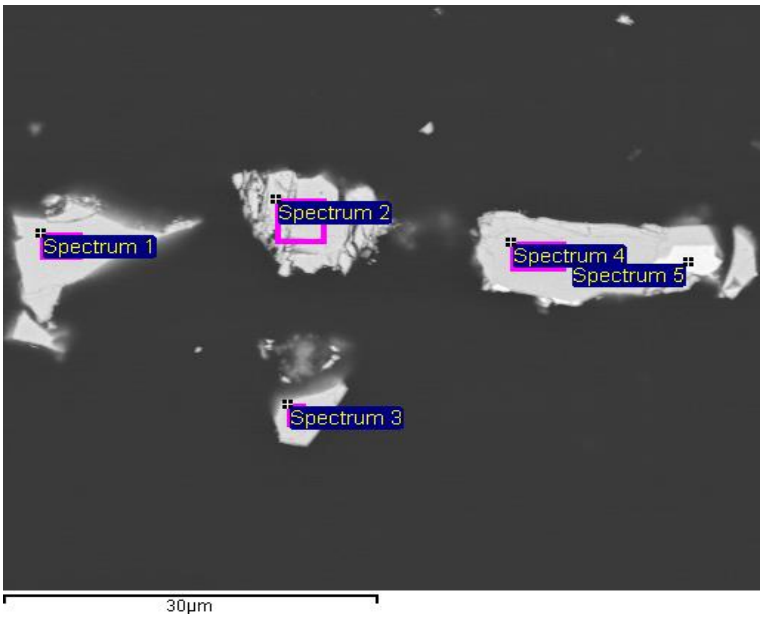

Figure 4.5 BSE micrograph of synthetic sperrylite of size fraction, -38µm

Table 4.9 EDS results for synthetic sperrylite of size fraction, -38µm

Spectrum -38µm	As (wt%)	Pt (wt%)	Pt/As Ratio from SEM	Pt/As Expected Ratio
Spectrum 1	42.64	57.36	1.35	1.3
Spectrum 2	43.04	56.96	1.32	1.3
Spectrum 3	43.04	56.96	1.32	1.3
Spectrum 4	43.04	56.96	1.32	1.3
Spectrum 5	0.47	99.53	212.07	1.3

4.2.2.5. Cooperite

The synthetic cooperite Back Scattered Electron (BSE) micrograph and its respective spectra are shown in Figure 4.6.

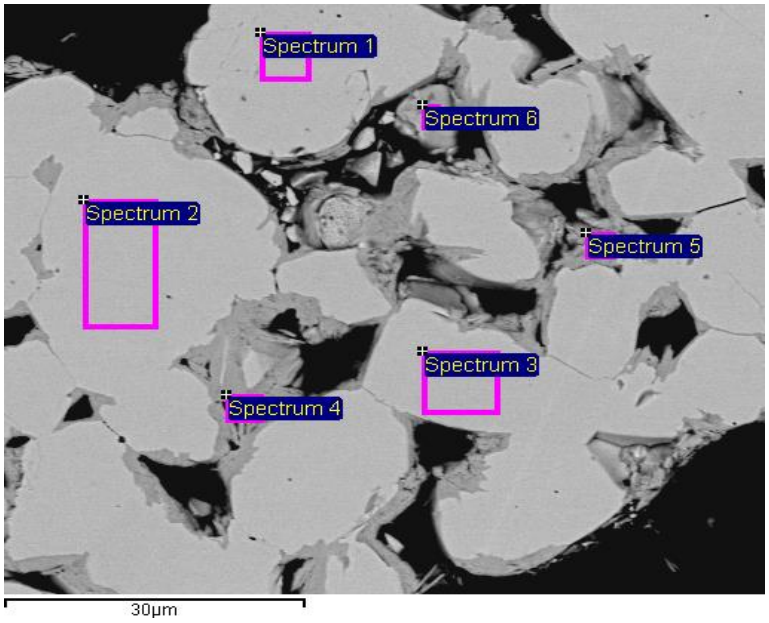

Figure 4.6 BSE micrograph of synthetic cooperite

The Energy Dispersive Spectroscopy (EDS) results given in Table 4.10 shows that the sample consists of a cooperite phase. However, the elemental compositions indicate there is a variation in the sulphur content as shown by the calculated ratios.

Table 4.10 EDS results of synthetic cooperite

Spectrum -106+38µm	S (wt%)	Pt (wt%)	Pt/As Ratio from SEM	Pt/As Expected Ratio
Spectrum 1	16.01	83.99	5.25	6.08
Spectrum 2	15.37	84.63	5.51	6.08
Spectrum 3	15.51	84.49	5.45	6.08
Spectrum 4	20.96	79.04	3.77	6.08
Spectrum 5	18.75	81.25	4.33	6.08
Spectrum 6	24.98	75.02	3.00	6.08

4.3. MICROFLOTATION RESULTS

Microflotation tests were carried out using the UCT microflotation cell as a measure of bubble-particle attachment efficiency of selected minerals under different pulp conditions. Pure minerals of size fraction of -106+38µm, as shown in the previous section, were used during all the microflotation tests to minimize the possibility of recovery by entrainment as much as possible and the effect of mineral association. It was important to determine the natural hydrophobicity of the minerals in order to clearly evaluate the effect of adding different collectors and to understand the possible factors that could influence the interaction of various collectors with sperrylite and other minerals. The methodology that was followed in carrying out the experiments has been outlined in Section 3.5.2.

In order to compare all the selected minerals, a standard test was carried out for all the minerals using the selected standard collectors with the normal butyl chain length. These tests were carried out at pH 9, which is approximately the normal operating pH in the PGM plants.

The selected standard thiol collectors were: potassium normal butyl xanthate (PNBX), sodium normal butyl dithiocarbamate (SNBDTC) and sodium di-normal butyl dithiophosphate collectors (SNDBDTP). These collectors were added at one monolayer coverage based on the BET results to only investigate the effect of primary chemisorption adsorption products. The 1 monolayer dosage was chosen because the collector adsorption process is limited to 1 monolayer thickness since electron exchange cannot be maintained for more than one monolayer of the underlying adsorbent (Rao, 2004).

MIBC frother was used in all the tests at a dosage of 20ppm, which is slightly higher than the determined critical coalescence concentration (CCC) to avoid bubble coalescence (Guven et al., 2020). Synthetic plant water was used during the tests to mimic the possible plant conditions and to also investigate the effect of plant water ions. A UCT synthetic plant water recipe was used and an ionic strength of 4.84E-2 (2SPW) was chosen, which is 2 times stronger than the normal plant water ionic strength (1SPW), which is usually exceeded in most plants. Further tests were carried out to determine the effect of plant water ions in the recovery of minerals as opposed to deionised water in some of the tests. Tests that investigated the effect of pH were also introduced to determine the effects of surface oxidation and surface characteristics on recovery. The effects of various standard and novel collectors will also be presented in this section. The SIBX collector, which is used in most PGM plants was also tested on sperrylite and cooperite so as to compare the effect of a straight and branched chain butyl collectors on the recovery of those PGM minerals.

4.3.1. Sperrylite

Synthetic sperrylite was used in the microflotation tests to measure the hydrophobicity before and after adding collectors. Sperrylite is the main mineral under investigation in this study that seeks to understand its interactions with different collectors and how it compares with other minerals so as to improve its flotation recovery.

4.3.1.1. Standard Test

The first set of tests were done under standard conditions of pH 9 in synthetic plant water. The collector types that were used were the standard thiol collectors found on many PGM concentrators. Dosage was maintained at 1 monolayer coverage, as explained in Section 4.3. Sperrylite recovery, under these conditions, in the absence of a collector was 14.5% (Figure 4.7) and indicates that the mineral has a poor natural flotation response. Adding the standard collectors at the equivalent of 1 pseudo-monolayer coverage (1 ML) resulted in little improvement in the mineral recovery, the recoveries being: PNBX (26.0%) > SNBDTC (24.3%) > SNDBDTP (23.3%) > SIBX (19.9%). It is worth noting that PNBX gave a recovery of 6% greater than SIBX which is currently used as the preferred collector in the PGM plants. Generally, sperrylite showed a poor flotation response even after adding the standard collectors under alkaline conditions.

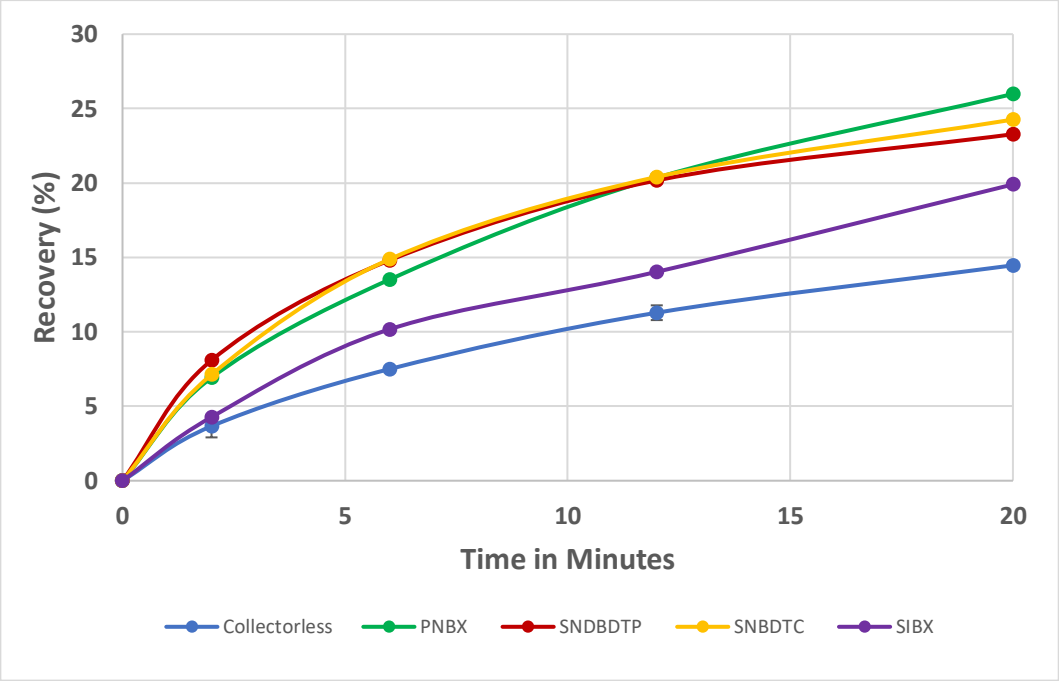

Figure 4.7 Microflotation recovery-time graphs of sperrylite with no reagent and standard collectors at pH 9 in synthetic plant water, I= 4.84E-2 M and 20 ppm MIBC frother.

4.3.1.2. Increased Collector Dosage

In an attempt to increase the flotation recovery of sperrylite, tests at higher collector dosages were carried out and the results are presented in Figure 4.8.

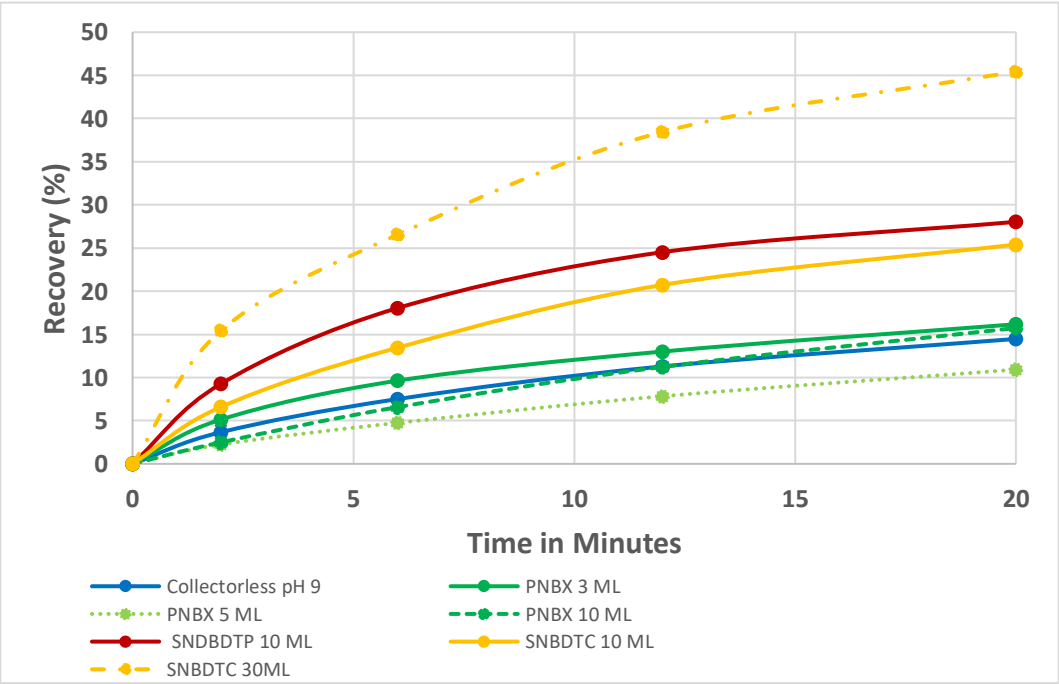

Figure 4.8 Microflotation recovery-time graphs of sperrylite with standard collectors at 3, 5, 10, and 30 pseudo-monolayer dosages at pH 9 in synthetic plant water, I= 4.84E-2 M and 20 ppm MIBC frother.

It was also hypothesized that increasing the collector dosage of the thiol collectors could lead to improved recoveries, as observed with pyrite and potassium amyl xanthate (PAX) (Fuerstenau et al., 1968). Increasing the collector dosage of PNBX to 3, 5 and 10 equivalent pseudo-monolayers, in fact, reduced the recovery to 16.2%, 10.9%, and 15.7% respectively. Adding SNBDTC and SNDBDTP at 10 monolayers did not result in any improvement in the recovery of sperrylite. The highest improvement, viz. to 45.4%, was obtained after adding the equivalent of 30 pseudo- monolayers of SNBDTC. This is equivalent to a dosage of 4421 g/t of the pure mineral. This would obviously be lower under plant conditions where the sperrylite is only present at less than one gram per ton concentrations.

4.3.1.3. Novel collectors

A set of novel collectors were identified as suitable candidates for testing as described in Section 1.8. It was hypothesized that collectors with nitrogen linking atoms that are electron-donating will result in stronger binding energy with sperrylite, resulting in improved flotation recoveries. Figure 4.9 shows the cumulative recovery of microflotation tests after 20 minutes of flotation time. Collectorless and standard collector tests, PNBX, SIBX, SNDBDTP and SNBDTC, are shown in Figure 4.9 for comparison.

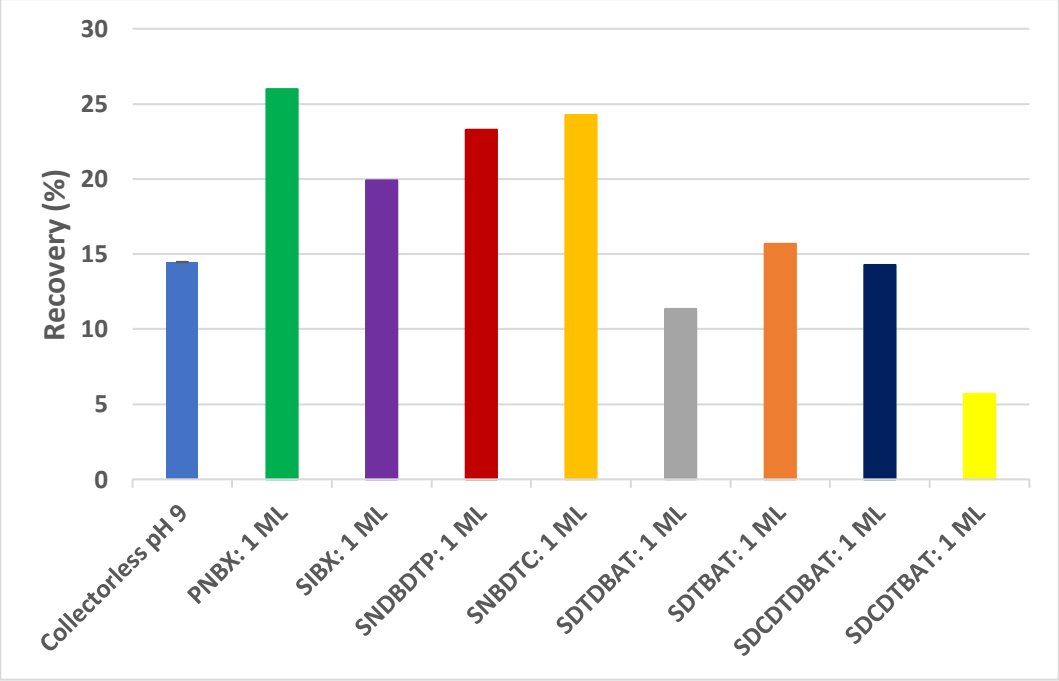

Figure 4.9 Flotation recoveries of sperrylite with no reagent and novel collectors and how they compare to standard collectors, at pH 9 in synthetic plant water, I= 4.84E-2 M and 20 ppm MIBC frother.

Novel collectors 2,6-dithio-4-butylamino-1,3,4-triazine (SDTBAT) and 2,6-dicarbonodithioate-4-di-butylamino-1,3,5-triazine (SDCDTDBAT), did not improve the recoveries of sperrylite beyond its natural floatability (Figure 4.9). In fact, 2,6-dithio-4-di-butylamino-1,3,4-triazine (SDTDBAT), and 2,6-dicarbonodithioate-4-butylamino-1,3,5-triazine (SDCDTBAT) had a depressing effect on the recovery of the mineral resulting in recoveries lower than the collectorless recovery.

The novel collectors did not offer any flotation recovery benefit on sperrylite at pH 9, even though they gave higher binding energies according to the isothermal titration calorimetry results (Figure 4.54).

4.3.1.4. Effect of pH

The effect of the pH was investigated, by carrying out the flotation tests at pH 4 in synthetic plant water. Figure 4.10 shows cumulative recoveries of selected collectors at 20 minutes flotation time for pH 4 and pH 9, for comparison. It is hypothesized that the hydroxide species formed on the mineral surface at high pH inhibit collector adsorption which results in poor recoveries. Flotation of sperrylite at pH 4 resulted in improved recoveries in the case of SNBDTC, SDTBAT and SDCDTDBAT to 48.5%, 41.7%, and 23.3% respectively (compared to 24.3%, 15.7%, and 14.3% at pH 9) (Figure 4.10). However, the recovery of PNBX remained unchanged even at low pH. A slight improvement in the collectorless recovery was also seen at pH 4.

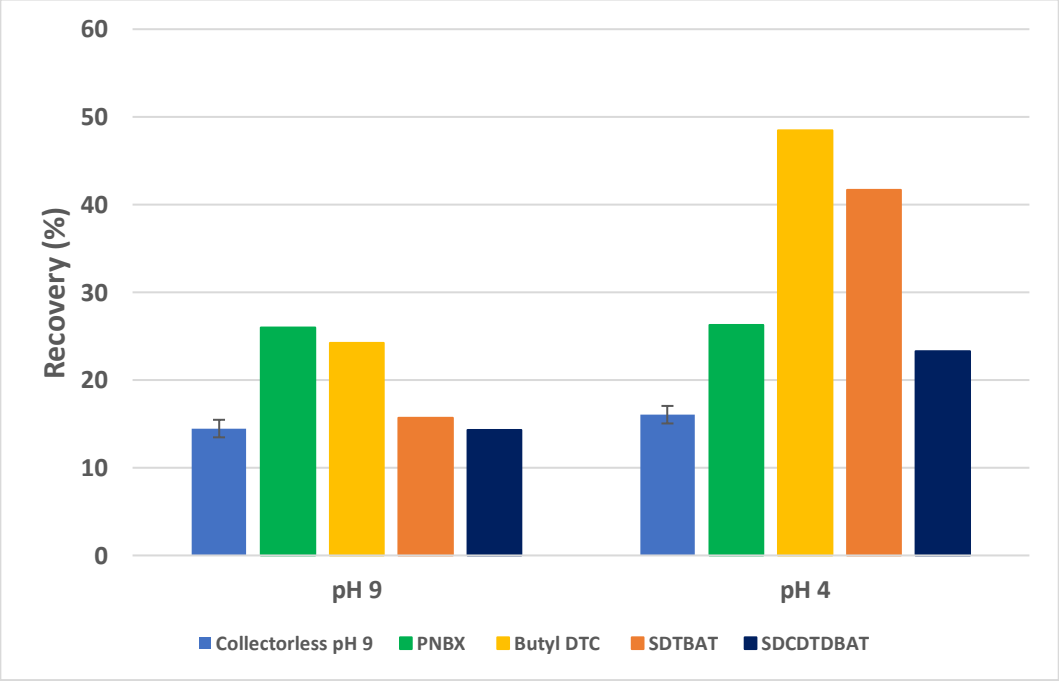

Figure 4.10 Effect of pH on the microflotation recoveries of sperrylite with standard and novel collectors, in synthetic plant water, I= 4.84E-2 M and 20 ppm MIBC frother

4.3.1.4.1. Recovery of Sperrylite with pH

The recovery profile of sperrylite at different pHs was investigated using SNBDTC as a collector. The dosage of the collector was 1 pseudo-monolayer. Figure 4.11 shows that the highest recovery was obtained at pH 4 while the lowest recovery was observed at pH 6.5.

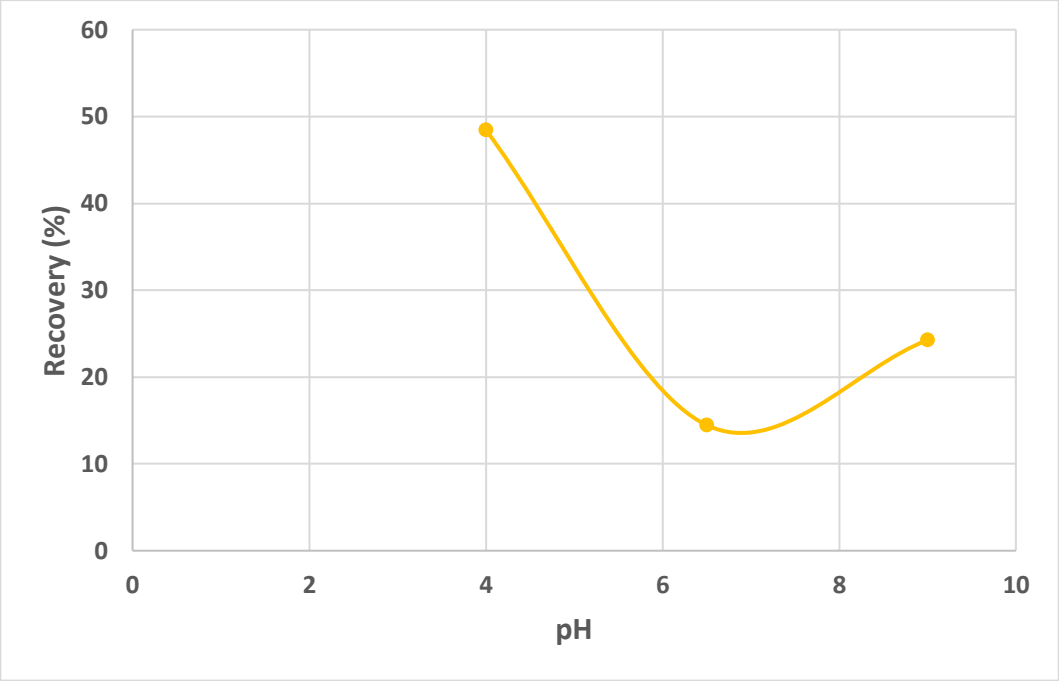

Figure 4.11 Microflotation recovery-pH profile of sperrylite with SNBDTC in synthetic plant water, I= 4.84E-2 M and 20 ppm MIBC frother.

4.3.1.5. Effect of Plant Water Ions

The effect of plant water ions on the floatability of sperrylite was investigated by floating sperrylite in distilled water. Figure 4.12 shows that the recovery of sperrylite was higher in distilled water (51.2%) as opposed to the synthetic plant water (26%).

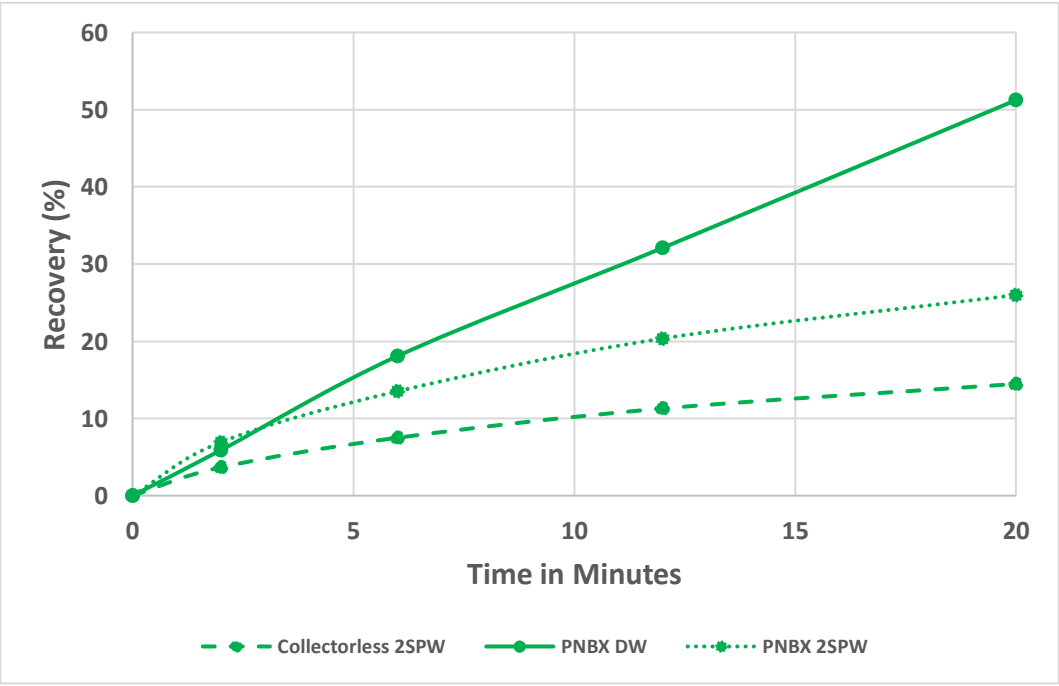

Figure 4.12 A comparison between the cumulative recovery of sperrylite with PNBX, at pH 9, in deionised water (DW) with 20ppm MIBC frother and sperrylite with PNBX collector, at pH 9 in synthetic plant water, I= 4.84E-2 M and 20 ppm MIBC frother.

This indicates that the plant water ions have a negative effect on the floatability of sperrylite. The collectorless recovery of sperrylite at pH 9 was not determined due to insufficient quantities of the mineral sample.

4.3.1.6. Increased Residence Time

Upon observing the slow rate of flotation for sperrylite, the flotation time was increased from 20 minutes to 30 minutes. As expected, there was an increase in the flotation recoveries with all these collectors (Figure 4.13). Increasing the flotation time to 30 minutes at pH 4 improved the recoveries in the order: SDTBAT (15.4%) > SNBDTC (11.9%) > SDCDTDBAT (7.3%). Moreover, at pH 9, the recovery for SNBDTC at 30 monolayers increased by 5.1% after increasing the flotation time to 30 minutes. This simply demonstrated the very slow floating nature of the sperrylite and the fact that improved recoveries can be obtained at longer residence times, which would come at the expense of a decrease in grade as gangue mineral recovery in the ore would increase correspondingly. It was also noted that increasing the dosage of SNBDTC from 1 monolayer to the equivalent of 10 monolayers at pH 4 had a depressing effect on the mineral, reducing the recovery by 37.2% (from 48.5 to 11.3%). This trend was also observed after increasing the PNBX collector dosage in the recovery of sperrylite at pH 9.

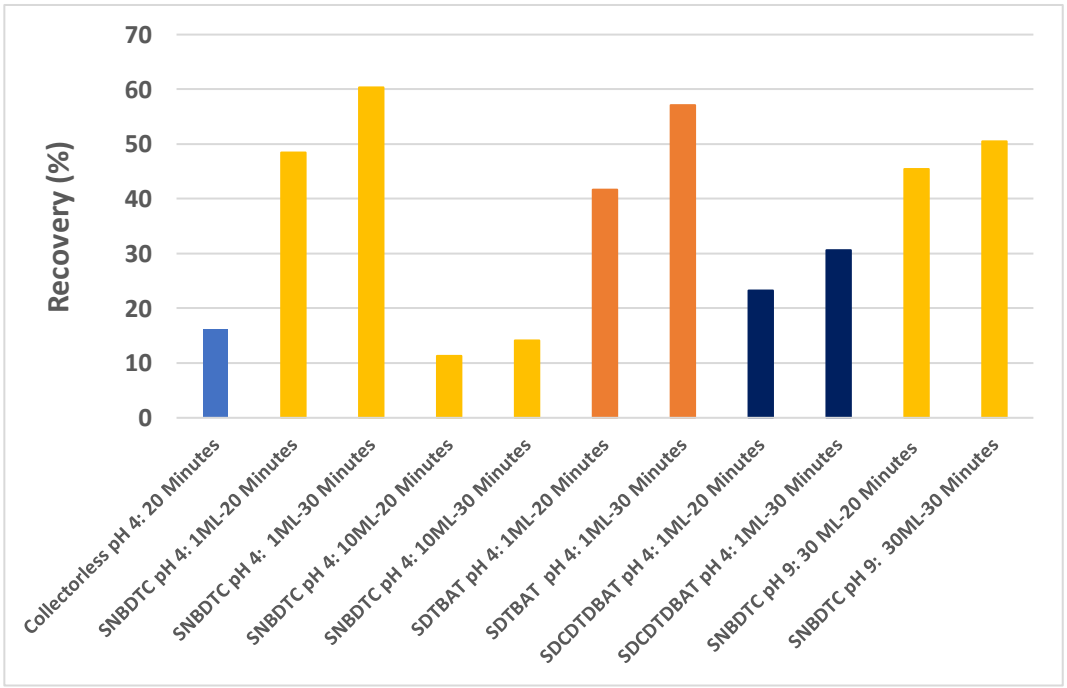

Figure 4.13 Effect of increasing the flotation time from 20 minutes to 30 minutes on the recovery of sperrylite with selected collectors in synthetic plant water, I= 4.84E-2 M and 20 ppm MIBC frother. In each case, the first result is after 20 mins. And the second is after 30 mins.

4.3.1.7. Collector Mixtures and Alternative Frothers

Tests to investigate the effect of collector combinations that mimic the current plant collector combination, viz. SIBX and sodium normal di-ethyl dithiophosphate (SNDEDTP) in the ratio of 3:1 were carried out.

Other conditions, such as pH (9) and dosage (1 monolayer) remained unchanged from standard conditions. Frother type was also varied since previous work (Pienaar et al., 2019) had suggested that MIBC may have favourable effects when used together with DTP. The recovery was slightly reduced by 1.7% when the collector combination of SIBX & SNDEDTP was used compared to SIBX at 1 pseudo-monolayer coverage (Figure 4.14). The use of a Dow 200 frother at a dosage of 15 ppm reduced the recovery of sperrylite by 8.3% compared to when tests were carried out with MIBC frother at a dosage of 20 ppm. Increasing the SIBX and SNDEDTP collector combination dosage to 10 monolayers with the Dow 200 frother improved the recovery by 4.4%, from 11.6 to 16%. Hence in these laboratory tests, using the SIBX and SNDEDTP collector combination did not increase the flotation recovery of sperrylite compared to the SIBX alone. MIBC frother produced slightly better results than the polyglycol frother, but overall recoveries were still poor for all tests.

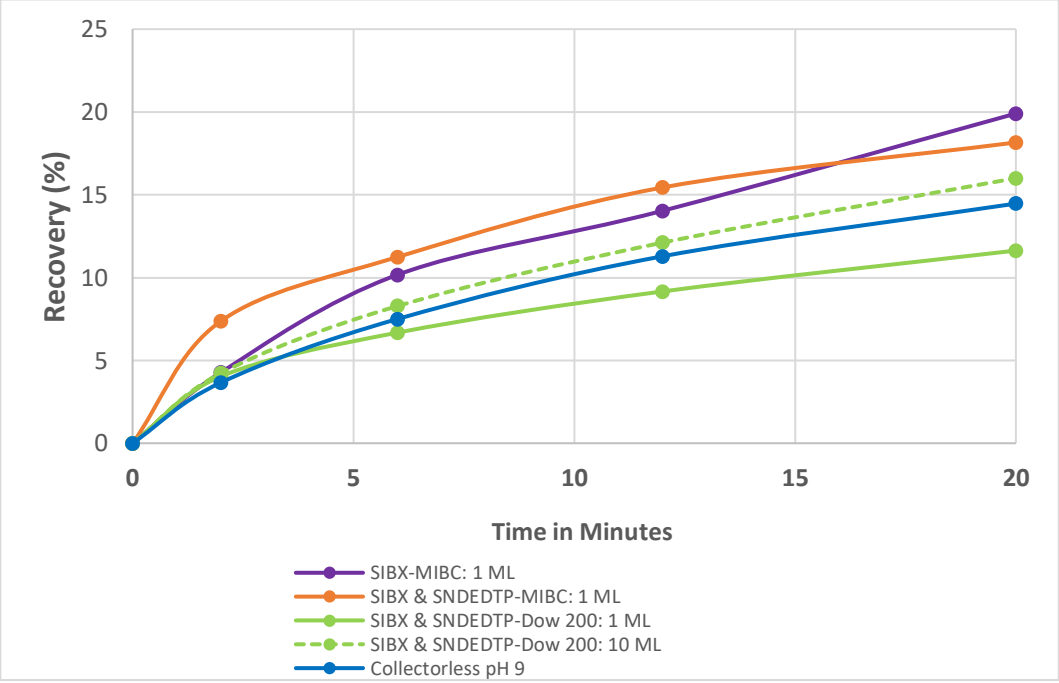

Figure 4.14 Effect of using a collector combination of SIBX and SNDEDTP with either 15 ppm Dow 200 frother and 20ppm MIBC frother on the recovery of sperrylite at pH 9 in synthetic plant water, I= 4.84E-2 M.

4.3.1.8. Increasing Eh

An investigation on the effect of increasing Eh at pH 9 on flotation recovery was carried out since it had been suggested in a paper by Vermaak et al., (2007) that an increase in Eh would improve xanthate collector adsorption onto sperrylite.

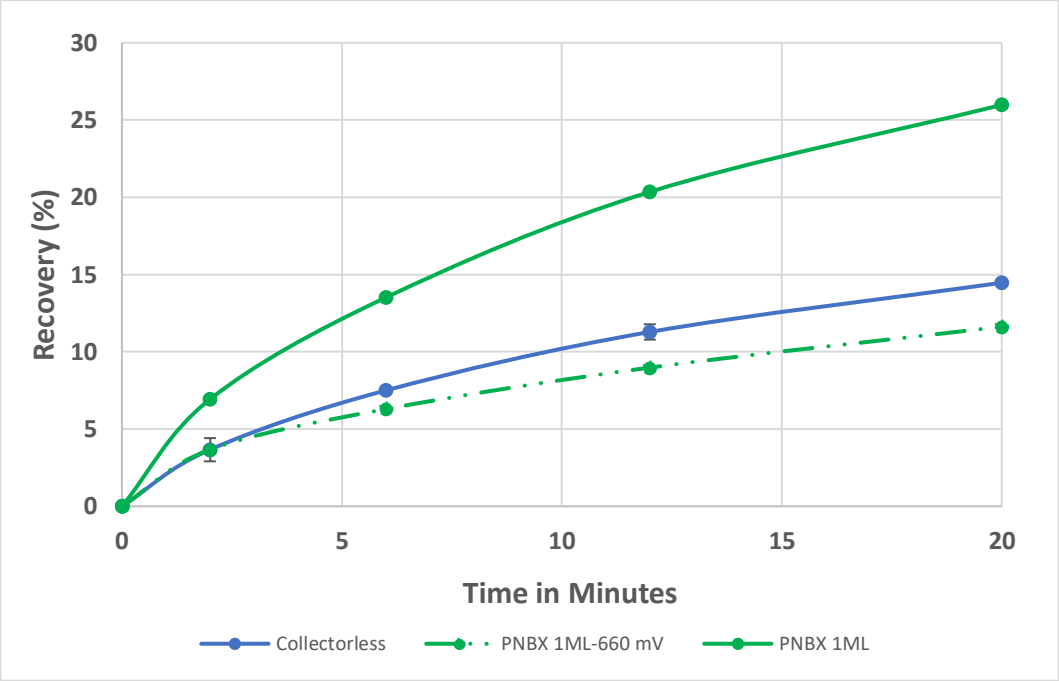

Figure 4.15 Effect of increasing the pulp Eh from natural Eh to 660 Mv on the recovery of sperrylite with PNBX collector, at pH 9 in synthetic plant water, I= 4.84E-2 M and 20 ppm MIBC frother.

The method used to increase the Eh has been described in Section 3.5.2.1. Increasing the pulp Eh from the natural Eh (160 mV) to 660 mV, in fact, depressed the recovery of sperrylite by 14.4%, back to the collectorless region (Figure 4.15). Collector was PNBX and other conditions were standard.

4.3.1.9. Activator Addition

Since copper sulphate is a known activator and assists in binding the thiol collectors to various mineral surfaces, the effect of adding copper sulphate was investigated (Figure 4.16). Copper sulphate ($CuSO_4$) was added at an equivalent molar dosage to the SNBDTC collector, but had a depressing effect on sperrylite, resulting in a reduced recovery by 14.4%.

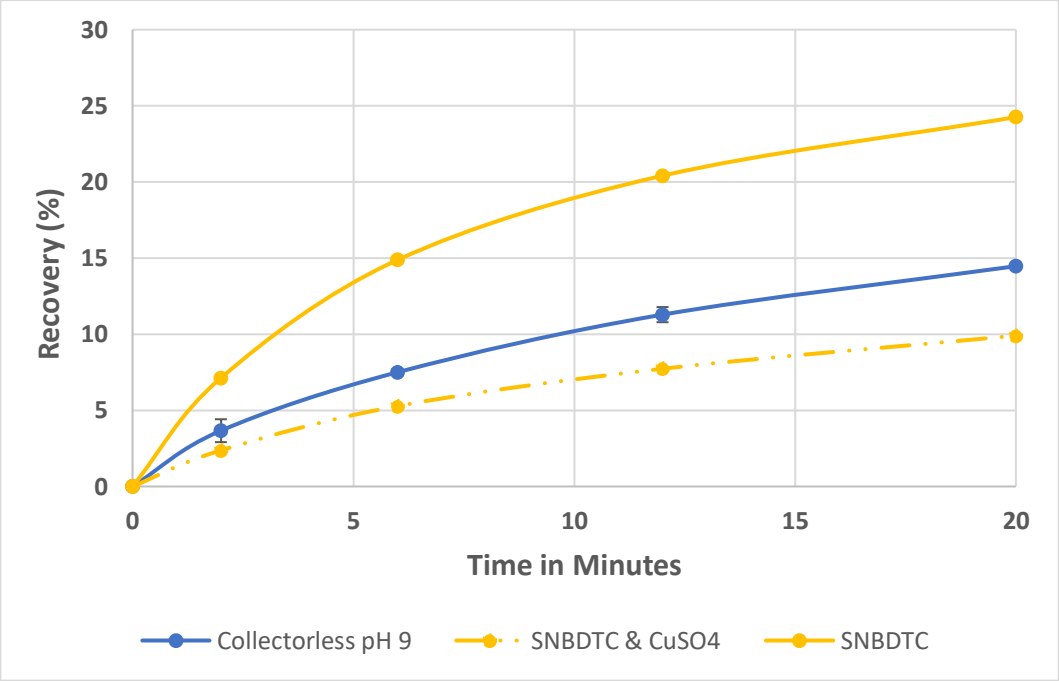

Figure 4.16 Microflotation recovery-time curves showing the effect of adding a copper sulphate activator and SNBDTC collector at pH 9 in synthetic plant water, I= 4.84E-2 M and 20 ppm MIBC frother.

4.3.1.10. Cationic, N-donor Collector

To investigate the behaviour of the nitrogen and oxygen bonding atoms as opposed to sulphur bonding atoms that are present in the thiol and novel collectors, an amide collector was tested at pH 9. It was not possible to measure the volume of the collector to make a monolayer coverage or to completely dissolve the collector in water, hence, a collector dosage equivalent to 5048.5 g/t was added for this test. This was found to be approximately 20 pseudo-monolayers coverage. Figure 4.17 shows that, surprisingly, the Flotigam 7100 collector increased the recovery to 40.9%. This was one of the highest recoveries seen under any conditions for sperrylite and compares to the recovery at 30 pseudo-monolayers with SNBDTC (45.4%), equivalent to 4421 g/t, under the same test conditions.

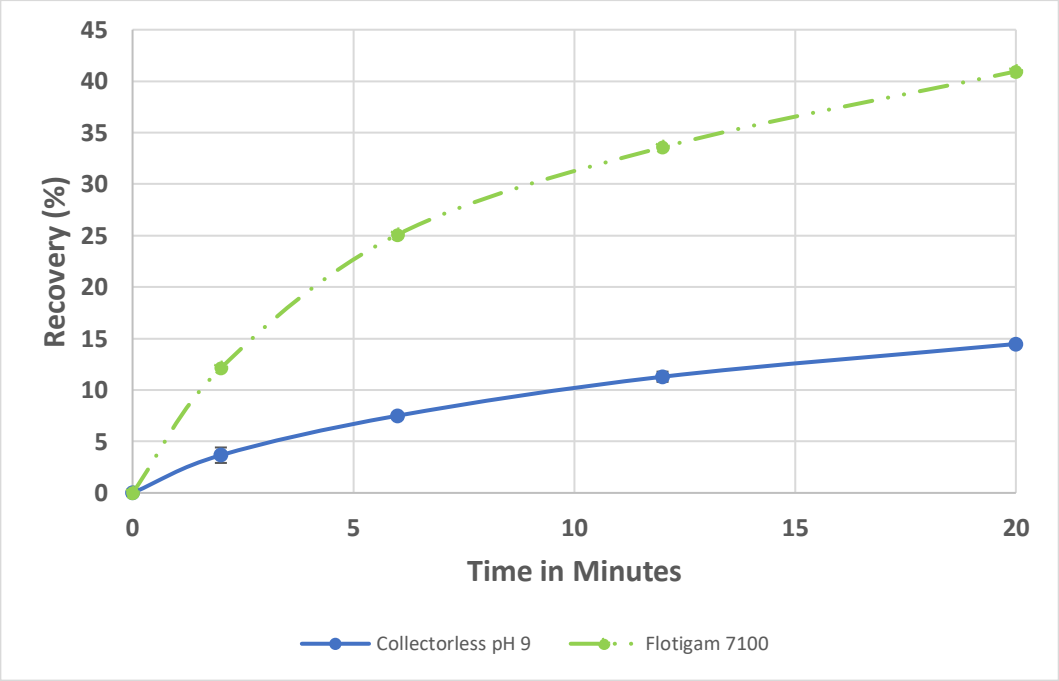

Figure 4.17 Microflotation recovery-time graphs of sperrylite with no reagent and Flotigam 7100 collector at pH 9 in synthetic plant water, I= 4.84E-2 M and 20 ppm MIBC frother.

4.3.2. Pyrite

Pyrite was investigated because it is a readily accessible sulphide mineral and has a similar crystal structure to sperrylite. It was considered that it may be possible to use pyrite as a cheap and accessible proxy for the flotation behaviour of sperrylite. In addition, these tests were done with a view to attempting to shed light on the behaviour of the mineral sulphur donor atoms and their interaction with collector molecules as opposed to the arsenic donor atoms in sperrylite. All tests were carried out at 1 pseudo-monolayer dosage of both the thiol and novel collectors. Parameters that were investigated in this section of tests included the effect of novel collectors, inclusion of ions in process water and the effect of pH on the microflotation recovery of pyrite.

4.3.2.1. Standard Test

The hydrophobicity of pyrite as indicated by microflotation recovery was determined before and after adding the different thiol collectors at a 1 pseudo-monolayer coverage (Figure 4.18). PNBX resulted in a significant improvement in recovery from 19% for the collectorless mineral to 94% for the PNBX-coated mineral. The other recoveries followed the order: PNBX (94.0%) > SNBDTC (43.4%) > SNDBDTP (18.8%). This is in contrast to the behaviour of sperrylite with these collectors under the same conditions where the highest recovery that was achieved was only 26%. The low collectorless pyrite recovery of 18.8% indicates that the mineral has only slight natural hydrophobicity.

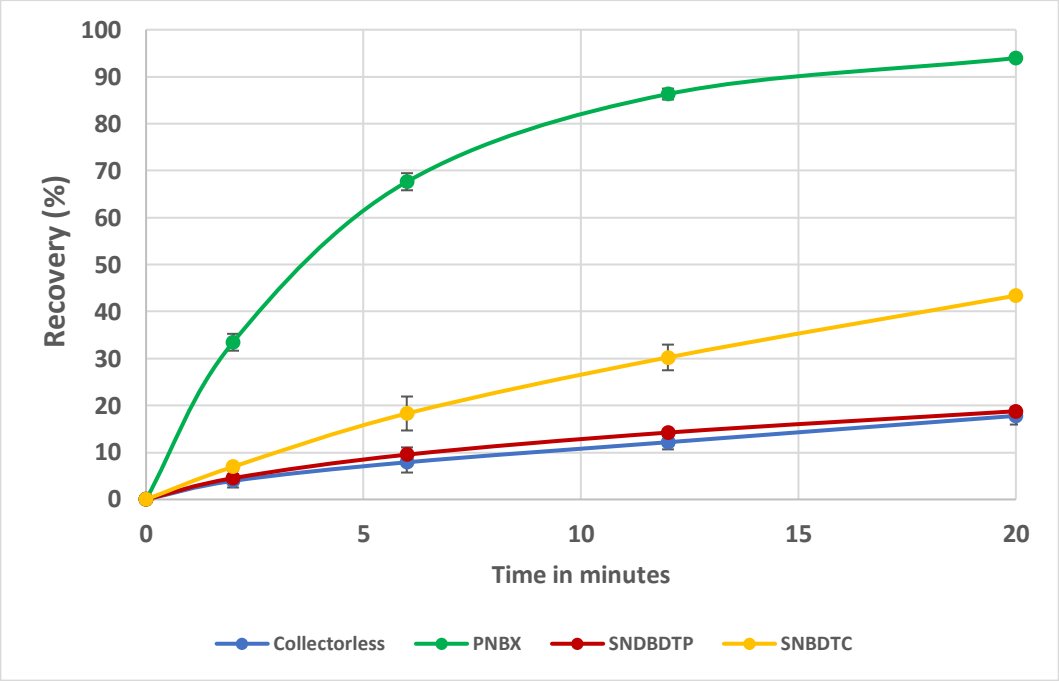

Figure 4.18 Microflotation recovery-time graphs of pyrite with no reagent and standard collectors at pH 9 in synthetic plant water, I= 4.84E-2 M and 20 ppm MIBC frother.

4.3.2.2. Novel Collectors

An investigation on the floatability of pyrite with the novel collectors that were developed during this collaborative study was carried out, to determine their performance as opposed to the thiol collectors.

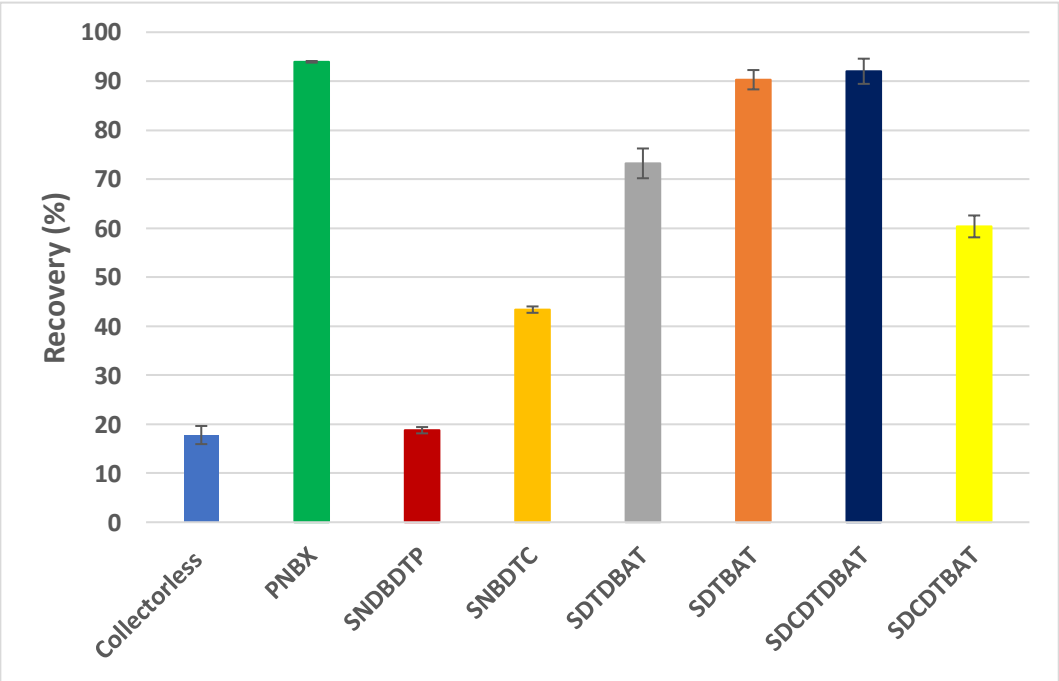

Figure 4.19 Microflotation recoveries of pyrite with no reagent and novel collectors and how they compare to standard collectors at pH 9 in synthetic plant water, I= 4.84E-2 M and 20 ppm MIBC frother.

SDTBAT and SDCDTDBAT gave the highest recoveries that were comparable to those of PNBX (Figure 4.19). SDTDBAT and SDCDTBAT gave moderate results and they also gave recoveries that were higher than SNBDTC and SNDBDTP. Therefore, it was found, during the flotation of pyrite, that these novel collectors were able to promote the floatability of a sulfide mineral but did not have the same effect on sperrylite, an arsenide mineral at pH 9.

4.3.2.3. Effect of Plant Water Ions

The flotation recoveries at pH 9 with distilled water resulted in the improved flotation recovery in the case of SNDBDTP, compared to the synthetic plant water, while the recoveries of PNBX and SNBDTC decreased considerably. Figure 4.19 indicates that the recoveries in distilled water follow the order: PNBX (43.4%) > SNDBDTP (28.6%) > SNBDTC (16.6%). In addition, the collectorless recovery was also reduced to 12.3%. When comparing these results with those in Figure 4.20, it can be noted that the recoveries of pyrite and the thiol collectors were greatly influenced by the presence of plant water. The action of PNBX and SNBDTC was enhanced by the plant water ions while the action of SNDBDTP was adversely affected.

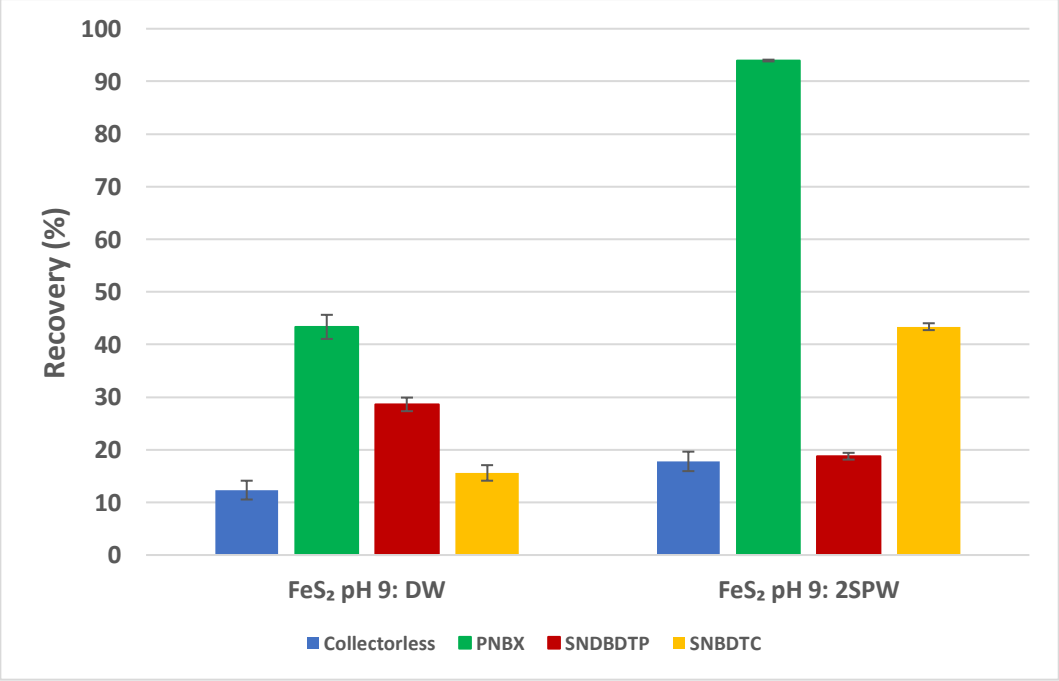

Figure 4.20 Microflotation recoveries of pyrite with no reagent and standard collectors at pH 9 in distilled water (DW) compared to plant water (2SPW), with 20 ppm MIBC frother.

4.3.2.3.1. Novel and Standard Collectors in Distilled Water

Since pyrite floatability was influenced by the synthetic plant water ions, the two best collectors were further tested on pyrite in distilled water.

There was a similar depressant effect when using distilled water with novel collectors as observed with the standard collectors under the same conditions. The recoveries of pyrite when using distilled water and the novel collectors were found to be higher than that of PNBX at pH 9 (Figure 4.21).

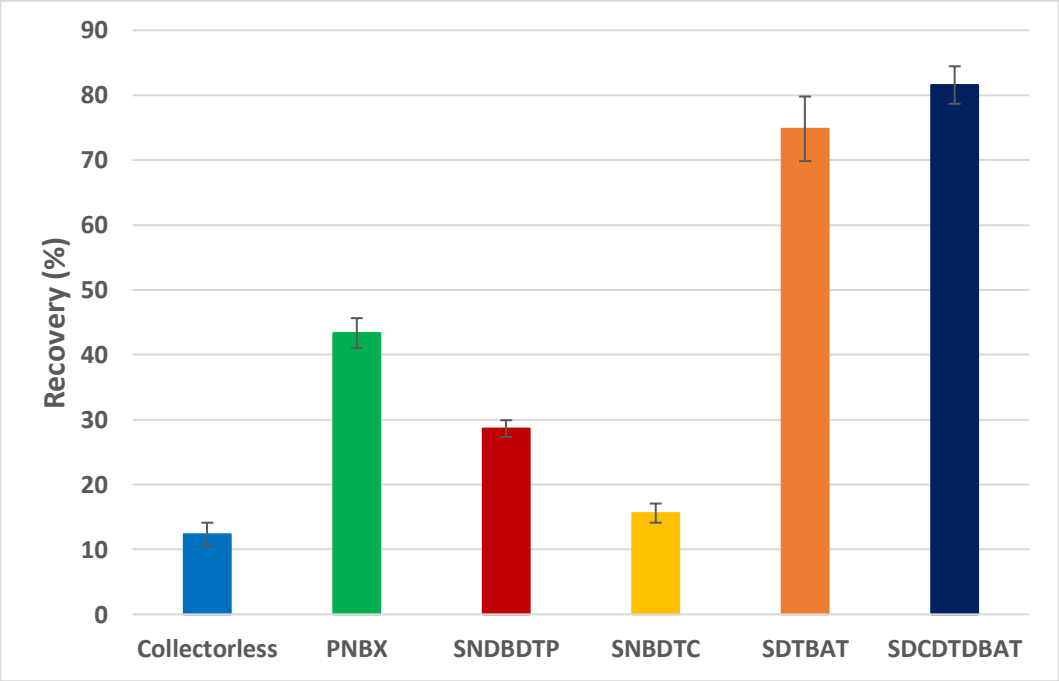

Figure 4.21 A comparison of microflotation recoveries of pyrite with no reagent, standard collectors and selected novel collectors at pH 9 in distilled water and 20 ppm MIBC frother.

The recoveries for SDTBAT and SDCDTDBAT were 74.8% and 81.6% respectively whereas that of PNBX was 43.4%.

4.3.2.4. Effect of pH

The recovery of pyrite in the presence of collectors increased at pH 4, compared to pH 9 (Figure 4.22) whereas its natural floatability was slightly reduced. The recoveries followed the order: SNDBDTP (85.0%) > PNBX (80.3%) > SNBDTC (31.9%). SNDBDTP recoveries increased substantially compared to the similar test at pH 9 (from 30% at pH 9 to 85% at pH 4). There is a well-documented effect of pH on pyrite recoveries, where recovery is depressed at higher pH's.

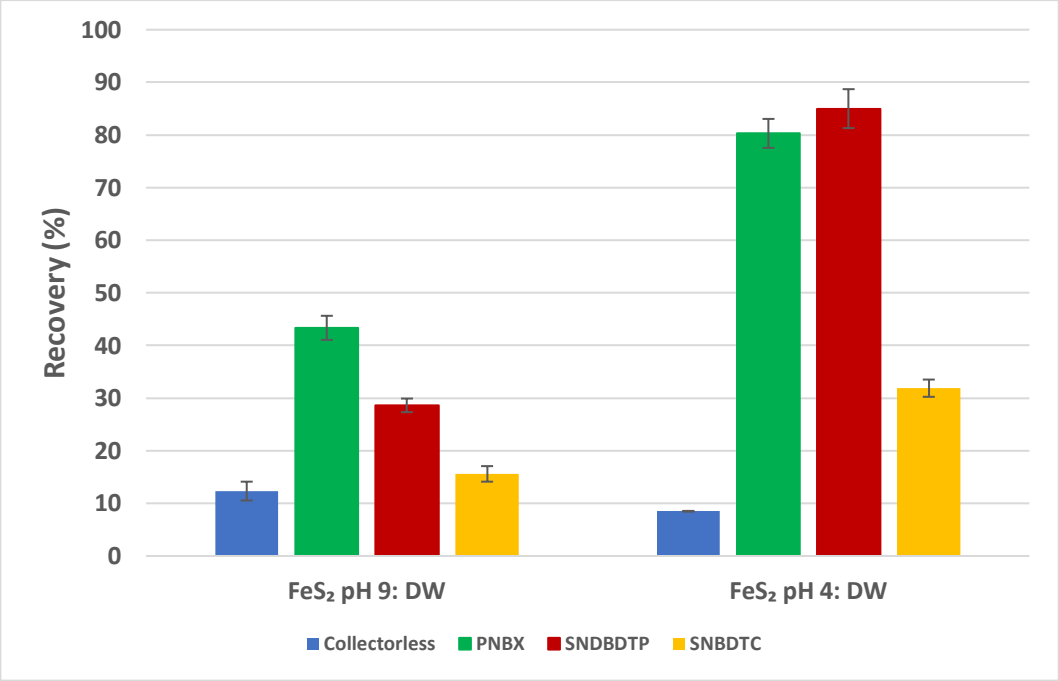

Figure 4.22 Effect of pH on the microflotation recoveries of pyrite with no reagent and standard collectors, in distilled water (DW) and 20 ppm MIBC frother.

4.3.3. Arsenopyrite

Arsenopyrite was selected to investigate the relative role of the presence of the mineral donor atoms (S, As) and how they influence the behaviour of the mineral. Furthermore, the arsenopyrite has a monoclinic crystal structure compared to the isometric crystal structure of pyrite and sperrylite. Standard microflotation tests were carried out to determine the natural and collector induced floatabilities of arsenopyrite. In addition, the effect of the addition of ions was investigated.

4.3.3.1. Standard Test

The flotation results for the standard test given in Figure 4.23 show that arsenopyrite had a high natural floatability of 86.2%. Adding the collectors only slightly increased the recoveries in the order: PNBX (94%) > SNDBDTP (91.5%) > SNBDTC (90.2%).

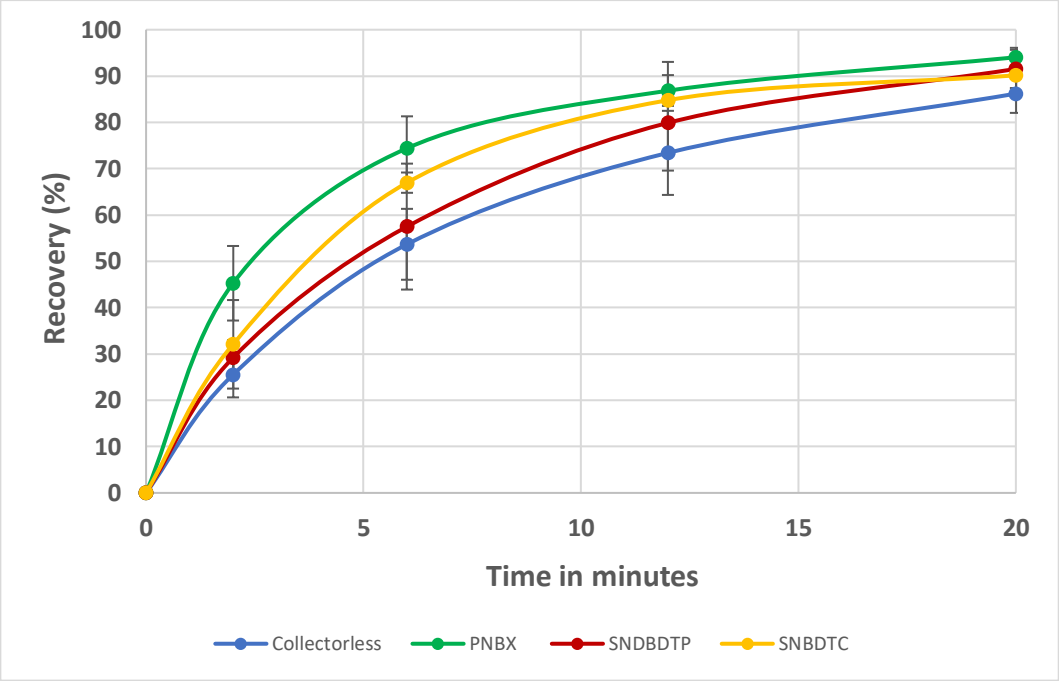

Figure 4.23 Microflotation recovery-time graphs of arsenopyrite with no reagent and standard collectors at pH 9 in synthetic plant water, I= 4.84E-2 M and 20 ppm MIBC frother.

4.3.3.2. Effect of Plant Water Ions

A test was also carried out to investigate the floatability of arsenopyrite in distilled water at pH 9. The natural floatability and SNDBDTP recoveries remained unchanged, while the recovery of SNBDTC was slightly increased by 3.2% (Figure 4.24).

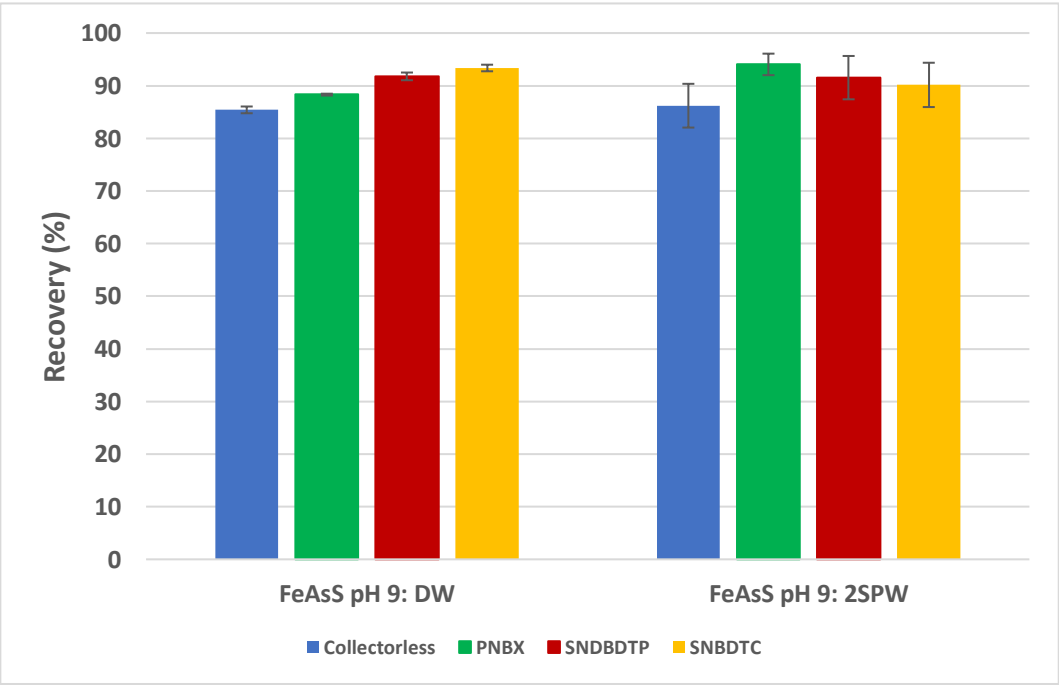

Figure 4.24 Microflotation recoveries of arsenopyrite with no reagent and standard collectors at pH 9 in distilled water (DW) compared to plant water (2SPW), with 20 ppm MIBC frother.

A decrease in the recovery using PNBX (5.7%) was observed, resulting in a similar trend observed for pyrite under the same conditions.

4.3.4. Cooperite

Cooperite was included in this study as a sulphide PGM that is known to float well. It is also a sulphide mineral that consists of one sulphur ligand, and it has a tetragonal crystal structure. It was hoped that these experiments would contribute to a better understanding of the behaviour of sperrylite by comparing their flotation behaviours, interactions with collectors and surface characteristics.

4.3.4.1. Standard Test

Cooperite had a very good natural flotation response of 94.8% (Figure 4.25). Adding 1 pseudo-monolayer coverage of the thiol collectors thus did not lead to much improvement in the mineral recovery. The highest recovery attained after adding the collectors was 97%, which confirmed the exceptionally good natural floatability of the cooperite mineral.

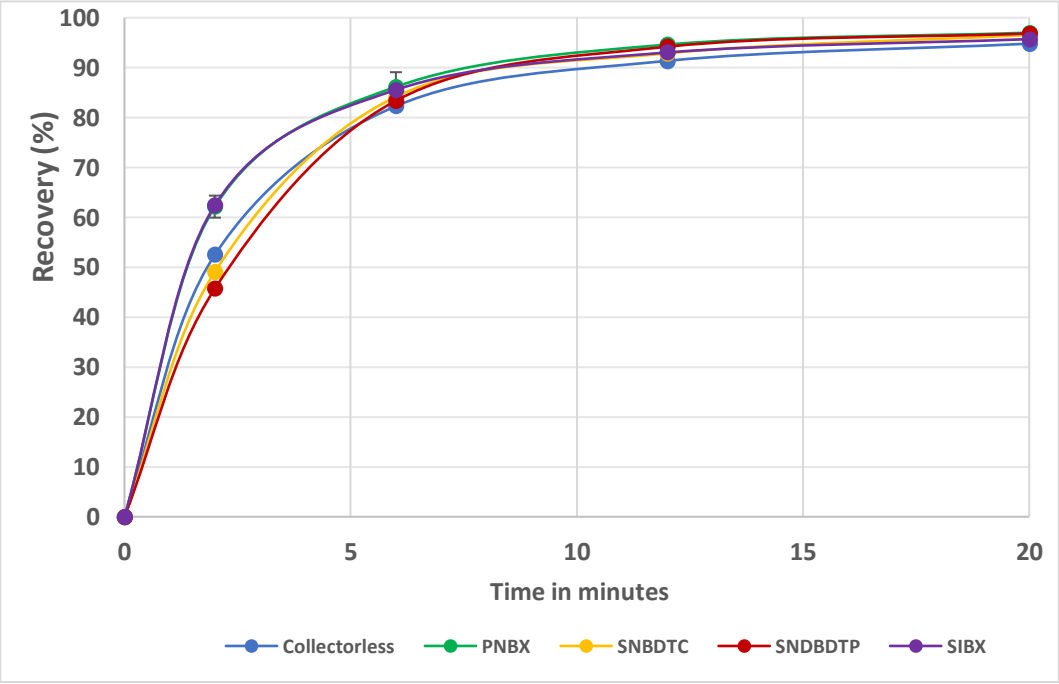

Figure 4.25 Microflotation recovery-time graphs of cooperite with no reagent and standard collectors at pH 9 in synthetic plant water, I= 4.84E-2 M and 20 ppm MIBC frother.

4.3.5. Summary of Flotation Results

This section gives a summary of the results across the different mineral types. The research approach sought to compare the behaviour of the different minerals based on their crystal structures and the number and types of bonding ligands on the mineral surface (As, S).

4.3.5.1. Comparing the floatability of the different minerals

Figure 4.26 shows the standard tests flotation recoveries of all the minerals at pH 9. Sperrylite (14.5%) and pyrite (17.8%), which have an isometric crystal structure gave low collectorless flotation recoveries. The collector-induced recoveries were significantly higher for pyrite with PNBX and, to a lesser extent SNBDTC while the response from both these collectors remained low on sperrylite.

On the other hand, arsenopyrite and cooperite, which have monoclinic and trigonal crystal structures, respectively, showed extremely good natural floatability. The addition of collectors had little effect since the natural floatability was already so high for both minerals.

Cooperite which consists of only one sulphur donor atom and a trigonal crystal structure gave the highest collectorless recovery and minimal improvement after adding the collectors compared to all the tested minerals. The symbol ND on arsenopyrite and pyrite indicates that no tests were done with SIBX.

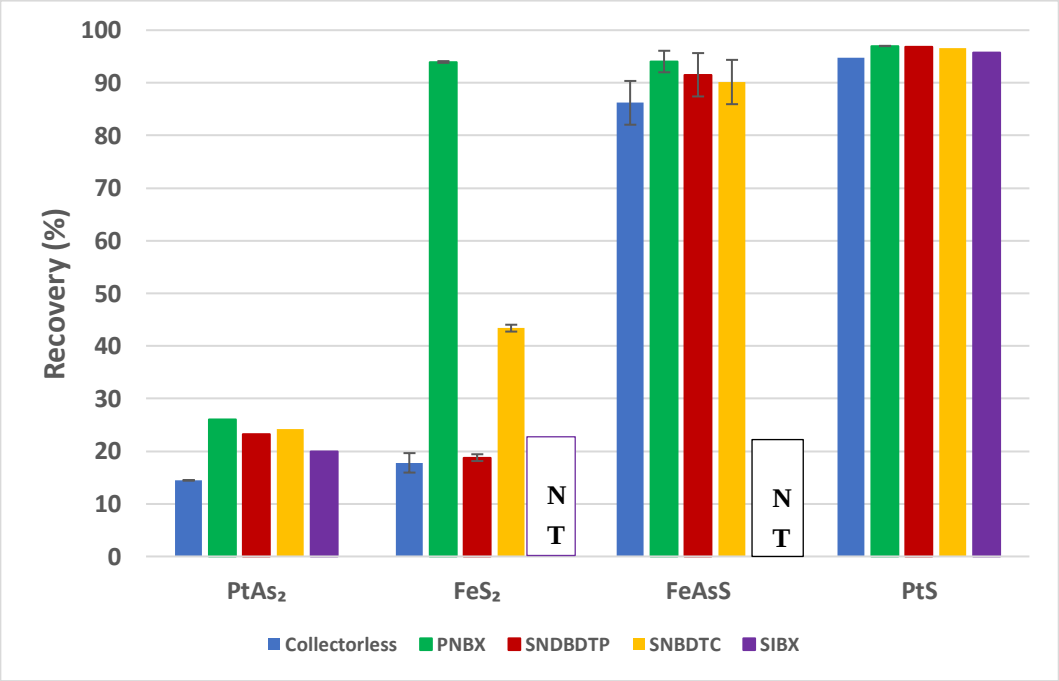

Figure 4.26 A comparison of microflotation recoveries of selected minerals with no reagent and standard collectors at pH 9 in synthetic plant water, I= 4.84E-2 M and 20 ppm MIBC frother. NT = not tested

4.3.5.2. *Effect of Dissolved Ions*

The effect of dissolved ions was also investigated on the recoveries of pyrite and arsenopyrite at pH 9 (Figure 4.27).

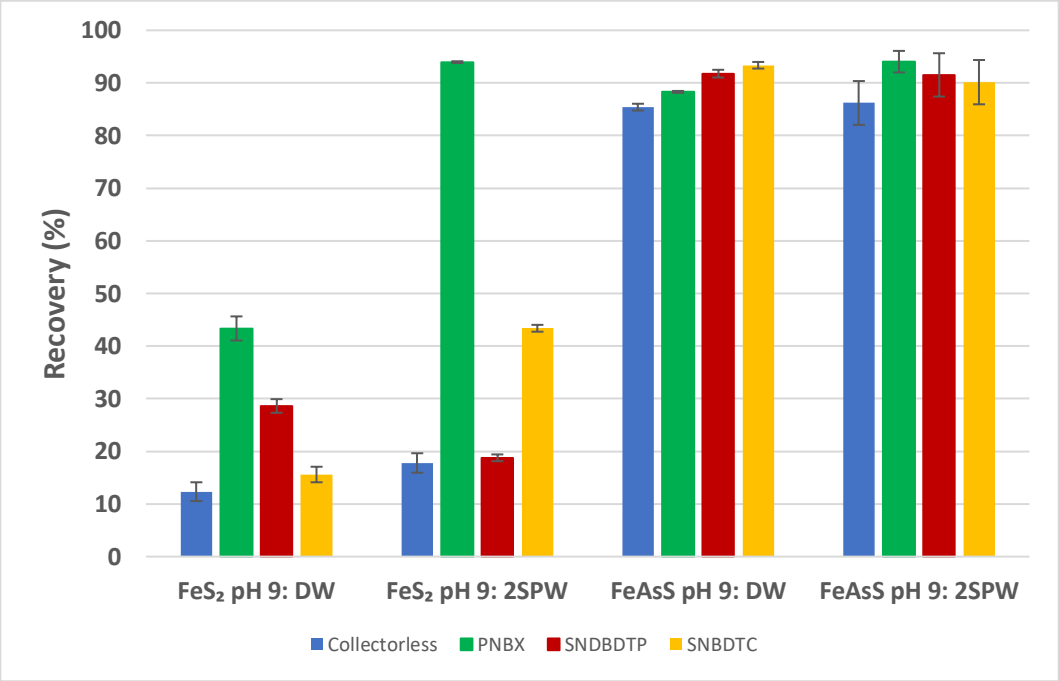

Figure 4.27 A comparison of microflotation recoveries of pyrite and arsenopyrite with no reagent and standard collectors at pH 9 in distilled water and synthetic plant water, I= 4.84E-2 M and 20 ppm MIBC frother.

There was an insufficient sample to extend these tests to the platinum-containing minerals. The natural floatability of pyrite was improved by 5.5% in plant water. In addition, the recovery with PNBX dramatically improved in the presence of ions, from 43% in DI water to 94% in synthetic plant water. The recovery of pyrite with SNBDTC also improved, although to a lesser extent, from 16% to 43%. However, in the presence of ions, the recovery when using SNDBDTP was reduced by 9.8%. The floatability of arsenopyrite was relatively unaffected by the presence of ions, except for the PNBX recoveries which improved by 5.8% in plant water.

4.3.5.3. *Effect of pH*

A decrease in pulp pH is shown to affect the flotation response of both sperrylite and pyrite as shown in Figure 4.28. The recovery of sperrylite when using PNBX remained unchanged, while the recoveries of SNBDTC, SDTBAT and SDCDTDBAT were improved under acidic conditions. The natural floatability of pyrite was slightly reduced at pH 4 in distilled water. Collector induced recoveries were improved at pH 4 for all the collectors, especially for PNBX and SNDBDTP.

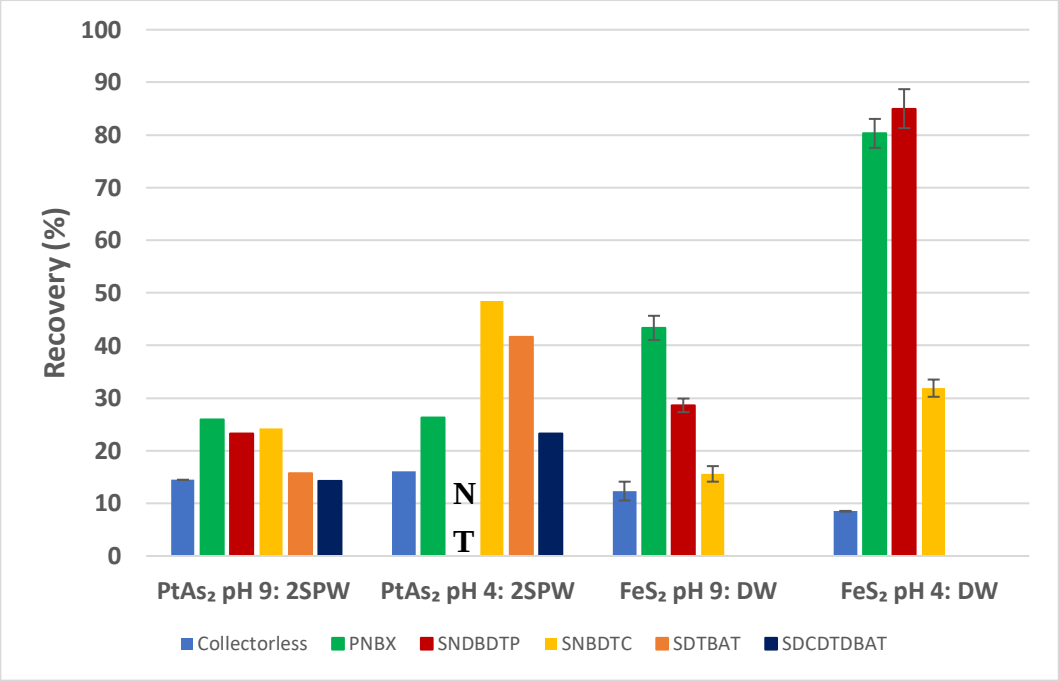

Figure 4.28 Microflotation recoveries of sperrylite and pyrite with no reagent and selected thiol collectors at pH 9 and pH 4 in distilled water and synthetic plant water, I= 4.84E-2 M and 20 ppm MIBC frother. NT = not tested

4.4. COLLECTOR ADSORPTION

Adsorption tests were carried out to further understand the interaction of the minerals with different collectors and to determine how the results relate to the flotation results of the respective minerals obtained. This will further shed light on the possible interaction of collectors on the tested minerals. All the tests were carried out at 1 pseudo-monolayer coverage based on the BET analysis of the mineral particles.

4.4.1. Sperrylite Adsorption at pH 9

UV-Vis spectrophotometry was used to determine the amount of standard and novel collectors adsorbed at pH 9, and to relate these results to the results obtained in the tests for flotation recovery of sperrylite. Figure 4.29 shows that there was minimal adsorption of the xanthate collectors at pH 9 with the exception of SNBDTC that had about 51.4% adsorption. Also, the novel collectors were not adsorbed onto sperrylite except for the SDTDBAT collector that which had the poor adsorption density of 1.7%. The lack of adsorption of these collectors onto the sperrylite surface corresponds with the poor flotation recoveries obtained when using these collectors. SNBDTC was the only collector that was tested that had an appreciable extent of adsorption onto the sperrylite surface at pH 9. However, this did not translate to an increase in flotation recovery as shown in Figure 2.27. The adsorption of SNDBDTP was not conclusive (NC) and the spectra are given in Appendix C.

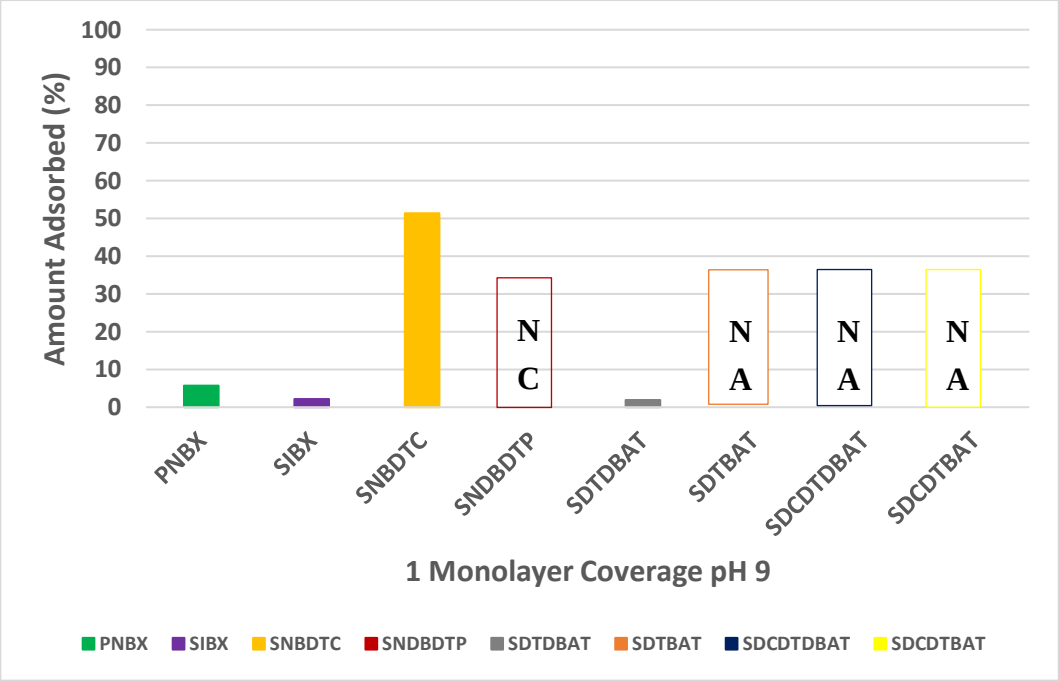

Figure 4.29 Amount of standard and novel collectors adsorbed on sperrylite, at 1 pseudo- monolayer coverage dosage, at pH 9, in distilled water. NC = not conclusive; NA = not adsorbed. For each collector the following wavelengths were used to calculate the adsorption densities: PNBX = 300nm, SIBX = 300nm, SNBDTC = 283nm, SNDBDTP = 231nm, SDTDBAT = 269nm, SDTBAT =266nm, SDCDTDBAT = 267nm, SDCDTBAT = 264nm.

4.4.1.1.1. Sperrylite Adsorption at pH 4

Figure 4.30 shows the amount of thiol and novel collectors adsorbed under acidic conditions. SNBDTC and the novel collectors, SDTBAT and SDCDTDBAT were adsorbed to a greater extent at pH 4 than pH 9 while PNBX was completely adsorbed under acidic conditions. On the other hand, the adsorption density of SNBDTC was reduced from 51.4% to 7.2% based on the peak at 317 nm as opposed to 283 nm at pH 9. This low calculated adsorption density is not consistent to the increase in the flotation recovery of sperrylite under acidic conditions.

There was a change in the SNBDTC, SDTBAT and SDCDTDBAT collectors' profiles, signifying a change in the collector molecules at pH 4, as addressed in Section 4.4.5. It was observed that there was a possible formation of the different surface products at pH 4 for the SDTBAT collector between the wavelengths of 250 nm to 300 nm (Appendix C) which could be responsible for the increased flotation recoveries. Hence, the adsorption density was calculated using the peaks at 317 nm, 318 nm and 316 nm respectively. The PNBX collector profile remained unchanged and the same peak of 300 nm was used to calculate the adsorption density at pH 4 and pH 9.

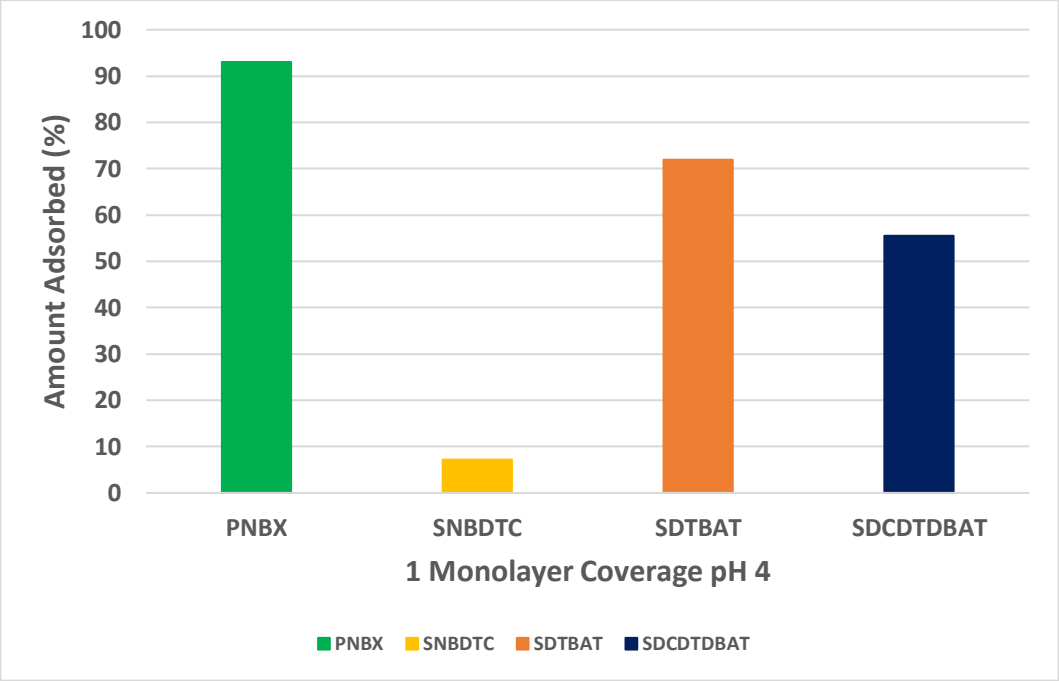

Figure 4.30 Amount of standard and novel collectors adsorbed on sperrylite, at 1 pseudo-monolayer coverage dosage, at pH 4, in distilled water. For each collector the following wavelengths were used to calculate the adsorption densities: PNBX = 300nm, SNBDTC = 317nm, SDTBAT =318nm, SDCDTDBAT = 316nm.

4.4.2. Pyrite Adsorption

Figure 4.31 shows the amount of thiol collectors adsorbed on pyrite at both pH 9 and pH 4.

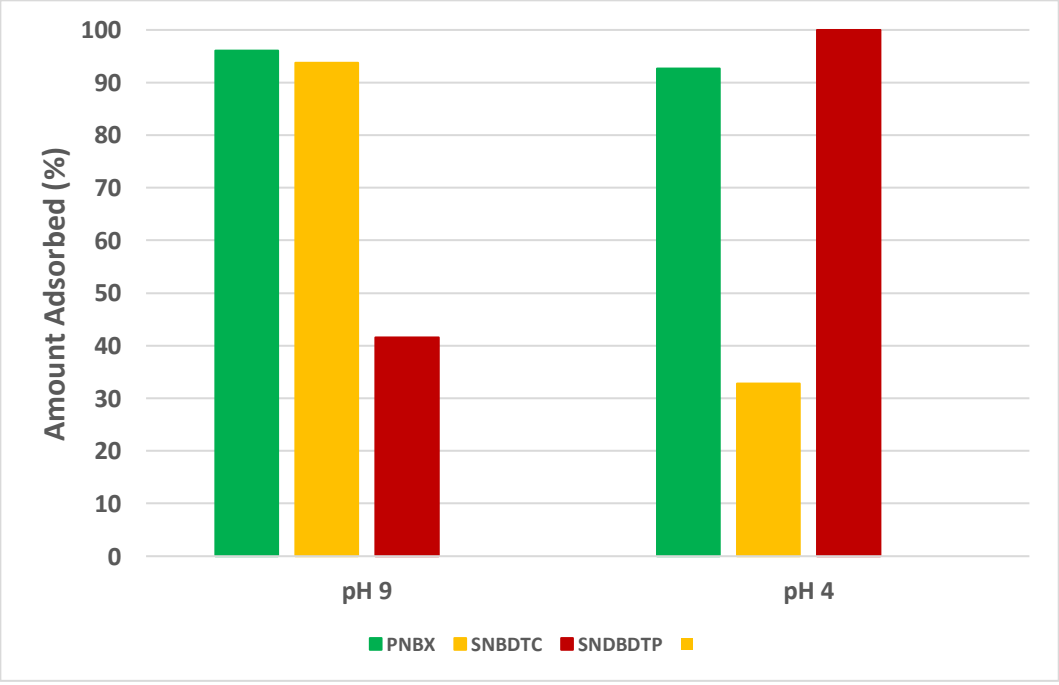

Figure 4.31 Amount of standard collectors adsorbed on pyrite, at 1 pseudo-monolayer coverage dosage, at pH 9 and pH 4, in distilled water. For each collector the following wavelengths were used to calculate the adsorption densities: PNBX = 300nm, SNBDTC = 283nm, SNDBDTP = 231nm at pH 9. Also, at pH 4 the wavelengths used for the calculations were PNBX = 300nm, SNBDTC = 317nm, SNDBDTP = 231nm.

The results show that at least 90% of the PNBX and SNBDTC collectors were adsorbed under alkaline conditions. SNDBDTP collector had the least adsorption density of 41.6% while it was fully adsorbed under acidic conditions. This is contrary to the behaviour of the same collectors with sperrylite where the highest amount of the adsorbed collector was 51.4% with SNBDTC at pH 9. There was a slight decrease in the PNBX collector adsorption at pH 9 while that of SNBDTC was reduced from 93.7% to 32.9%. Even though all the standard collectors exhibited a greater extent of adsorption onto the pyrite surface, these were associated with varying degrees of recovery from 19% (SNDBDTP at pH 9) to over 90% (PNBX pH 9). The moderate recovery with the SNBDTC did not correspond to the fairly high collector adsorption onto the mineral. The mineral adsorption spectra are given in Appendix D.

4.4.2.1. Novel Collectors

The adsorption of the novel collectors on pyrite at pH 9 was also investigated and compared to that of sperrylite. Figure 4.32 shows that the novel collectors were adsorbed on the pyrite mineral surface to a greater extent (above 80%) than sperrylite. The extent of adsorption also corresponds well with the flotation recoveries obtained, which ranged from 60.4% to 92%.

On the other hand, the three novel collectors were not adsorbed onto sperrylite, while 1.9% of SDTDBAT collector was adsorbed on sperrylite under the same test conditions.

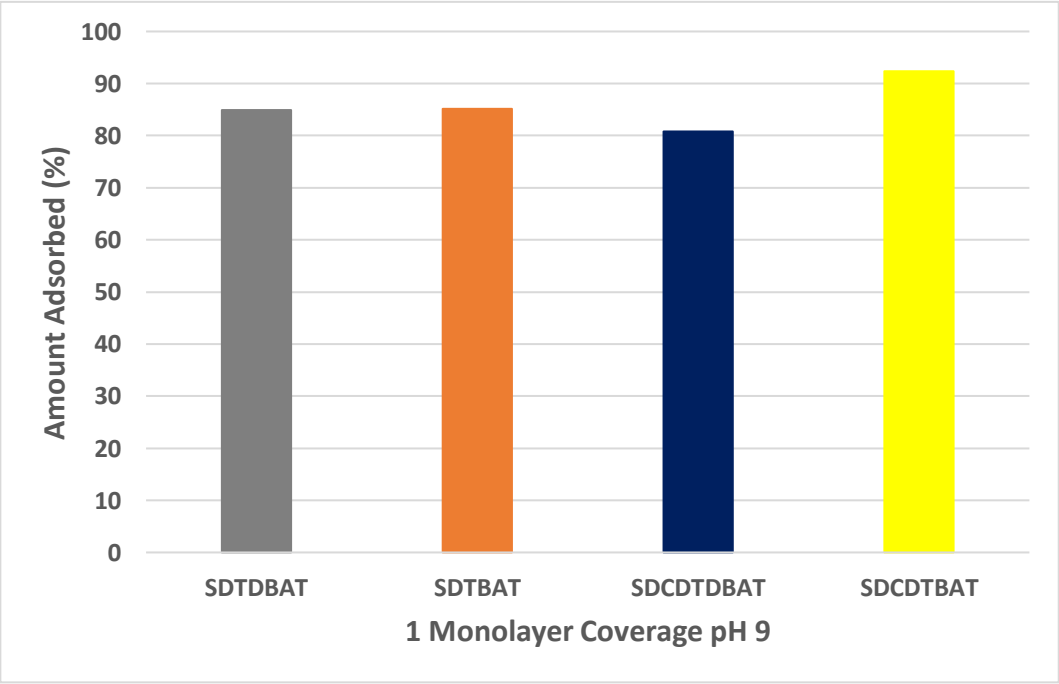

Figure 4.32 Amount of novel collectors adsorbed on pyrite, at 1 pseudo-monolayer coverage dosage, at pH 9, in distilled water. For each collector the following wavelengths were used to calculate the adsorption densities: SDTDBAT = 269nm, SDTBAT =266nm, SDCDTDBAT = 267nm, SDCDTBAT = 264nm.

4.4.3. Arsenopyrite Adsorption

Adsorption tests were carried out at pH 9 and pH 4, at one monolayer collector dosage using the thiol collectors. The results given in Figure 4.33 show that the amount of PNBX and SNBDTC adsorbed were 29.9% and 78.4% respectively.

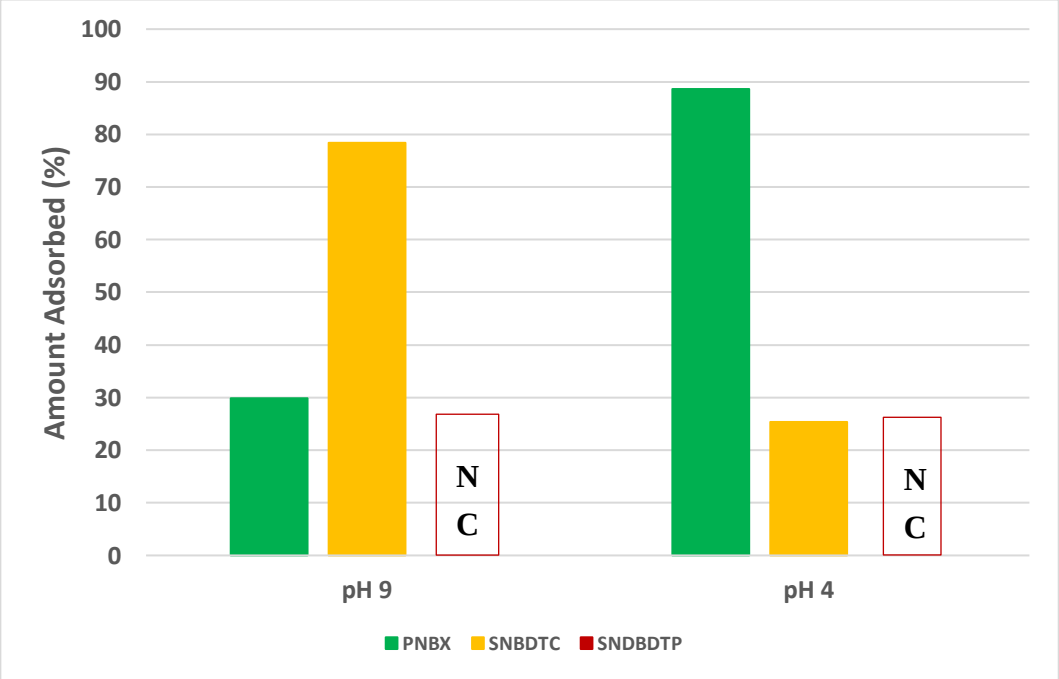

Figure 4.33 Amount of standard collectors adsorbed on arsenopyrite, at 1 pseudo-monolayer coverage dosage, at pH 9 and pH 4, in distilled water. NC = not conclusive. For each collector the following wavelengths were used to calculate the adsorption densities: PNBX = 300nm, SNBDTC = 283nm, SNDBDTP = 231nm at pH 9. Also, at pH 4 the wavelengths used for the calculations were PNBX = 300nm, SNBDTC = 317nm, SNDBDTP = 231nm

The SNDBDTP profile indicated a possible transformation to another product with an absorption peak at around 300 nm, and the result was not conclusive (Figure 4.34). There was an increase in the adsorption density of PNBX to 88.6% at pH 4. SNBDTC adsorption density was reduced from 78.4% to 25.4% under acidic conditions. The SNDBDTP peak was obscured beneath the spectrum of the arsenopyrite "blank" (dissolution of FeAsS into solution, with no collector present) and it was, thus, not possible to draw any conclusions with respect to SNDBDTP adsorption at pH 4. However, it could be reliably concluded that it was not the same transformation as an alternative SNDBDTP product, as was noted at pH 9 (Appendix E).

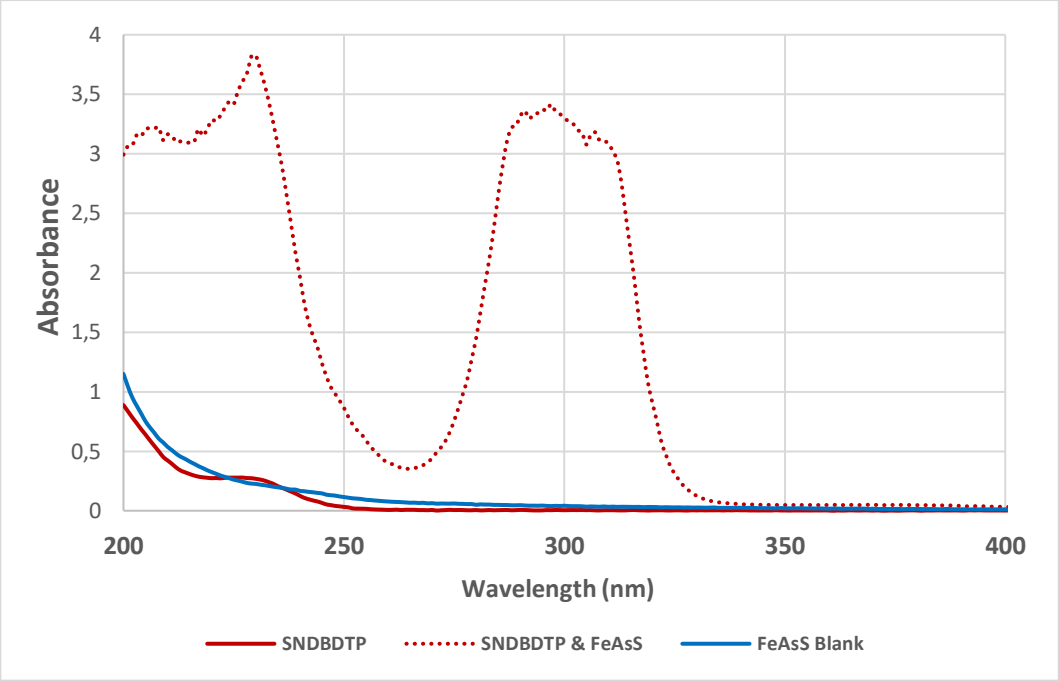

Figure 4.34 The adsorption profiles of the SNDBDTP, FeAsS blank and SNDBDTP contacted with FeAsS that suggested the formation of the unknown product.

4.4.4. Cooperite Adsorption

Adsorption tests were also carried out to understand the cooperite interactions with the collectors. Figure 4.35 shows that PNBX was not fully adsorbed on the mineral surface, at 83.6%, while SNDBDTP was not adsorbed at all. SNBDTC gave the highest adsorption density of 88.2% under alkaline conditions and the lowest adsorption density of 56.3% under acidic conditions. However, at pH 4, the adsorption densities of PNBX and SNDBDTP were increased to 97.3 and 100% respectively. The mineral adsorption spectra are given in Appendix F.

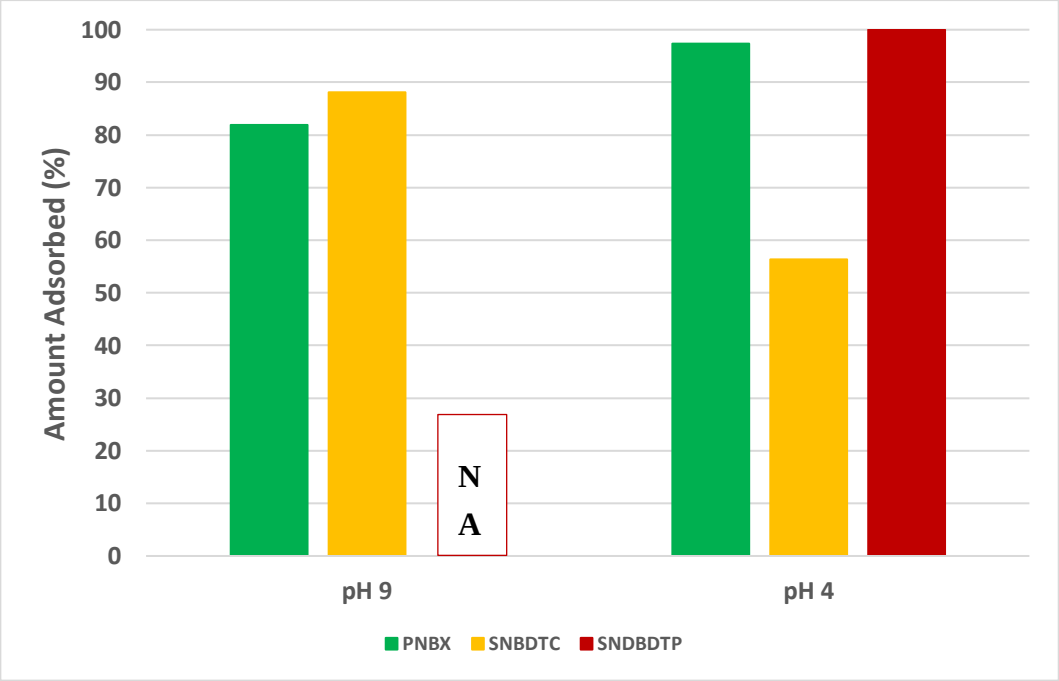

Figure 4.35 Amount of standard collectors adsorbed on cooperite, at 1 pseudo-monolayer coverage dosage, at pH 9 and pH 4, in distilled water. NA = not adsorbed. For each collector the following wavelengths were used to calculate the adsorption densities: PNBX = 300nm, SNBDTC = 283nm, SNDBDTP = 231nm at pH 9. Also, at pH 4 the wavelengths used for the calculations were PNBX = 300nm, SNBDTC = 317nm, SNDBDTP = 231nm.

4.4.5. Transformation of Collector Molecules with pH

A transformation of collectors, indicated by a change in the UV-Vis spectra, under acidic conditions was noted for SNBDTC, SDTBAT, and SDCDTDBAT collectors.

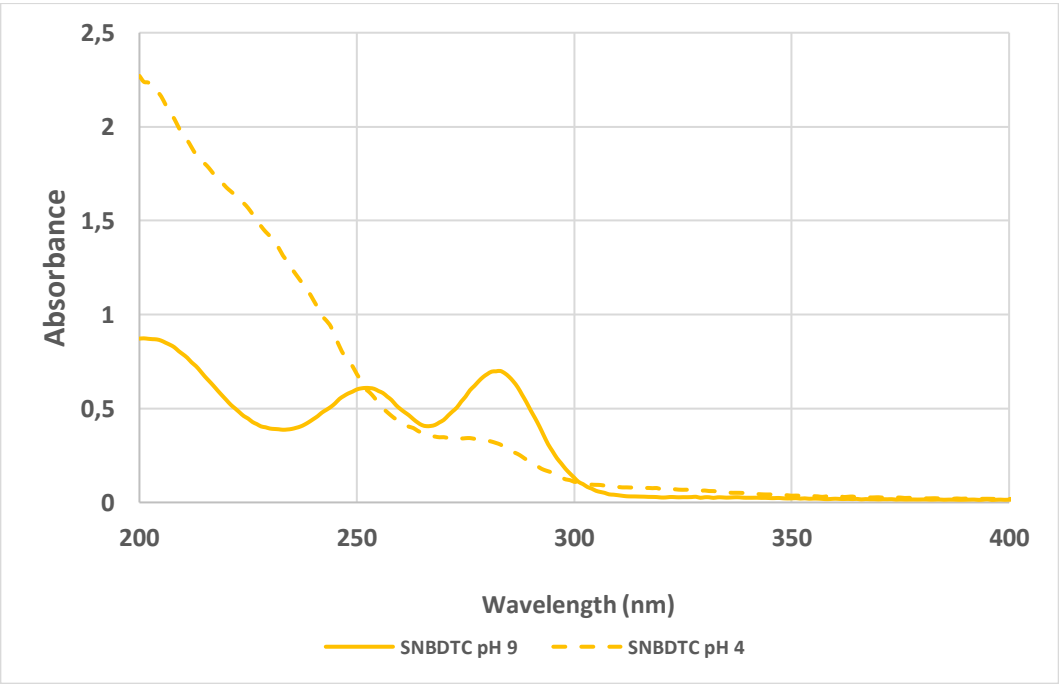

Figure 4.36 A comparison of the SNBDTC profiles and absorbance peaks at pH 9 and pH 4

It can be seen in Figure 4.36 that SNBDTC at pH 9 has 2 peaks at 252 nm and 283 nm, respectively. At pH 4, there is only a single peak visible with a peak at approximately 276 nm and a lower molar extinction coefficient. The profiles of the SDTBAT given in Figure 4.37 also show a transformation of the absorption spectra under acidic conditions.

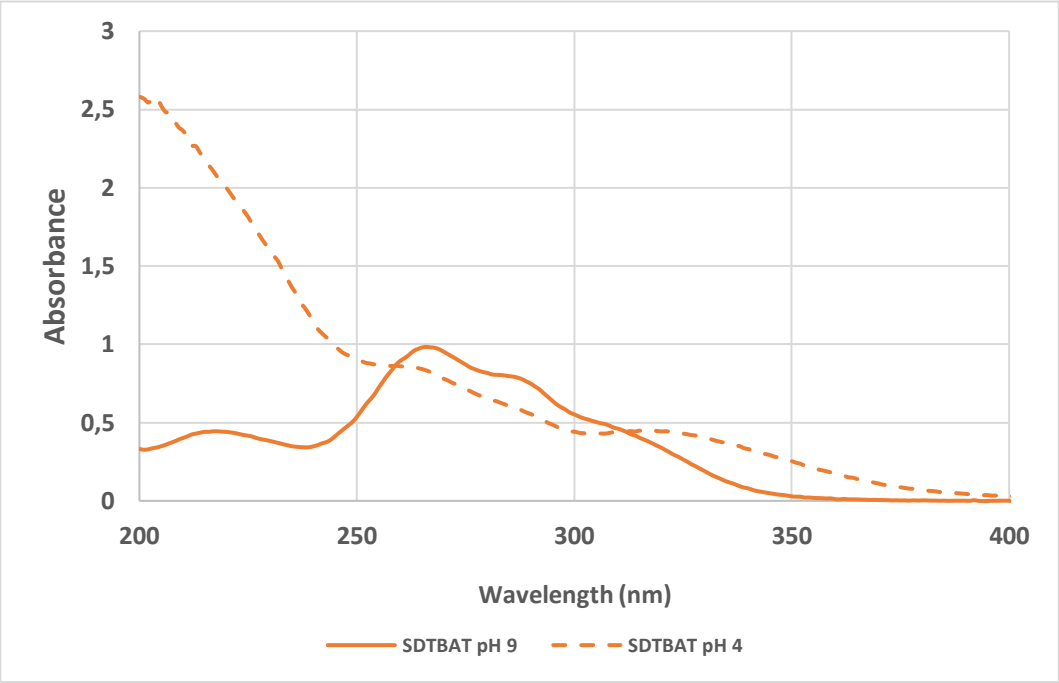

Figure 4.37 A comparison of the SDTBAT profiles and absorbance peaks at pH 9 and pH 4

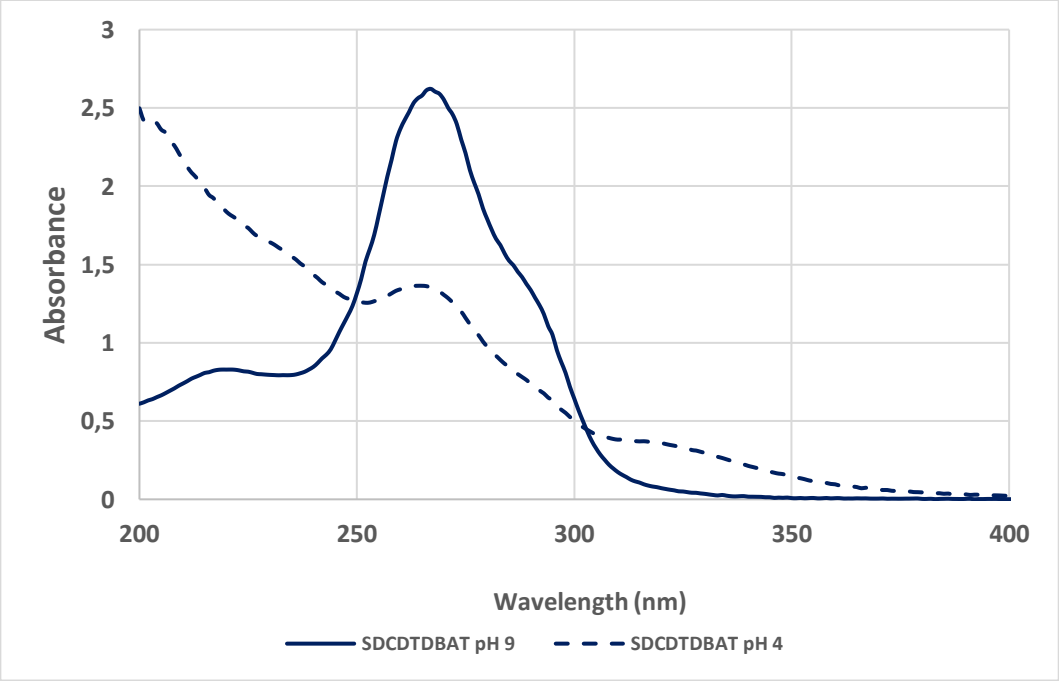

Figure 4.38 A comparison of the SDCDTDBAT profiles and absorbance peaks at pH 9 and pH 4

It appeared that the peak at 269 nm was maintained for the SDCDTDBAT collector under acidic conditions, but that incomplete transformation to another product may have occurred (Figure 4.38).

4.4.6. Summary of Adsorption Tests at pH 9

A comparison of the amount of collectors adsorbed on the minerals at pH 9 is given in Figure 4.39. SNDBDTP collector was only adsorbed onto pyrite. Also, relatively lower amounts of PNBX were adsorbed onto sperrylite and arsenopyrite compared to the sulphide minerals.

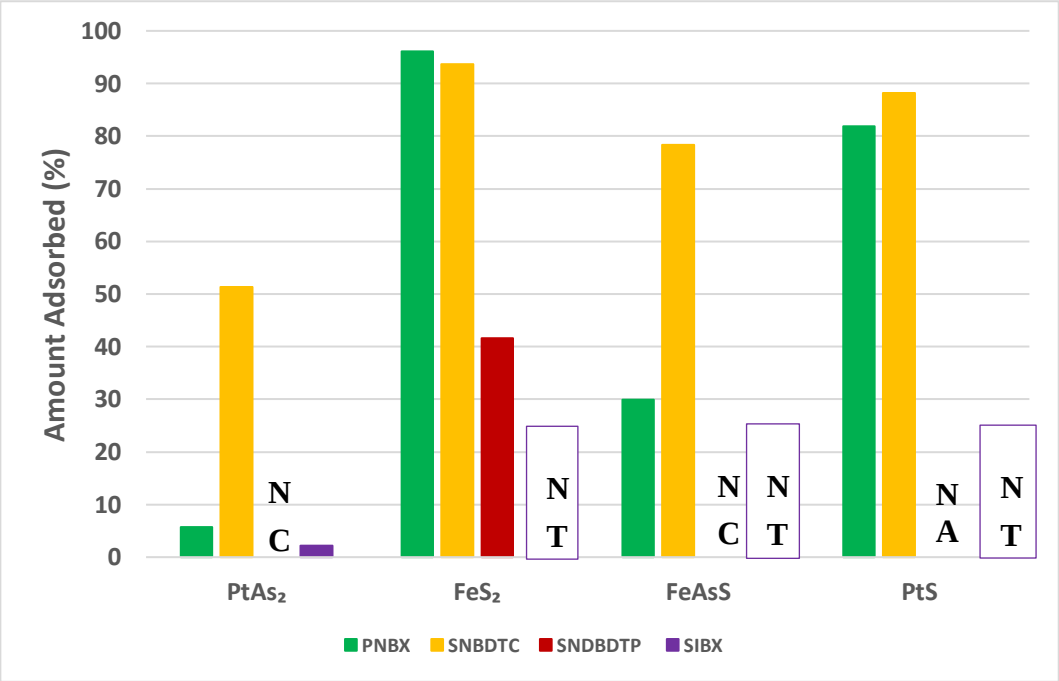

Figure 4.39 Amount of standard collectors adsorbed on minerals, at 1 pseudo-monolayer coverage dosage, at pH 9, in distilled water. SIBX adsorption was only carried out using sperrylite. NC = not conclusive. NT = not tested. NA = not adsorbed. For each collector the following wavelengths were used to calculate the adsorption densities: PNBX = 300nm, SNBDTC = 283nm, SNDBDTP = 231nm.

4.4.6.1. Novel Collectors

A comparison between the amount of novel collectors adsorbed onto sperrylite and pyrite is given in Figure 4.40. The novel collectors were adsorbed to a greater extent onto pyrite as opposed to sperrylite, which has the As donor atoms on its surface.

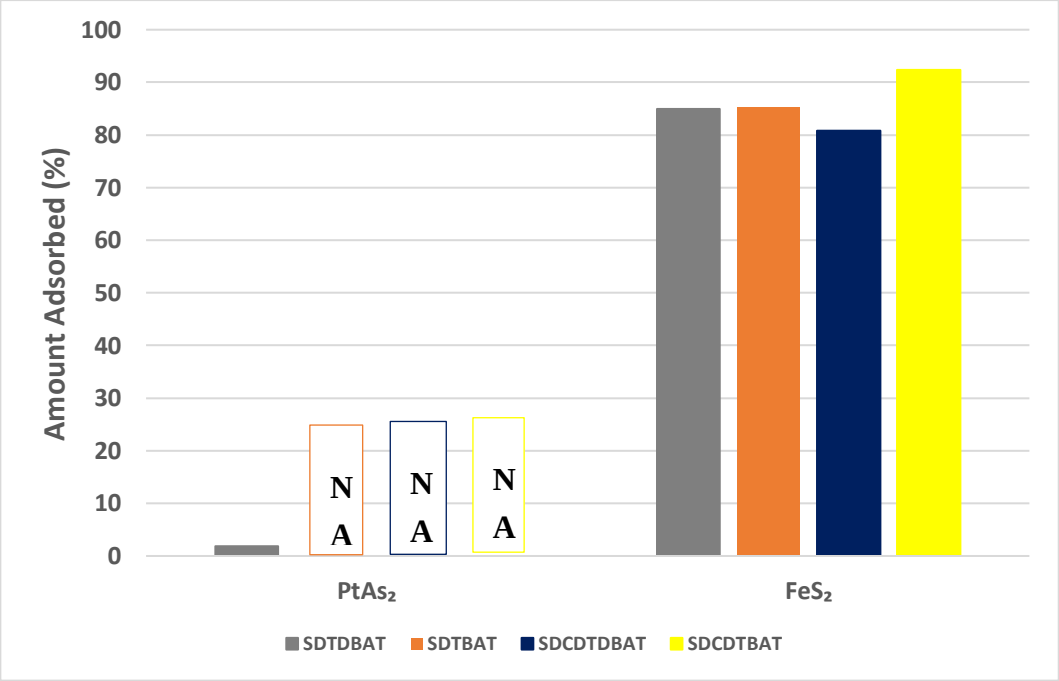

Figure 4.40 Amount of novel collectors adsorbed on sperrylite and pyrite, at 1 pseudo-monolayer coverage dosage, at pH 9, in distilled water. NA = not adsorbed. For each collector the following wavelengths were used to calculate the adsorption densities: SDTDBAT = 269nm, SDTBAT =266nm, SDCDTDBAT = 267nm, SDCDTBAT = 264nm.

4.5. REST POTENTIAL TEST RESULTS

The rest potentials of selected minerals were determined before and after adding the standard collectors at pH 9.5 and pH 3.5, and collector dosages were maintained at a concentration of 6.24 x 10^{-4} M in the reaction vessel for all the experiments. The extent of interaction with collectors, indicated by the magnitude of the decrease in potential after adding the collectors, at 600 seconds, was determined. Furthermore, surface products that are likely to be formed after adding the collector are determined by the final rest potential of the mineral at 1200 seconds. If the final rest potential lies above the dithiolate/metal thiolate equilibrium potential line of the collector, a dithiolate is most likely to be formed. On the contrary, when the final rest potential of the mineral lies below the dimerization equilibrium potential of a collector, a metal thiolate will most probably be formed. All the rest potential values in this study were converted to the Standard Hydrogen Electrode (SHE) values.

4.5.1. Sperrylite

Rest potential measurements were carried out to determine the rest potentials of both the natural and synthetic sperrylite electrodes before and after adding the standard collectors. The synthetic sperrylite electrode will act as a guiding factor on the extent to which the synthetic mineral resembles the natural sperrylite.

4.5.1.1. Natural Sperrylite at pH 9.5

The average rest potential of the natural sperrylite from the plotted data before adding the collectors at 600 seconds was 233.7 ± 7.2 mV as shown in Figure 4.41. The mineral showed very little interaction with all the collectors as indicated by the small decrease in potential after adding the collectors. The order for the extent of interaction as indicated by the decrease in rest potential: SNBDTC (24.9 mV) > PNBX (17.6 mV) > SNDBDTP (7.9 mV). Despite the minimal interaction of the mineral with the collectors, the prediction of surface products suggests that dithiolates would form on the mineral surface.

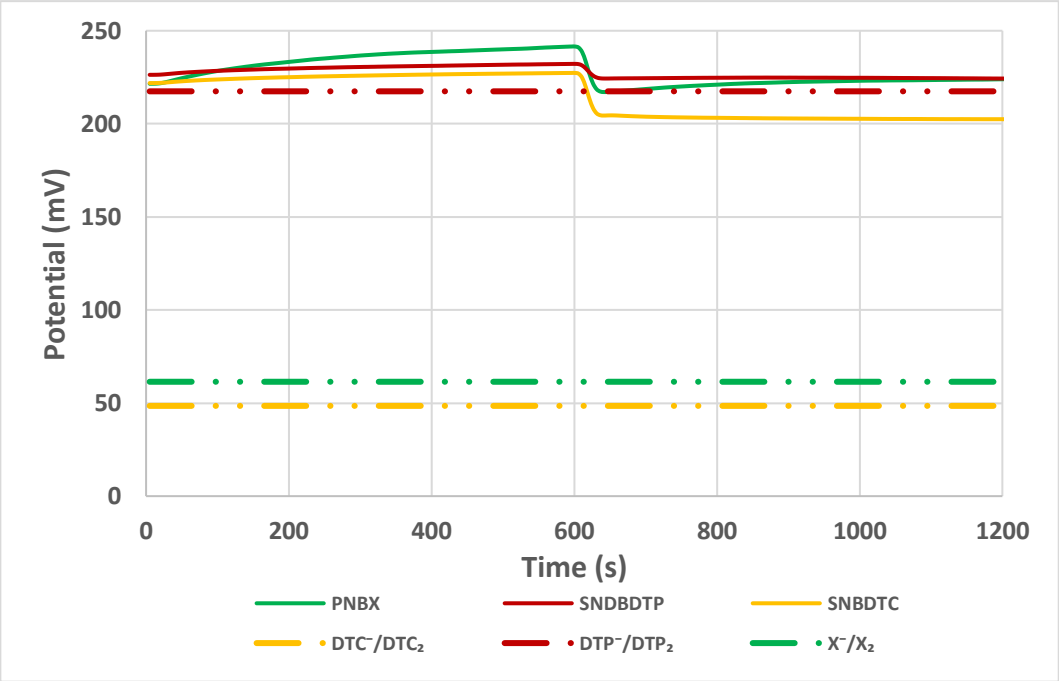

Figure 4.41 Rest potential results of natural sperrylite in the absence and presence of standard collectors, after 600 seconds, at pH 9.5 The dotted lines indicate the oxidation potential of the standard collectors.

4.5.1.2. Natural Sperrylite at pH 3.5

The interactions of the natural sperrylite electrode with the thiol collectors at pH 3.5 is given in Figure 4.42. The average rest potential of the natural sperrylite before adding the collectors at 600 seconds was 243.7 ± 10.7 mV. It is worth noting that there was only a slight increase of 10 mV in the rest potential of sperrylite under acidic conditions. This increase is within the calculated standard deviation of the rest potentials at pH 3.5 and pH 9.5 and it can be concluded that the sperrylite surface remained unaltered. The mineral showed a marked increase in the extent of interaction upon the addition of the collectors compared to higher pH's. PNBX and SNBDTC reacted to a far greater extent compared to SNDBDTP. In this case, a change in the order of interaction as indicated by the decrease in rest potential was observed as opposed to the one at pH 9.5, where PNBX had the greater extent of interaction as opposed to SNBDTC: PNBX (126 mV) > SNBDTC (107 mV) > SNDBDTP (44.4 mV).

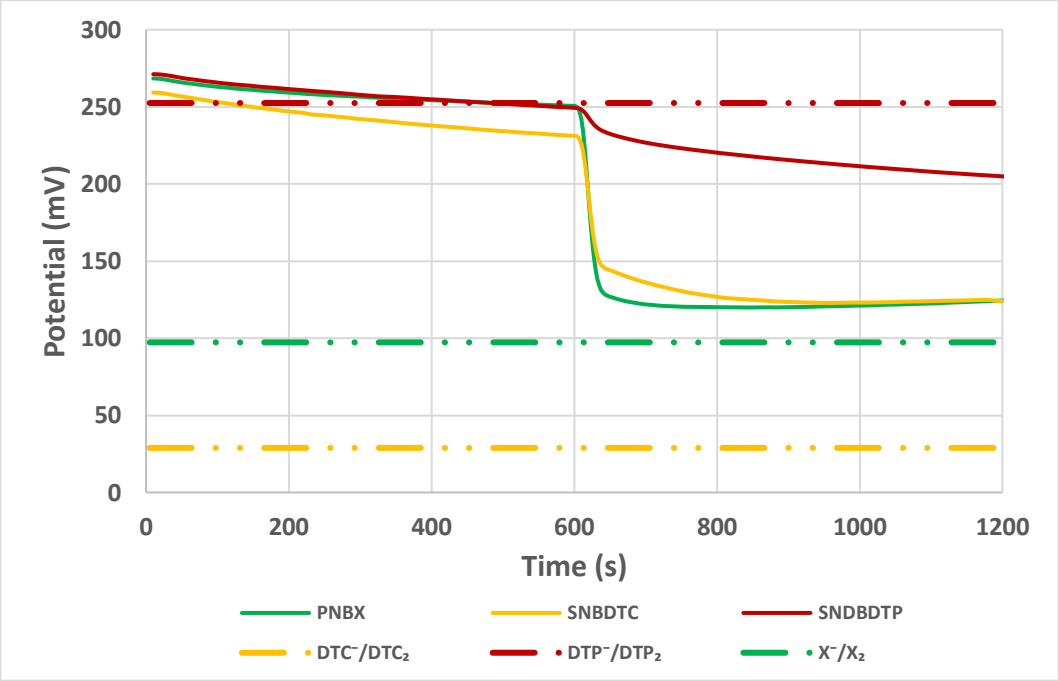

Figure 4.42 Rest potential results of natural sperrylite in the absence and presence of standard collectors, after 600 seconds, at pH 3.5 The dotted lines indicate the oxidation potentials of the standard collectors.

Dithiolates were expected to form with PNBX and SNBDTC. However, due to the high oxidation potential of SNDBDTP, it is suggested that, if anything, the metal thiolate will be formed with sperrylite.

4.5.1.3. Synthetic Sperrylite at pH 9.5

The synthetic electrode gave an average rest potential of 204.6 ± 3.2 mV before adding the collectors at 600 seconds (Figure 4.43) which was 29.1 mV less than the natural sperrylite. The standard deviation of the rest potentials is also an indication that the mineral surface was fairly similar throughout the tests. Also, the difference in the rest potentials of the natural and synthetic sperrylite electrodes did not exceed 50 mV indicating that the minerals were relatively similar. This indicates that the electrochemical potential of the two surfaces was relatively similar, with the synthetic sperrylite being slightly less cathodic than the natural sperrylite.

Just like in the case of the natural sperrylite, the synthetic mineral showed very little interaction with all the collectors as indicated by the final rest potentials after adding the collectors. For the tested collectors, the order for the extent of interaction as indicated by the decrease in rest potential was SNBDTC (10.4 mV) > PNBX (6.7 mV) > SIBX (3.2 mV). The dithiolates were predicted to form on the synthetic sperrylite with all the collectors under alkaline conditions.

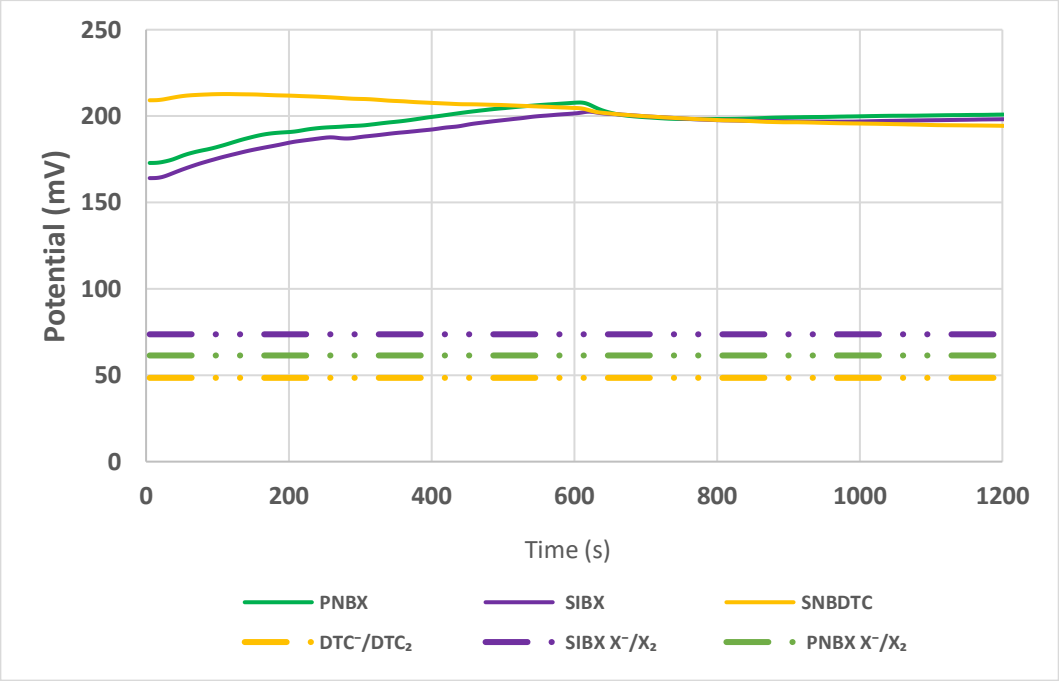

Figure 4.43 Rest potential results of synthetic sperrylite in the absence and presence of xanthate and SNBDTC collectors, after 600 seconds, at pH 9.5 The dotted lines indicate the oxidation potentials of the xanthate and SNBDTC collectors.

4.5.1.4. Synthetic Sperrylite at pH 3.5

The average rest potential for the synthetic sperrylite electrode at pH 3.5 was 262.6 ±1.3 mV, with the difference between the natural sperrylite and synthetic sperrylite rest potentials at pH 3.5 being 18.6 mV.

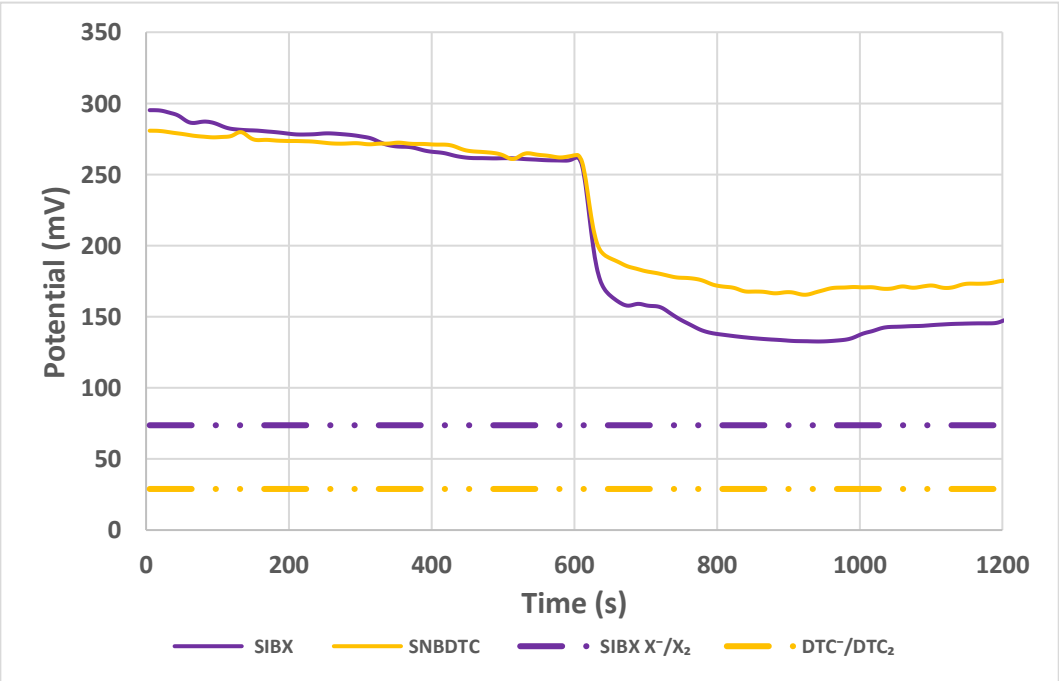

Figure 4.44 Rest potential results of synthetic sperrylite in the absence and presence of SIBX and SNBDTC, after 600 seconds, at pH 3.5 The dotted lines indicate the oxidation potentials of SIBX and SNBDTC collectors.

The synthetic electrode average rest potential increased by 58 mV under acidic conditions as shown in Figure 4.44, compared to the 10 mV increase noticed for the natural sperrylite. Once again, this illustrates relatively little change in the mineral surface with decreasing pH. After adding SIBX and SNBDTC collectors, the decrease in the rest potentials trend was the same as that observed on the natural sperrylite, whereby the extent of interaction was greater for the xanthate collector in comparison to SNBDTC. The decrease in potentials was 114.2 mV and 88.2 mV, respectively. Both collectors indicated the formation of the dithiolate with the mineral surface. Tests could not be carried out with the other standard collectors because the electrode was no longer in working condition. However, the results generated were enough to draw conclusions that the electrode resembled the natural sperrylite electrode in rest potentials and extent of interactions. The interactions with SIBX and SNBDTC collectors predicted the formation of dithiolates under alkaline conditions.

4.5.2. Pyrite Rest Potential Results

The interaction of pyrite with different thiol collectors was investigated to determine the effect of the isometric crystal structure and the sulphur donor atoms as opposed to arsenic donor atoms in sperrylite. The results are given below.

4.5.2.1. Pyrite at pH 9.5

The average rest potential of pyrite before adding the collectors at 600 seconds was 284.2 ±3.7 mV (Figure 4.45).

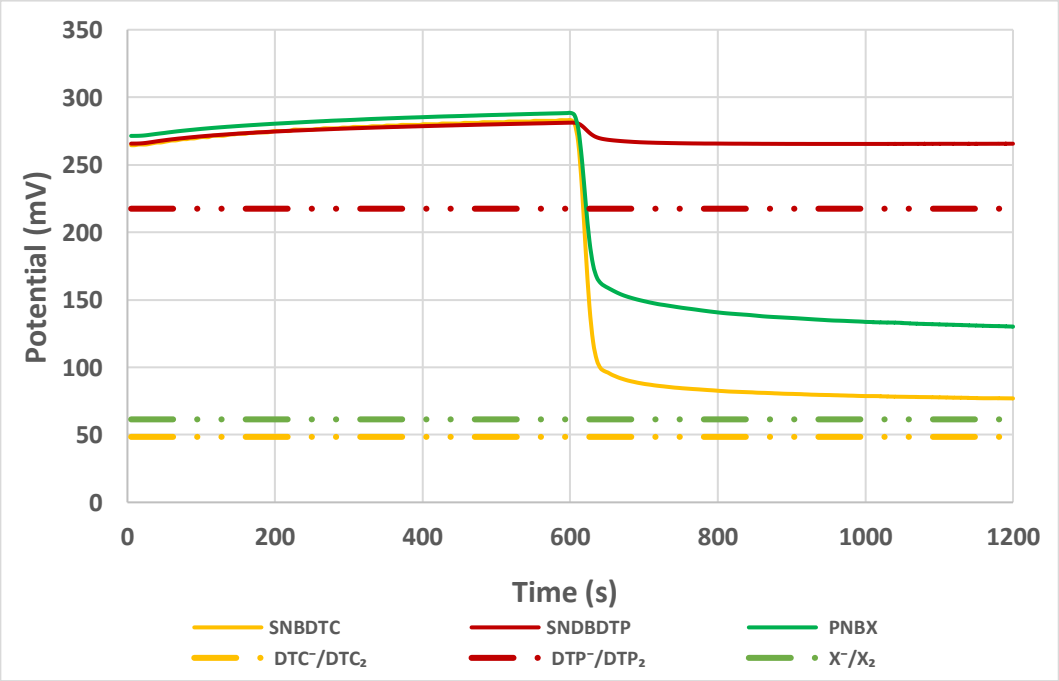

Figure 4.45 Rest potential results of pyrite in the absence and presence of standard collectors, after 600 seconds, at pH 9.5 The dotted lines indicate the oxidation potentials of the standard collectors.

The mineral showed a greater extent of interaction with PNBX, and SNBDTC as indicated by the final rest potentials after adding the collectors when compared to sperrylite. The decrease in potentials after each collector addition were in order: SNBDTC (206.1 mV) > PNBX (158.3 mV) > SNDBDTP (15.6 mV). There was still very little interaction between the pyrite and SNDBDTP. The final rest potentials suggest the formation of the dithiolates for all the collectors.

4.5.2.2. Pyrite at pH 3.5

Compared to pH of 9.5 a more positive average rest potential of pyrite, viz. 411.5 +1.1 mV, an increase of 127.3 mV was observed at pH 3.5, before adding the collectors (Figure 4.46).

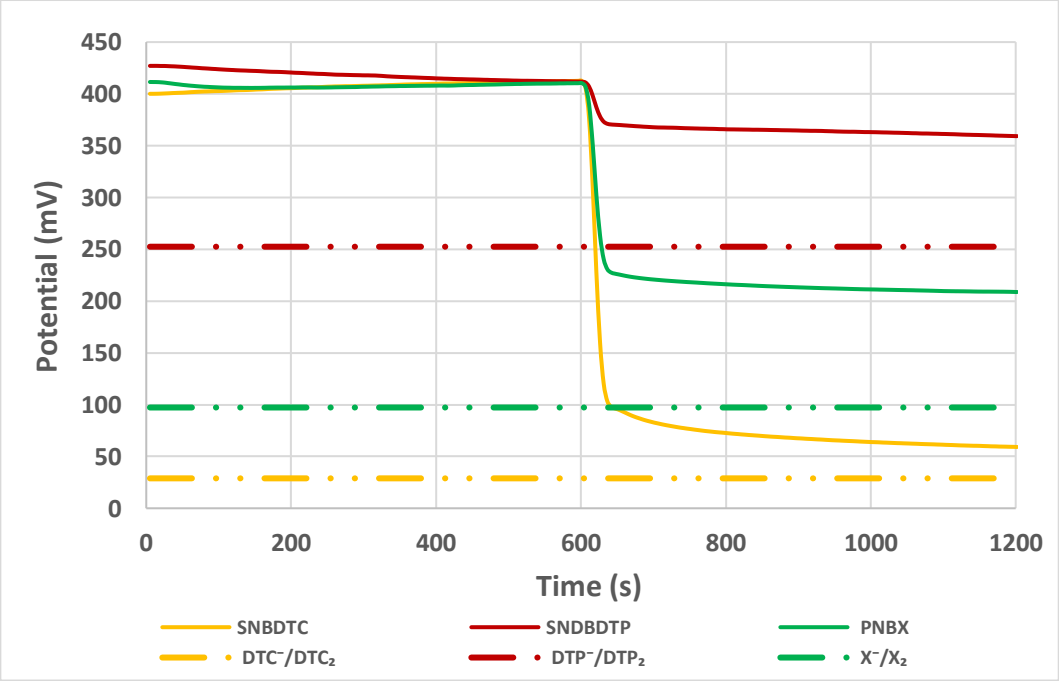

Figure 4.46 Rest potential results of pyrite in the absence and presence of standard collectors, after 600 seconds, at pH 3.5 The dotted lines indicate the oxidation potentials of the standard collectors.

This is a significant increase in the rest potential of pyrite at pH 3.5 as opposed to sperrylite which hardly showed any change in potential at the same pH. The mineral showed a greater extent of interaction with all the collectors as indicated by the final rest potentials after adding the collectors as opposed to sperrylite under the same conditions. The order for the extent of interaction was SNBDTC (353.3 mV) > PNBX (201.6 mV) > SNDBDTP (52.6 mV). The decrease in potential was also greater than that of pyrite at pH 9.5 after adding the thiol collectors. The formation of the dithiolates was also predicted to form on the mineral surface.

4.5.3. Arsenopyrite Rest Potential Results

Rest potential measurements were carried out with arsenopyrite to further investigate the effects of donor atoms (S, As) on the mineral surface and the effect of a monoclinic crystal structure.

4.5.3.1. Arsenopyrite at pH 9.5

The average rest potential of arsenopyrite, given in Figure 4.47, before adding the collectors at 600 seconds was 179 ± 26.7 mV. It gave the lowest rest potential of all the selected minerals at a pH of 9.5. The mineral showed a lesser extent of interaction with all the collectors as indicated by the potential drop after adding the collectors compared to pyrite and cooperite.

However, the drop in potential was greater than that observed for sperrylite after adding the collectors. The order for the extent of interaction was: SNBDTC (95.4 mV) > PNBX (45 mV) > SNDBDTP (10.4 mV). The final rest potentials indicate that, if anything, a metal thiolate is likely to form with SNDBDTP whereas the formation of the dithiolate was predicted for PNBX and SNBDTC.

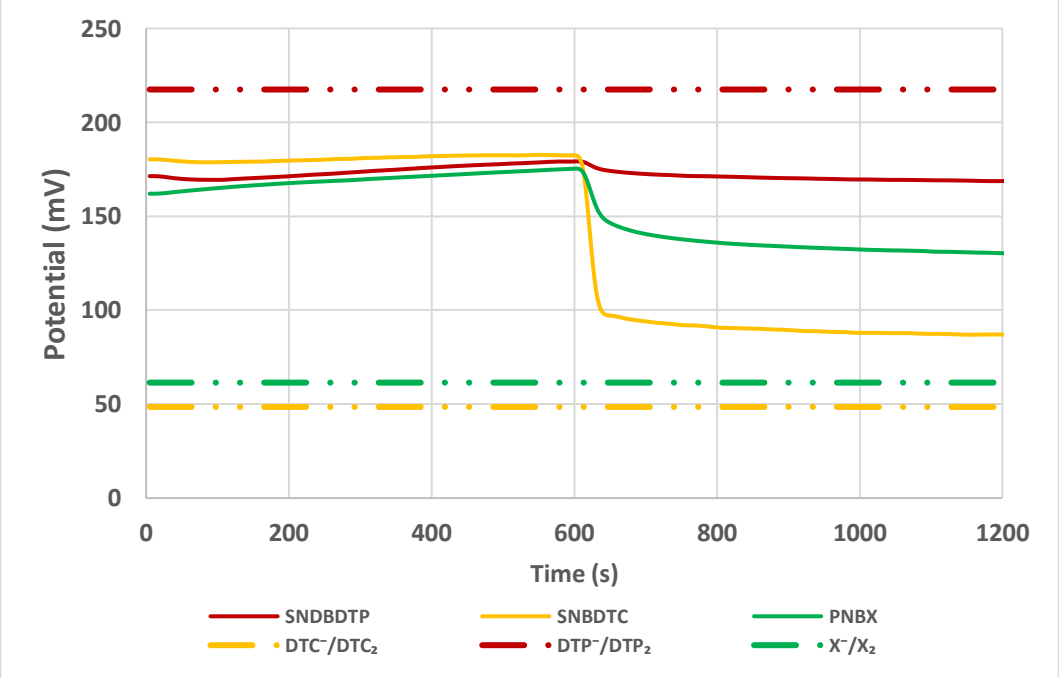

Figure 4.47 Rest potential results of arsenopyrite in the absence and presence of standard collectors, after 600 seconds, at pH 9.5 The dotted lines indicate the oxidation potentials of the standard collectors.

4.5.3.2. Arsenopyrite at pH 3.5

A more positive average rest potential of 355 mV, an increase of 176 mV was observed before adding the collectors in comparison to the rest potential of 179 mV at pH 9.5 (Figure 4.48).

The extent of interaction as indicated by the change in rest potential upon the addition of PNBX was 183.7 mV.

Unfortunately, the full set of data could not be generated at pH 3.5 because the electrode was no longer in a working condition. However, just like all the other selected minerals, a greater extent of interaction was observed at low pH compared to high pH. The formation of a dithiolate was predicted under acidic conditions.

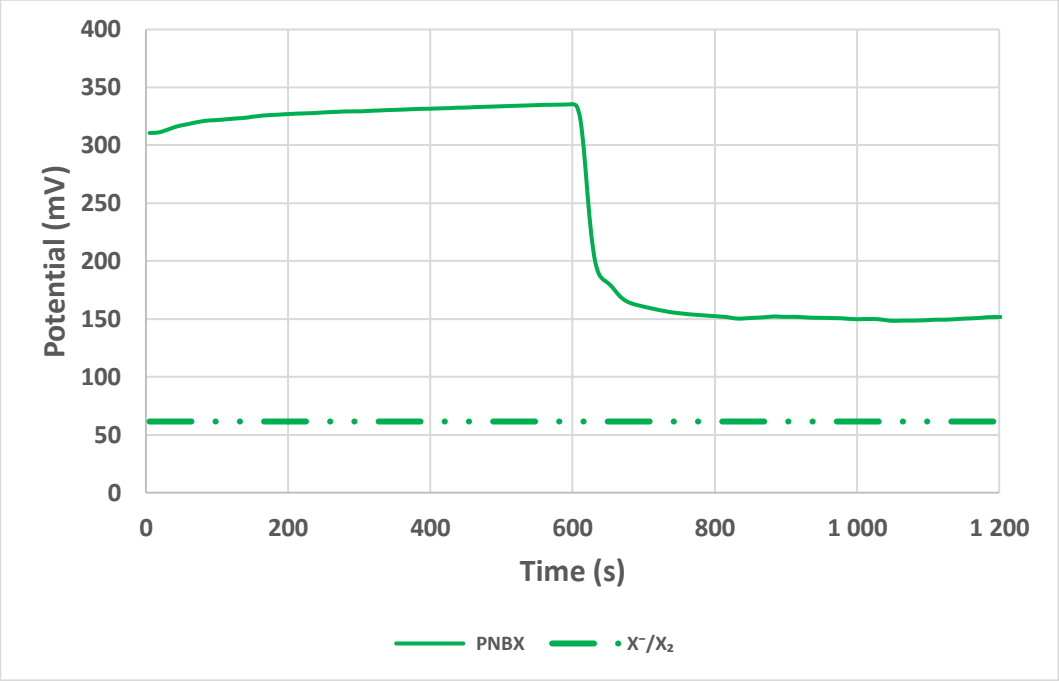

Figure 4.48 Average Rest potential of arsenopyrite in the absence and presence of PNBX collector, after 600 seconds, at pH 3.5 The dotted line indicates the oxidation potential of the PNBX collector.

4.5.4. Cooperite Rest Potential Results

Rest potential measurements of cooperite were carried out to investigate its interaction with the thiol collectors at pH 9.5 and 3.5. The results are given below.

4.5.4.1. Cooperite at pH 9.5

The average rest potential of cooperite before adding the collectors at 600 seconds was 256.2 ± 10.4mV (Figure 4.49). The mineral showed the greatest extent of interaction with all the collectors as indicated by the decrease of rest potentials after adding the collectors compared to all the other minerals. The rest potential values followed the order: SNBDTC (241.2 mV) > PNBX (161.9 mV) > SNDBDTP (26.5 mV). The rest potential tests predicted the formation of the dithiolates with SNDBDTP and PNBX, and the metal thiolate with SNBDTC. On the contrary, the adsorption tests showed that SNDBDTP was not adsorbed on the cooperite surface under alkaline conditions.

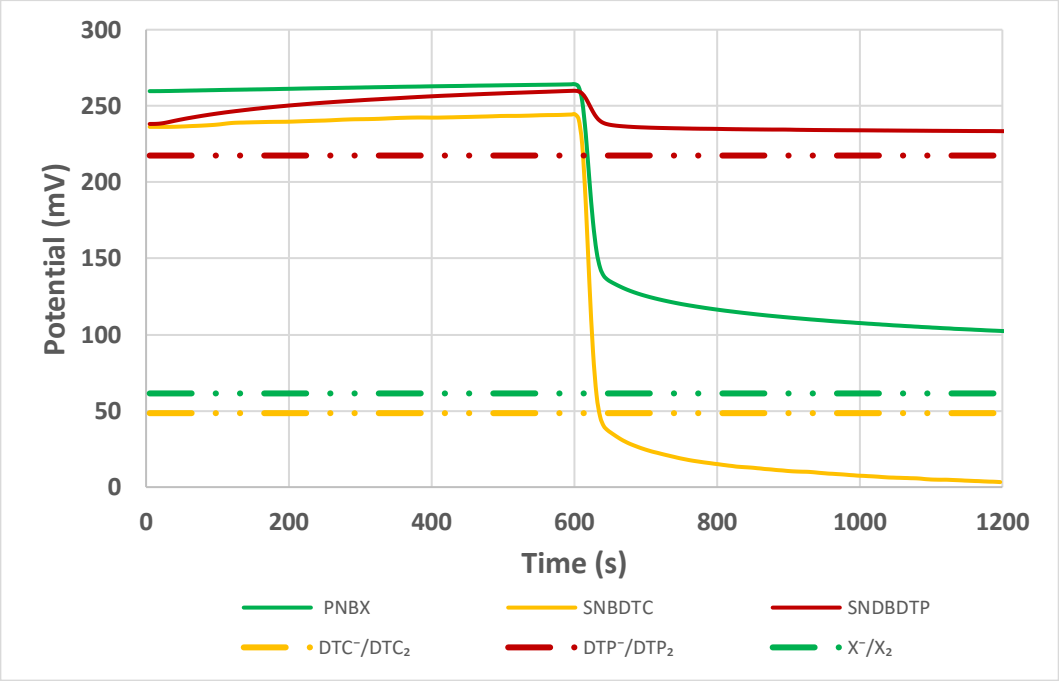

Figure 4.49 Rest potential results of synthetic cooperite in the absence and presence of standard collectors, after 600 seconds, at pH 9.5 The dotted lines indicate the oxidation potentials of the standard collectors.

4.5.4.2. Cooperite at pH 3.5

Similarly to pyrite and arsenopyrite, Figure 4.50 shows an increase in the average rest potential of cooperite in the absence of a collector at pH 3.5 compared to pH 9.5.

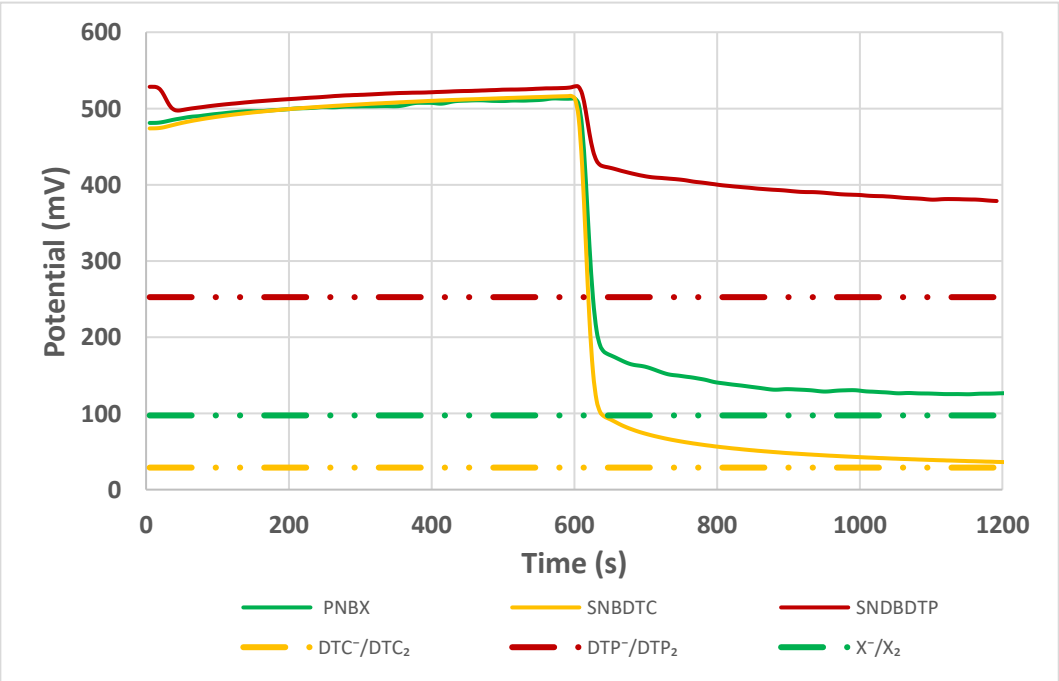

Figure 4.50 Rest potential results of synthetic cooperite in the absence and presence of standard collectors, after 600 seconds, at pH 3.5 The dotted lines indicate the oxidation potentials of the standard collectors.

In the case of cooperite, the increase in the rest potential was significant, from 256 mV at pH 9.5 to 518 ± 9.5 mV at pH 3.5, an increase of 262 mV. This is in contrast to the sperrylite, which showed an increase of 10 mV from high pH to low pH. Cooperite showed a greater extent of interaction with all the collectors at pH 3.5 compared to the other minerals. The extent of interaction, indicated by the potential drop, followed the order: SNBDTC (476.1 mV) > PNBX (386.4 mV) > SNDBDTP (150.7 mV). The formation of the dithiolates was predicted by the tests for all the thiol collectors under acidic conditions.

4.5.5. Summary of Rest Potential Results

A summary of the rest potential results of the minerals and their extent of interaction is given in the following sections.

4.5.5.1. Change in Rest Potentials with pH

Figure 4.51 shows the average rest potentials of the minerals under alkaline and acidic conditions. Sperrylite had a fairly moderate rest potential of 233.7 mV at pH 9.5, which was only greater than that of arsenopyrite (179 mV), indicating that arsenopyrite is more reactive than sperrylite (Rao and Finch, 1988).

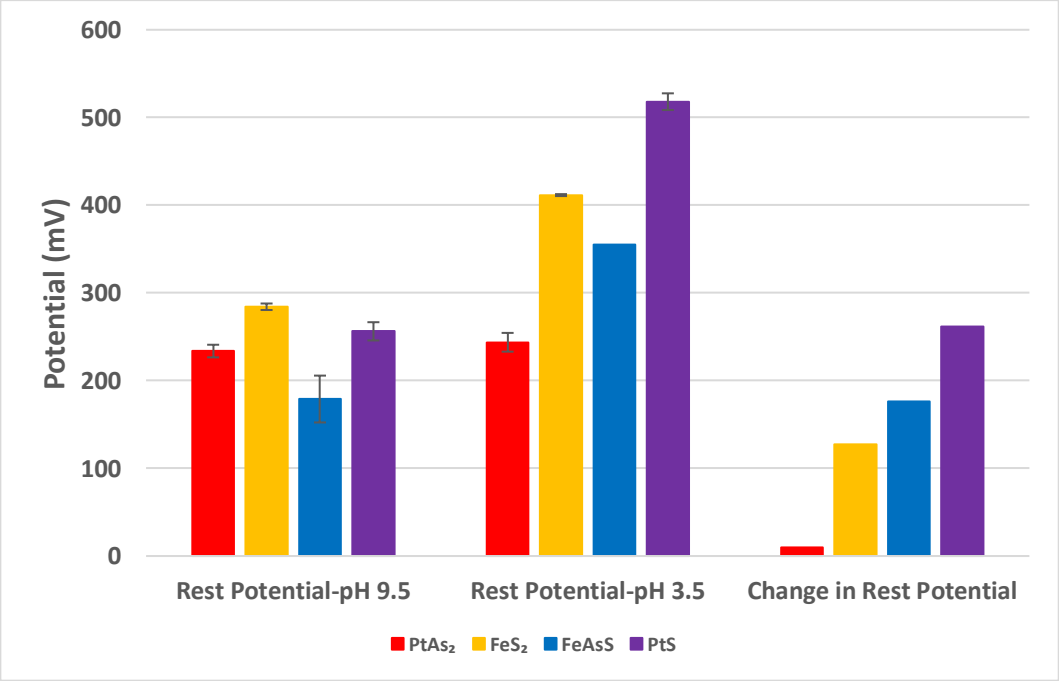

Figure 4.51 Change in minerals' rest potentials with change in pH

Also, the rest potential of cooperite (256.2 mV) was found to be lower compared to that of pyrite (284.2 mV). An important point to note is that all minerals experienced an increase in rest potential at pH 3.5 compared to pH 9.5, except for sperrylite. The rest potentials of the minerals before adding the collector at 600 seconds show that the there was only an increase of 10 mV in the sperrylite potential under acidic conditions: PtS (518 mV) > FeS_2 (411.5 mV) > FeAsS (355 mV) > $PtAs_2$ (243.7 mV).

The changes in the rest potentials of sperrylite, pyrite, arsenopyrite and cooperite were 10 mV, 127.3 mV, 176 mV and 261.8 mV respectively. The change in rest potential values signifies the ease with which the mineral surface can be altered resulting in the formation of surface products at pH 9.5 (Figure 4.61). Sperrylite has the lowest change in potential with pH compared to the other minerals. In addition, pyrite which also has the isometric crystal structure, had a lower change in potential as opposed to arsenopyrite and cooperite. This also indicates that the minerals with the isometric crystal structure were not readily oxidized compared to the other tested minerals.

4.5.5.2. The extent of Interaction of all Minerals with Collectors

The extent of interaction of the minerals with different collectors is given in Figure 4.52. Sperrylite gave the least extent of interaction with all the collectors under alkaline and acidic conditions. For example, the extent of interaction of cooperite, pyrite, arsenopyrite and sperrylite with PNBX as indicated by the drop in potential was 161.9 mV, 158.3 mV, 45 mV and 17.7 mV respectively.

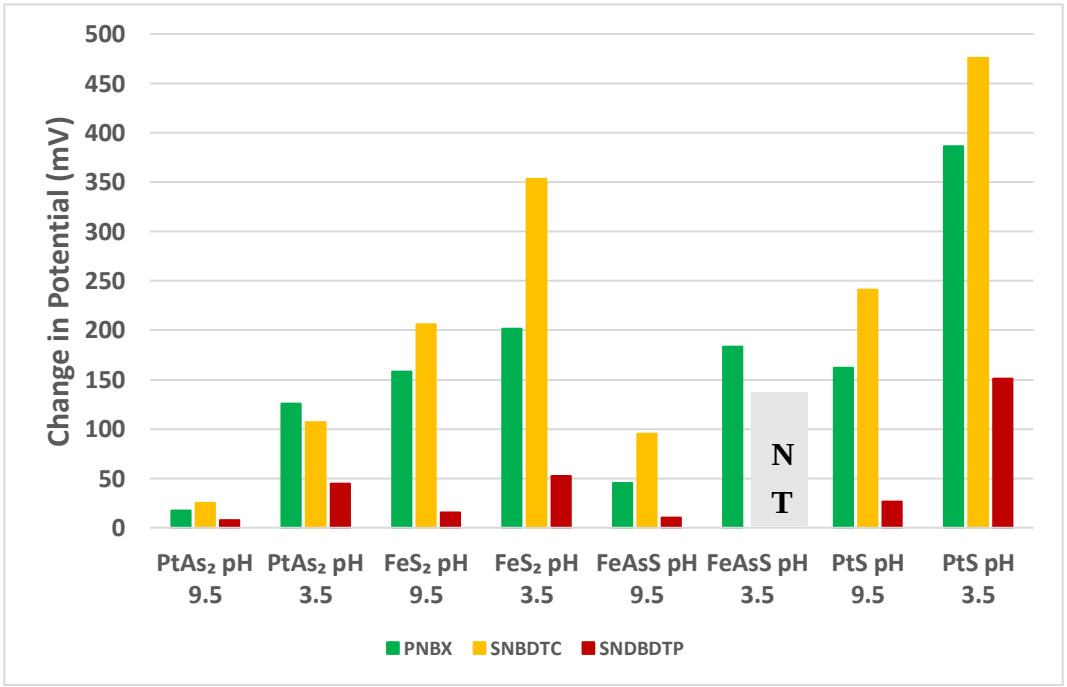

Figure 4.52 Minerals' extent of interaction with standard collectors is signified by the drop in potential at pH 9.5 and pH 3.5. NT = not tested.

Minerals that contain the arsenic donor atom, particularly sperrylite, gave the lowest extent of interaction with all the collectors in comparison to the minerals containing the sulphur ligand. DTP consistently shows very low interaction with all mineral surfaces. The tests of arsenopyrite with SNBDTC and SNDBDTP were not carried out.

At pH 3.5, the extent of interaction for all the minerals increased, however, sperrylite still had the least extent of interaction as opposed to the other minerals.

For instance, the decrease in the potential of cooperite, pyrite, arsenopyrite and sperrylite after adding the PNBX collector at pH 3.5 was 386 mV, 216.6 mV, 183.7 mV and 126 mV respectively.

4.6. ISOTHERMAL TITRATION CALORIMETRY TEST RESULTS

The extent of interaction with the thiol and novel collectors at 1 pseudo-monolayer coverage was determined by isothermal titration calorimetry tests. Due to the difficulty in controlling the pH of the slurry in the reaction vessel, the tests were carried out at the natural pH of each mineral.

4.6.1. Heats of Adsorption of Minerals

Figure 4.53 shows the calculated molar heats of adsorption for the minerals after adding a monolayer coverage of the thiol collectors in the mineral slurry, initially at its natural pH.

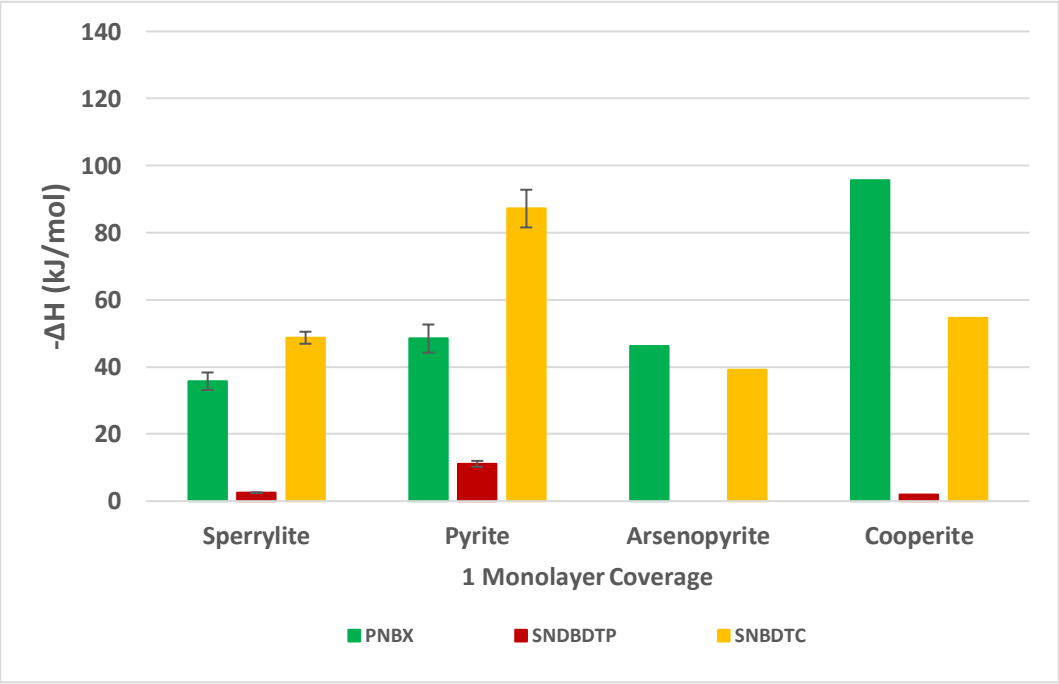

Figure 4.53 Heats of adsorption of minerals at 1 pseudo-monolayer coverage using standard collectors, at minerals' natural pH, in distilled water

A rise in pH is expected during the experiment after adding the collectors, however, it was not possible to measure the pH during the experiments. Sperrylite and pyrite with the same isometric crystal structure showed the same trend in the energy of adsorption: SNBDTC > PNBX > SNDBDTP. On the other hand, cooperite and arsenopyrite which showed good natural floatability had energies of adsorption that followed the order: PNBX > SNBDTC > SNDBDTP. The sulphide minerals generally gave the highest adsorption energies compared to sperrylite and arsenopyrite. SNDBDTP had the lowest heats of adsorption with all the minerals and the lowest value of 0 kJ/mol was recorded with arsenopyrite.

4.6.1.1. Heats of Adsorption with Novel collectors

The calculated molar heats of adsorption for the novel collectors with sperrylite are given in Figure 4.54.

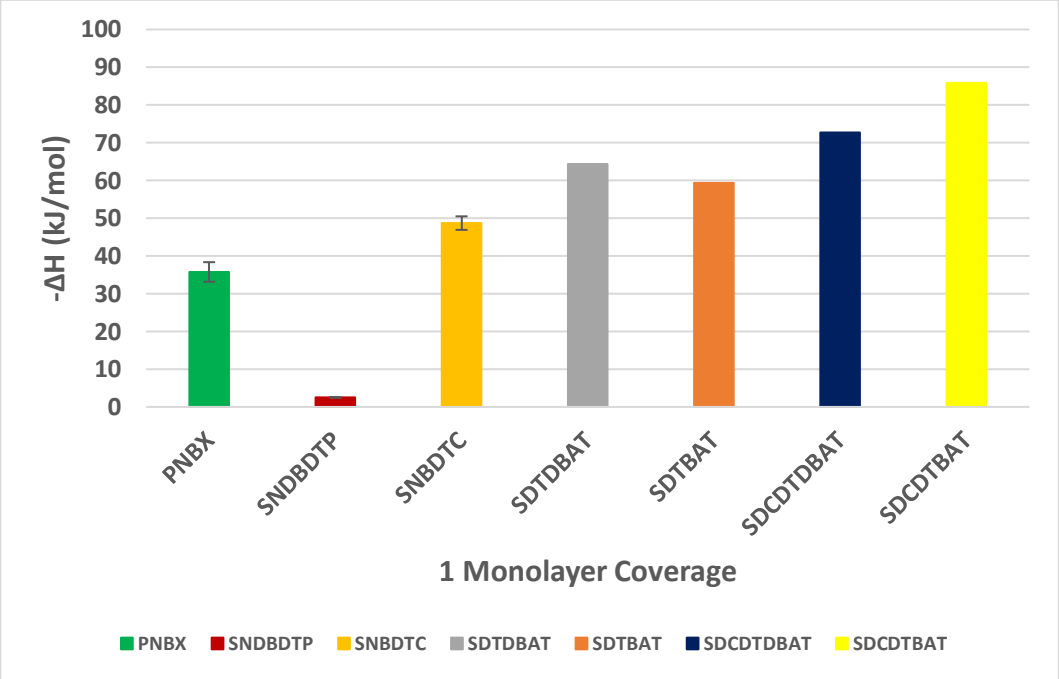

Figure 4.54 Heats of adsorption of sperrylite at 1 pseudo-monolayer coverage using novel collectors and how they compare to standard collectors, at natural pH of 6.3, in distilled water

The novel collectors gave higher heats of adsorption compared to the thiol collectors as predicted by the molecular modelling computational studies carried out in collaboration with the University of Limpopo.

Also, hydroxide ions were titrated into sperrylite to determine the binding energy of the hydroxide ions. After integrating the peaks, it was observed that the solution gave the average binding energy of 16 kJ/mol which is lower than the binding energy of the tested collectors, except for SNDBDTP. This shows that collectors should be able to displace adsorbed hydroxide ions from the sperrylite surface.

4.7. SURFACE ANALYSIS RESULTS

XPS and TOF-SIMS surface analysis tests were carried out using the sperrylite and arsenopyrite samples. Untreated samples were used as a standard reference in the test. A change in the relevant individual species was compared to those of the standard samples to determine the effect of conditioning the samples in plant water and the selected collectors. The TOF-SIMS results could not give detailed information on the individual species found on the mineral surface, hence only the carbon content could be analysed to check if the collectors with the butyl chain length were adsorbed.

Moreover, the O and S peaks could not be distinguished from each other, and it was recommended that the O peak must be used as an indication of the presence of O2. All the samples had some carbon and oxygen contamination. The C1s line is always present in the samples and gets introduced from the laboratory environment or a glove box. The O1s line and CO_2 gas are also introduced from the atmosphere during the handling of the samples. The survey spectra for the sample gave an insight into identifying the most important species on the minerals' surface

4.7.1. Sperrylite

The sperrylite was investigated to determine its surface characteristics when conditioned in synthetic plant water and the PNBX and SNBDTC collectors. In addition, the possible adsorption products were investigated after conditioning the mineral in the collector solution. The collectors were added to make up a concentration of 5 x 10^{-3}M in 100 ml water.

4.7.1.1. XPS Results

Table 4.11 shows the peak analysis of the species on the mineral surface that are key to explaining the surface composition and surface species that were introduced under given conditions.

Table 4.11 Sperrylite XPS results showing the species of interest and their atomic compositions measured from the surface of the mineral

			Atomic %				
Line	**Species**	**Peak BE**	**Untreated Standard**	**2SPW**	**PNBX**	**SNBDTC**	**Summary**
As3d5	As, Arsenide	41.8	9.3	10.4	10.5	11.2	Platinum arsenide content in respective samples
As3d5	As_2O_3	45	16.7	10.1	13.4	12.3	Reduction of arsenolite content by 39.5% after conditioning the sample in plant water. A reduction was also noted after conditioning the sample in plant water with collectors.
S2p3	Mercaptan	162.2	1.1	0.7	0.7	1.3	There was no increase in the RSH group observed in the sample that was treated with PNBX and SNBDTC
C1s	C-C	284.7	20.1	21.6	19.5	21.3	There was no increase in the C-C group after adding the thiol collectors. This could indicate that no chemisorption took place. The physisorbed collectors could have been washed away after washing the samples with distilled water
O1s	Metal Oxide	530.2	0.8	11	5	6.1	Minimal to no oxidation took place on the dry sperrylite sample. There is increase in metal oxide content in the sample after conditioning with synthetic plant water. There was a reduction in the amount of metal oxides found on the mineral surface by 44.5% and 54.5% when the mineral was conditioned in the presence of the PNBX and SNBDTC collectors respectively. This indicates that some of the plant water ions could have formed complexes with the collectors instead of metal oxides.

4.7.1.2. Sperrylite TOF-SIMS Results

Sperrylite TOF-SIMS results and the peak intensity of each species given in spectral images have been summarised in Table 4.12. The sperrylite TOF-SIMS images under different conditions are given in Appendix F. The results corroborate with the XPS results that gave an indication that the collectors were not chemisorbed onto the mineral surface.

This contradicts with the adsorption tests results, especially for SNBDTC. It is however important to note that distilled water was used during the adsorption test, as plant water ions were also found to introduce their individual spectra, making it difficult to analyse the results.

Table 4.12 TOF-SIMS results showing the species detected on the sperrylite samples and their spectral peak intensity

Species	Untreated Standard	2SPW	PNBX	SNBDTC	Summary
O	483937	502105	509228	496553	
O_2/S	53441	26019	56328	24126	The sulphur and oxygen peaks could not be differentiated
AsO_2/AsS	362524	408712	362262	314681	
C	56832	62892	47650	50521	There was no increase in the carbon content indicating that there was no chemisorption of the collectors on the sperrylite surface.
As	25679	24412	21587	18331	

4.7.2. Arsenopyrite

Arsenopyrite was also investigated to determine especially the cause for its natural floatability and also its interaction with the PNBX collector. Its surface characteristics will also further give an insight on how it differs with sperrylite.

4.7.2.1. Arsenopyrite XPS Results

Table 4.13 shows the arsenopyrite XPS analysis results and the composition of the surface species under different conditions. Surface oxidation on the standard sample was observed on arsenopyrite resulting in the formation of arsenolite and metal oxides detected on the untreated sample.

Table 4.13 Arsenopyrite XPS results showing the species of interest and their atomic compositions measured from the surface of the mineral

			Atomic %			
Line	**Species**	**Peak BE**	**Untreated Standard**	**2SPW**	**PNBX**	**Summary**
S2p3	Mercaptan	162	2.4	2.5	4.1	A 39% increase in mercaptan content was noted after adding the PNBX collector, indicating that the collector was chemisorbed on the mineral.
S2p3	Sulfide	43.3	0.7	0.9	1.2	There was a slight increase in the sulphide content after adding the PNBX collector
As3d5	As_2O_3	44.6	7.7	4.5	5.1	The dry standard sample was slightly oxidized to form arsenolite. The content was reduced after conditioning the sample with plant water and with PNBX.
C1s	C-C	284.6	28.3	24.8	26.8	There was no increase in the C-C peak observed.
O1s	Metal Oxide	530.5	6.6	17.1	15.9	There was an initial oxidation of the sample as indicated by the content of 6% in the dry untreated sample. After conditioning the sample in synthetic plant water there was an increase of 61.4% in the metal oxide content. This increase in the metal oxide content due to the presence of plant water ions was the same as that noted in sperrylite, hence, the natural floatability of the mineral could be attributed to the initial surface oxidation of the untreated mineral. There was a reduction on the amount of the metal oxides formed on the mineral surface by 7% after adding the PNBX collector and collectors were still adsorbed to a greater extent as opposed to sperrylite, an indication that these oxides are not detrimental to the collector adsorption.
Fe2p3	$FeSO_4$	711.9	2.5	2.7	3.1	An increase in sulphate content was also noted after conditioning the sample in synthetic plant water and after adding the PNBX collector.

4.7.2.2. Arsenopyrite TOF-SIMS Results

Table 4.14 shows the arsenopyrite TOF-SIMS results and the images of the mineral samples under given conditions are given in Appendix E. Only the carbon content could be used to deduce if the PNBX collector was adsorbed onto the mineral surface. The result also corroborates what was shown by the XPS data.

Table 4.14 TOF-SIMS results showing the species detected on the sperrylite samples

Species	Untreated Standard	2SPW	PNBX	Summary
O	339856	398132	442397	
O_2/S	58742	43917	114075	The sulphur and oxygen peaks could not be differentiated. However, the higher sulphur content after adding PNBX could be an indication that the collector was chemisorbed.
AsO_2/AsS	70808	46733	82804	
C	75217	101376	113039	There was an increase in the carbon content indicating that there was chemisorption of the PNBX collector on the surface.
Fe	258920	281699	327152	
As	16671	23950	44712	

4.8. OVERALL SUMMARY OF THE BEHAVIOUR OF SELECTED MINERALS

This section gives a summary on the floatability of the minerals and how they compare to respective collector adsorption densities at pH 9 (Figure 4.55).

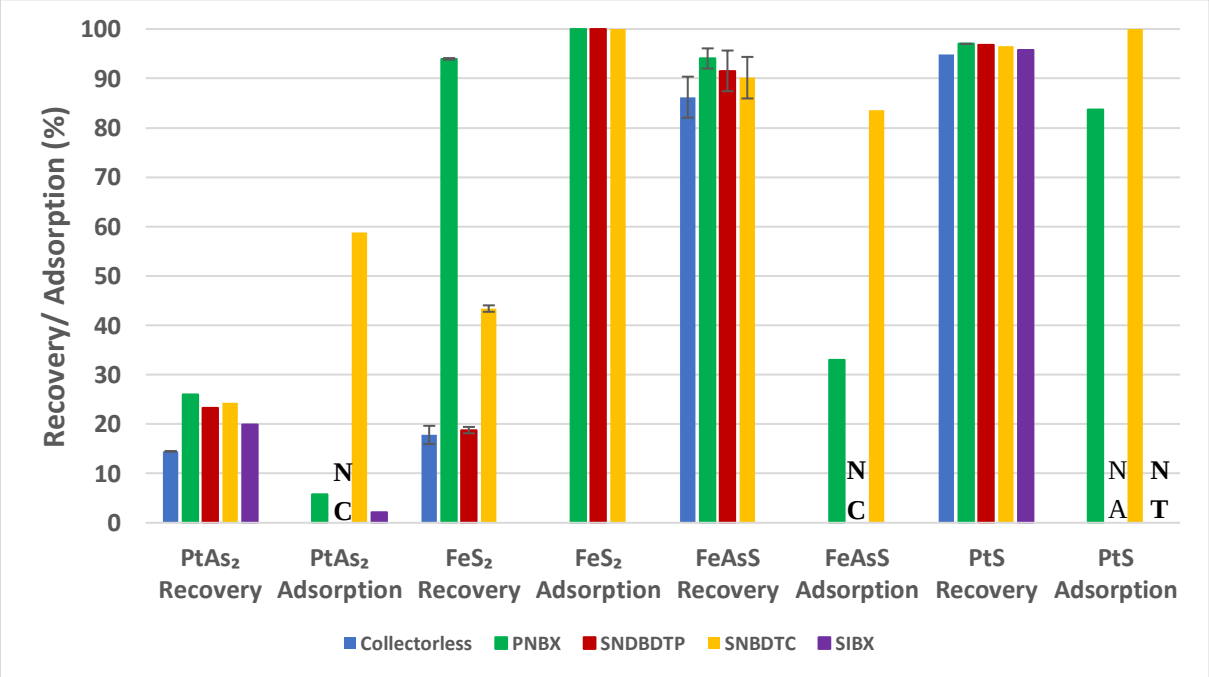

Figure 4.55 Minerals' flotation recoveries with standard collectors and their respective collector adsorption densities at pH 9. NC = not conclusive. NT = not tested.

It can be seen that sperrylite which had the least flotation recoveries also had the least amount of collectors adsorbed. The complete adsorption of collectors on pyrite did not translate to high flotation recoveries except for PNBX. The adsorption of the PNBX collector was much lower on sperrylite and arsenopyrite compared to the other minerals.

The adsorption of SNBDTC was higher for all the minerals, however, sperrylite and arsenopyrite still gave the least adsorption densities. It can also be concluded that high collector adsorption cannot be linked to improved recoveries for cooperite and arsenopyrite, which had a high natural flotation response.

Figure 4.56 shows a comparison between the flotation recoveries and adsorption densities of sperrylite and pyrite with the novel collectors. The poor floatability of sperrylite with novel collectors can be directly linked to poor collector adsorption. The presence of the As donor atoms in sperrylite as opposed to S donor atoms in pyrite could be responsible for poor collector adsorption which ultimately leads to poor flotation recoveries of sperrylite.

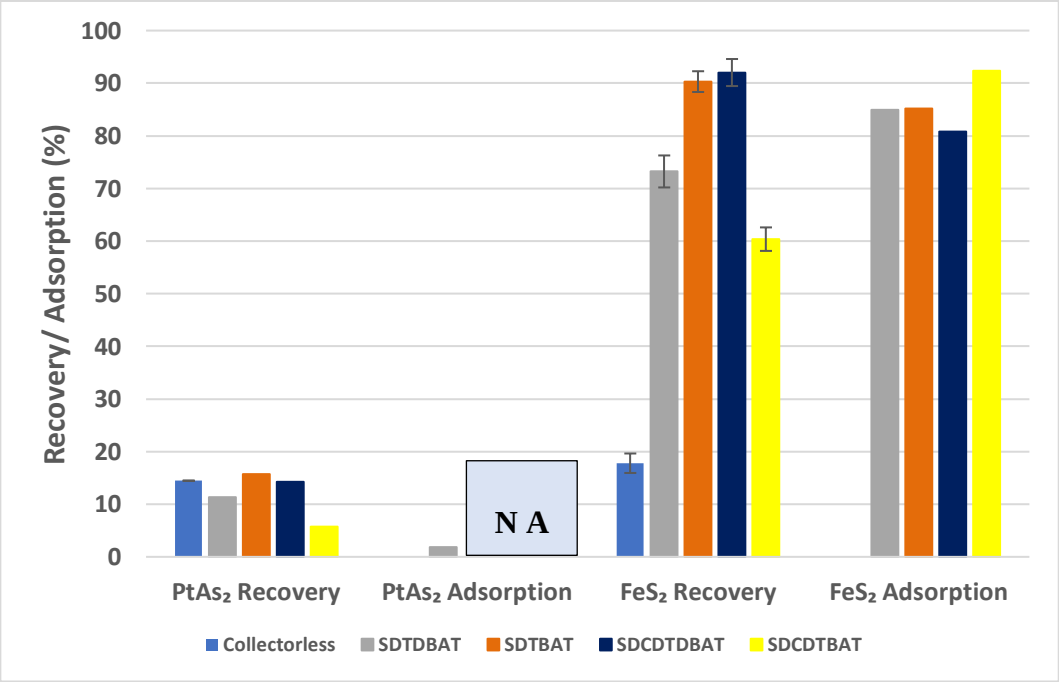

Figure 4.56 Flotation recoveries of sperrylite with novel collectors and their respective adsorption densities at pH 9. NA= not adsorbed

A summary of the interaction of the minerals with collectors and their respective crystal structures is also given in Table 4.15.

Table 4.15 Overall tabulated results of the selected minerals under different conditions. NC = not conclusive.

Mineral	**Sperrylite ($PtAs_2$)**	**Pyrite (FeS_2)**	**Arsenopyrite (FeAsS)**	**Cooperite (PtS)**
Crystal Structure	Isometric	Isometric	Monoclinic	Tetragonal
Member of	Pyrite Group	Pyrite Group	Arsenopyrite Group	Dimorph of Braggite
Collectorless Recovery (%)	14.5	17.8	86.2	94.8
Recovery PNBX (%)	26 (↑ 11.5%)	94.0 (↑ 76.2%)	94.0 (↑ 7.8%)	97.0 (↑ 2.2%)
Amount of collector adsorbed at pH 9	PNBX: 5.7% DTP: NC DTC: 51.4%	PNBX:96.1% DTP: 41.6% DTC: 93.7%	PNBX: 29.9% DTP: NC DTC: 78.4%	PNBX: 81.9% DTP: 0% DTC: 88.2%
Extent of interaction (mV) pH 9.5	PNBX: 17.6 DTP: 7.9 DTC: 24.9	PNBX: 158.3 DTP: 15.6 DTC: 206.1	PNBX: 45 DTP: 10.4 DTC: 95.4	PNBX: 161.9 DTP: 26.5 DTC: 241.2
Surface Products predicted by Electrochemistry at pH 9.5	$(PNBX)_2$ $(DTC)_2$	$(PNBX)_2$ $(DTC)_2$	$(PNBX)_2$ $(DTC)_2$	$(PNBX)_2$ DTC^-
Rest Potential (mV) pH 9.5	233.7	284.2	179	256.2
Rest Potential (mV) pH 3.55	243.7	411.5	355	518
Extent of interaction (mV) pH 3.55	PNBX: 126 DTP: 44.4 DTC: 107	PNBX: 201.6 DTP: 52.6 DTC: 353.3	PNBX: 183.7	PNBX: 386.4 DTP: 150.7 DTC: 476.1

5. DISCUSSION

This study sought to understand why sperrylite is slow floating compared to the other PGM minerals with the aim of improving its recoveries. One major question to be answered by this study was to determine why the xanthate collectors seemed to be selective against sperrylite and floated the other PGM minerals well? Microflotation, adsorption, rest potential and isothermal titration calorimetry tests were carried out to understand the interactions of sperrylite with different collectors under various pulp conditions of pH, ionic strength and redox potential. Pyrite, arsenopyrite and cooperite were also investigated to understand how crystal structures and the donor atoms (S, As) on the mineral surface influence the minerals' floatability.

A discussion will be presented that, firstly, covers aspects of mineral synthesis and characterisation that was central to being able to conduct this study. Secondly, the floatability of sperrylite will be interpreted based on the supplementary experiments that were carried out, such as the extent of collector adsorption, electrochemical and calorimetric interactions. Moreover, surface products on sperrylite and arsenopyrite determined using XPS and TOF-SIMS analysis for the untreated, conditioned in plant water and conditioned in plant water with collectors were discussed and how they affected the floatability of the minerals. Finally, sperrylite flotation response will be compared to that of the other minerals selected for this study in order to interpret the effect of crystal structure and donor atoms.

5.1. MINERAL SYNTHESIS AND CHARACTERISATION

Mineral synthesis was the key aspect of this study due to the limited availability of the PGM minerals in the ore. Moreover, these minerals are finely disseminated in the ore making it difficult to carry out the tests on natural sperrylite and other PGM minerals. The operating temperatures of the synthesis process for sperrylite and cooperite were limited to 800ºC and 1000ºC respectively, due to the highly volatile nature of arsenic and sulphur. Even though the complete fusion of the mineral components was not possible during the synthesis process, sperrylite and cooperite samples obtained resembled the natural minerals in composition as indicated by the XRD and EDS results.

The rest potential results for the natural sperrylite electrodes were also a good indicator of the quality of the synthetic sample produced (Figure 4.41; Figure 4.42). The synthetic sperrylite electrode behaved in a similar manner to a natural sperrylite electrode (Figure 4.43; Figure 4.44). The rest potentials and extent of interaction of the synthetic sperrylite electrode with thiol collectors were found to be fairly similar to that of the natural sperrylite electrode. The rest potentials of the synthetic sperrylite electrode were found to be within 12% of those of the natural sperrylite electrodes. Moreover, the very low extent of collector interaction observed with the natural sperrylite electrode under alkaline conditions corroborates well with the poor collector adsorption results observed with the synthetic sperrylite sample and standard collectors.

This confirms the success of the synthesis process of the major mineral required for the completion of this study. Also, the collectorless flotation recovery of cooperite of 94% (Figure 4.25) is the same as that obtained during the study by Shackleton (2007) indicating the reliability and reproducibility of the synthesis process applied.

5.1.1. Sperrylite

The EDS results (Table 4.5) and the BSE micrograph of the natural sperrylite electrode (Figure 4.1) revealed that it was homogenous and ~100% sperrylite. The Rietveld analysis in Table 4.1 indicated that the synthetic sperrylite sample was 87% sperrylite and 12% arsenolite and 1% platinum. The EDS analysis results given in Tables 4.8 and 4.9 showed that the sample was fairly homogenous, with some spectra (cf. Appendix B) showing the presence of excess arsenic, indicating the presence of arsenolite. The presence of arsenolite on the surface of the particles is most likely to have had no impact on the flotation and adsorption results. Arsenolite dissolves in water to form arsenous acid (H_3AsO_3) and its solubility in 100g of water is 2.1g at 25^0C (https://www.ncbi.nlm.nih.gov›books). This was demonstrated by the XPS results that showed that the arsenolite content on the mineral surface decreased by 39.5% after conditioning the sperrylite sample in synthetic plant water. The formation of arsenolite could have resulted from the residual oxygen in the silica ampoule and the vacuum pump may not have evacuated all the oxygen. It is recommended that in future studies the vacuuming time be increased from 24 hours to 36 hours.

In addition, free platinum specks (less than 20µm) were observed in the core of a few -106+38 µm size fraction particles in Figure 4.4. Most of the free platinum specks were locked within the particles of around 100 µm and would not have greatly affected the floatability of the mineral particles. The floatability of the mineral samples is mainly determined by their surface properties. It can be concluded that most of the raw platinum and arsenic particles were successfully converted to sperrylite using the low temperature sintering process, where the reagents were heated below the melting temperature of sperrylite, as explained in Section 3.2.1.

5.1.2. Cooperite

The cooperite XRD Rietveld analysis (Table 4.2) showed that the sample contained 97% cooperite and it was pointed out that it matched the Bushveld complex cooperite. EDS results indicated that the sample was homogenous and the composition was almost uniform (Table 4.10). The synthetic cooperite electrode that was synthesized previous to this study, contained cooperite as the main phase. EDS results indicated that the outer parts of the electrode sections had higher sulphur content compared to the core because the mineral is formed by the diffusion process during synthesis. This was also noticed in sperrylite particles that were greater than 100µm, where arsenic could not completely diffuse to the core of some particles.

5.1.3. Pyrite and Arsenopyrite

The XRD results showed that the natural pyrite sample had a good purity of 89% (Table 4.3). The natural arsenopyrite sample had a purity of 74.2% and 16.5% pyrite was the major impurity in the sample (Table 4.4). The presence of 16.5% pyrite in arsenopyrite may have influenced the interaction of the mineral with the thiol collectors to a certain extent. However, arsenopyrite and pyrite showed totally different behaviours with collectors, which appears to indicate that they are interacting differently based on their different compositions. Therefore, some impurities can influence the behaviour of the mineral depending on their composition. It is also important to note that it is only those portions of pyrite that are exposed to the surface not necessarily the total content that is able to influence the flotation behaviour of the mineral and its interaction with different collectors. However, in this study, there was a limitation in determining the percentage of impurities that were exposed at the surface of each mineral particle and the extent to which they could influence the test results.

5.2. SPERRYLITE

This section will interpret the sperrylite flotation behaviour with reference to the supplementary experimentation that was performed in order to assist in this interpretation.

5.2.1. Sperrylite Floatation Response with standard thiol collectors

Sperrylite showed very poor floatability after adding the standard collectors at pH 9 with synthetic plant water, giving a maximum recovery of around 26% with PNBX (Figure 4.26). All standard thiol collectors, PNBX, SNDBDTP and SNBDTC, gave poor recoveries that ranged from 19% to 26% (Figure 4.7). This corroborates the poor floatability that was also observed in the study by Shackleton et al., (2007) using SIBX as the collector. The main reason for the poor floatability of sperrylite is the poor interaction of the mineral with collectors. This was reflected by the adsorption and rest potential test results. The adsorption behaviour of sperrylite with the xanthate collectors could be closely linked to the poor flotation response the mineral exhibited at pH 9, given in Figure 4.29. The amount of xanthate collectors adsorbed onto sperrylite were 2.2% and 5.7% for SIBX and PNBX respectively. Therefore, the poor flotation recoveries of sperrylite could be attributed to the poor adsorption of the xanthate collectors, which are the main collectors that are employed in the PGM flotation circuits. The n-butyl chain resulted in a slightly higher recovery of 6% than the isobutyl chain of the xanthate derivative. This corroborates the findings in the study by Taguta et al., (2017) and others that the straight chain collectors are stronger collectors than the branched chain collectors.

Also, it was observed that the different standard collectors had different adsorption densities onto the sperrylite mineral. SNBDTC (51.4%) was adsorbed to a greater extent compared to the xanthate collectors while SNDBDTP was not adsorbed at all (Figure 4.29).

This behaviour could be linked to the presence of the nitrogen and oxygen linking atoms that are electron donating and electron withdrawing respectively.

Dithiocarbamates are known to be stronger collectors as opposed to the xanthates towards certain types of minerals, even though xanthates generally gave higher recoveries. In addition, the XPS (Table 4.11) and TOF-SIMS (Table 4.12) surface analysis results further shed light on the possible interactions of the collectors with sperrylite. There was no increase in the mercaptan peaks and C-C peaks after treating the mineral with PNBX and SNBDTC collectors at dosages much higher than the single monolayer. This shows that the collectors, especially SNBDTC, may have been physisorbed on the mineral surface and could be easily removed after washing the sample with distilled water or during drying in the vacuum oven. The TOF-SIMS results also confirmed that none of the collectors was chemisorbed onto sperrylite since no increase in carbon content was observed after treating the samples with the collectors.

The XPS results also showed that the poor collector adsorption observed was not caused by the surface oxidation of sperrylite. There were metal oxides that were found on the mineral surface after conditioning the sample in synthetic plant water, which contains some metal ions. However, a reduction in the metal oxides formed on the mineral surface was seen after treating the samples with the collectors, indicating that the collectors could remove the metal oxide coating on the mineral surface. Hence, these metal oxides were not responsible for the poor collector adsorption observed. Also, the sperrylite sample was not oxidised in its standard state and this was indicated by the very low metal oxide content in the untreated sample.

Furthermore, the rest potential tests also confirmed the minimal interaction of sperrylite with the standard collectors (Figure 4.41). The potential drop after adding the collectors ranged from 7.9 mV to 24.9 mV and these were very low compared to the other minerals. Tests showed that the extent of interaction with PNBX and SNBDTC was very low. These results, although unexpected, correlate with the poor collector adsorption that was observed with sperrylite. This confirms that there is indeed very little interaction that takes place between sperrylite and the tested standard collectors. This finding is very key because the natural sperrylite electrode results confirmed the similarity in behaviours between natural and synthetic sperrylite and, therefore, substantiated the microflotation tests and adsorption tests results that were obtained using synthetic sperrylite.

The rest potential results can also be used to predict the possible surface products that can form on a mineral when it interacts with different collectors. Despite, the low interaction with collectors at pH 9.5, the rest potential tests predicted the formation of the dithiolates, if anything, on the mineral surface with PNBX and SNBDTC. This was indicated by the final rest potentials after adding the respective collectors which were above the oxidation potential of the collectors. This observation is however not consistent with the TOF-SIMS analysis results obtained by Shackleton (2007) on synthetic PGM minerals in which it was suggested that dixanthogen was formed on all the tested minerals except sperrylite.

In addition, a study by Vermaak et al., (2007) indicated that dixanthogen only formed on sperrylite after it was anodically polarized at potentials greater than 300 mV. The rest potential of sperrylite at pH 9.5 was 233.7 ± 7.2 mV. This shows that xanthate cannot be oxidized on the sperrylite mineral surface under normal flotation conditions.

The sperrylite surface was also less than 300 mV under both alkaline and acidic conditions, making the prediction of the formation of dithiolates also debatable in the case of PNBX. Hence, the rest potential measurements are not always consistent with the surface analysis results of minerals as seen with the platinum arsenide. It can be assumed that the rest potential data simply corroborates the adsorption data, in that very little, if any, collector adsorbed onto the sperrylite surface at basic pH's except SNBDTC.

5.2.1.1. Floatability of Sperrylite with Novel Collectors

Novel collectors were tested with sperrylite, and the recoveries were lower than those observed using standard collectors as indicated by the results in Figure 4.9. The maximum recovery obtained for SDTBAT was just above the collectorless recovery, viz. 15.7%, while SDTDBAT and SDCDTBAT collectors seemed to have a depressing effect on the mineral. These collectors were designed based on hypothesis 3, which proposed that linking atoms that are less electronegative, or more electron donating should be selected since this will increase the electron density around coordinating atoms and that, consequently, stronger bonds will be formed between the mineral and collector. In addition, SDCDTDBAT and SDCDTBAT collectors, based on hypothesis 2 suggested that a longer inter-atomic distance between the two chelating atoms compared to that of typical thiol collectors will have a better crystal structure compatibility with $PtAs_2$. This sought to make the Pt atoms more accessible to the bonding ligands with possible minimal steric hindrances. The standard test flotation results did not validate the proposed hypotheses 2 and 3.

Moreover, the molecular modelling computations by Nemutudi et al., (2020) revealed that the sulphur bonding ligands in the collector molecules have the ability to bond with both the Pt and As atoms on the sperrylite mineral surface thereby increasing the possible number of adsorption sites that the ligands are attracted to (Figure 1.13). Consequently, this might reduce the binding energy of the collector molecules onto sperrylite.

The poor recoveries with the novel collectors were also reflected by their poor adsorption onto sperrylite. Minimal adsorption of the novel collectors on sperrylite surface at pH 9 also confirms that poor collector adsorption is the cause of poor recoveries. The adsorption density of the novel collectors ranged from 0% to 1.9% (Figure 4.29). The minimal adsorption could also have been caused by the steric hindrances posed by the ring collector structures, even though they gave the higher binding energies as opposed to the PNBX collector during the screening process, using the molecular modelling computations (Nemutudi et al., 2022). This also reveals the limitations of the collector screening using molecular modelling computations as it only focuses on the binding energies of single collector molecules.

Moreover, it does not take into account the presence of the hydroxides on the mineral surface under alkaline conditions which also competitively adsorb onto the mineral or forms hydroxy compound that can coat the mineral surface.

5.2.1.2. Effect of Increased Collector Dosage

Increasing the collector dosage (Figure 4.8) of PNBX to 3, 5 and 10 monolayer equivalents proved to have a depressing effect on the mineral, resulting in reduced recoveries. An improvement in the recoveries was only obtained at a dosage of 30 monolayer equivalents with SNBDTC (45.4%). Tests at higher collector dosages were carried out because increasing collector dosages improved the flotation recoveries of pyrite. Studies have shown that pyrite can float well at xanthate concentrations greater than 10^{-3}M, due to the formation of oily dixanthogen species at pH 9 which leads to the passivation of the mineral surface (Smart et al., 1998). Moreover, work by Fuerstenau et al., (1968) also showed that the recovery of pyrite improved with the increase in ethyl xanthate collector dosage. The action of xanthates on sperrylite is different from pyrite as it led to a decrease in recoveries at higher dosages. Effect of Increasing Residence Time

Increasing the residence time was also investigated since plant data has also indicated that sperrylite is slow floating (Chetty et al., 2009). When the residence time was increased from 20 minutes to 30 minutes (Figure 4.13) the recoveries of sperrylite with SNBDTC, SDTBAT and SDCDTDBAT collectors, at 1 monolayer dosage, increased by 11.9%, 15.4% and 7.3% respectively at pH 4. This could be an indication that the interactions of sperrylite with the collectors are poor and slow, even though they were adsorbed onto the mineral to a much greater extent compared to pH 9, as indicated by the adsorption results. It is equally likely that the bubble-particle interaction is poor and it takes many bubble-particle collisions before the particle makes it to the concentrate.

Also, when the residence time was increased from 20 to 30 minutes, the recovery of SNBDTC increased by 5.1% at a collector dosage of 30 pseudo-monolayers, under alkaline conditions. This indicates the slow flotation response of the mineral, hence increasing the residence time could be beneficial. This attests to the findings by Chetty et al., (2009) that revealed that the arsenide minerals were recovered at the end of the rougher bank of the UG2 concentrator.

5.2.1.3. Effect of pH

The effect of pH on the floatability of sperrylite was investigated by carrying out tests under acidic conditions. The improved interaction of the mineral with different collectors was observed compared to alkaline conditions. Sperrylite gave moderate recoveries with SNBDTC and no recovery improvement with PNBX at pH 4 (Figure 4.10). This recovery did not correspond to the high adsorption density of the xanthate collector (5.7% to 93%) at pH 4. The recovery of sperrylite with SNBDTC, SDTBAT and SDCDTDBAT increased by 24.2%, 26% and 9% respectively.

This could be attributed to improved collector adsorption for all the collectors at pH 4 (Figure 4.30), and especially for the SDTBAT (0 to 71.9%) and SDCDTDBAT (0 to 55.5%) collectors. Interestingly, the UV-Vis spectra of SNBDTC (Figure 4.36), SDTBAT (Figure 4.37) and SDCDTDBAT (Figure 4.38) collectors before adding sperrylite at pH 4 were altered, indicating that they existed as different molecules under acidic conditions. Nevertheless, an improved recovery was obtained with the SNBDTC collector at pH 4 even though the adsorption density of the collector onto the mineral was reduced from 51.4% to 7.2%.

The SDTBAT product that forms as observed in the UV-VIS spectra between the 250 nm to 300 nm at pH 4, may be responsible for the improved recoveries. Also, it was noted that the whole spectrum appeared to have changed before and after contact with the sperrylite compared to the spectrum at pH 9. SNBDTC has an aliphatic chain and is prone to acid hydrolysis to liberate carbon disulphide (CS_2) under acidic and neutral conditions (Szolar, 2006). The novel collectors, SDTBAT and SDCDTDBAT consist of the aromatic chain and it was beyond the scope of this study to determine the products that form under acidic conditions. This method is only useful when the spectrum remains completely unchanged and is just reduced after contact with the mineral. When reactions occur the calculated adsorption densities under acidic conditions are unreliable. On the contrary, that phenomenon was not observed with PNBX and there was no improvement in the recovery, despite the increased adsorption density from 5.7% to 93% (Figure 4.29; Figure 4.30; Appendix B).

The instability of the above collector molecules under acidic conditions could be linked to their high pKa values. High pKa values are associated with the electron donating linking atoms in the collectors (N, S), which make the collector molecule a strong base. Also, the opposite is true for the PNBX and SNDBDTP collectors which possess oxygen, viz. electron-withdrawing linking atoms which have low pKa values, making the collector molecules acidic (Rao, 2004). For example, the reported pKa values of PNBX, sodium normal diethyl dithiocarbamate (SNDEDTC) and SNDEDTP are 2.23 (Huyashi et al., 1984), 7.5 (Raju & Forsling, 1991) and ~ 0 (Rao, 2004) respectively. The pKa values for the novel collectors were not determined in this study but are expected to be in the same range as the SNBDTC pKa since they also contain the N, electron donating atom. Studies have shown that the decomposition of xanthate collector takes place below the pH of 2 as reflected by the decrease in the pyrite recoveries of pyrite below the pH 2 (Leppinen, 1990; Fuerstenau et al., 1968).

Unexpectedly, the recovery of sperrylite with PNBX did not improve despite the 93% collector adsorption at pH 4. This indicates that, even though the xanthate collectors may adsorb on the platinum arsenide mineral surface, the resultant hydrophobicity was not sufficient to allow bubble-particle attachment. In another study, molecular xanthate was detected on the slow floating Pd-Bi-Te and gave rise to a contact angle of 63° which gave sufficiently high recoveries (97%) of the mineral in the size range of -106+38µm (Vermaak et al., 2005). However, no molecular xanthate was detected on the surface of sperrylite under alkaline conditions (Vermaak et al., 2007).

This also shows that collector adsorption alone as determined by the differences in concentration in the aqueous phase before and after contact with the mineral, does not translate to higher flotation recoveries, a hydrophobic surface layer is the main requirement and is mainly dependent on the surface products formed on the mineral.

The rest potential tests also revealed another unexpected result about sperrylite. Under acidic conditions the rest potential of sperrylite was 243.7 ± 10.7 mV as opposed to 233.7 ± 7.2 mV at pH 9.5, giving an increase of 10 mV, which was still within the standard deviation of the rest potential average values (Figure 4.51). This is an indication that the surface potential before adding the collectors remained unchanged under acidic and alkaline conditions. This shows that sperrylite is resistant to surface alteration and remained unoxidized under alkaline conditions. Studies have revealed that superficial surface oxidation is necessary for collector adsorption, whereas heavy oxidation is a major cause of the poor floatability of minerals (Nakazawa & Iwasaki, 1986; Shackleton et al., 2007). Hence, this study has shown that surface oxidation is not the cause of the poor floatability of sperrylite under alkaline conditions, nor did it assist in collector adsorption. However, there was a greater extent of electrochemical interaction with all the collectors at low pH as opposed to alkaline conditions. This observation also corresponds with the extent of collector adsorption observed at pH 4. Sperrylite seems to exhibit refractory characteristics and since froth flotation is mainly dependent on the chemisorption of collectors, a process that also involves concurrent oxidation of the collector and the mineral surface, hence, there are very slim chances of improving the recovery of sperrylite by chemical means.

Thiol collectors can be adsorbed on the mineral surfaces by either chemisorption or physical adsorption or both. Chemisorption involves an exchange of electrons involved between the collector and the mineral surface, resulting in the formation of chemical bonds (Rao, 2004). In this study, the XPS and TOF-SIMS results also corroborate that the PNBX and SNBDTC collectors were not chemisorbed onto the sperrylite surface.

This study further indicates that the poor collector adsorption and poor extent of interaction of the collectors during the rest potential tests were not caused by excessive surface oxidation. This study has revealed that no oxidation takes place on the sperrylite surface under alkaline conditions. Further support for the refractory nature of the sperrylite surface is found in a study by Mwase (2016) which indicated that sperrylite leached slowly with cyanide and cyanide-ferricyanide lixiviants, suggesting the refractory nature of the mineral. This reveals the difficulty experienced in trying to break the Pt-As bonds, resulting in the poor dissolution of platinum.

5.2.1.4. Effect of Plant Water Ions

Plant water ions are known to influence the floatability of the minerals in different ways (Shackleton et al., 2012). This part of the study focused on the floatability of sperrylite in synthetic plant water. The flotation recovery of sperrylite with 1 pseudo-monolayer coverage of PNBX in distilled water was 51% while that with synthetic plant water at pH 9 was 26% (Figure 4.12). This shows that the recovery of sperrylite was negatively impacted by the presence of plant water ions. Further studies still need to be carried out to determine the effect of the individual ions in the water on the recovery of sperrylite.

The XPS results also indicated the presence of the metal oxides on the sperrylite surface after conditioning the sample in synthetic plant water at pH 9. The synthetic plant water consists of metal ions that can easily be oxidized when exposed to air or form metal hydroxides under alkaline conditions. These compounds could be responsible for the poor natural floatability of the mineral in plant water; however, the natural floatability of the mineral was not determined in deionised water. A study by Pikinini et al., (2020) gave a fairly moderate collectorless recovery of sperrylite of 34.8% deionised water.

There was a reduction of the metal oxides formed on the mineral surface after conditioning the sample in the collector solution of PNBX and SNBDTC, by 54.5% and 44.5% respectively (Table 4.11). However, the amount of oxides which were formed could have hindered the mineral collector interactions resulting in lower recoveries. In terms of which ions, specifically, which negatively affect the mineral flotation, these would almost certainly be the divalent cations, which can form oxyhydroxo species at high pH's and cause mineral surfaces to become hydrophilic.

Collectors can form complexes with the metal ions in synthetic plant water and dithiocarbamate collectors form stable complexes with metal ions, hence their application in metal ions removal (Szolar, 2007). On the other hand, pyrite was activated by the plant water ions resulting in high recoveries as opposed to distilled water. The rest potential tests revealed that the surface of sperrylite was unreactive, hence the ions which activated other minerals could have acted as contaminants on the mineral surface resulting in reduced recoveries. The addition of the Cu^{2+} ions in this study also further depressed the recovery of the mineral further showing the sensitivity of the sperrylite mineral surface to any changes in the pulp chemistry (Figure 4.16).

5.2.1.5. Effect of Increased Eh

Figure 4.15 shows that the recovery of sperrylite at a high Eh of 660 mV with PNBX decreased by 14.4%. Increasing the pulp Eh had a depressing effect on sperrylite. This result contradicted electrochemical and Raman spectroscopic studies carried out by Vermaak et al., (2007) that concluded that the hydrophobicity of sperrylite should increase with an increase in potential. The electrochemical contact angle measurements, in the presence of ethyl xanthate, gave the highest contact angle of 54º at a potential of 400 mV (vs SHE). The surfaces of sperrylite were found to be hydrophilic at low potentials, with contact angles of 0º at potentials of 200 mV and below.

Also, when sperrylite was anodically polarized at 300 mV (vs SHE), there was a rapid formation of the dixanthogen bands on the mineral surface after 2 minutes (Vermaak et al., 2007). This is an indication that under normal flotation pulp potentials the mineral cannot catalyze the oxidation reaction of the xanthate collector to form dixanthogen.

The potential range of the natural sperrylite electrode, from the rest potential measurements, was 233.7 ± 7.2 mV to 243.7 ± 10.7 mV at pH 9.5 and pH 3.5. In the presence of ethyl xanthate, at 250 mV, the potential controlled contact angle measured was ~ 25° (Vermaak et al., 2007). The recoveries obtained with PNBX at pH 9 seem to be consistent with the minimal contact angle that was measured at the potential of 250 mV. This study also clearly confirms that particle size effects are not the major cause of the poor floatability of sperrylite as suggested by the study by Vermaak et al., (2007).

The fact that high pulp potentials failed to improve the floatability of the sperrylite may be due to the fact that pulp Eh is different to the electrochemical potential at the mineral surface. However, this was a brief and preliminary test on pulp Eh conditions and further work is required to make definitive conclusions.

5.2.1.6. Effect of Adding Copper Sulphate Activator

An investigation was carried out to determine the effect of adding copper sulphate during the flotation of sperrylite with SNBDTC. Pyrite, which has the same isometric crystal structure as sperrylite can be activated by Cu^{2+} ions thereby increasing its recovery (O'Connor et al., 1988). Hence, the possible activation of the sperrylite surface by the adsorption of the Cu^{2+} ions was investigated. Copper sulphate (Figure 4.16) had a depressing effect on the recovery of sperrylite and the recovery was reduced by 14.4%. The results give an indication that the ions were not adsorbed onto the mineral surface as Cu^{2+} ions but were possibly forming hydrophilic $Cu(OH)_2$ colloids that had a passivating effect on the surface of the mineral. Different mechanisms have been proposed that lead to the activation of the mineral surfaces by transition metal ions: ion exchange and redox reaction upon the adsorption of the Cu^{2+} ions (Finkelstein, 1997). None of these two mechanisms could have taken place on the sperrylite mineral surface since there was no increase in sperrylite's recovery. In addition, copper ions in solution act as acceptors or competitive adsorption sites and could react with the SNBDTC collector to form a stable complex leading to reduced flotation recovery of the mineral. This corroborates with the cyclic voltammetry findings from a study by Tadie et al., (2017), which showed that there was a reduction of collector activity on the tested mineral surfaces in the presence of copper sulphate. A study by Shackleton et al., (2007) also indicated that adding copper sulphate with SIBX collector was detrimental to the recovery of most PGM minerals that were investigated. It was concluded that the formation of $Cu(OH)_2$ colloids, detected during the TOF-SIMS analysis, was responsible for reduced collector adsorption.

5.2.1.7. Effect of Adding an Ether Amine Collector

Figure 4.17 gave the recovery curve of the Flotigam 7100 collector. The ether amine collector that is mainly used for the flotation of oxide minerals, dosed at about 20 pseudo-monolayers at pH 9, gave a recovery of 40.9%, which is fairly comparable to the 30 pseudo-monolayers recovery with SNBDTC under the same conditions.

Although a nitrogen ligand in the collector can bond with the metal on the mineral surface, it does not have the ability to back-bond since it does not have vacant d-orbitals. Nitrogen, being a donor atom, is also able to bond with the As donor on the sperrylite mineral surface. A study by Mkhonto et al. (2018) revealed that one of the exocyclic nitrogen ligands in the 2-mercaptobenzothiazole (MBT), 2-mercaptobenzoxazole (MBO) and 2-mercaptobenzimidazole (MBI) collectors directly bonded with the Fe atoms in pyrite. The molecular modelling studies by Nemutudi et al., (2022) also revealed that the N in the SDTBAT collector could also form a bond with As on the sperrylite surface.

5.3. PYRITE

Pyrite was selected as a readily available proxy for sperrylite since it has the same crystal structure as sperrylite. Also, the mineral was used to further understand the effect of the sulphur bonding ligand on the mineral surface as opposed to the arsenic donor atom on the sperrylite surface.

5.3.1. Pyrite Flotation Response

Pyrite showed a different flotation response to that of sperrylite under the standard test conditions (pH 9, 1 pseudo-monolayer). Just like sperrylite (14.5%), pyrite (17.8%) had poor natural floatability when floated without a collector. However, a notable increase in recovery to 94% after adding PNBX collector was realized with pyrite as opposed to 26% with sperrylite (Figure 4.26). Also, SNBDTC gave a moderate recovery of 43.4% for pyrite, which was only attained after adding 30 pseudo-monolayers of the same collector with sperrylite. The increase in recovery corresponded to a greater extent of adsorption onto the pyrite, giving an adsorption density that ranged from 41.6% to 96.1% (Figure 4.31). On the contrary, minimal adsorption of the standard collectors was observed on sperrylite at pH 9. SNDBDTP gave the lowest recovery of 18.8% which was slightly lower than the recovery of sperrylite under the same conditions. However, dithiophosphates have recently been shown to have a different interaction mechanism to other thiol collectors (Pienaar et al., 2019). The difference in the flotation performance between sperrylite and pyrite with standard collectors may be an indication that the presence of the arsenic donor atoms on the sperrylite mineral surface has a greater effect on its collector induced floatability. Even though they also differ in the metal atom (Pt versus Fe), it is known that certain platinum minerals such as cooperite have excellent floatability. Therefore, it is proposed, that the problematic floatability is as a result of the presence of the arsenic atoms.

The rest potential tests also showed that pyrite had a greater extent of interaction as signified by the drop in potential after adding the standard collectors for pyrite compared to sperrylite. The rest potential values, indicating the extent of interaction of pyrite, ranged from 15.6 mV to 206.1 mV while that of sperrylite ranged from 7.6 mV to 24.9 mV (Figure 4.52). SNDBDTP extent of interactions was the least in all the instances. The final rest potentials of pyrite after adding all the collectors predicted the formation of dithiolates and this is consistent with what has been shown in literature (Finkelstein & Poling, 1977).

It is generally proposed that the formation of dithiolates is desirable for higher flotation recoveries of the minerals. Sulphide minerals have been found to float well in the presence of either the dithiolate or metal thiolate, even though the presence of the dithiolate often resulted in higher floatability (Finkelstein & Poling, 1977). However, there is some controversy regarding the flotation recoveries that result from the formation of metal thiolates and dithiolates. It has been shown that the adsorbed butyl xanthate gave a contact angle of 74° and di-butyl dixanthogen gave a contact angle of 95° on the galena surface. Indeed, it can be argued that the higher recoveries could have been caused by the surface products that form on galena since it has high natural floatability, indicated by the recovery of 97.3% without adding the collector (Taguta, 2015). This clearly suggests that many factors influence the floatability of minerals other than the surface products that are formed after adding the collector.

Another study by Tadie (2015) indicated the reliability of the rest potential tests in predicting the products that are formed on the mineral surface and indicated the difference in the behaviour of the sulphide and telluride minerals. A similar trend was also observed in this study that clearly shows the difference in the interaction of the sulphides and arsenides minerals. The collector dosage used in the rest potential tests is somewhat greater than that used in the flotation tests and the extent of interaction in some cases does not correspond to the flotation recoveries of the minerals.

The surface products that form on the mineral in the absence of collector can determine the floatability of some minerals. Studies have clearly indicated that electrochemical oxidation leads to the formation of a sulfur-rich surface with the hydrophilic iron hydroxide species that coat pyrite when conditioned at pH 9. This results in pyrite's poor flotation response at pH 9 while only a sulphur-rich surface is formed under acidic conditions (Ahlberg et al., 1990). It was shown in this study that the rest potential of pyrite (284.2 ± 3.7 mV) at pH 9.5 was found to be higher than that of sperrylite (233.7 ± 7.2 mV).

Under alkaline conditions, it has been shown that the collector primarily removes the hydroxide ions on the mineral surface to a certain extent before adsorbing onto the mineral surface (Smart et al., 1998). This was indicated by surface analysis where valuable mineral particles that reported to the tailings contained less hydroxide ions on their surface compared to the feed particles (Smart et. al., 1998). The isothermal titration test also confirmed the possibility of the removal of the hydroxide ions by the collectors. Results showed that the binding energy of hydroxide ions at high pH (pH 13.2) on sperrylite was lower than that of SNBDTC and PNBX collectors. However, this result contradicts the molecular modelling studies that predicted that the binding energy of the hydroxide ions was greater than that of SEX (Waterson et al.,

2016). This could have been caused by the factors that are not taken into consideration during the molecular modelling computations: aqueous condition and the surface products that are formed on the mineral during conditioning. This makes the isothermal titration calorimetry results more reliable except that it was not possible to control the pH due to the size of the ampoules used.

The improved collector adsorption was also corroborated by the isothermal titration calorimetry results which showed that the binding energy of standard collectors with pyrite was greater than that with sperrylite (Figure 4.53). This also corroborates that the presence of the As atoms on sperrylite result in reduced binding energies as opposed to the S donor atoms on pyrite. This was confirmed by the molecular modelling studies by Nemutudi et al., (2020) where the binding energy of pyrite with PNBX was greater than that with sperrylite.

5.3.1.1. Floatability of Pyrite with Novel Collectors

The flotation recovery of pyrite in the presence of novel collectors was much greater than that of sperrylite, even though the same trend in recoveries was observed for each novel collector. The recoveries ranged from 60% to 92% as shown in Figure 4.58. The improved recoveries also corresponded with the improved extent of collector adsorption onto the pyrite as opposed to sperrylite at pH 9 (Figure 4.39). The extent of adsorption ranged from 80.8% to 92.4% resulting in fairly high pyrite recoveries as opposed to sperrylite.

The novel and the standard collectors have sulphur ligands and this could be an indication that they are not suitable or powerful enough to adsorb to and impart hydrophobicity to sperrylite, but making them most suitable for sulphide minerals.

The adsorption test results further shed insight into the effects of surface topography and the respective bonding ligands (S, As) on the mineral surface. Even though sperrylite and pyrite have the same isometric crystal structure, the behaviour of the S and As atoms on these mineral surfaces might differ to a greater extent. The study by Waterson (2015) indicated that the surface clefts in $PtAs_2$ are deeper by 0.28A° and have a higher rise angle than pyrite making it more difficult to access Pt atoms in sperrylite. The adsorption results have also been confirmed by the isothermal titration calorimetry tests that showed that the binding energy of thiol collectors on pyrite was greater compared to sperrylite.

Figure 4.21 shows that SDCDTDBAT and SDTBAT collectors gave recoveries that are superior to those of standard collectors: 81.5% and 74.8% respectively in deionised water at pH 9. This is proof that hypothesis 2 was correct when it comes to pyrite, as the increase in the inter-atomic distance between the two chelating atoms compared to that of typical thiol collectors resulted in higher recoveries. It can be concluded that much stronger collectors are required in the recovery of sperrylite or collectors with different binding ligands.

Theoretically, the sulphur ligand in the collectors has a high affinity for the Pt metal and the arsenic donor atom on the mineral surface (Somasundaran & Nagaraj, 1984; Nagaraj & Ravishankar, 2007), which can weaken the binding energy of ligands due to increase in the number of binding sites since the ligands get attracted to more than one site. The affinity of sulphur for arsenic can also be seen in the existence of realgar (As_4S_4) in nature. The affinity of a sulphur ligand for arsenic was also confirmed by molecular modelling computations that indicated that the collector can either dock on Pt or As atoms or both (Nemutudi et al., 2020). This could have resulted in weakened collector strength resulting in poor sperrylite recoveries with both novel and standard collectors. Figure 1.13 shows that the sulphur ligand passes over an As atom in order to bond with Pt atoms, hence bridging on two Pt atoms gave the lowest binding energy. On the other hand, collectors with sulphur ligands can effectively adsorb to the pyrite mineral because the two sulphur atoms cannot approach closely, hence all the ligand binding energy is directed towards the Fe metal ions, resulting in higher recoveries.

In addition, a computational study by Nemutudi et al. (2020) also confirmed that the binding energy of PNBX on pyrite (-306 kJ/mol) was greater than that on sperrylite (-270 kJ/mol). During molecular modelling studies on pyrite, docking the sulphur collector ligands on the sulphur ions on the mineral surface failed and the ligands moved away from the sulphur atoms to bind with the Fe ions (Nemutudi et al, 2020 personal communication). This gives us insight into what could be taking place on the mineral's surfaces and the possible binding sites. This is caused by the steric hindrance on sulphur atoms and hence they cannot approach closely to form a desirable bond. This factor seems to be favourable for the formation of stronger collector bonds, as the sulphur ligands are attracted to the metal ions in sulphide minerals.

On the other hand, the bonding of S with the As ion is most likely to take place because the arsenic ion is bigger and it is less sterically hindered for bonding resulting in no repulsive forces between the two approaching ligands. The lowest binding energy was obtained when bridging with two Pt ions (Nemutudi et al., 2020), confirming the presence of attracting forces from projected arsenic atoms, indicative of the steric hindrance they pose to the approaching collector ligands.

5.3.1.2. Effect of Synthetic Plant Water Ions on the Floatability of Pyrite

Figure 4.27 shows that the recoveries of pyrite were generally higher in 2SPW plant water than in distilled water, except for SNDBDTP which had a recovery that was similar to the collectorless recovery in pyrite. The presence of plant water ions enhanced the recovery of pyrite with PNBX and SNBDTC. In distilled water, the recoveries of PNBX and SNBDTC were reduced by 50.6% and 26.8% respectively, while that of SNDBDTP was increased by 9.8%. The same behaviour was noted when pyrite was floated using the SDTBAT and SDCDTDBAT novel collectors, where the plant water recoveries were higher in synthetic plant water than distilled water recoveries at pH 9.

From the given results, it can be concluded that the effect of plant water depends on the type of the mineral and the collector added to the system. The performance of xanthates is enhanced by the presence of plant water ions for pyrite while that of SNDBDTP was negatively impacted in pyrite flotation only. A study by Mhonde et al., (2020) showed that the cationic ions in plant water, Ca^{2+} and Mg^{2+}, enhanced the chemisorption of SIBX on chalcopyrite. Another study by Davia-Pulido et al., (2015) also indicated within the pH ranges that are below 10, the presence of Ca^{2+} resulted in the improved adsorption of xanthate on sphalerite (ZnS).

Furthermore, the zeta potential tests indicated that the charge on the PbS and ZnS mineral surfaces became more positive as the concentration of Ca^{2+} and Mg^{2+} cations increased, making the surfaces more attractive to the adsorption of the xanthate collectors (Bulut & Yenial, 2016). On the other hand, the S_2O_3 ions were competitively adsorbed on the chalcopyrite mineral surface to form a copper thiosulphate complex thereby preventing the adsorption of SIBX (Mhonde et al., 2020).

The interesting part of this study is the difference between the effect of ions on the floatability of pyrite compared to sperrylite. The absence of ions enhanced the recovery of sperrylite with PNBX, compared to depressing floatability for pyrite. This will be discussed in further detail when discussing arsenopyrite below.

5.3.1.3. Effect of pH on the Floatability of Pyrite

Unlike sperrylite, pyrite showed good floatability at pH 4 in distilled water with both PNBX and SNDBDTP (Figure 4.28). It is well documented, that the recovery of pyrite is high under acidic conditions. SNBDTC collector was found to be unstable at pH 4 due to the hydrolysis of the collector molecules, as a result, it gave the lowest increase in the recovery of pyrite at pH 4 as opposed to PNBX and SNDBDTP. As indicated previously, the low pKa values of PNBX and SNDBDTP are associated with the relative stability of the collectors under acidic conditions and high pyrite recoveries at pH 4. Studies have indicated that electrochemical oxidation leads to the formation of a hydrophobic sulfur-rich surface which aids good collector adsorption resulting in higher recoveries under acidic conditions (Ahlberg et al., 1990). Sperrylite, on the other hand, gave moderate recoveries with SNBDTC and no recovery improvement with PNBX at pH 4. Carrying out tests with sperrylite and PNBX at pH 4 in deionised water could help to further explain this unexpected behaviour of sperrylite.

Just like sperrylite, pyrite also showed a greater extent of electrochemical interaction with the standard collectors at pH 3.5. Moreover, the extent of interaction of pyrite with PNBX and SNBDTC was also found to be more than 1.7 times greater than that of sperrylite at pH 3.5. Also, it confirms that high pH negatively affects the interaction of these minerals with the collectors.

At pH 3.5 the rest potential of pyrite (411.5 ± 1.1 mV) was more positive than that at pH 9.5 (284.2 ± 3.7 mV) (Figure 4.52). This significant increase in the rest potential values of pyrite shows that different surface behaviour occurs on the pyrite mineral under alkaline and acidic conditions. Evidently, surface alteration does take place on pyrite as documented in literature (Fuerstenau et al., 1968). On the contrary, the rest potential of sperrylite remained unchanged with change in pH, showing that the mineral could not be oxidized under alkaline conditions. The other major difference between sperrylite and pyrite is that As is bonded to a noble metal (Pt), whereas S is bonded to iron which is fairly reactive.

5.4. ARSENOPYRITE

Tests were carried out using arsenopyrite to determine the effect of the sulphur and arsenic atoms and the monoclinic crystal structure. They were compared to sperrylite and pyrite and their isometric crystal structures.

5.4.1. Arsenopyrite Flotation Response

Arsenopyrite showed good natural floatability (86.2%) and a maximum increase in recovery obtained after adding the standard collectors was 7.8%, with the PNBX collector (Figure 4.26). It appears that the presence of 16.5% pyrite as indicated by the XRD analysis results has had little effect on the arsenopyrite behaviour. The natural floatability of arsenopyrite is beneficial when processing the arsenopyrite gold ores. However, in the flotation of base metal sulphides, studies have focused on depressing the mineral. Unlike pyrite and sperrylite, the mineral showed very good natural floatability and very little improvements were noted after adding the standard collectors. The difference in recoveries using the standard collectors was greater for pyrite and SNDBDTP gave the lowest recovery as opposed to arsenopyrite and sperrylite.

Notably poor collector adsorption of PNBX collector was noted on arsenopyrite but this did not have any impact on the recovery of the mineral (Figure 4.39). Surface oxidation could be the major cause of the fairly low adsorption of the PNBX collector.

XPS results also indicated the presence of the arsenolite and metal oxides on the surface of the untreated arsenopyrite sample (Table 4.13). The XPS results also corroborated the poor adsorption of the PNBX onto the mineral sample. There was a 39% increase in the mercaptan content after treating the sample with PNBX, indicating that the collector was chemisorbed onto the mineral. Furthermore, the TOF-SIMS results confirmed the chemosorption of the PNBX collector on the arsenopyrite surface by the increase in carbon content (Table 4.14). Arsenopyrite has a monoclinic crystal structure and its behaviour was found to be totally different from that of sperrylite and pyrite. The effect of surface topography could also explain the reactivity of the mineral. The mineral has two bonding ligands (S, As), the working surface of arsenopyrite given in Figure 1.6 shows that both arsenic and sulphur atoms are exposed at the surface as opposed to the sulphur atoms in pyrite.

On the other hand, the formation of the hydrophobic surface layer on arsenopyrite, which is responsible for its natural floatability, could be responsible for poor collector adsorption.

Literature shows the variation in the floatability of arsenide minerals and the factors that influence their floatability. In the case of NiAs, the poor floatability was caused by the formation of nickel hydroxide and high recoveries of the mineral could be obtained between pH 4 to pH 8 (Nakazawa and Iwasaki, 1986) due to the reduction in the hydroxide ions concentrations. This shows that the Ni acceptor was available for bonding with the OH^- ions and that resulted in the poor floatability of the mineral.

However, the surface oxidation in Pd_2As seems to have aided its natural floatability and had no effect on its collector induced fairly high floatability (Shackleton, 2007). Studies have also shown that excessive oxidation of arsenopyrite using oxidants like hydrogen peroxide could depress the mineral (Monte et al., 2002; Beattie and Polling, 1987). One thing is common in the above minerals; their surfaces can be altered at any given time to either float or depress them. This is the missing factor when it comes to sperrylite, which exhibits high surface sensitivity and yet it cannot be chemically altered under the normal flotation conditions and at elevated Eh. It can also be seen that some minerals can be adversely affected by the high concentration of the hydroxide ions at pH 9, like FeS_2, NiAs, $PtAs_2$, while the other minerals like PbS, PtS, FeAsS did not seem to be affected by the same conditions.

The rest potential of arsenopyrite at pH 9 (179 ± 26.7 mV) was lower than that of sperrylite (233.7 ± 7.2 mV) and pyrite (284.2 mV) (Figure 4.51). The low rest potential of the mineral in comparison to other minerals is usually associated with the ease with which the mineral can be oxidized. Therefore, its high collectorless recovery can be attributed to a hydrophobic oxidation layer that could have been formed during the conditioning period. Studies have shown that arsenopyrite releases S and As under acidic and alkaline conditions (Buckley & Walker, 1988). A study that investigated the oxidation of arsenopyrite in oxygenated solutions indicated the presence of As and S in multiple oxidation states close to the unaltered surface (Nesbitt et al., 1995). Also, when arsenopyrite was reacted with oxygenated distilled water, the Fe^{3+} oxyhydroxide species were the major iron species found and the As^{+5}, As^{+3}, As^{+1}, and As^{-1} species were also found in greater quantities. Appreciable amounts of sulphate were also found on the mineral surface.

Moreover, it was also revealed that arsenic was readily oxidized compared to S on the mineral surface and that similar oxidation rates of As^{-1} and Fe^{+2} were observed during the study by Nesbitt et al., (1995). Under the acid mine drainage conditions, arsenopyrite was found to be more reactive than other minerals such as pyrite, chalcopyrite, galena and sphalerite. This corroborates with our results that indicated that the rest potential of arsenopyrite was lower than that of pyrite, indicating that the mineral was readily oxidised as opposed to pyrite under both acidic and alkaline conditions.

A study by Corkhill & Vaughan (2009) revealed that the naturally weathered arsenopyrite samples had an effective passivation layer that protected the mineral from further oxidation. Similar observations were also made on the arsenopyrite in tailings dams, where particles were protected from further oxidation by the rims of secondary minerals such as scorodite, arseniosiderite and goethite (Paktunc et al., 2004).

The behaviour of arsenopyrite and pyrite clearly sheds more light on the surface of sperrylite as indicated by the rest potential tests. Sperrylite could be unreactive because the As atoms are bonded to a noble metal, platinum. This shows that the behaviour of the arsenic donor atom on a mineral surface is dependent on the type of the mineral and the crystal structure of the mineral. It is important to note that it was cited that the rate of oxidation of the As^{-1} and Fe^{2+} were the same in arsenopyrite.

The same was reported in literature on pyrite which has the same crystal structure as sperrylite, indicating an alteration of both the iron and the sulphur donor atom on the mineral surface. Also, the oxidation states of Pt and As could play a role in the ease with which the mineral could be oxidised. There is still uncertainty that surrounds the oxidation state of Pt and As in literature. Platinum could take a +4 or +2 oxidation state. Also, the Pt-As bond could be much stronger compared to Fe-S and Fe-As bonds, rendering sperrylite unreactive. It is important to note that these transition metals all form the dπ-dπ bonds with S and As donor atoms since they all possess empty d-orbitals.

The extent of electrochemical interaction of arsenopyrite under alkaline conditions was greater than that with sperrylite. Strikingly, the extent of interaction of arsenopyrite (45 mV) with PNBX was 2 times greater than that with sperrylite (17.7 mV). Its extent of interaction with SNBDTC was also 3.8 times that of sperrylite. This corroborates with the collector adsorption results that showed SNBDTC was adsorbed to a greater extent on arsenopyrite as opposed to PNBX. The dithiolate prediction for PNBX and arsenopyrite matches with the prediction in literature. However, with DTC and DTP, no positive identification was made (Finkelstein & Goold, 1972) and it was concluded that small quantities of the surface products were extracted from the mineral.

5.4.1.1. Effect of Synthetic Plant Water Ions

The floatability of arsenopyrite was also enhanced by the presence of plant water ions as was the case with pyrite but to a much lesser extent (Figure 4.27). Also, the mineral showed high natural floatability as opposed to pyrite and sperrylite. The same trend was observed in the flotation of arsenopyrite with PNBX and SNDBDTP while the opposite was observed for SNBDTC recoveries. The recovery of arsenopyrite with PNBX was reduced by 5.7% in distilled water.

This further confirms that the presence of plant water ions, when adsorbed onto the mineral surface, may enhance the floatability of certain minerals. However, it had the opposite effect with sperrylite. Shackleton (2007) proposed that the formation of $Cu(OH)_2$ species on the mineral surface may have had a competitive effect with adsorbing collector species.

The same argument could be extended to the effect of other cations in solution forming their corresponding hydroxide species and competitively adsorbing onto the sperrylite surface. However, in the absence of any further experimental evidence, this is a hypothesis that requires further investigation.

5.4.2. Effect of pH

The extent of PNBX adsorption increased on arsenopyrite under acidic conditions, from 29.9% to 88.6% (Figure 4.33). A decrease in adsorption of the dithiocarbamate collector was observed (78.4% to 25.4%) as seen with the other minerals. Rest potential tests also indicated that the rest potential of arsenopyrite at pH 4 was more positive than that obtained at pH 9.5.

This behaviour was not seen in sperrylite, hence from the rest potential results, it can be deduced that surface alteration of arsenopyrite is likely to take place at pH 9.5. Both minerals showed an increased extent of interaction with the PNBX collector at pH 3.5, however, the extent of interaction of arsenopyrite was greater than that of sperrylite (Figure 4.52). These results all agree with the adsorption tests obtained for the arsenic containing minerals. The extent of interaction of PNBX with arsenopyrite (183.7 mV) was 1.4 times greater than that with sperrylite (126 mV) under acidic conditions.

5.5. COOPERITE

Cooperite is a sulphide mineral with one sulphur bonding ligand and it is well known for its good floatability compared to other PGM minerals. Its behaviour will shed light on how it differs from sperrylite and the possible reasons for its natural floatability.

5.5.1. Cooperite Flotation Response

There was very little improvement in the recovery of cooperite after adding the standard collectors (Figure 4.26). The mineral, which consists of one S donor atom gave the highest collectorless recovery (94.8%) such that there was very little room for improvement. There was no clear distinction between the thiol collector induced recoveries of cooperite and arsenopyrite after adding different thiol collectors, even though PNBX still gave the highest recoveries. The results are in agreement with the study carried out by Shackleton (2007) that also gave the collectorless recovery of 94% and thereafter showed no improvement after adding SIBX. This confirms the findings from a study by Chetty et al., (2009) that indicated that fully liberated sulphide PGMs were fast floating as they were recovered from the first 2 cells of the UG2 rougher bank that consists of 10 cells. Cooperite behaved in a different manner compared to pyrite. The difference between these two minerals is in their crystal structures and the number of the S donor atoms on the mineral surface.

Thiol collectors were adsorbed on cooperite to a greater extent compared to sperrylite and arsenopyrite (Figure 4.39). SNDBDTP collector was only adsorbed under acidic conditions (Figure 4.35). The presence of the sulphur ligands on the mineral surface could be the reason why the collectors were adsorbed to a greater extent on cooperite and pyrite.

However, the floatability of cooperite was not dependent on the extent of collector adsorption because of the high natural floatability of the mineral (94%). The effect of a surface coating formed during conditioning that usually leads to the natural floatability of the minerals still needs to be investigated. The high adsorption density of SNBDTC on all the minerals shows that it is a stronger collector than xanthates but that did not lead to good flotation recoveries in all cases. Hence, again it is shown that collector adsorption does not necessarily result in good floatability of the mineral as indicated by the results of this study. Generally, the sulphide minerals showed a greater extent of collector adsorption compared to the arsenide minerals.

The rest potential of cooperite (256.2 ± 10.4 mV) was higher than that of sperrylite (233.7 ± 7.2 mV), but it was lower compared to pyrite (Figure 4.51). Pyrite is known to be fairly resistant to oxidation compared to the other sulphide minerals, hence from the rest potential results it can be deduced that the surface oxidation is greater in cooperite compared to pyrite. As a result, it had good natural floatability. Studies by Shackleton (2007) indicated that there was mild surface oxidation on cooperite. The prediction for the formation of the dithiolate on cooperite with PNBX is consistent with the surface analysis results carried out in the study by Shackleton (2007). This also confirms that the xanthate collector was chemisorbed onto the mineral surface even though it gave no improvement on the recovery of the mineral. Hence, a degree of surface oxidation is a requirement for the chemisorption of collectors as shown by the arsenopyrite XPS results with PNBX. The rest potential of cooperite at pH 9.2 in a study done by Tadie (2015) was 240 mV and it is within the acceptable range from our recorded average rest potential of the mineral.

The extent of electrochemical interaction with the thiol collectors under alkaline (Figure 4.42) and acidic (Figure 4.52) conditions followed the order: PtS > FeS_2 > FeAsS > $PtAs_2$. Minerals with Arsenic as a donor atom had little interaction with the collectors, especially sperrylite, whereas the sulphide minerals had the greatest interaction with all the thiol collectors. The surface chemistry of these minerals when conditioned in water differs from one mineral to the other and this study has shown that it greatly determines the interaction of the mineral with collectors.

In addition, the functional groups of the standard collectors play a role in the change in potential of the minerals after adding the collectors. The trend of potential drop was SNBDTC > PNBX > SNDBDTP. The decrease in potential shows the ease with which the different collectors can donate electrons to the mineral surface and also the ease with which the mineral accepts the electrons from the collector as it is reduced. As indicated, the nitrogen linking atom in SNBDTC is electron donating resulting in greater extent of interaction.

PNBX which has one oxygen linking atom which is electron withdrawing, gave the extent of interaction which is less than that of SNBDTC. SNDBDTP has two oxygen linking atoms which are electron withdrawing, making it very difficult for the collector to be oxidised. Hence, it gave the least extent of interaction with all the minerals. This behaviour is also demonstrated by the oxidation potentials of the collectors that follows the order SNDBDTP > PNBX > SNBDTC, with the lowest potential indicating the ease which the collector can donate electrons to the mineral surface.

5.5.2. Effect of pH

Under acidic conditions, the rest potential of cooperite was more positive than the rest potential at pH 9.5 (Figure 4.51). That behaviour was observed for all the minerals except for sperrylite under acidic conditions. The rest potentials of the minerals before adding the collectors at pH 9.5 at 600 seconds: PtS (518 mV) > FeS_2 (411.5 mV) > FeAsS (355 mV) > $PtAs_2$ (243.7 mV).

The less positive rest potentials of pyrite, arsenopyrite and cooperite minerals at pH 9.5, as opposed to the more positive rest potentials at pH 3.5, are an indication that the minerals are more prone to surface oxidation at pH 9.5 than at pH 3.5. The findings are consistent with the study by Tadie et al., (2015) that indicated that the rest potentials of the pure platinum and palladium metals were higher than those of the respective minerals that could be oxidised. Cooperite, a sulphide mineral with one sulphur donor atom, had the greatest interaction with PNBX and SNBDTC.

The extent of interaction of the minerals with collectors was generally greater under acidic conditions as indicated by the potential drop after adding the thiol collectors (Figure 4.52). The extent of interaction with the thiol collectors followed the order: SNBDTC > PNBX > SNDBDTP except with sperrylite at pH 3.5 where the extent of interaction of PNBX was greater than that of SNBDTC. There was an increase in the adsorption density of the PNBX and SNDBDTP collectors under acidic conditions.

SNDBDTP showed very little interaction with all the minerals at pH 9.5 and pH 3.5, even though there was an improvement under acidic conditions.

Under acidic conditions, dithiolates were predicted for all the minerals with the exception of sperrylite and SNDBDTP. All the minerals showed a greater potential drop after adding the collectors under acidic conditions. This is an indication that the higher concentration of the hydroxide ions greatly impacted the interaction of the minerals with the collectors. However, sperrylite still gave the lowest extent of interaction.

5.6. THE NATURAL FLOATABILITY OF MINERALS

The flotation recoveries of the minerals were also determined without adding the collector. Sperrylite had the lowest collectorless flotation recovery compared to the other minerals at pH 9 in synthetic plant water as given in Figure 4.26. It was observed that pyrite (17.8%) and sperrylite (14.5%) which have isometric crystal structures had very low natural floatabilities. On the contrary, cooperite (94.8%) and arsenopyrite (86.2%) which have tetragonal and monoclinic crystal structures respectively showed good natural floatability. The difference in the minerals' natural floatability has been attributed to their crystal structures and their cleavage surfaces or working surfaces, for example, the high floatability of realgar has been linked to its crystal structure (Rao, 2004).

Surface analysis techniques have been used in different studies to determine the surface products that form on the mineral surfaces under different pulp conditions. The formation of surface products has been attributed to either low or high natural floatability of the minerals. The XPS results showed that the behaviour of sperrylite was different from that of arsenopyrite after conditioning with synthetic plant water. Sperrylite, which has poor natural floatability had no surface oxidation before the sample was treated with synthetic plant water.

According to the atomic percentage of the surface elements and products quantified by the XPS analysis, it was shown that there was a 92.7% increase of metal oxides on the surface of sperrylite after conditioning with plant water (Table 4.11) and this could be responsible for its poor natural floatability. A reduction of 54.5% of the metal oxides found on the mineral when conditioned in synthetic plant water after adding the PNBX collector (Table 4.11) resulted in the improved floatability of the mineral.

On the other hand, there was initial surface oxidation of 6.6% by atomic weight that was detected on the surface of the untreated arsenopyrite sample. The XPS results indicated an increase in the metal oxide atomic species by 61.4% after conditioning the arsenopyrite sample in synthetic plant water (Table 4.13). When the sample was conditioned in synthetic plant water with PNBX collector, the metal oxides found on the mineral surface were reduced by 7% (Table 4.13). The initial surface oxidation on the untreated arsenopyrite sample could be responsible for the natural floatability of the mineral because the same change in metal oxide content was noted for both arsenopyrite and sperrylite after conditioning the minerals in synthetic plant water of around 10% atomic weight.

The metal oxides formed from the synthetic plant water ions that could not enhance the floatability of sperrylite, could not have been responsible for the natural floatability of sperrylite. Moreover, the surface oxidation layer could have also been responsible for the poor interaction of the mineral with collectors, especially PNBX. Arsenopyrite forms $FeAsO_4$ when exposed to the atmosphere and the mineral is generally more reactive than pyrite (Corkhill and Vaughan, 2009; Paktunc et al., 2004). This could be the reason why it is difficult to depress arsenopyrite except by further oxidizing it with strong oxidizing agents such as hydrogen peroxide.

This study has also shown that pyrite has poor natural floatability under both alkaline (12.3%) and acidic (8.5%) conditions in deionized water. It has been proposed that pyrite forms a hydrophobic sulphur rich surface under acidic conditions and a hydrophobic sulfur-rich surface with the hydrophilic iron hydroxide species under alkaline conditions (Ahlberg et al., 1990). This study shows that both surfaces are hydrophilic, except that the former offers no hindrance to collector adsorption which results in higher flotation recoveries. This behaviour was noted in NiAs which also form nickel hydroxide which results in poor recoveries.

Even though it is well known that the formation of the hydrophilic species under alkaline conditions reduces the floatability of minerals, the natural floatability of sperrylite and pyrite did not improve at pH 4 as shown in Figure 4.28. This is an indication that these minerals are naturally hydrophilic, and this behaviour could be attributed to their crystal structure. It is documented that before the collector adsorbs onto the pyrite surface at pH 9, the collector cleans the surface before adsorbing onto pyrite to improve its recovery (Smart et al., 1998). In the case of pyrite, the Fe atom on the mineral surface provided a free binding site for the hydroxide ions. This could also be the case with sperrylite where some species that form in the pulp do obstruct the adsorption of the collectors on a naturally hydrophilic mineral surface. The increase in hydroxide ions under alkaline conditions which readily complexes with the dissolved metal ions in synthetic plant water or pulp to form the metal hydroxide species results in poor collector adsorption.

It has been hypothesized that the natural floatability of minerals is directly related to their surface energies. Minerals with lower surface energy are expected to have high natural floatability. Figure 5.1. shows that minerals with the lowest collectorless flotation recoveries belong to the pyrite group. The surface energy of arsenopyrite is slightly higher than that of sperrylite, but its natural floatability is much greater than that of sperrylite. There could be a connection between surface energy and natural floatability as seen in galena and cooperite. However, the minerals on the graph could be a good pointer that the crystal structure and the mineral group also play a role in the natural floatability of the mineral. Generally, the naturally floatable minerals react when exposed to aqueous conditions and quickly form a hydrophobic passive layer that makes the mineral naturally floatable.

A study carried out by Shackleton (2007) confirmed the presence or absence of the oxidation products after conditioning the synthetic PGMs in plant water at pH 9. According to the study by Shackleton (2007), the ToF-SIMS results indicated that palladium minerals: PdS, $PdTe_2$ and Pd_2As were heavily oxidized by synthetic plant water during the conditioning process. Their flotation rates and recoveries were found to be higher than those of platinum minerals and did not appear to be adversely affected by surface oxidation. Platinum minerals showed minimal surface oxidation, with the exception of sperrylite, which showed no evidence of surface oxidation (Shackleton, 2007). Surface oxidation can also be attributed to fairly good natural floatability of PdS (64%), $PdTe_2$ (63%) and $PdPt(BiTe)_2$ (75%).

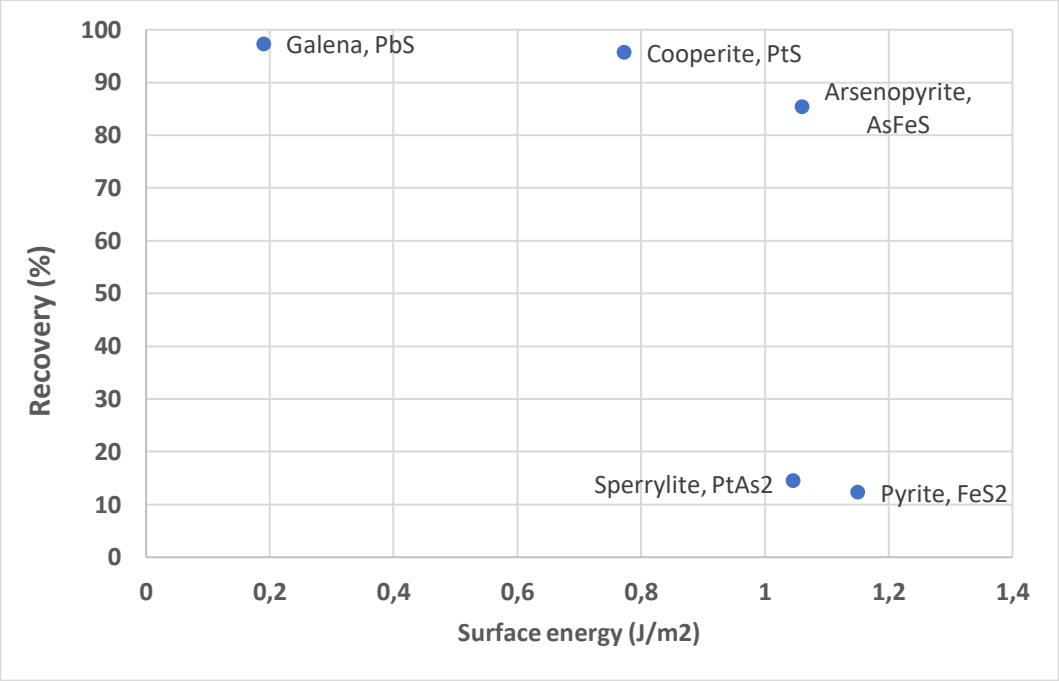

Figure 5.1 Relationship between the minerals' natural floatability and their surface energies

6. CONCLUSION

The main objective of this study was to determine the reasons for the poor floatability of sperrylite and to identify novel and known collectors that could possibly improve its recovery. Microflotation, adsorption, rest potential and isothermal titration calorimetry tests were carried out to understand the interactions of sperrylite with different collectors under various pulp conditions of pH, ionic strength and redox potential. To further shed light on the behaviour of sperrylite, the research approach also included the minerals: pyrite, arsenopyrite and cooperite with a view to understanding how crystal structures and the presence of (S, As) donor atoms on the mineral surface influenced the floatability of those minerals in comparison with sperrylite.

This study revealed that the poor interaction of sperrylite with different collectors is the major reason for its poor flotation response. Sperrylite gave poor collector-induced recoveries and poor interaction with the standard and the tested novel collectors. The poor recoveries were linked to the poor adsorption of the collectors tested. The design of the novel collectors was based on the hypotheses 2 and 3 in order to improve the recovery of sperrylite. Hypothesis 3 proposed to increase the binding energy of sulphur ligands by using the nitrogen and sulphur linking atoms which are electron donating would lead to stronger bonds and improved recoveries while hypothesis 2 proposed increasing the interatomic distance between the bonding ligands to reduce the steric hindrances, thereby increasing crystal structure compatibility with sperrylite. The hypotheses were only sustained in the case of pyrite which has the sulphur bonding ligands as opposed to sperrylite.

The XPS results showed that collectors were not chemisorbed onto the sperrylite surface, indicating that the collectors were only physisorbed onto the mineral as shown by the adsorption test results. Chemisorption is the preferred mechanism so as to form a strong bond between the mineral and the collectors and concurrent oxidation of the collector and the mineral should also take place for the chemisorption process to take place. In addition, the adsorption tests at pH 9 indicated that only 5.7% of the PNBX collector, dosed at 1 pseudo-monolayer coverage, was adsorbed and this appears to be insufficient to render the mineral hydrophobic. It was also revealed that the mineral is naturally hydrophilic under alkaline and acidic conditions and its interaction with collectors is the key to improving its recovery.

Furthermore, the mineral also showed some resistance to surface alteration as seen in the rest potential results, which remained unchanged under alkaline and acidic conditions before adding the thiol collectors. This also corroborates the fact that no surface oxidation takes place on the mineral surface. The adsorption of collectors and the recovery of sperrylite were also affected by an increase in pH but the study showed that pH was not the major factor for poor flotation recoveries. This was indicated by the PNBX recoveries that remained unchanged despite the 93.1% adsorption of the collector at pH 4 in synthetic plant water.

This study also showed that the synthetic plant water ions had a negative impact on the recovery of sperrylite. The recovery of sperrylite with PNBX was 51% in deionised water at pH 9 as opposed to the 26% in synthetic plant water. This former recovery was achieved despite the poor collector adsorption of around 5.7% when using deionised water. XPS results revealed the presence of metal oxides on the mineral surface when the sample was conditioned in synthetic plant water at pH 9. Even though almost half of these oxides were removed after adding the collectors as revealed by the XPS results, the mineral surface could not catalyse the oxidation of the adsorbed collectors because its surface was unreactive. This further revealed that the mineral surface is sensitive to any form of contamination by dissolved metal ions, as also seen by the detrimental effect of copper sulphate on the recovery of sperrylite.

In an unreactive surface of sperrylite, arsenic donor atoms on the mineral surface can also act as acceptor atoms thereby increasing the number of collector adsorption sites which consequently results in reduced overall binding energy onto the Pt of sperrylite. In a sense, the presence of the As atoms dilutes the overall strength of the binding energy of the collector with the sperrylite, especially when the collector has two bonding ligands. This was demonstrated by the lesser extent of interaction of sperrylite with the standard collectors, which contains an arsenic donor atom, as opposed to pyrite since in the latter case the sulphur ligands are only attracted to the Fe atoms which results in higher overall binding energies. Molecular modelling computations by Nemutudi et al. (2020) also showed that the sulphur ligands in the collectors had the ability to bond with Pt and As. Literature has shown that sulphur ligands have an affinity for both the Pt and As atoms on the mineral surface, which has its As atoms projected above the Pt atoms. This unique behaviour could also result in the reduced overall binding energies of the collectors with sperrylite as seen in the case of 2 Pt bonds with collector ligands. It can be concluded that collectors with sulphur bonding ligands are more suitable for sulphide minerals like pyrite. These findings sustained hypothesis 1, which proposed that both Pt and As on the sperrylite surface had a potential to bond with collector ligands by virtue of being a soft acid and a soft base respectively but that this ultimately resulted in a reduced overall binding energy of the collectors with the sperrylite.

Another objective was to determine the effect of S and As bonding ligands on the floatability of the selected minerals. Even though the minerals that contained arsenic bonding atoms had a poor interaction with the collectors, it was revealed that As bonding atoms had different reactivities in these minerals. It can be concluded that the reactivity of these ligands was mainly dependent on the metals (Fe, Pt) bonded to them and also on the crystal structure of the minerals. Hence, hypothesis 4 was also sustained which states that the crystal structure and the donor atoms (As, S) on the minerals' surfaces will have a great influence on the floatability of the minerals because they also have an ability to act as electron acceptors. The reactivity of these minerals leads to the formation of the surface products that determine the natural floatability of the minerals under different pulp conditions. It was also seen that sperrylite and pyrite, which have the isometric crystal structures, had poor natural floatability under both alkaline and acidic conditions. Hence their floatability is mainly dependent on their interaction with different collectors.

Moreover, the rest potential results showed that all the other minerals except sperrylite could be oxidised under alkaline conditions.
Due to the inertness of the sperrylite surface, the mineral could not be activated by the plant water ions or by adding copper sulphate, instead, it was depressed. The success of the froth flotation process hinges on the ability to alter different mineral surfaces in order to either depress or impart hydrophobicity and hence the resistance to surface alteration observed in sperrylite makes it difficult to recover the mineral.

It was also proposed that the surface energy of minerals determines the natural hydrophobicity of minerals, the lower the surface energy the greater the natural hydrophobicity of the mineral. This hypothesis was partly sustained but when it came to sperrylite and arsenopyrite it was not upheld. The analysis revealed that the minerals that had poor natural floatability, sperrylite and pyrite, had a common isometric crystal structure. It was also proposed that the OH^- ions can act as a ligand and have the ability to form strong bonds with the sperrylite mineral under the PGM plant operating conditions thus resulting in reduced collector adsorption which ultimately results in low recoveries. The hypothesis was not sustained as the isothermal titration test showed that the binding energy of hydroxide ions was lower than that of PNBX and SNBDTC indicating that these collectors are able to displace the hydroxide ions that are adsorbed onto the mineral surface. However, this would also require some energy, as indicated by generally higher adsorption densities of collectors at pH 4.

6.1. RECOMMENDATIONS

- Fresh water shortages have seen an increase in the use of recycled plant water and this study pointed out that synthetic plant water ions had a negative impact on the recovery of sperrylite. It is recommended that a further study should be carried out to determine the effect of the different plant water ions on the floatability of sperrylite. It should also be taken into account that the plant water ions also react with each other to form different compounds, making the study of plant water ions complex.

- Optimum conditions and collector dosages still need to be determined for the recovery of sperrylite.

- There is also a need to design collectors that have higher binding energies with sperrylite, which are stable under acidic conditions for improved recoveries. Collectors were adsorbed onto sperrylite mineral particles to a greater extent under acidic conditions as opposed to alkaline conditions.

- Since sperrylite was found to be relatively inert under conditions of increasing pH, it is suggested that a complete mapping of floatability as a function Eh and pH be made to determine floatability domains, as is common for base metal sulphide minerals.

7. REFERENCES

Ahlberg, E., Forssberg, K. S. E., & Wang, X. (1990). The surface oxidation of pyrite in alkaline solution. Journal of Applied Electrochemistry, 20, 1033-1039.

Allison, S. A., Goold, L., Nicol, M., & Granville, A. (1972). A determination of the products of reaction between various sulfide minerals and aqueous xanthate solution and a correlation of the products with electrode rest potentials. Metallurgical and Materials Transactions A: Physical Metallurgy and Materials Science, 3 (10), 2613-2618.

Bai, L., Barnes, SJ., & Baker, D. R. (2017). Sperrylite saturation in magmatic sulfide melts: Implications for formation of PGE-bearing arsenides and sulfarsenides. American Mineralogist, Volume 102, Pages 966-974.

Becker, M., Brough, C., Reid, D., Smith, D., Bradshaw, D. (2008). Geometallurgical Characterization of the Merensky Reef at Northam Platinum Mine–Comparison of Normal, Pothole and Transitional Reef Types. Ninth International Congress for Applied Mineralogy, Australasian Institute for Mining and Metallurgy, pp. 391–399.

Becker, M., Wiese, J., Ramonotsi, M. (2014). Investigation into the mineralogy and flotation performance of oxidised PGM ore. Minerals Engineering, 65, 24-32.

Beattie, M. J. V., & Polling, G. W. (1987). A study of the surface oxidation of arsenopyrite using cyclic voltametry. The Journal of Mineral Processing, 20, 87-108.

Bradshaw, D. J., & O'Connor, C. T. (1996). Measurement of the sub-processes of bubble loading in flotation. Minerals Engineering, 9 (4), 443-448.

Buckley, A. N., & Walker, G. W. (1988). The surface composition of arsenopyrite exposed to oxidizing environments. Applied Surface Science, 35(2), 227-240.

Bulatovic, S. M. (2007). Handbook of Flotation Reagents. Elsevier Ltd., Amsterdam.

Bulut, G., & Yenial, Ü. (2016). Effects of major ions in recycled water on sulfide minerals flotation. Minerals & Metallurgical Processing, 33, 137-143.

Bushell, C. (2011). A new SEM-EDS based automated mineral analysis solution for PGM-bearing ores and flotation products. Minerals Engineering, 24, 1238-1241.

Cabri, L. J. (1981). Relationship of mineralogy to the recovery of platinum-group elements from ores. In: Cabri l. J (Ed.), Platinum Group elements: Mineralogy, Geology, Recovery. Canadian Institute of Mining and Metallurgy, Special Volume 23, pp 233-252.

Canali, A. C., Brenam, J. M., & Sullivan, N. A. (2017). Solubility of platinum-arsenide melt and sperrylite in synthetic basalt at 0.1 MPa and 1200ºC with implications for arsenic speciation and platinum sequestratin in mafic igneous systems. Geochemica et Cosmochimica Acta, 216, 153-168.

Cawthorn, R. G. (1999). The platinum and palladium resources of the Bushveld Complex, South African Journal of Science, 95, 481-489.

Chen, J. H., Lan, L. H., & Chen, Y. (2013). Computational simulation of adsorption and thermodynamic study of xanthate, dithiophosphate and dithiocarbamate on galena and pyrite surfaces. Minerals Engineering, 46, 136‑43.

Chetty, D., Gryffenberg, L., Lekgetho, T. B., & Molebale, I. J. (2009). Automated SEM study of PGM distribution across the UG2 flotation concentrate bank: Implications for understanding PGM floatability. The Southern African Institute of Mining and Metallurgy, 109, 587-593.

Chimonyo, W., Wiese, J., Corin, K., & Connor, C. O. (2017). The use of oxidising agents for control of electrochemical potential in flotation. Minerals Engineering, 109, 135-143.

Cho, Y.S. & Laskowski, J.S. (2002). Effect of flotation frothers on bubble size and foam stability. International Journal of Mineral Processing, 64, 69-80.

Chryssoulis, Stowe, K., Niehuis, E.,Cramer, H. G., Bendel, C., & Kim, J. (1995). Detection of collectors on mineral grains by TOF-SIMS. Transactions of the Institution of Mining and Metallurgy, C101, C1-C6.

Clark-Mostert, V. (2006). Benchmark Mineralogy Investigation of the PPL concentrator-February 2006 Report No M/06/37, Anglo Research, Internal Report.

Cole, S., Ferron, C. J. (2002-3). A review of the beneficiation and extractive metallurgy of the platinum group elements, Highlighting recent process innovations. SGS Mineral Services.

Corkhill, C. L., & Vaughan, D. J. (2009). Arsenopyrite oxidation–A review. Applied Geochemistry, 24(12), 2342-2361.

Cotton, F.A., Wilkinson, G., Murillo, C. A., Bochmann, M. (1999). Advanced inorganic chemistry. John Wiley and Sons, Inc, pp 434-436.

Dàvila-Pulido, G. I., Uribe-Salas, A., Alvarez-Silva, M., & Lôpez-Saucedo, F. (2015). The role of calcium in xanthate adsorption onto sphalerite. Minerals Engineering, 71, 113-119.

Dzinza, L. (2018). An investigation into the effect of potential modifiers on the flotation of a copper sulphide ore. Masters Thesis, University of Cape Town, Faculty of Engineering and the Built Environment, Chemical Engineering Department, Cape Town, South Africa.

Finkelstein, N. P., & Polling, G. W. (1977). The role of dithiolates in the flotation of sulphide minerals. Minerals Science Engineering, 9 (4), 177-196.

Finkelstein, N. P. (1997). The activation of sulphide minerals for flotation: a review. International Journal of Mineral Processing, 52, 81-120.

Finkelstein, N., & Goold, L. (1972). The reaction of sulphide minerals with thiol compounds. National Institute for Metallurgy, ProjectC. 33/62, Project Report No 14.

Fuerstenau, M. C., Kuhn, M. C., & Elgillani, D. A. (1968). The role of dixanthogen in xanthate flotation of pyrite. Society for Mining, Metallurgy & Exploration Transaction, pp. 148-156.

Fuerstenau, M. C., Jameson, G., & Yoon, R. (2007). Froth flotation, A century of Innovation. Society for Mining, Metallurgy and Exploration Inc, Englewood, CO.

Gonzalez Chavez, J. L., & Bessiere, J. (1989). Influence of oxidants on flotation of arsenopyrite and pyrite. Proceedings XI Meeting on Metallurgical Research, Saitillo, Mexico, pp. 224-241 (In Spanish)

Gorain, B. K., Franzidis, J. P., & Manlapig, E. V. (2000). Flotation Cell Design : Application of Fundamental Principles, 1502–1512.

Grano, S. R., Prestidge, C. A., & Ralston, J. (1997). Solution interaction of ethyl xanthate and sulphite and its effect on galena flotation and xanthate adsorption. International Journal of Mineral Processing, 52(2-3), 161-186.

Guo, B., Peng, Y., & Espinosa-Gomez, R. (2014). Cyanide chemistry and its effect on mineral flotation. Minerals Engineering, 66, 25-32.

Guven, O., Batjargal, K., Ozdemir, O., Karakashev, S. I., Grozev, N. A., Boylu, F., & Çelik, M. S. (2020). Experimental procedure for the determination of the critical coalescence concentration (CCC) of simple frothers. Minerals, 10(7), 617.

Hochreiter, R. C., Kennedy, D. C., Muir, W., & Wood, A. I. (1985). Platinum in South Africa, Journal of the South African Institute of Mining and Metallurgy, June, pp.165-185.

Hayashi, Y., Sasaki, K., Inomata, S., & Yanagidani, T. (1984). Acid dissociation constants of alkyl xanthic acids and formation constants of cadmium (ll) and zinc (ll) xanthato complexes in 1:1 v/v H2 DMF Medium. The Chemical Society of Japan, 57 (11), 3074-3076.

Hicks, D., Mehl, M. J., Esters, M., Oses, C., Levy, O., Hart, G. L.W., Toher, C., & Curtarolo, S. (2021). The AFLOW Library of Crystallographic Prototypes: Part 3, Computational Materials Science, 199, 110450. (doi=10.1016/j.commatsci.2021.110450).

Hu, Y., Gao, Z., Sun, W Colloids and Surfaces A: Physicochemical and Engineering Aspects, 415, 439-448.., & Liu, X. (2012). Anisotropic surface energies and adsorption behaviors of scheelite crystal.

Iwasaki, I., Nakazawa, H., Malicsi, A. S., & Xiaowei, L. (1988). Recovery of Platinum-Group Metals from Gabbroic Rocks. The Journal of The Minerals, Metals & Materials Society, 40(6), 36-39.

Liu, GY., Zeng, HB., Lu, QY., Zhong, H., Choi, P., & Xu, ZH. (2012). Adsorption of mercaptobenzo heterocyclic compounds on sulfide mineral surfaces: A density functional theory study of structure-reactivity relations. Colloids Surface A: Physicochemical and Engineering Aspects, 409, 1-9.

Liu, GY., Xiao, JJ., Zhou, DW., Zhong, H., Choi, P., Xu, ZH., (2013). A DFT study on the structure reactivity relationship of thiophosphorus acids as flotation collectors with sulfide minerals: implication of surface adsorption. Colloids Surface A: Physicochemical and Engineering Aspects, 434, 243-52.

Liu, GY., Zhong, H., Dai, T. G., & Xia LY. (2008). Investigation of the effect of N-substituents on performance of thionocarbamates as selective collectors for copper sulfides by ab initio calculations. Minerals Engineering, 21, 1050-4.

Liu, GY., Zhong, H., Xia, LY., Wang, S., & Dai, T G. (2010). Effect of N-substituents on performance of thiourea collectors by density functional theory calculations. Transactions of Nonferrous Metals Society of China, 20, 695-701.

Liu, GY., Yang, X., & Zhong, H. (2017). Molecular design of flotation collectors: A recent progress. Advances in Colloid and Interface Science, 246, 181-195.

Leppinen, J. O. (1990). FTIR and flotation investigation of the adsorption of ethyl xanthate on activated and non-activated sulphide mineral. International Journal of Mineral Processing, 30 (3-4), pp 245-263.

Lewis, A., & Lima, O. (2018). Tecflote - new collector chemistry for sulphide flotation. In 14th International Mineral Processing Conference. 5th International International Seminar on Geometallurgy. Procemin GEOMET, 321-33, Santiago, Chile, November 28-30.

Lopez Valdivieso, A., Sànchez Lòpez, A. A., Ojeda Escamilla, C., & Fuerstenau, M. C. (2006). Flotation and depression control of arsenopyrite through pH and pulp redox potential using xanthate as the collector. International Journal of Mineral Processing, 81, 27-34.

Lopez Valdivieso, A., Escamilla, C. O., Song, S., Baez, I. L., & Martinez, I. G. (2003). Adsorption of isopropyl xanthate ions onto arsenopyrite and its effect on flotation. International Journal of Mineral Processing, 69, 175-184.

Mhonde, N., Schreithofer, N., Corin, K., & Mäkelä, M. (2020). Assessing the combined effect of water temperature and complex water matrices on xanthate adsorption using multiple linear regression. Minerals, 10, 733.

Miller, J. D., Du Plessis, R., Kotylar, D. G., Zhu, X., & Simmons, G. L. (2002). The low-potential hydrophobic state of pyrite in amyl xanthate flotation with nitrogen. International Journal of Mineral Processing, 67(1-4), 1-15.

Mkhonto, P. P., Zhang, X., McFadzean, B., Taguta, J., & Ngoepe, P. E. (2018). Enthalpy of adsorption of MBT, MBO and MBI and modified MBT onto pyrite surfaces: A Computational and Experimental Approach. Proceedings of the International Mineral Processing Congress (IMPC 2018), 15-21 September, Moscow, Russia.

Mkhonto. P. P, (2001, 2022). Personal Communication.

Monte, M. B. M., Dutra, A. J. B., Alburqueque, C. F. R., Tondo, L. A., & Lins, F. F. (2002). The influence of the oxidation state of pyrite and arsenopyriteon the flotation of an auriferous sulphide ore. Minerals Engineering, 15, 1113-1120.

Mwase, J. M. (2016). An investigation of cyanide-based heap leaching for extracting precious metals from Platreef ore. PhD Thesis, University of Cape Town, Faculty of Engineering and the Built Environment, Chemical Engineering Department, Cape Town, South Africa.

Nagaraj, D.R., & Ravishanker, S.A. (2007). Flotation Reagents - A critical overview from an industry perspective, in Froth flotation: A century of innovation. Ed. M.C.Fuerstenau, G.Jameson, R-H Yoon, SME, 2007. p.375-424).

Nakazawa, H., & Iwasaki, I. (1986). Flotation behaviour of nickel arsenide. International Journal of Mineral Processing , 18, pp 191-202.

Nemutudi, B., Pikinini, S., Mkhonto, P. P., McFadzean, B., Zhang, X., & Ngoepe, P. E. (2020). Experimental and density functional theory comparison study of xanthate and dithiocarbamateadsorption on sperrylite surface. Proceedings of the International Mineral Processing Congress (IMPC 2020), 18-22 October 2020, Cape Town, South Africa.

Nemutudi, B., Pikinini, S., Mkhonto, P. P., McFadzean, B., Zhang, X., & Ngoepe, P. E. (2022). Computational density functional theory study of triazine adsorption on sperrylite (100) surface. Proceedings of the International Mineral Processing Congress (IMPC Asia-Pacific 2022), 22-24 August 2022, Melbourne, Australia + online.

Nesbitt, H. W., Muir, I. J., & Prarr, A. R. (1995). Oxidation of arsenopyrite by air and air-saturated, distilled water, and implications for mechanism of oxidation. Geochimica et Cosmochimica Acta, 59(9), 1773-1786.

Nichol, S. (2006). Benchmark Mineralogical Investigation of the Waterval UG2 concentrator-March 2006, Report No M/06/44, Anglo Research, Internal Report.

O'Connor, C. T., & Shackleton, N. J. (2013). Investigations into the recovery of Platinum Group Minerals from the Platreef Ore of the Bushveld Complex of South Africa. Platinum Metals Review, 57, (4), 302-309.

O'Connor, C.T., Bradshaw, D. L., & Upton, A. E. (1990). The use of dithiophosphates and dithiocarbamates for the flotation of arsenopyrite. Minerals Engineering, 3 (5), 447-459.

O'Connor, C. T., Botha, C., Walls, M. J., & Dunne, R. C. (1988). The role of copper sulphate in pyrite flotation. Minerals Engineering, 1, 203-212.

Okamoto, H. (1990). As-Pt (arsenic-platinum). Journal of Phase Equilibria and Diffusion, 17, 456.

Owusu, C., Abreu, S. B., Skinner, W., Addai-Mensah, J., & Zanin, M. (2014). The influence of pyrite content on the flotation of chalcopyrite/ pyrite mixtures. Minerals Engineering, 55, pp 87-95.

Paktunc, D., Foster, A., Heald, S., & Laflamme, G. (2004). Speciation and characterization of arsenic in gold ores and cyanidation tailings using X-ray absorption spectroscopy. Geochimica et Cosmochimica Acta, 68(5), 969-983.

Penberthy, C. J., Oosthuyzen, E. J., & Merkle, R. K. W. (2000). The recovery of platinum-group elements from the UG2 chromite Bushveld Complex- A mineralogical perspective. Mineralogy and Petrology, 68, 213-222.

Pienaar, D., Jordaan T., McFadzean, B., & O'Connor C. T. (2019). The synergistic interaction between dithiophosphate collectors and frothers at the air-water and sulphide mineral interface. Minerals Engineering, 138, 125-132.

Pikinini, S., McFadzean, B., & O'Connor, C. T. (2020). The interactions of butyl thiol collectors with sperrylite ($PtAs_2$) at different pulp chemistries. Proceedings of the International Mineral Processing Congress (IMPC 2020), 18-22 October 2020, Cape Town, South Africa.

Raju, B. G., & Forsling, W. (1991) Adsorption mechanism of diethyl dithiocarbamate on covellite, cuprite and tenorite. Colloids and surfaces, 60, 53-69.

Ralston, J. (1991). E_h and its consequences in sulphide mineral flotation. Minerals Engineering, 4 (7-11), pp 859-878.

Rao, S. R., (2003). Surface Chemistry of Froth Flotation Volume 1: Fundamentals. Kluwer Academic/Plenum Publishers, Second Edition, New York.

Rao, S. R., (2004). Surface Chemistry of Froth Flotation Volume 2: Reagents and Mechanisms. Kluwer Academic/Plenum Publishers, New York.

Rao, S. R., & Finch, J. A. (1988). Galvanic interactions studies on sulphide minerals. Canadian Metallurgical Quarterly, 27 (4), 253-259.

Rule, C. M., Knopjes, L., Clermont, B., & Philippe, C. (2008). Fine grinding-Developments in ceramic media technology and resulting improved plant performance at Anglo Platinum. SAIMM Platinum in transformation.

Rule, C. M. (2011). Stirred milling-new comminution technology in the PGM industry. Journal of the Southern African Institute of Mining and Metallurgy, 111(2), 101-107.

Schalkwyk, G. A. C. (2007). Benchmark Mineralogical Investigation of the PPL concentrator-August 2006, Report No M/06/137, Anglo Research, Internal Report.

Schouwstra, R. P., & Kinloch, E. D. (2000). A short geological review of the Bushveld Complex. Platinum Metals Review., 44(1), 33-39.

Shabalala, N. Z. P., Harris, M., Leal Filho, L. S., & Deglon, D. A. (2011). Effect of slurry rheology on gas dispersion in a pilot-scale mechanical flotation cell. Minerals Engineering, 24, 1448-1453.

Shackleton, N. J. (2007). Surface characterisation and flotation behaviuor of the platinum and palladium arsenide, telluride and sulphide mineral species. PhD Thesis, University of Cape Town, Faculty of Engineering and the Built Environment, Chemical Engineering Department, Cape Town, South Africa.

Shackleton, N. J., Malysiak, V., & O'Connor, C. T. (2007b). Surface characteristics and flotation behaviour of platinum and palladium tellurides. International Journal of Mineral Processing, 85(1–3), 25–40.

Shackleton, N. J., Malysiak, V., & O'Connor, C. T. (2007a). Surface characteristics and flotation behaviour of platinum and palladium arsenides. International Journal of Mineral Processing, 85(1–3), 25–40.

Shackleton, N. J., Malysiak, V., De Vaux, D., & Plint, N. (2012). Water quality–A comparative study between moncheite and pentlandite in mixture with pyroxene. Minerals Engineering, 36, 53-64.

Shamaila, S., & O' Connor, C. T. (2008). The role of synthetic minerals in determining the relative flotation behaviour of Platreef PGE tellurides and arsenides. Minerals Engineering, 21, 899-904.

Shamaila, S. (2007). A study of the flotation behaviour of Pt and Pd tellurides and arsenides. Masters Thesis, University of Cape Town, Faculty of Engineering and the Built Environment, Chemical Engineering Department, Cape Town, South Africa.

Smart, R. St. C., Amarantidis, J., Skinner, W., Prestige, C. A., LaVanier, L., & Grano, S. (1988). Surface analytical studies of oxidation and collector adsorption in sulphide mineral flotation, Scanning Microscopy, 12 (4), 553-583.

Somasundaran, P., & Wang, D. (2006). Application of flotation agents and their structure-property relationships. Developments in Mineral Processing, 17, 143-201.

Somasundaran, P., & Nagaraj, D. R. (1984). Chemistry and applications of chelating agents in flotation and flocculation. Reagents in Mineral Industry. Institute of Mining and Metallurgy, London, 209–219.

Szolar, O. H. J. (2007). Environmental and pharmacetical analysis of dithiocarbamates (Review). Analytica Chimica Acta, 582, 191-200.

Szymanski, J. T. (1979). The crystal structure of platarsite, $Pt(As,S)_2$, and a comparison with sperrylite, $PtAs_2$. Canadian Mineralogist, 17, pp.117-123.

Tadie, M. (2015). An electrochemical investigation of Platinum Group Minerals. PhD Thesis, University of Cape Town, Faculty of Engineering and the Built Environment, Chemical Engineering Department, Cape Town, South Africa.

Tadie, M., Corin K. C., Wiese, J. G., Nicol, M., & O'Connor, C. T. (2015). An investigation into the electrochemical interactions between platinum group minerals and sodium ethyl xanthate and sodium diethyl dithiophosphate collectors: Mixed potential study. Minerals Engineering, 83 44-52.

Tadie, M., Corin, K. C., Wiese, J. G., & O'Connor, C. T. (2017). Electrochemical interactions of platinum group minerals with copper sulphate. Minerals Engineering, 112, 43-49.

Taguta, J. (2015). The thermochemical behaviour of thiol collectors and collector mixtures with sulphide minerals. Masters Thesis, University of Cape Town, Faculty of Engineering and the Built Environment, Chemical Engineering Department, Cape Town, South Africa.

Taguta, J., Connor, C. T. O., & McFadzean, B. (2017). The effect of the alkyl chain length and ligand type of thiol collectors on the heat of adsorption and floatability of sulphide minerals. Minerals Engineering, 110, 145–152.

Taguta, J., Connor, C. T., & McFadzean, B. (2018). The relationship between enthalpy of immersion and flotation response. Colloids and Surfaces A, 558, 263-270.

Taguta, J., McFadzean, B., O'Connor, C., (2019). The relationship between the flotation behavior of a mineral and its surface energy properties using calorimetry. Minerals Engineering, 143

Taguta, J., & Ross, V. (2021). The application of a Nitrile-based collector in the flotation of a Platreef PGM ore. Mineral Processing and Extractive Metallurgy Review, DOI: 10.1080/08827508.2021.1920411

Taggart, A. F., Taylor, T. C., & Knoll, A. F. (1930). Chemical reactions in flotation. The American Institute of Mining, Metallurgical, and Petroleum Engineers, Incorporated Publ, 312, 3-33.

Tolun, R., & Kitchener, J. A. (1963-64). Transactions of the Institution of Mining and Metallurgy, 73, pp 313-22.

Van Staden, A. (2006). Benchmark Mineralogical Investigation of the Waterval UG2 Feed, Concentrate, and Final tailings samples-September 2005, Report No M/05/31, Anglo Research, Internal Report.

Van Staden, A. (2007). Benchmark Mineralogical Investigation of the Waterval UG2 Concentrator-December 2006, Report No M/07/129, Anglo Research, Internal Report.

Vermaak, M. K. G., Pistorius, P. C., & Venter, J. A. (2007). Fundamental electrochemical and Raman spectroscopic investigations of the flotation behaviour of $PtAs_2$. Minerals Engineering, 20 (12), 1153–1158.

Vermaak, M. K. G., Pistorius, P. C., & Venter, J. A. (2005). Electrochemical and Raman spectroscopic studies of the interaction of ethyl xanthate with Pd-Bi-Te. Minerals Engineering, 18, 575-584.

Vermaak, M. K.G. (2005). Fundamentals of flotation behaviour of palladium bismuth tellurides. PhD Thesis, University of Pretoria, Faculty of Engineering, Built Environment and Information Technology, Pretoria, South Africa.

Wadso, I., & Goldberg, R. N. (2001). Standards in isothermal microcalorimetry (IUPAC Technical Report). Pure and Applied Chemistry, 73 (10), 1625-1639.

Wang, X. H., & Forssberg, K. S. E. (1991). Mechanisms of pyrite flotation with xanthates. International Journal of Mineral Processing, 33 (1-4), 275-290.

Wang, X-H. (1995). Interfacial electrochemistry of pyrite oxidation and flotation, II: FTIR studies of xanthate adsorption on pyrite surfaces in neutral pH solutions. Journal of Colloid and Interface Science, 171, pp. 413-428.

Waterson, C. N. (2015). Design, synthesis and testing of reagents for high-value mineral collection. PhD Thesis, University of Edinburgh, School of Chemistry and EaSTCHEM Research School, Edinburgh, U.K.

Waterson, N. W., Tasker, P. A., Farinato, R., Nagaraj, D. R., Shackleton, N., & Morrison, C. A. (2016). A computational and experimental study on the binding of dithio ligands to sperrylite, pentlandite and platinum. The journal of physical chemistry, 120 22476-22488.

Weller, M., Overton, T., Rourke, J., Armstrong, F. (2014). Inorganic chemistry. Oxford University Press, USA.

Wiese, J., Harris, P., Bradshaw, D. (2005). The influence of the reagent suite on the flotation of ores from the Merensky reef, Minerals Engineering, 18, 189-198.

Wills, B.A., & Napier-Munn, T. J. (2006). Mineral Processing Technology. 7th edition. Elsevier Science and Technology Books.

https://www.mindat.org/min-1123.html

Xiao, Z., Laplante, A. R., (2004). Characterizing and recovering the platinum group minerals- a review. Minerals Engineering, 17, 961-979.

Yekeler, H., Yekeler, M., (2005). Molecular modelling study on the relative stabilities of the flotation products for arsenic-containing minerals: dixanthogens and arsenic (III) xanthates. Journal of Colloid and Interface Science, 284, 694‑7.

Yekeler, H., Yekeler, M., (2006). Predicting the efficiencies of 2-mercaptobenzothiazole collectors used as chelating agents in flotation processes: a density-functional study. Journal of Molecular Modelling, 12, 763‑8.

Yuan, L., Zhong, H., Li, LQ., Xiao, JJ. (2012). A novel dithiourea and its response to metal ions. Chinese Chemical Letters, 23, 93‑6.

8. LIST OF APPENDICES

APPENDIX A: MINERAL CHARACTERISATION

XRD SPECTRA OF MINERALS

Sperrylite

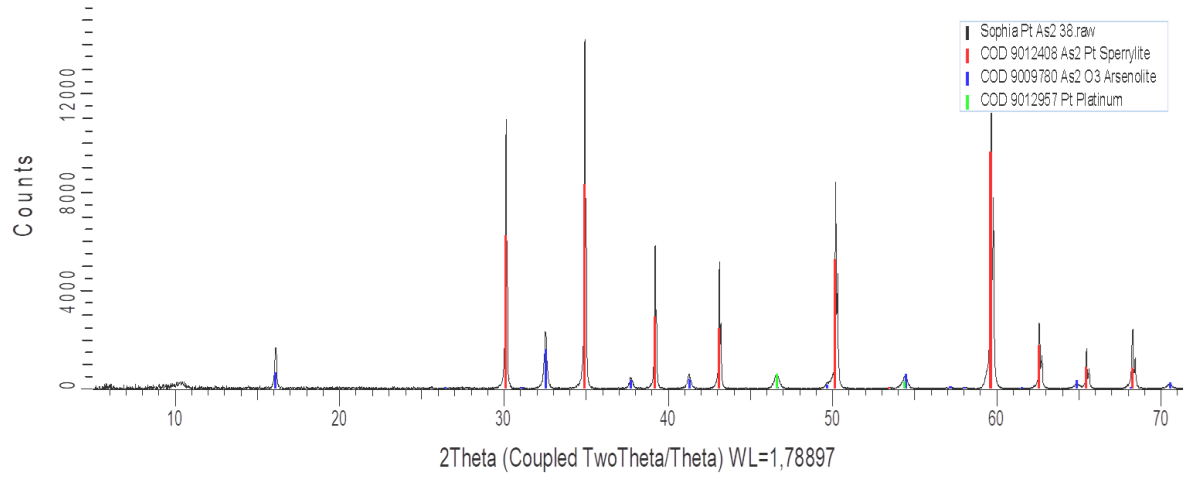

Cooperite

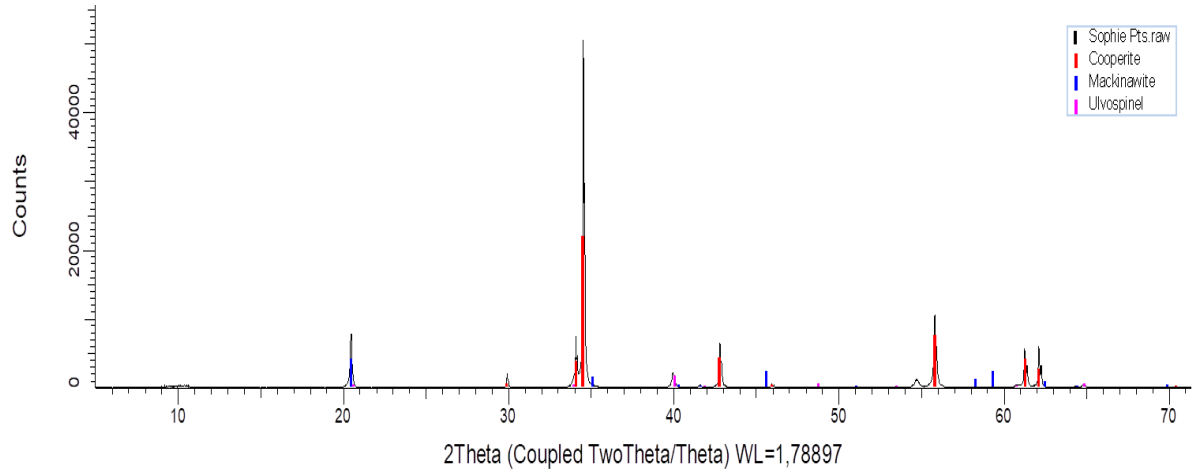

Pyrite

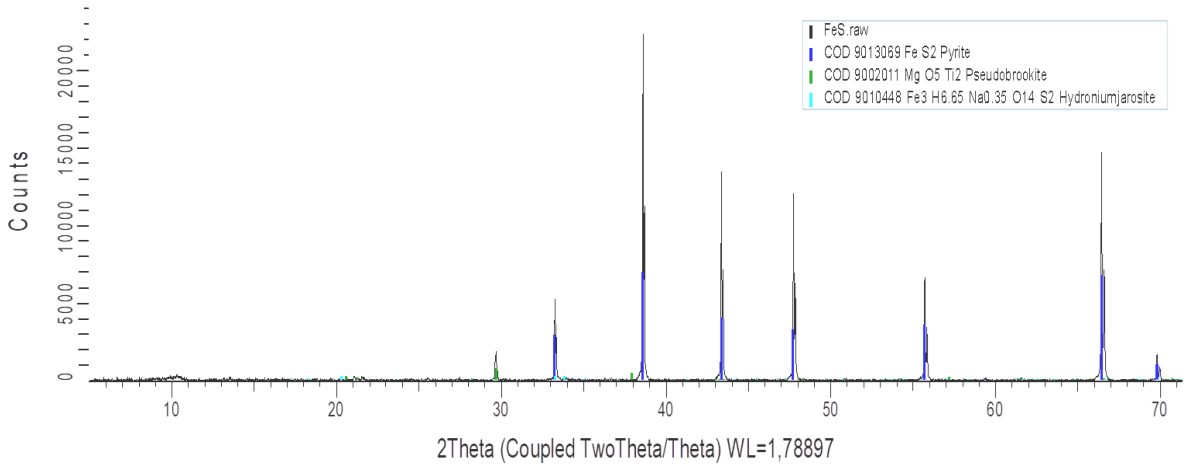

Arsenopyrite

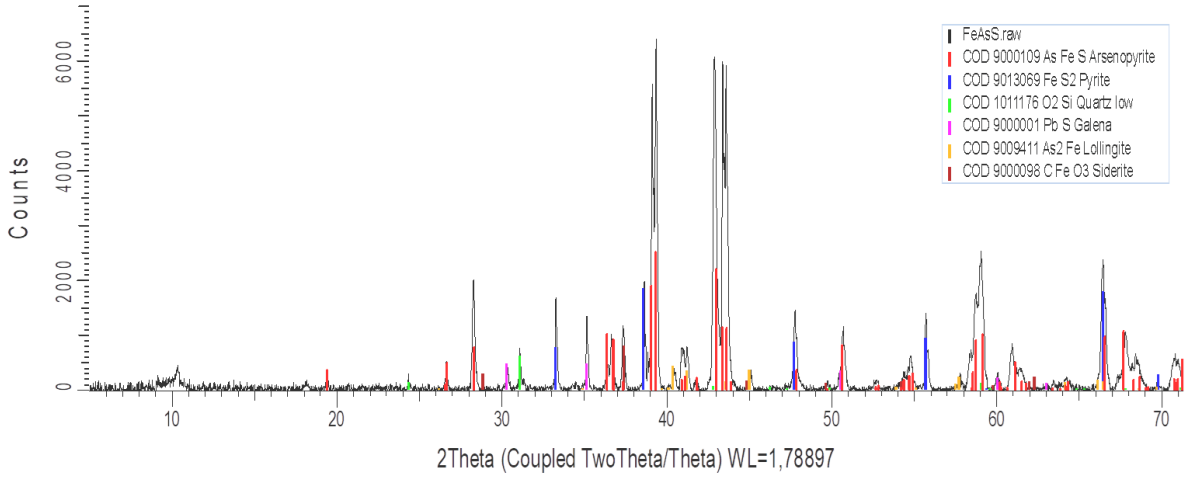

EDS RESULTS

Expected Calculated ratio of Minerals

Pt = 52.68 wt% (atomic wt.=195)

As = 38.41 wt % (atomicwt. = 74)

For PtAs2 we have 1 atom of Pt and 2 of As i.e. 195/(2x74) = 1.32. Ratio from the spreadsheet is 1.37. For the 2nd spectrum we have 1.28. Hence it looks as if we do have PtAs2.

Cooperite electrode

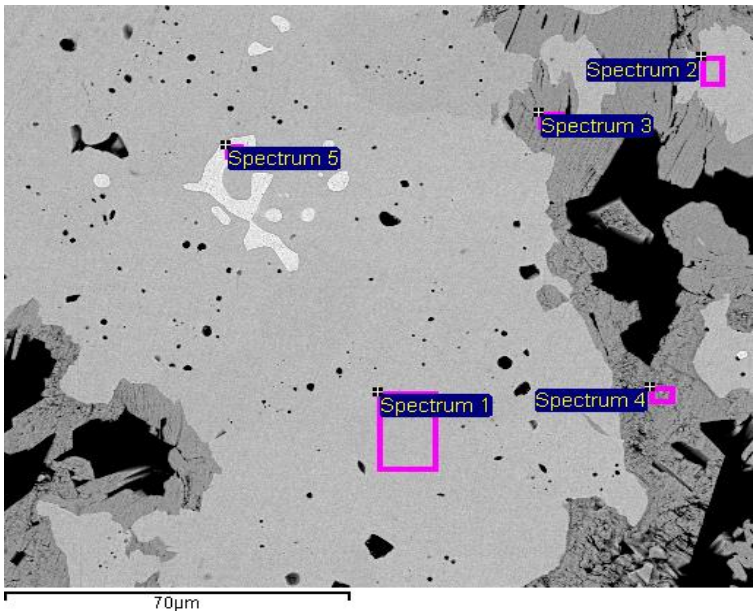

Spectrum	S	Pt	Pt/As Ratio from SEM	Pt/As Expected Ratio
Spectrum 1	14.99	85.01	5.67	6.08
Spectrum 2	15.03	84.97	5.65	6.08
Spectrum 3	25.60	74.40	2.91	6.08
Spectrum 4	26.78	73.22	2.73	6.08
Spectrum 5	0	100.00	≈100	6.08

Synthetic Cooperite

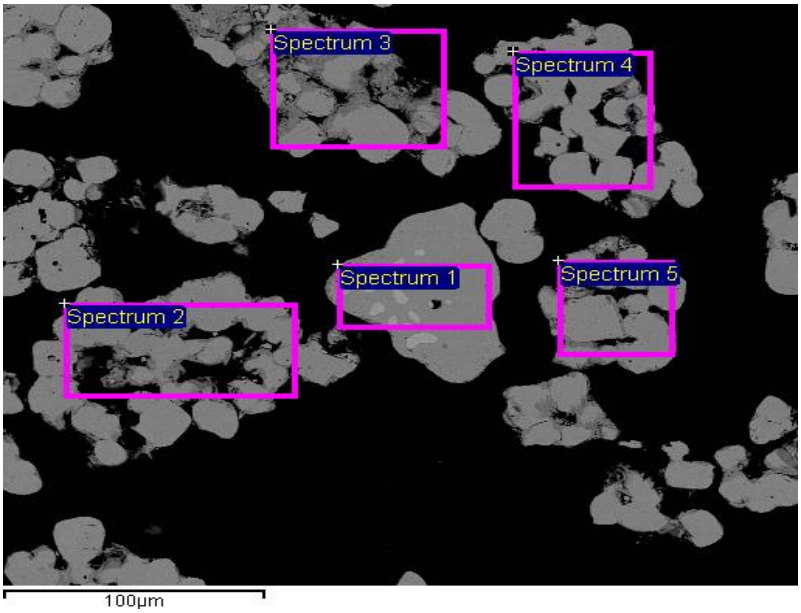

Spectrum	S	Pt	Pt/As Ratio from SEM	Pt/As Expected Ratio
Spectrum 1	13.45	86.55	6.44	6.08
Spectrum 2	18.19	81.81	4.50	6.08
Spectrum 3	21.34	78.66	3.69	6.08
Spectrum 4	16.51	83.47	5.06	6.08
Spectrum 5	17.69	82.31	4.65	6.08

Synthetic Sperrylite Electrode

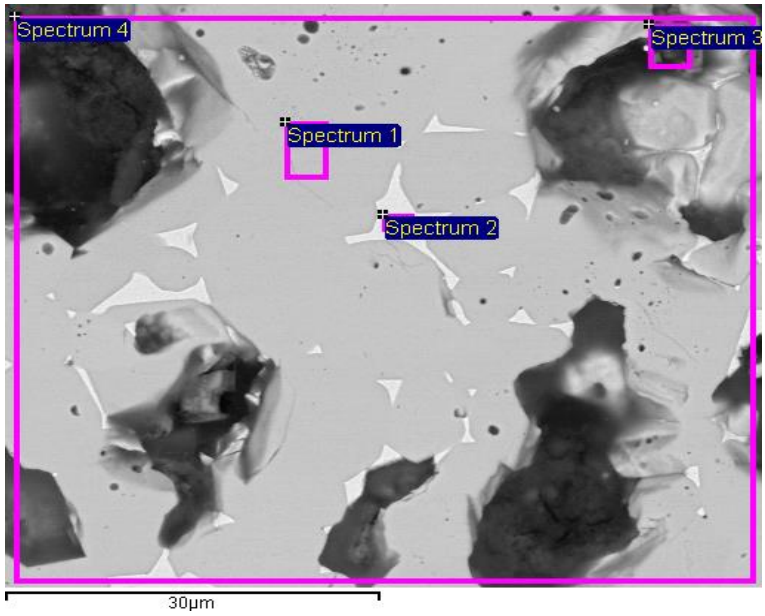

Spectrum	O	As	Pt	Pt/As Ratio from SEM	Pt/As Expected Ratio
Spectrum 1		42.99	57.02	1.33	1.3
Spectrum 2		0.68	99.32	145.77	1.3
Spectrum 3	60.40	14.43	25.17	1.74	1.3
Spectrum 4	17.77	36.76	45.47	1.24	1.3

Sperrylite -38 microns

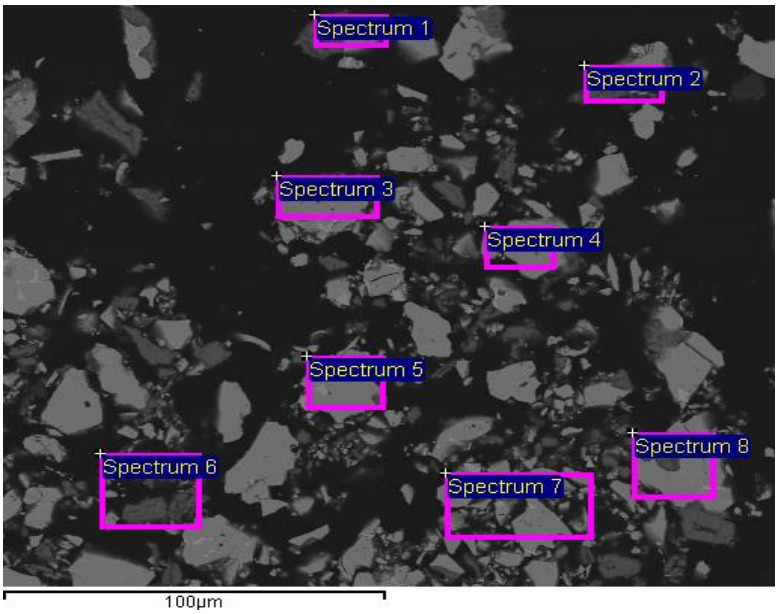

Spectrum	O	As	Pt	Pt/As Ratio from SEM	Pt/As Expected Ratio
Spectrum 1	16.20	49.54	34.26	0.69	1.3
Spectrum 2	19.11	48.20	32.69	0.68	1.3
Spectrum 3		43.77	56.23	1.28	1.3
Spectrum 4		43.76	56.24	1.29	1.3
Spectrum 5		41.93	58.07	1.38	1.3
Spectrum 6	24.45	52.88	22.67	0.43	1.3
Spectrum 7		43.96	56.04	1.27	1.3
Spectrum 8		47.37	52.63	1.11	1.3

APPENDIX B: ADSORPTION PROFILES OF THE MINERALS

ADSORPTION OF SPERRYLITE WITH STANDARD AND NOVEL COLLECTORS AT pH 9

PNBX

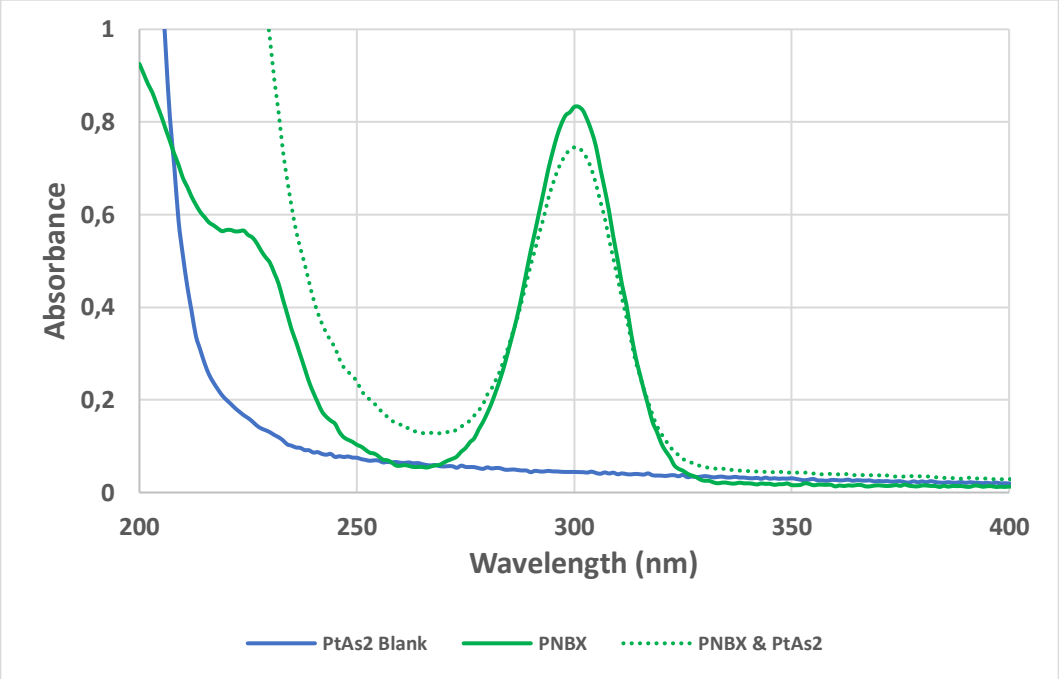

SIBX

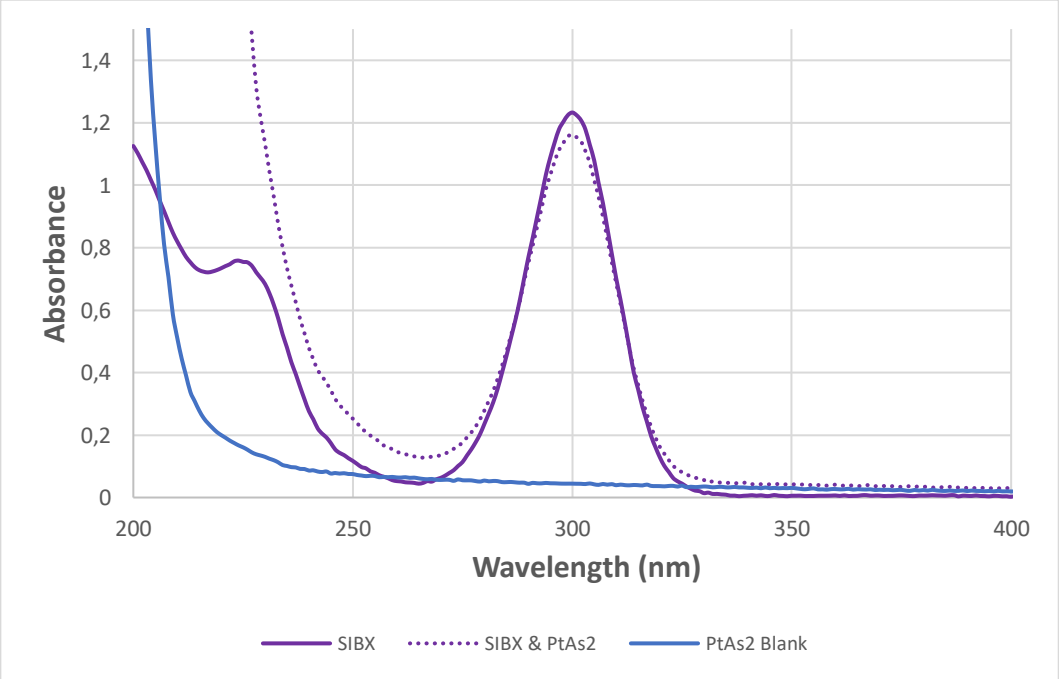

SNBDTC

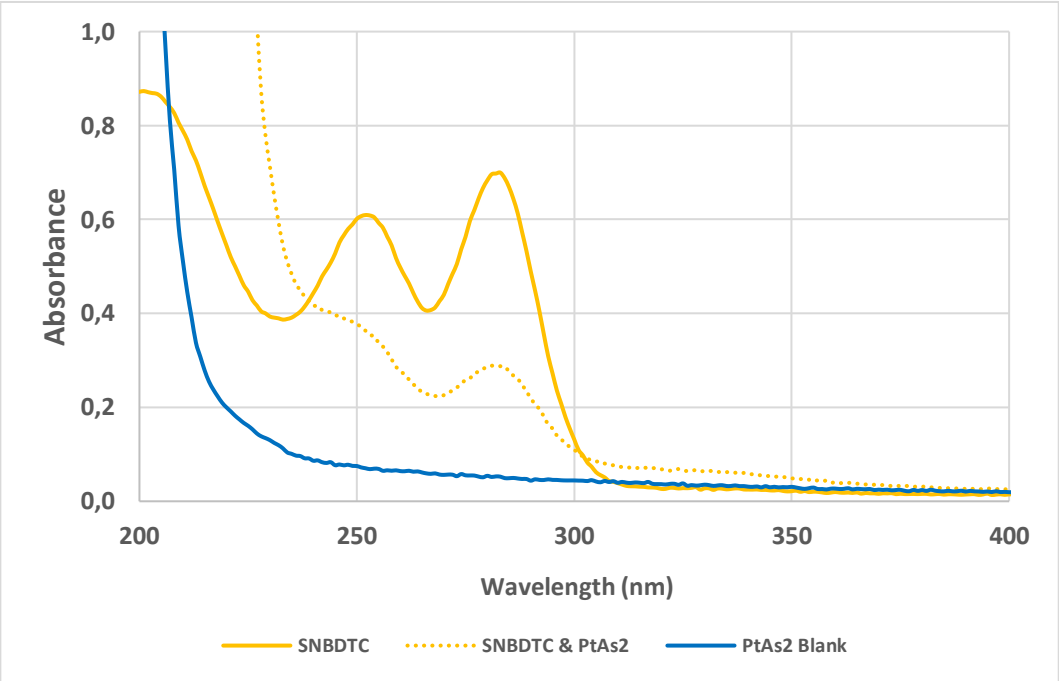

SNDBDTP

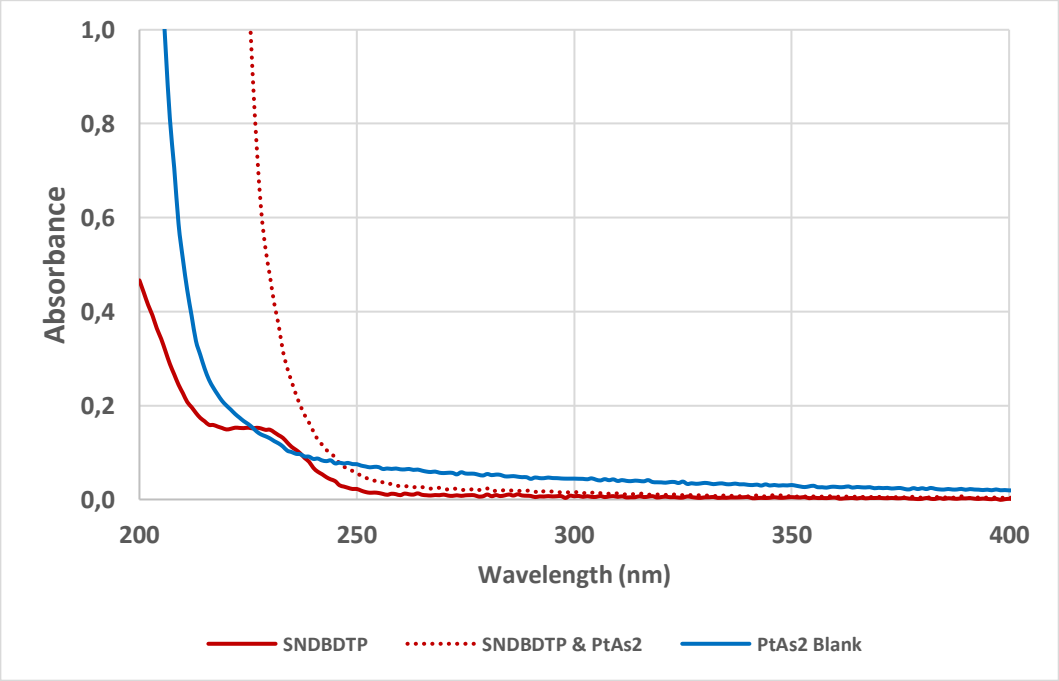

SDTDBAT

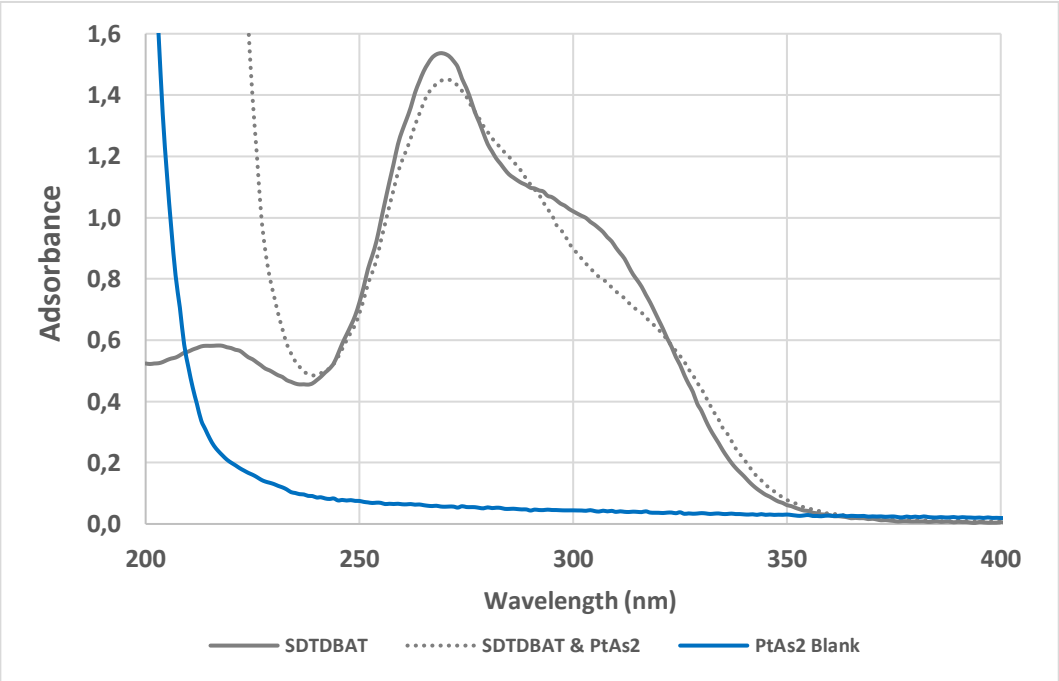

SDTBAT

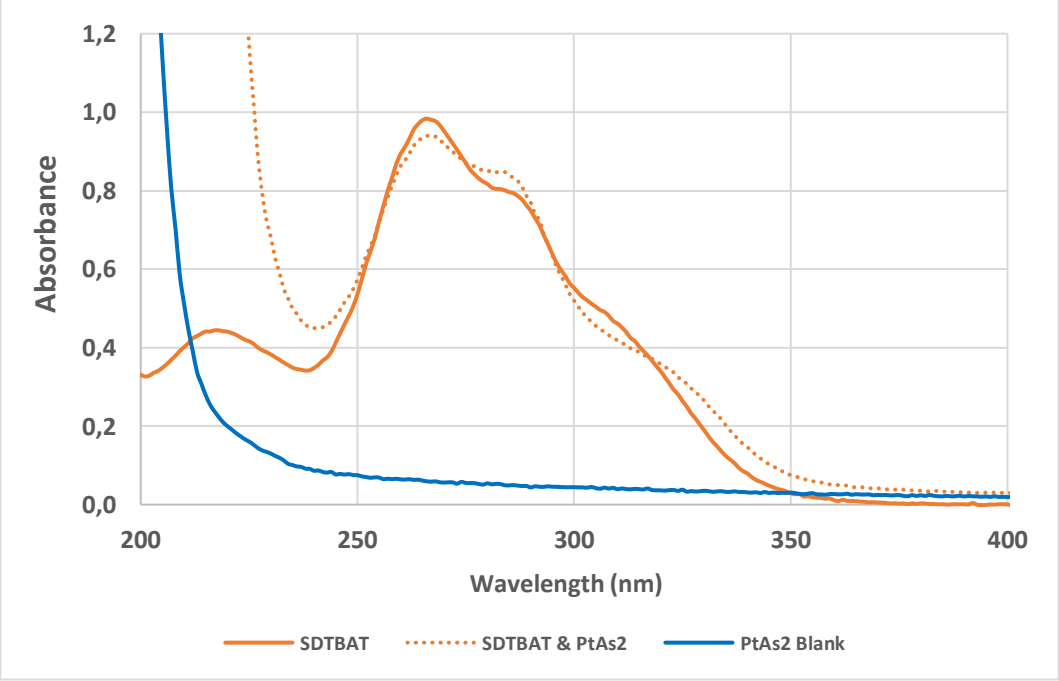

SDCDTDBAT

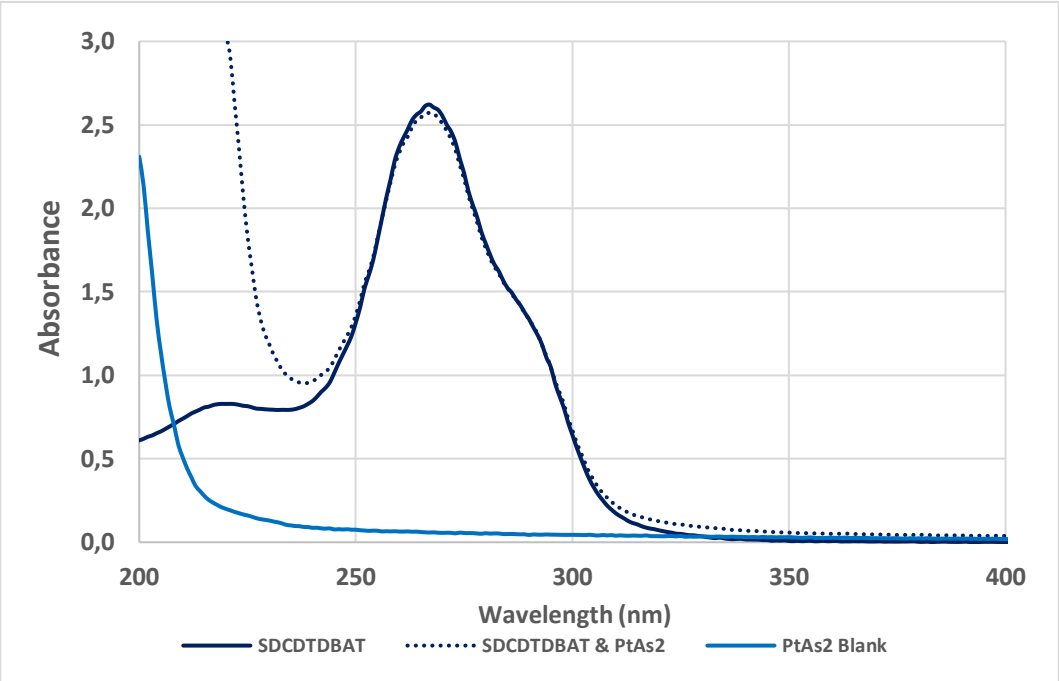

SDCDTBAT

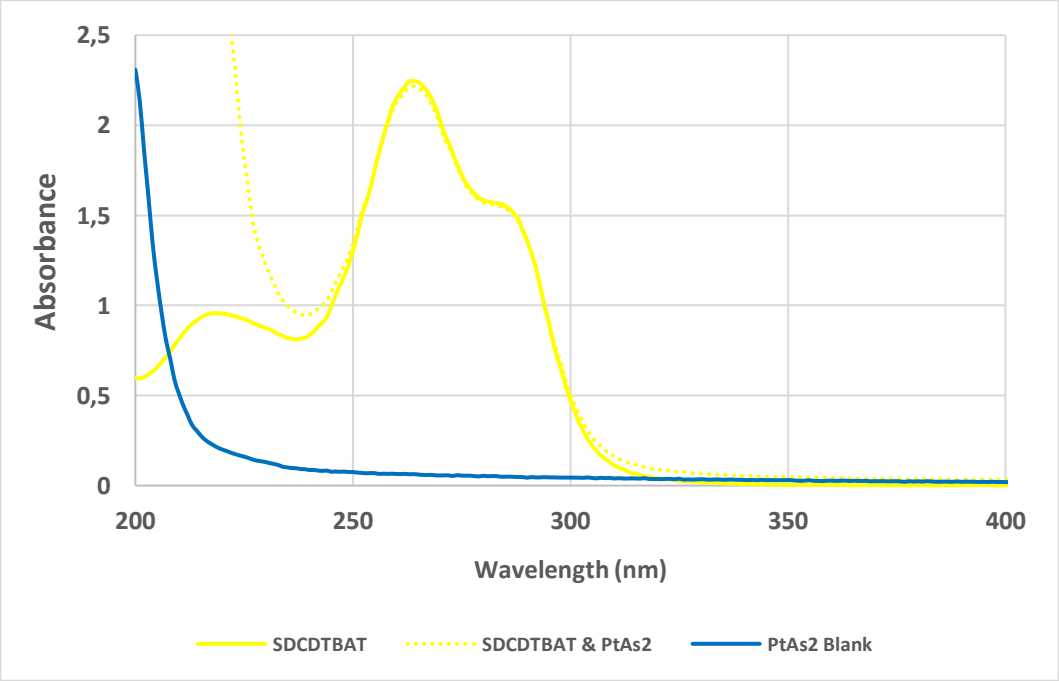

ADSORPTION OF SPERRYLITE WITH STANDARD AND NOVEL COLLECTORS AT pH 4

PNBX

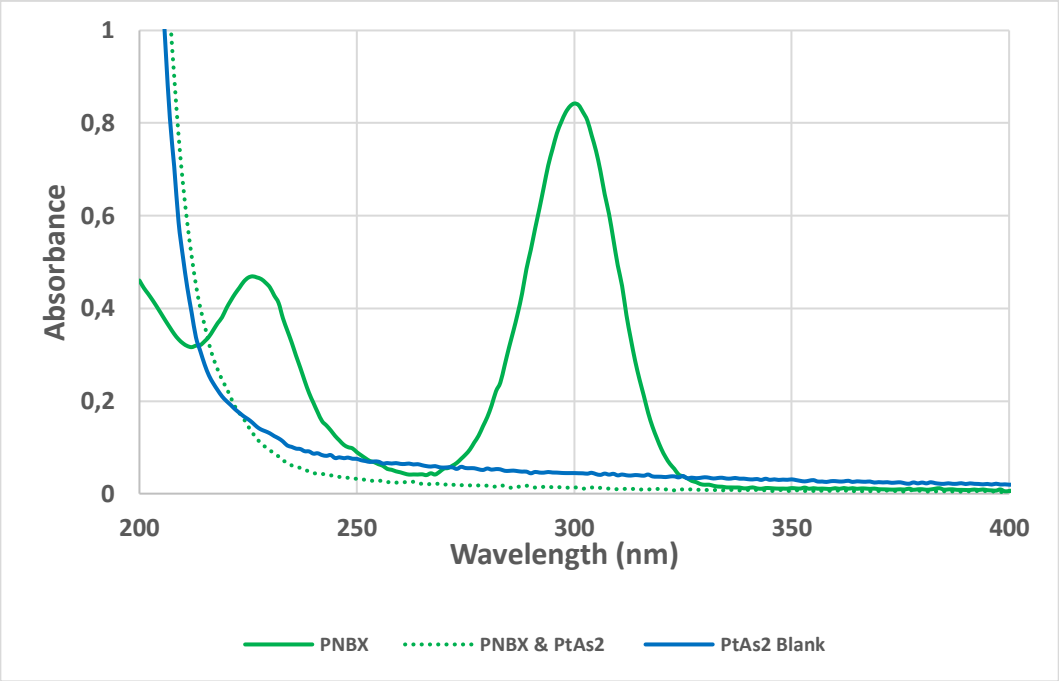

SNBDTC

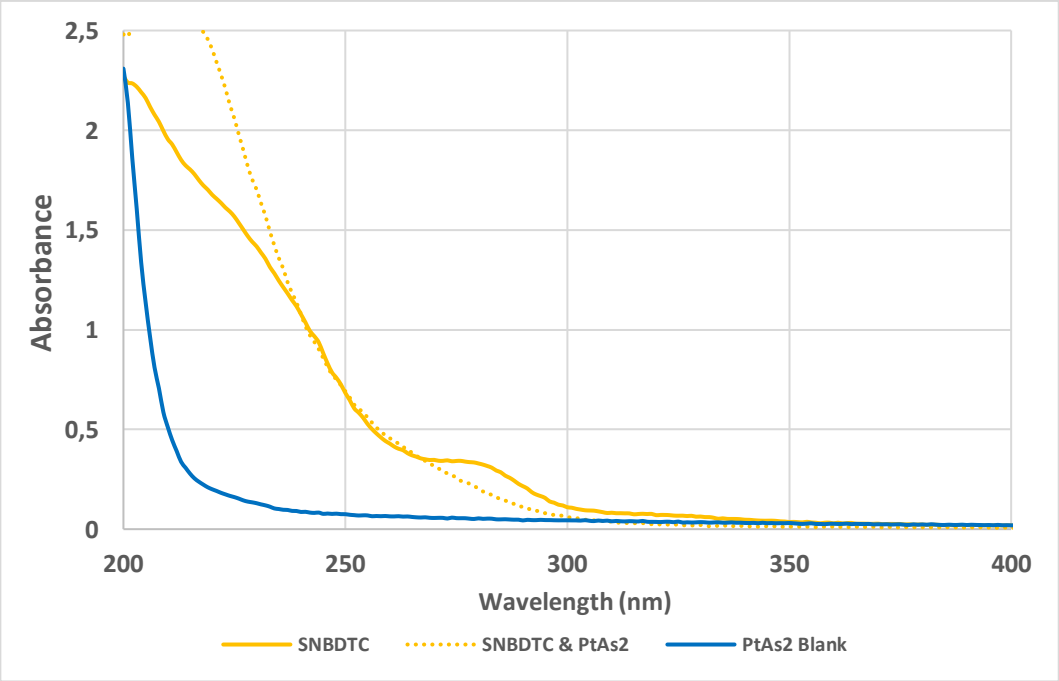

SDTBAT

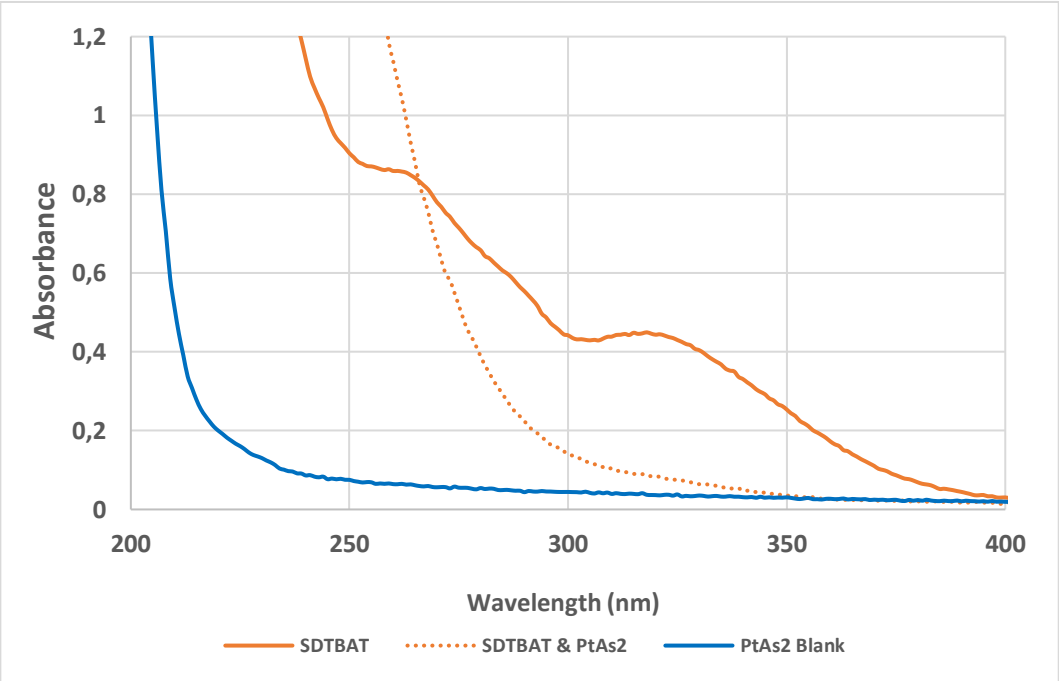

SDCDTDBAT

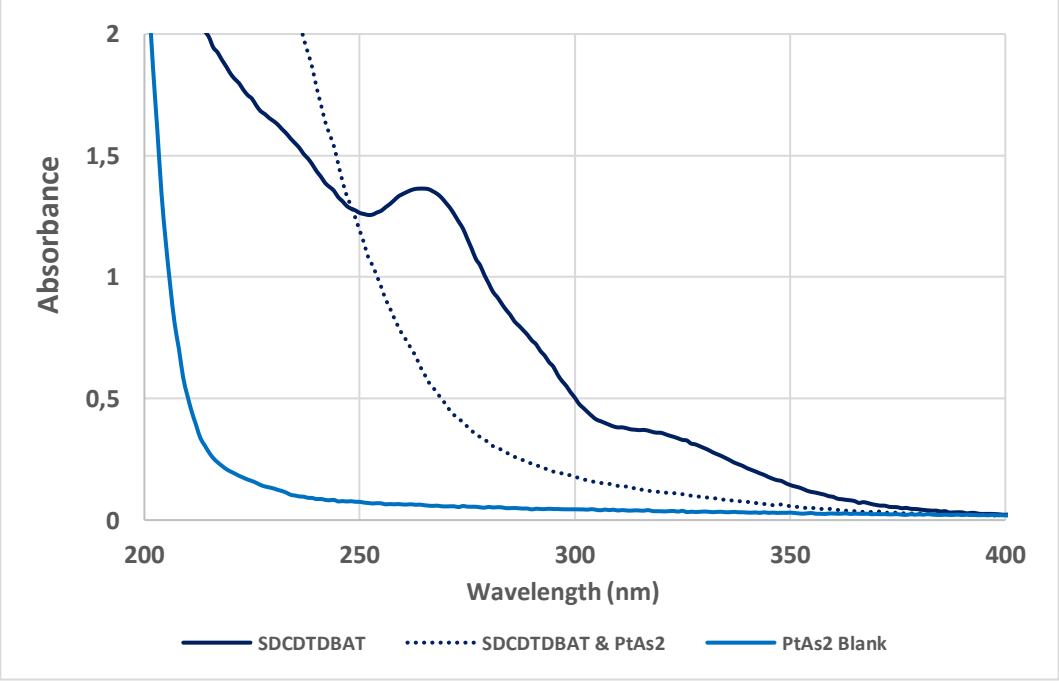

ADSORPTION OF PYRITE WITH STANDARD AND NOVEL COLLECTORS AT pH 9

PNBX

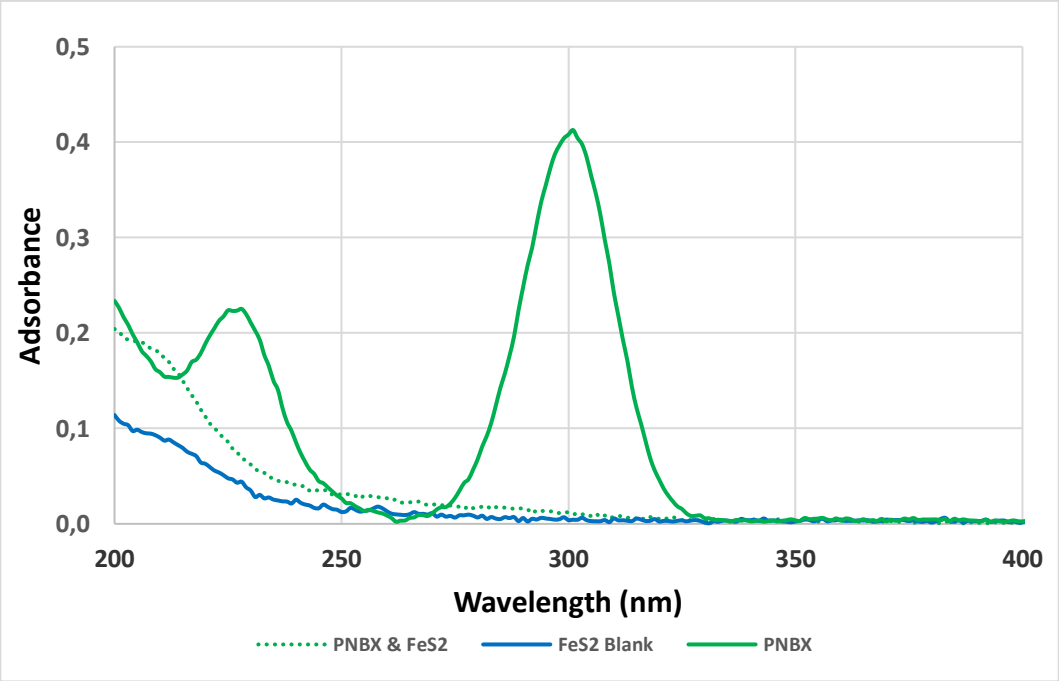

SNBDTC

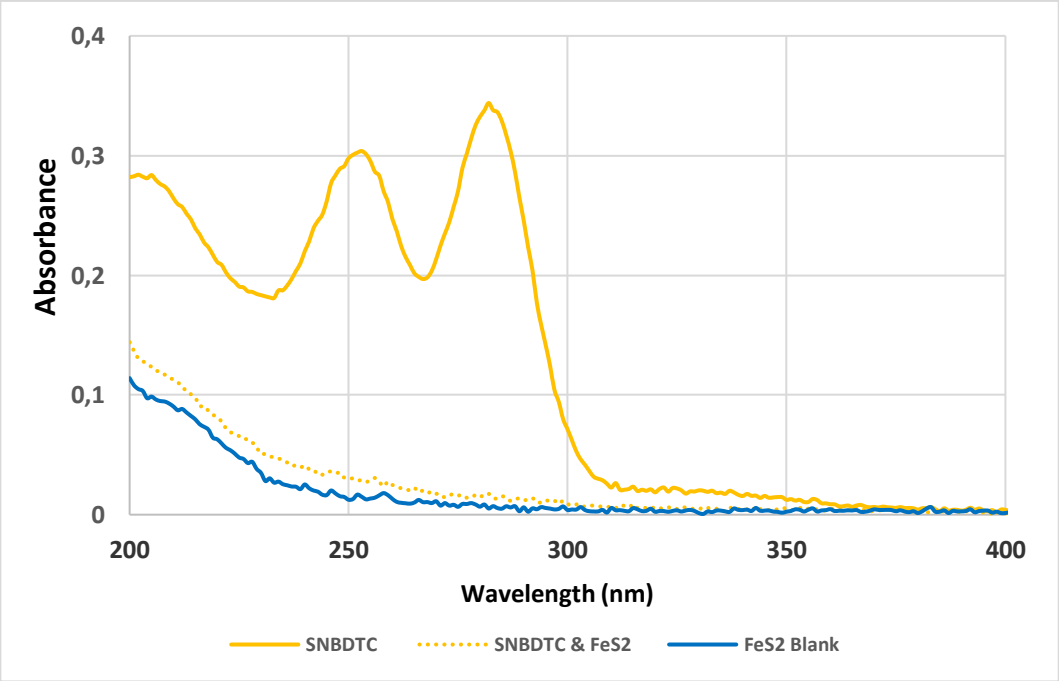

SNDBDTP

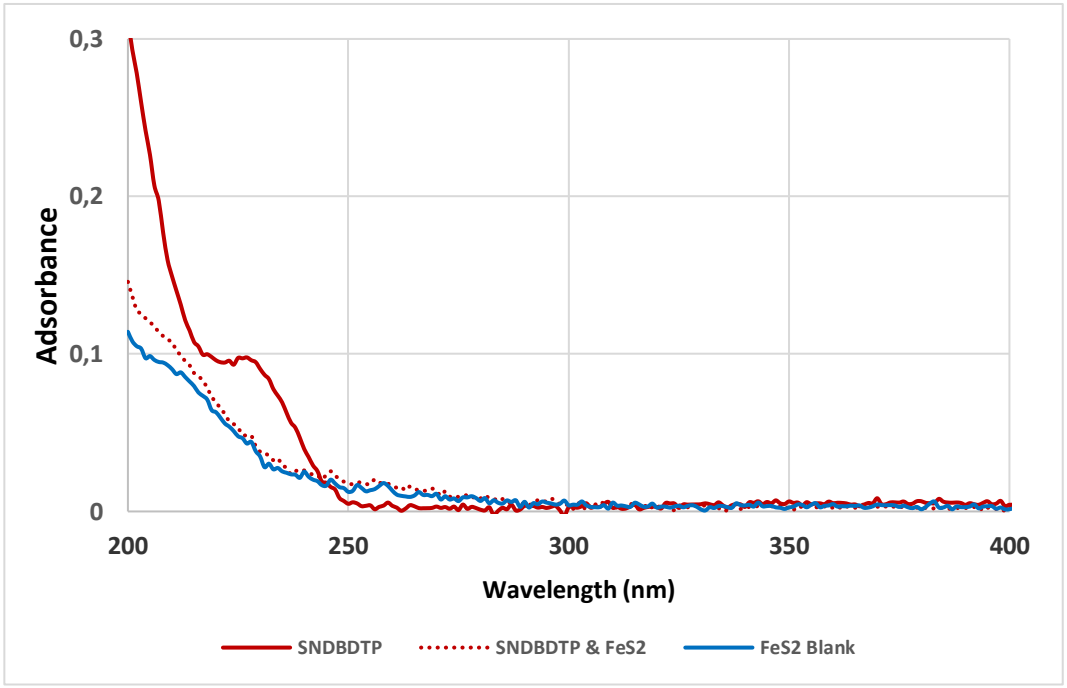

SDTDBAT

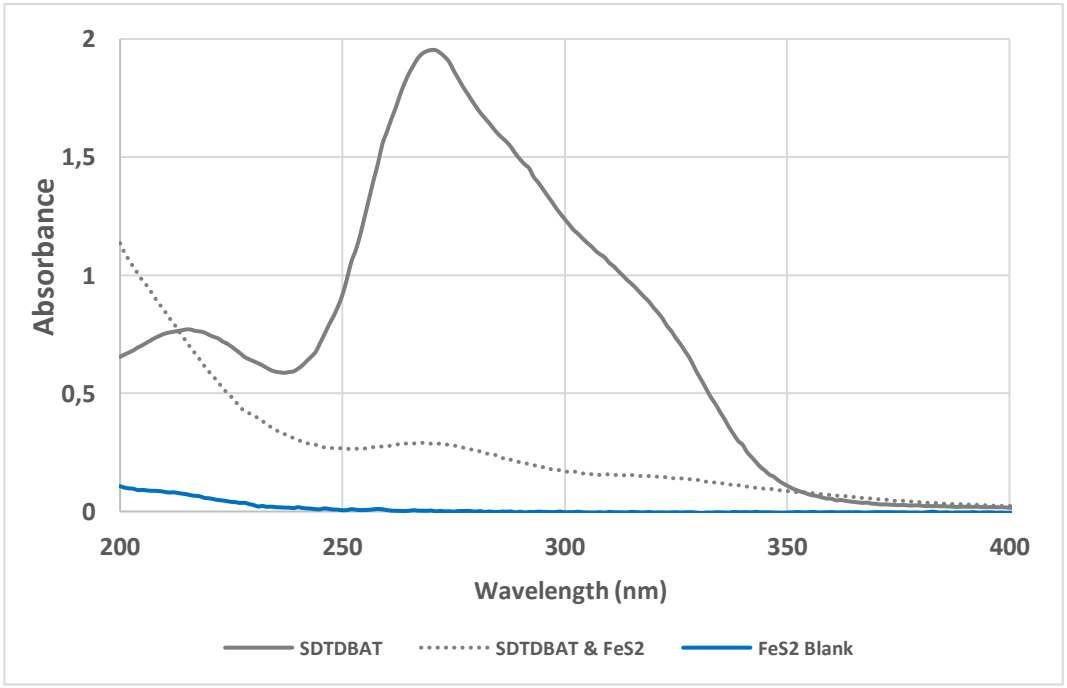

SDTBAT

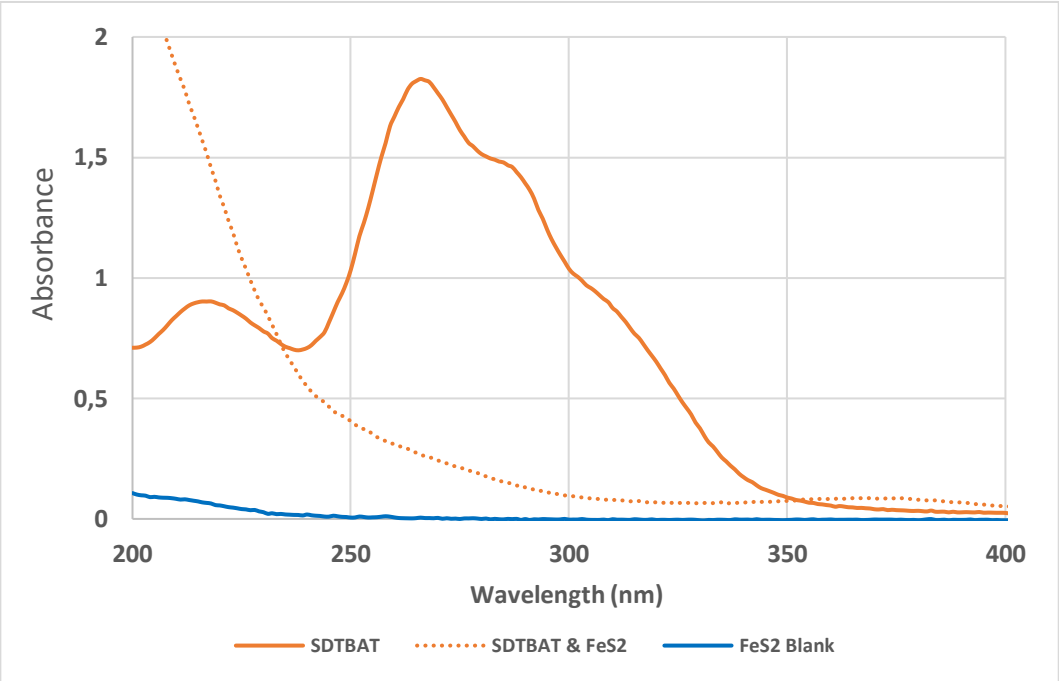

SDCDTDBAT

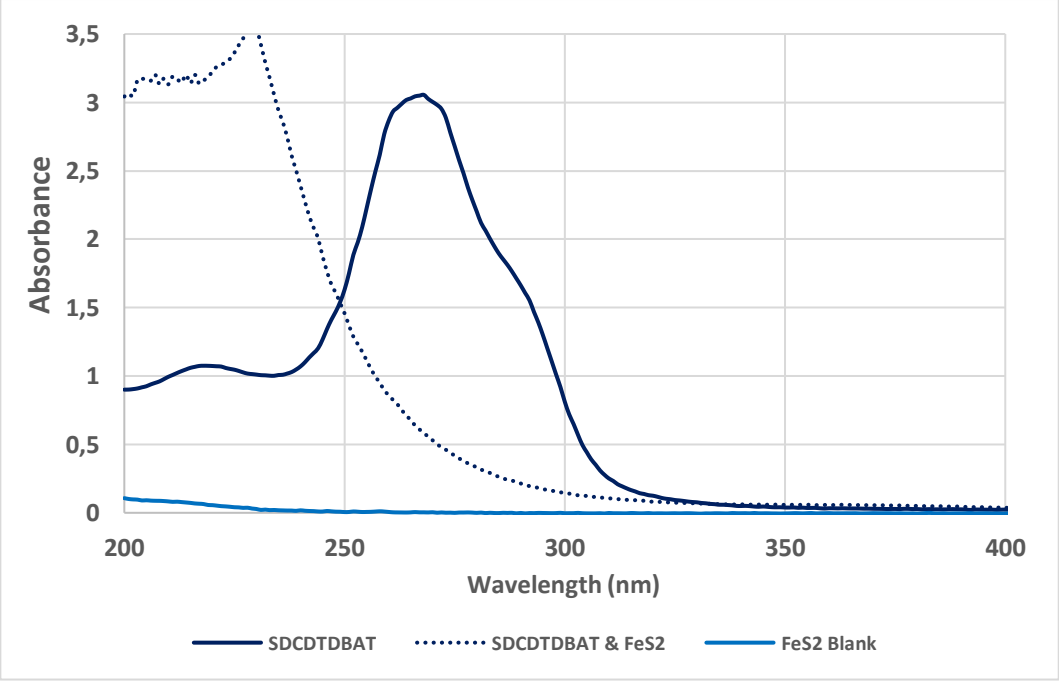

SDCDTBAT

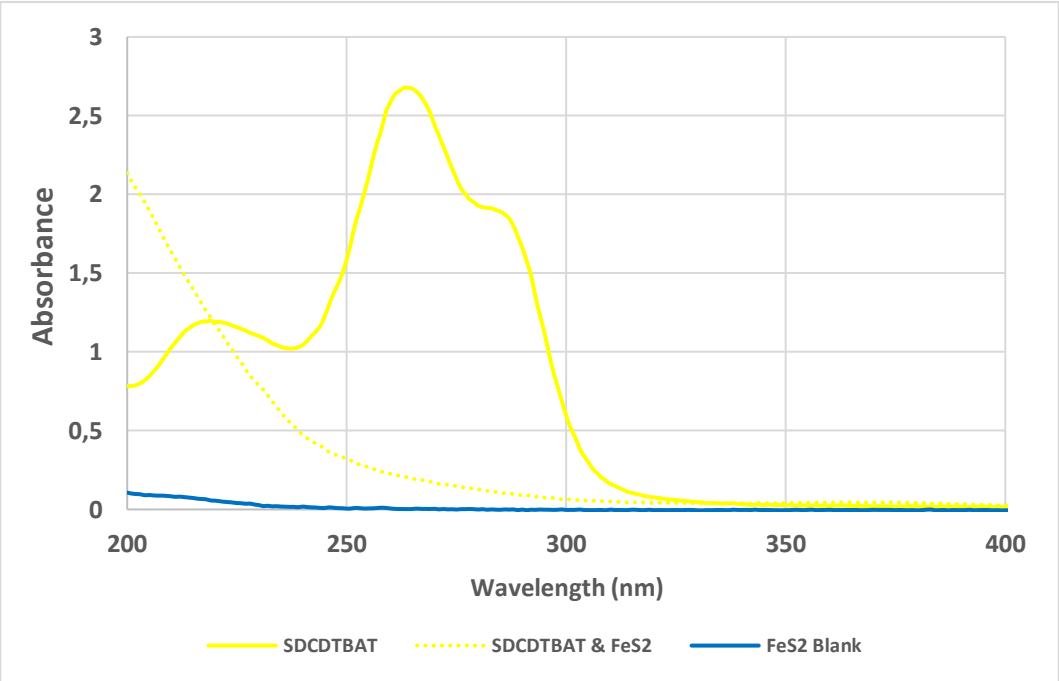

ADSORPTION OF PYRITE WITH STANDARD COLLECTORS AT pH 4

PNBX

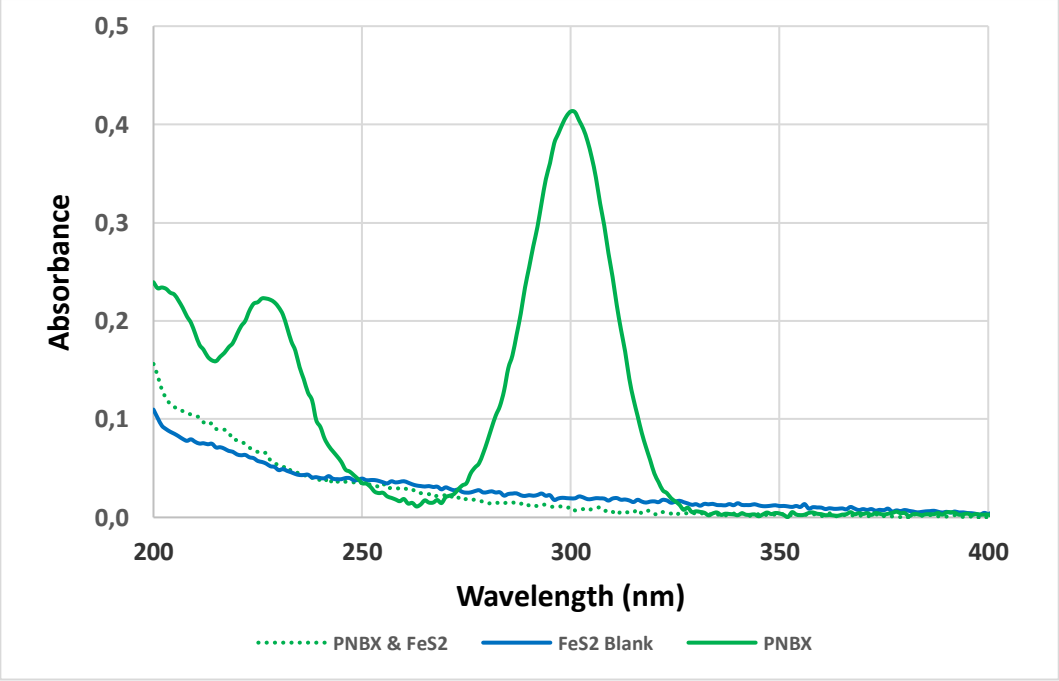

SNBDTC

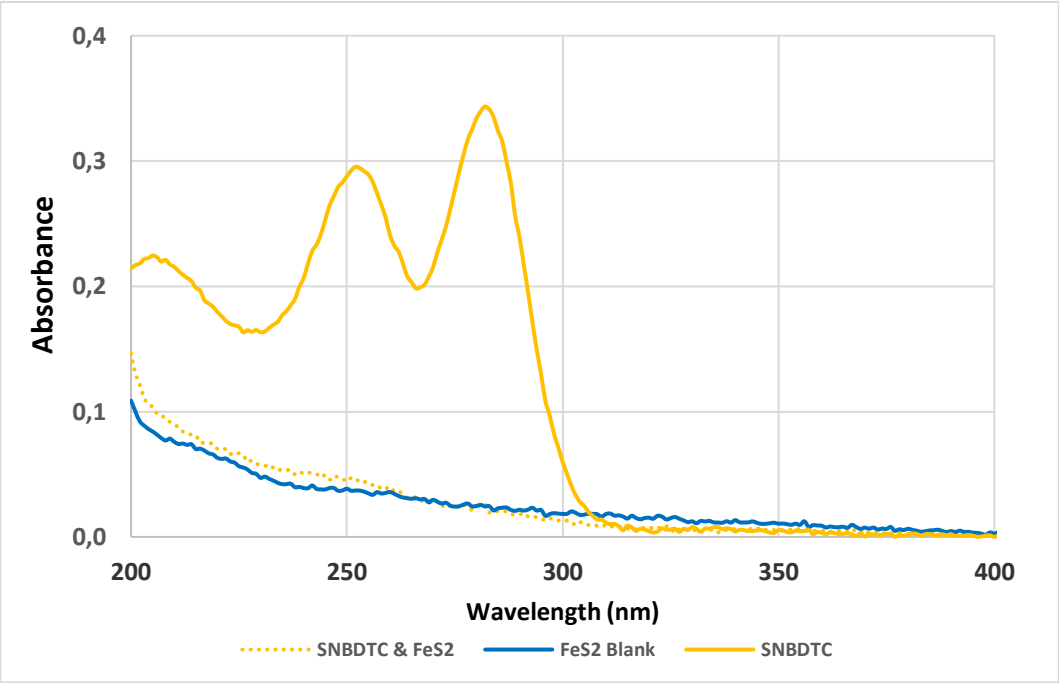

Beer Lambert law to calculate the peak for the distorted spectra at pH 4 in order to calculate the adsorption density.

SNDBDTP

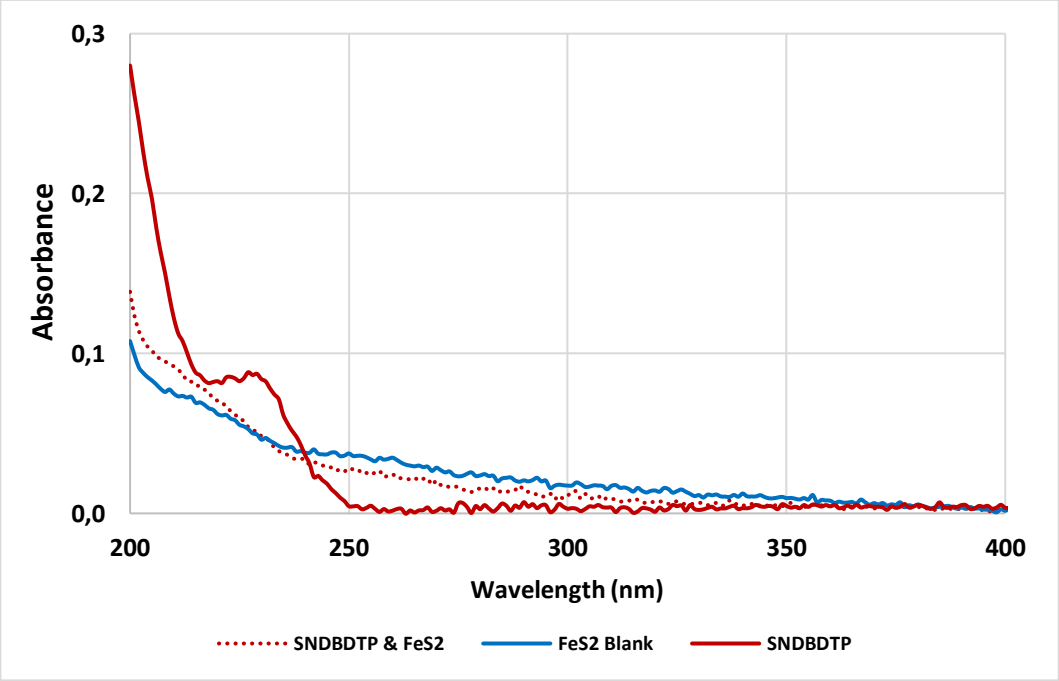

ADSORPTION OF ARSENOPYRITE WITH STANDARD COLLECTORS AT pH 9

PNBX

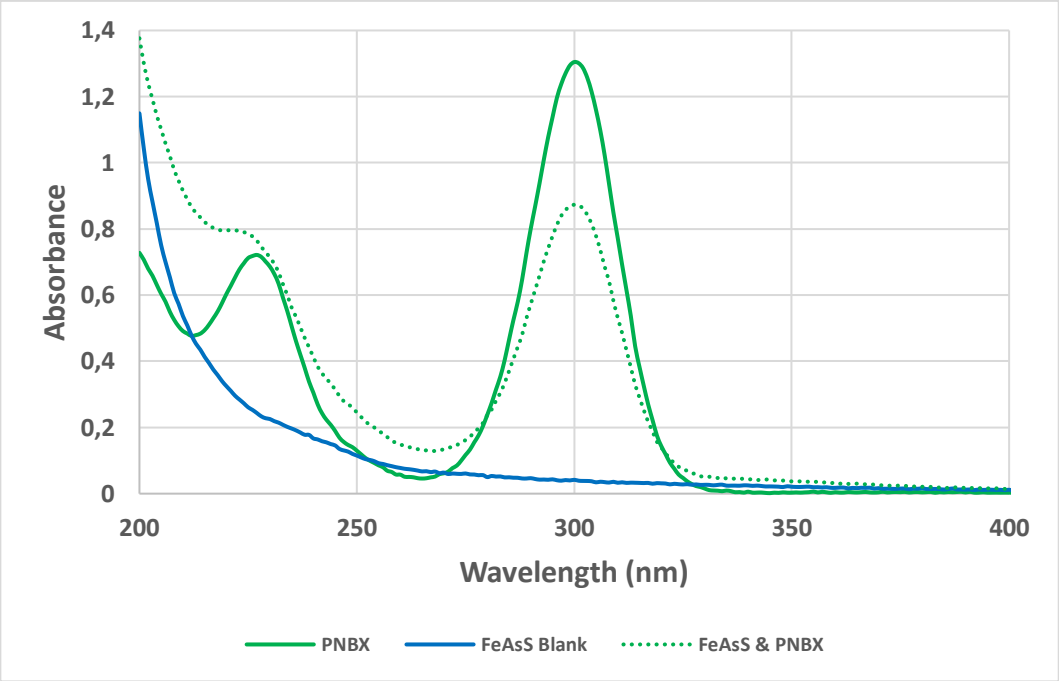

SNBDTC

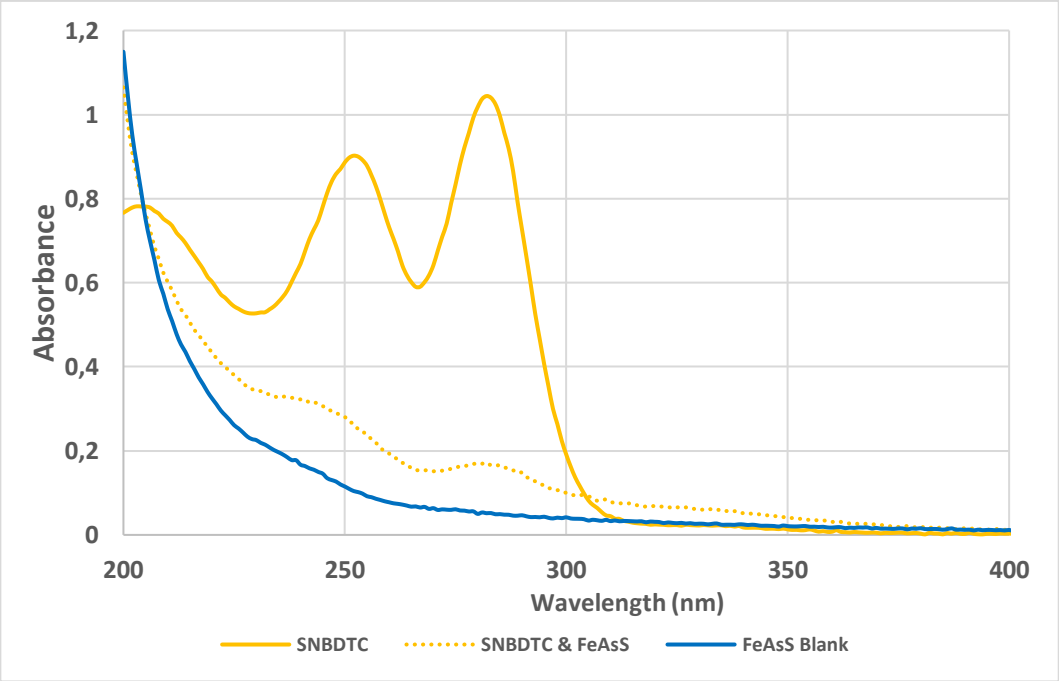

SNDBDTP

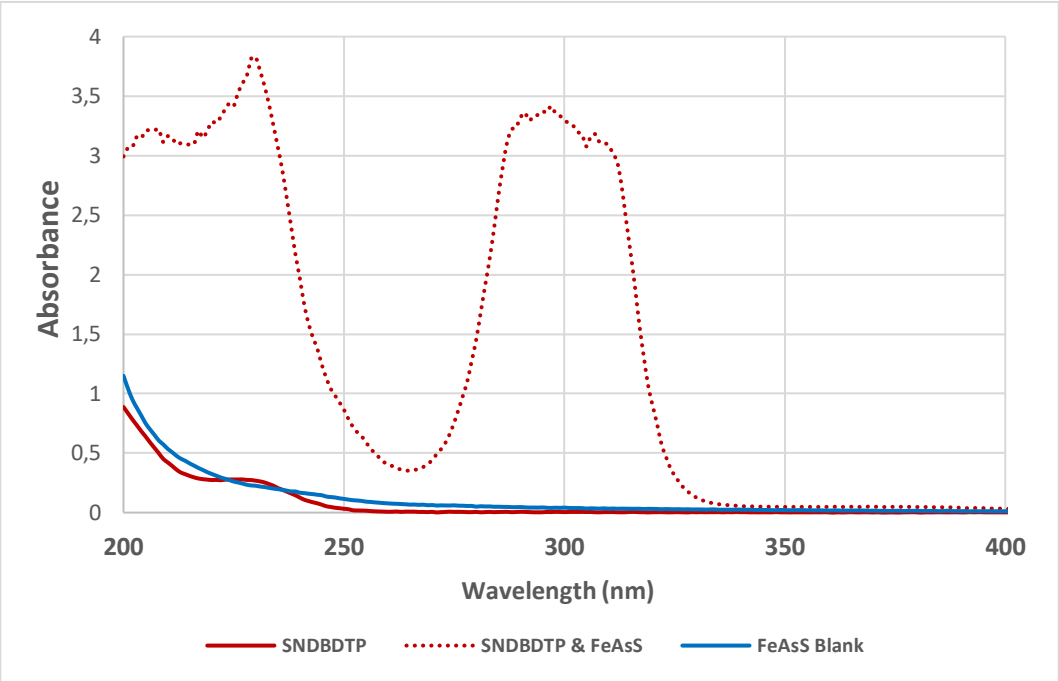

ADSORPTION OF ARSENOPYRITE WITH STANDARD COLLECTORS AT pH 9

PNBX

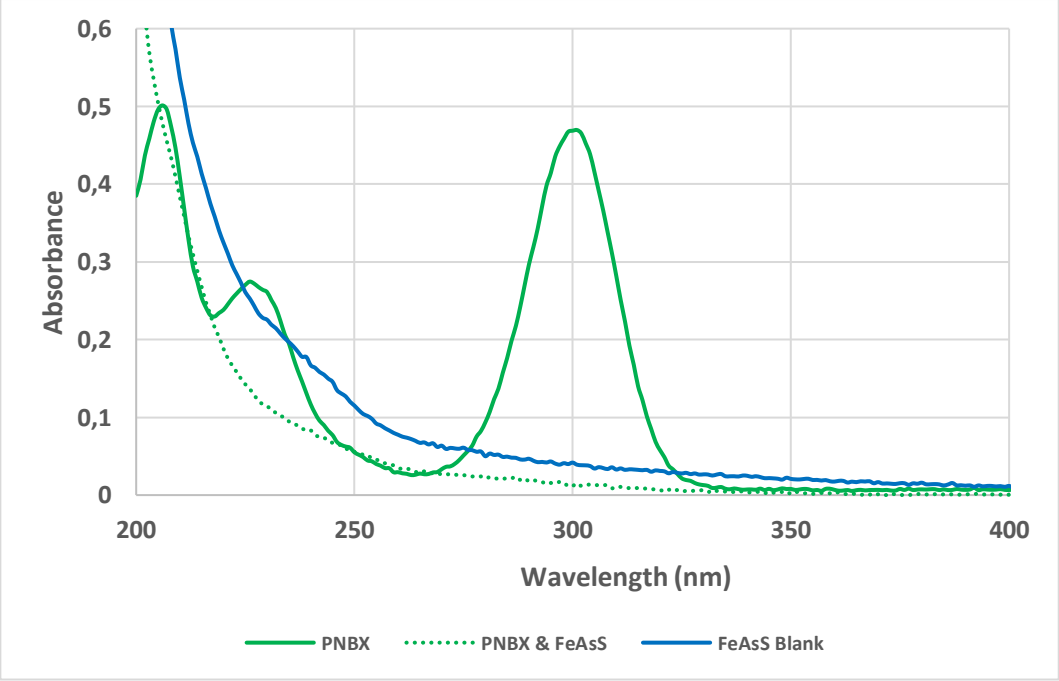

SNBDTC

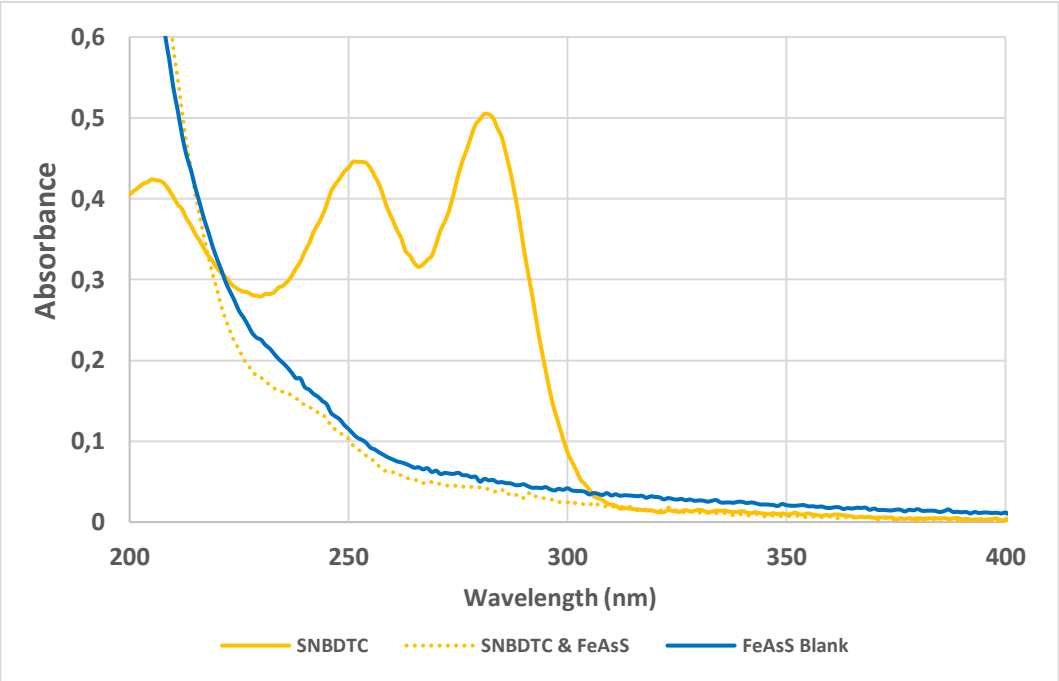

Beer Lambert law to calculate the peak for the distorted spectra at pH 4 in order to calculate the adsorption density.

SNDBDTP

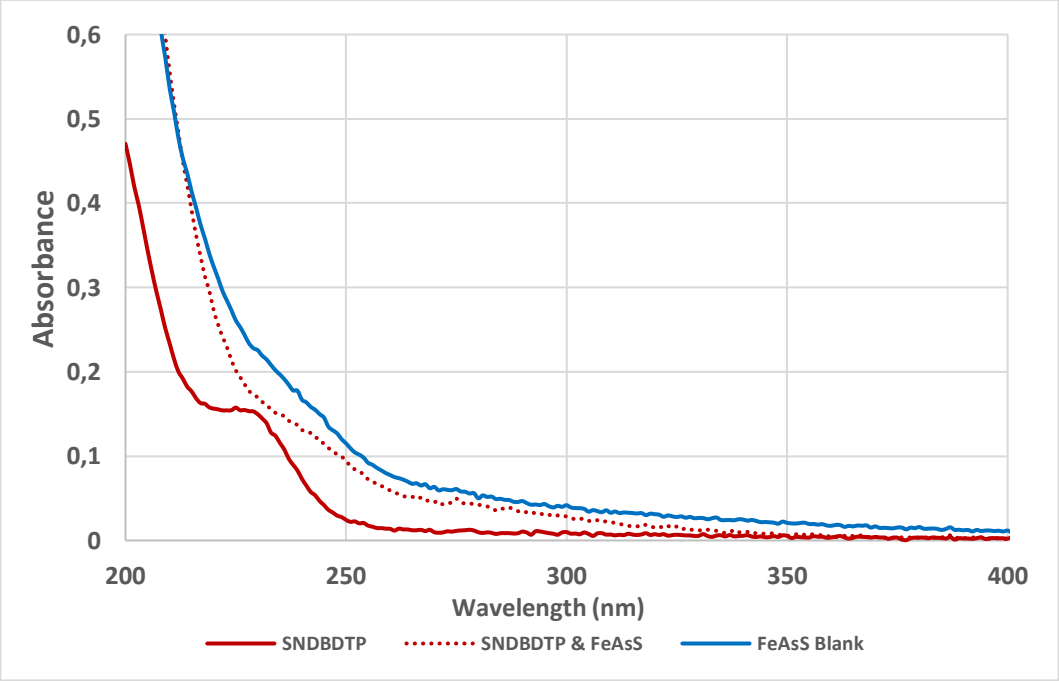

ADSORPTION OF COOPERITE WITH STANDARD COLLECTORS AT pH 9

PNBX

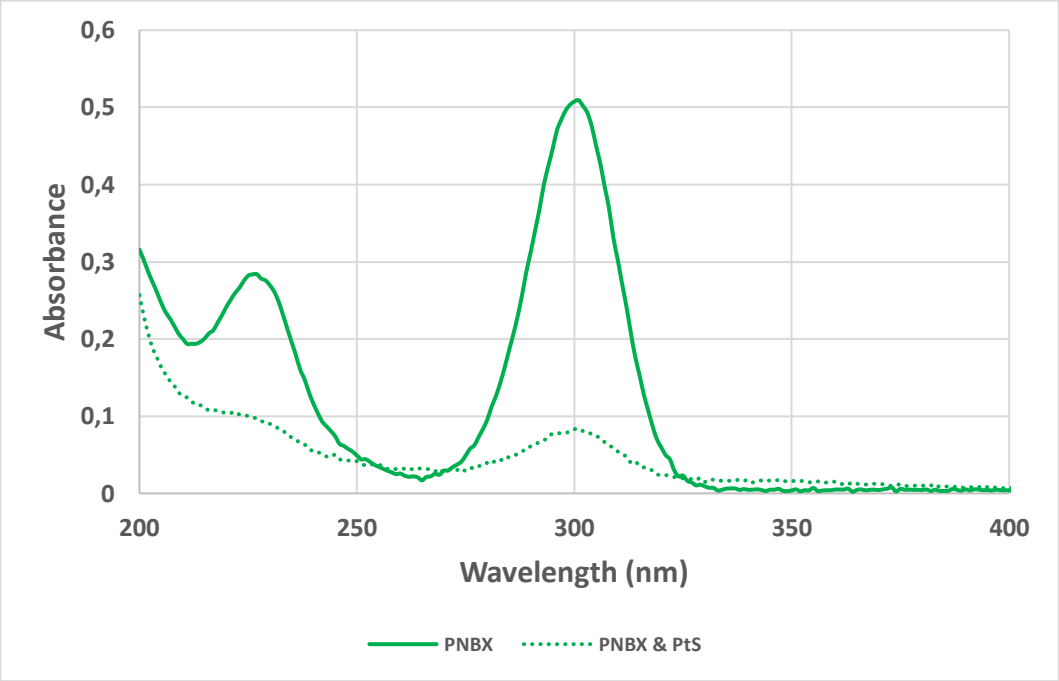

SNBDTC

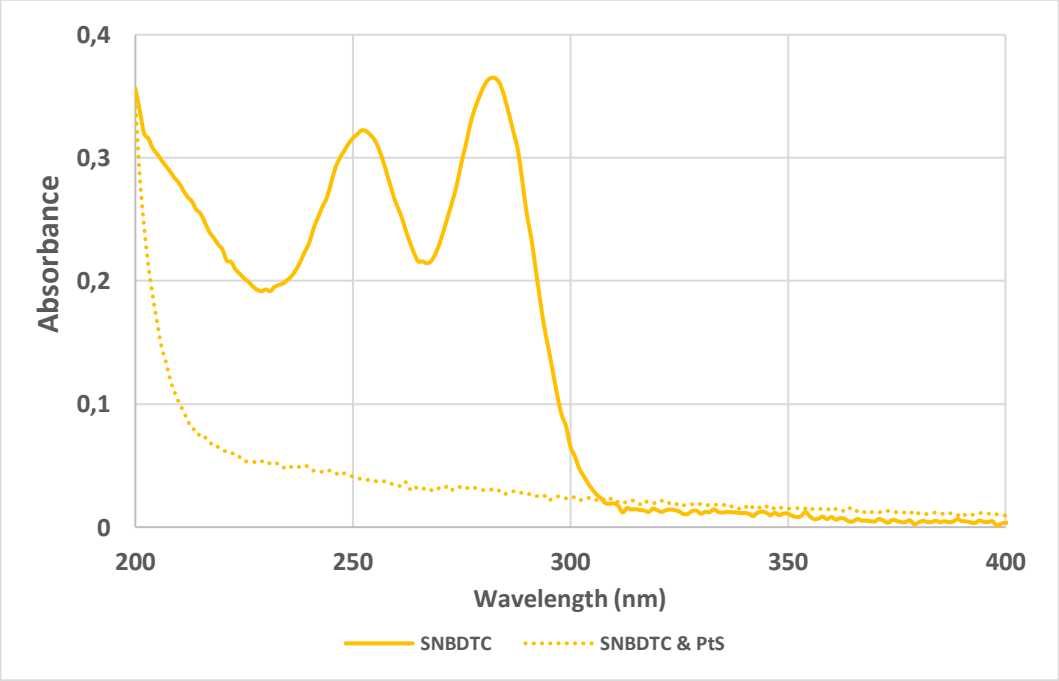

SNDBDTP

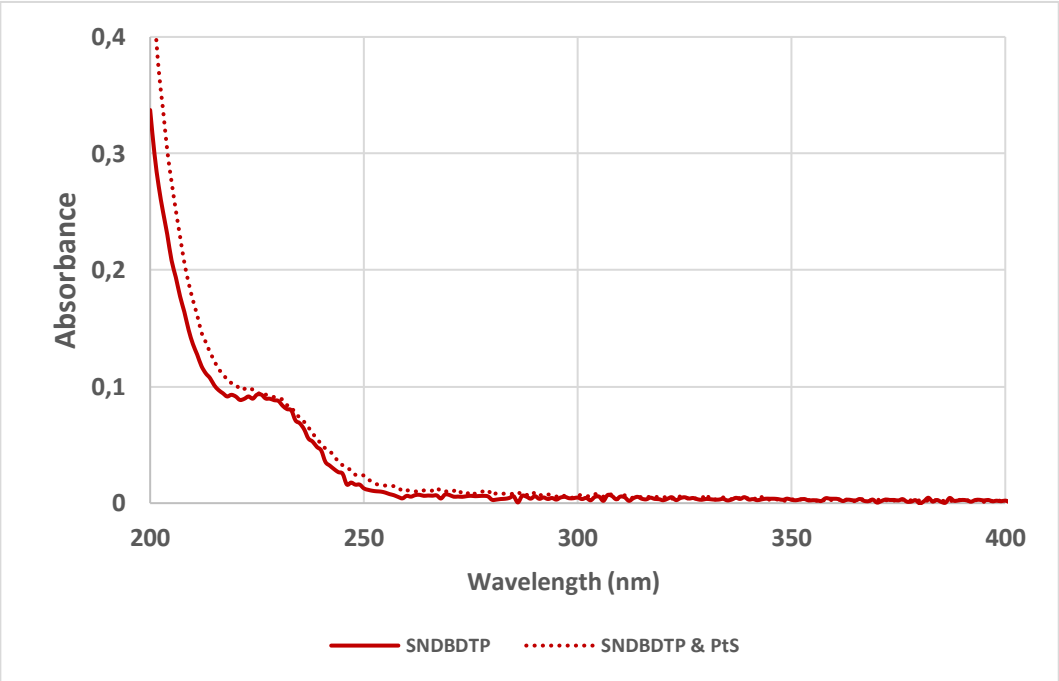

ADSORPTION OF COOPERITE WITH STANDARD COLLECTORS AT pH 4

PNBX

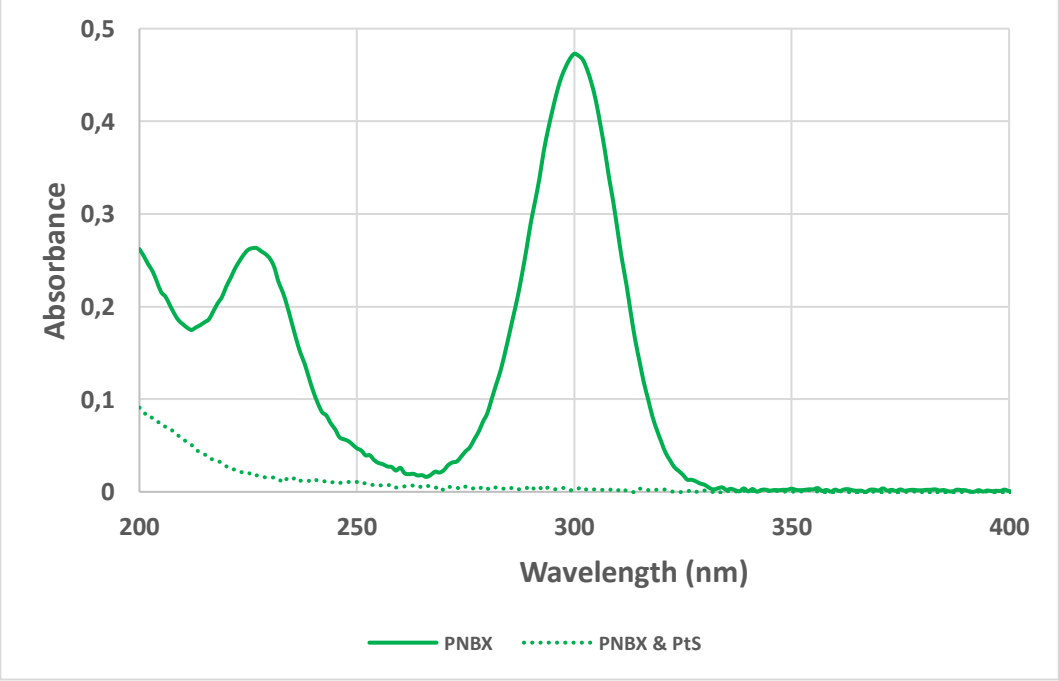

SNBDTC

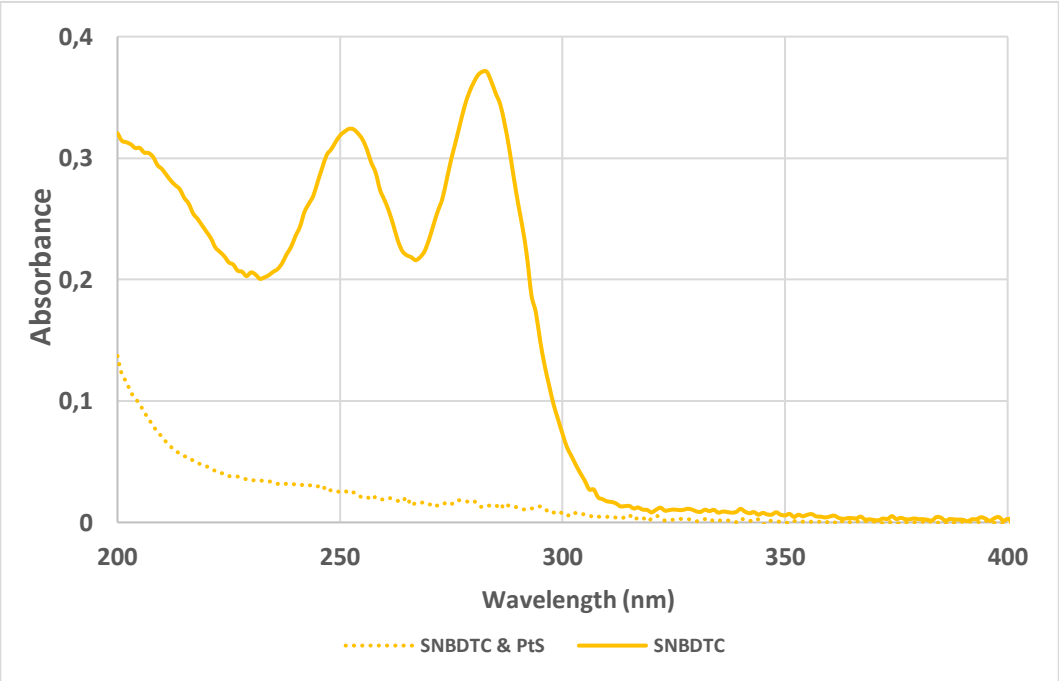

Beer Lambert law to calculate the peak for the distorted spectra at pH 4 in order to calculate the adsorption density.

SNDBDTP

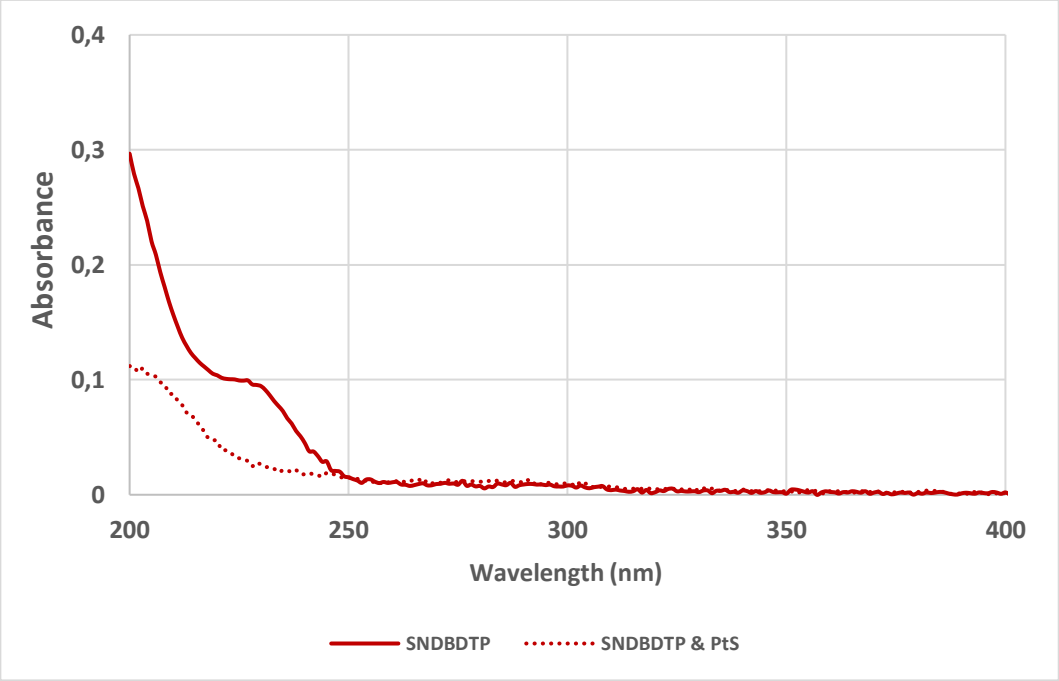

APPENDIX C: SPERRYLITE XPS RESULTS

C-C Peaks

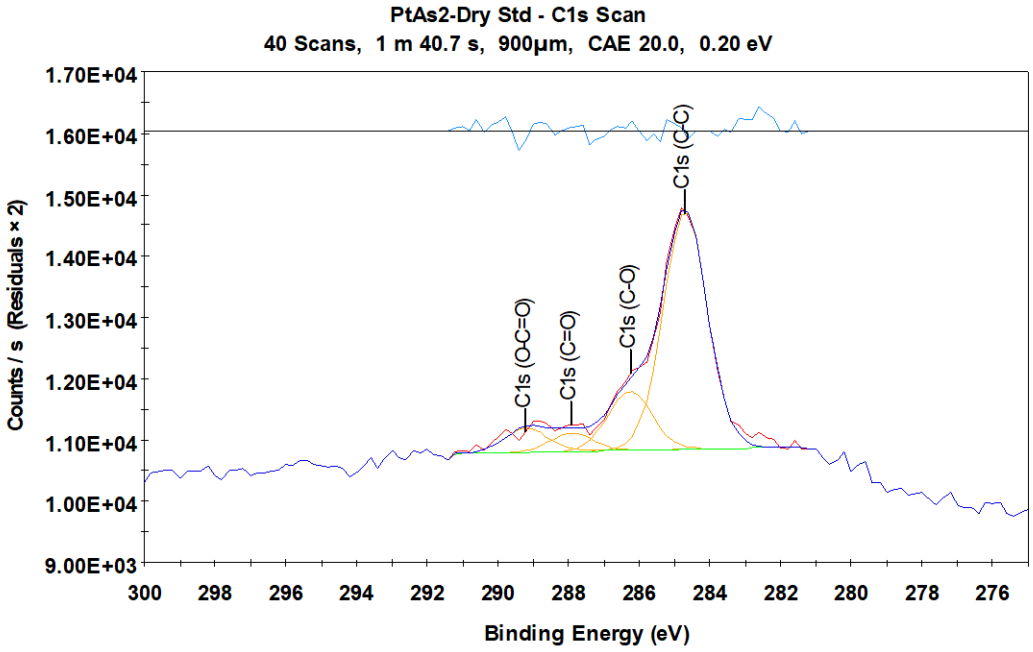

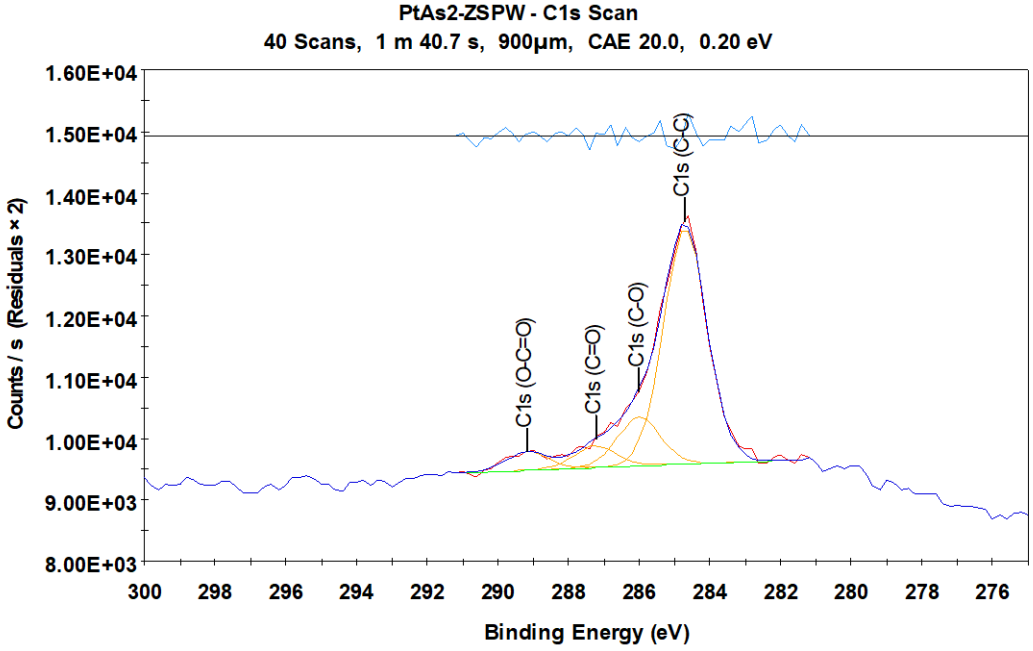

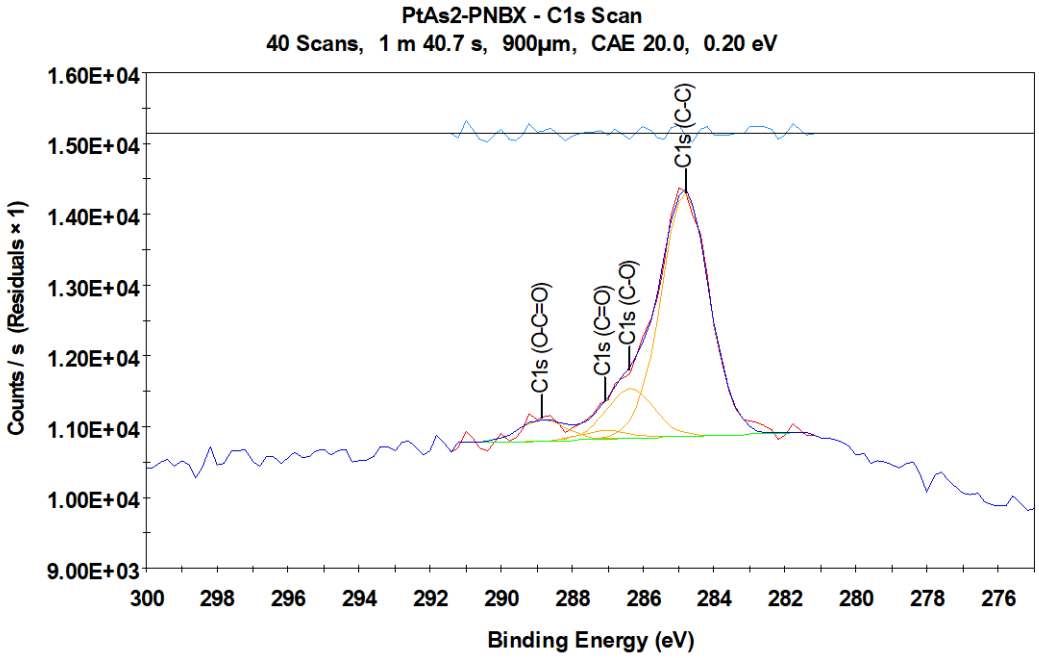
PtAs2-PNBX - C1s Scan
40 Scans, 1 m 40.7 s, 900µm, CAE 20.0, 0.20 eV
Counts / s (Residuals × 1)
1.60E+04
1.50E+04
1.40E+04
1.30E+04
1.20E+04
1.10E+04
1.00E+04
9.00E+03
C1s (C-C)
C1s (C-O)
C1s (C=O)
C1s (O-C=O)
300 298 296 294 292 290 288 286 284 282 280 278 276
Binding Energy (eV)

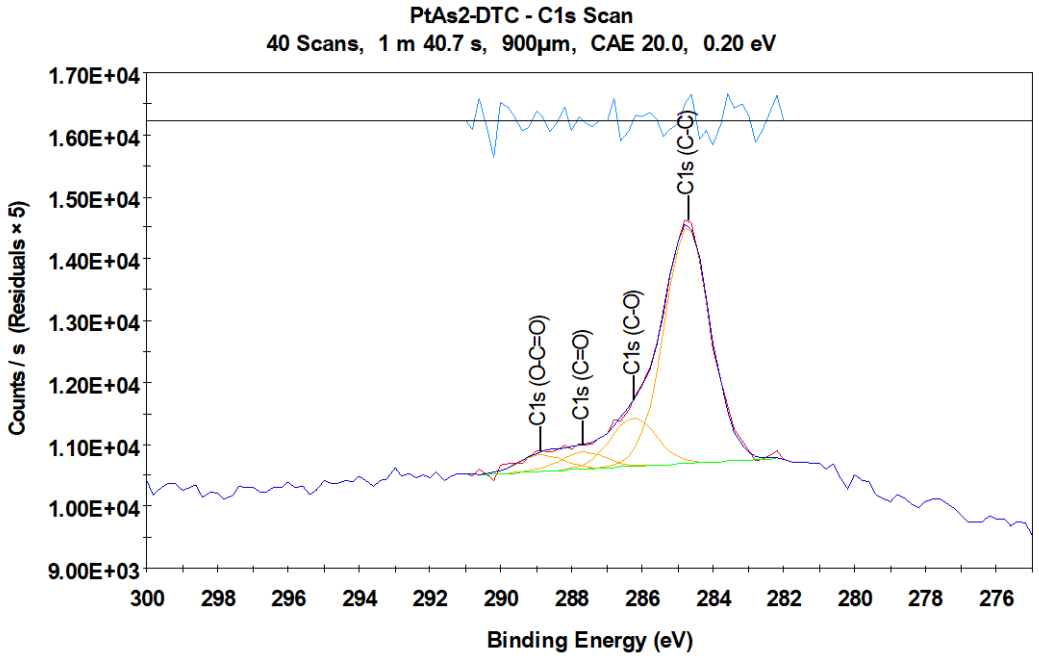
PtAs2-DTC - C1s Scan
40 Scans, 1 m 40.7 s, 900µm, CAE 20.0, 0.20 eV
Counts / s (Residuals × 5)
1.70E+04
1.60E+04
1.50E+04
1.40E+04
1.30E+04
1.20E+04
1.10E+04
1.00E+04
9.00E+03
C1s (C-C)
C1s (C-O)
C1s (C=O)
C1s (O-C=O)
300 298 296 294 292 290 288 286 284 282 280 278 276
Binding Energy (eV)

Sulfide Peak

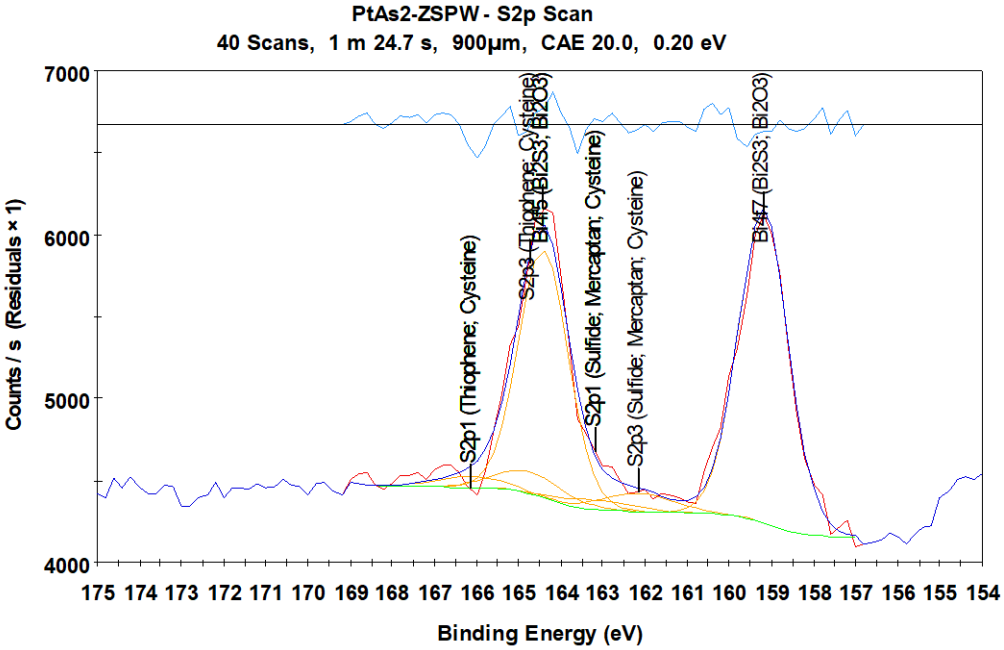

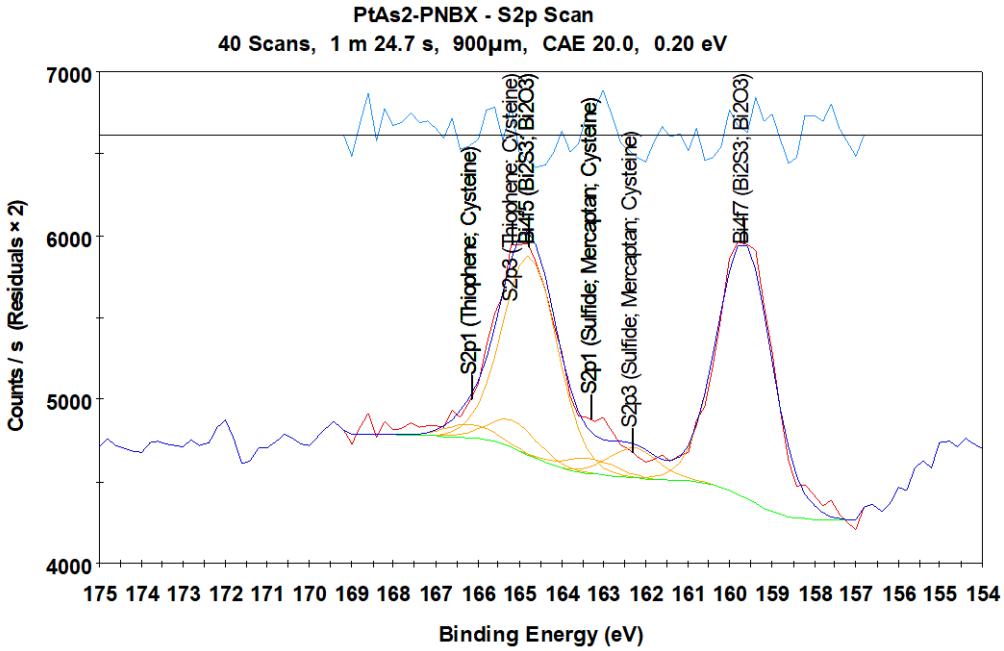

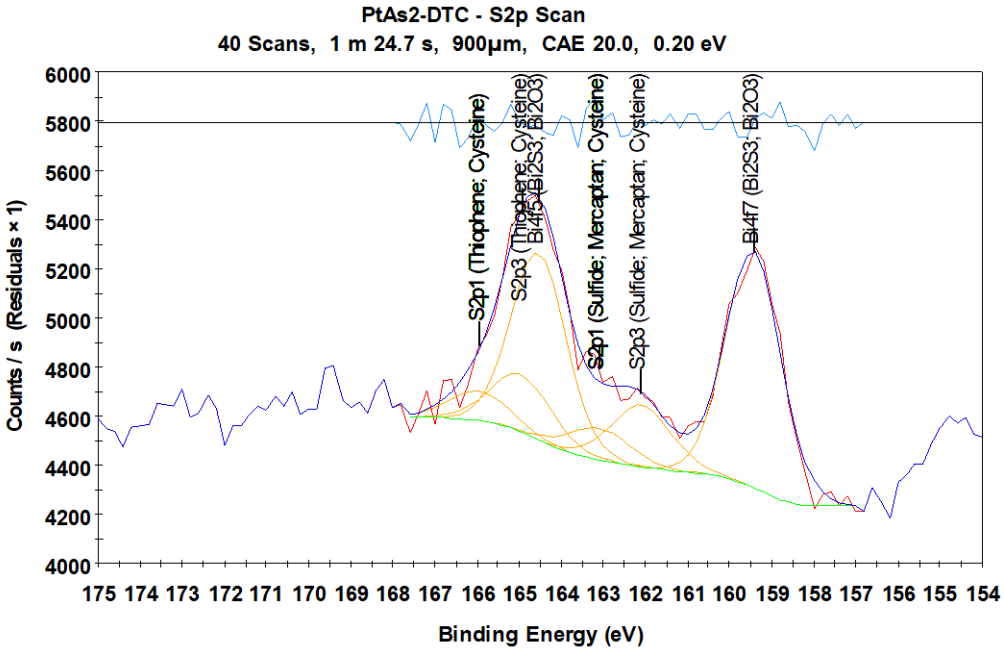
PtAs2-DTC - S2p Scan
40 Scans, 1 m 24.7 s, 900µm, CAE 20.0, 0.20 eV
Counts / s (Residuals × 1)
Binding Energy (eV)
S2p1 (Thiophene; Cysteine)
S2p3 (Thiophene; Cysteine)
Bi4f5 (Bi2S3; Bi2O3)
S2p1 (Sulfide; Mercaptan; Cysteine)
S2p3 (Sulfide; Mercaptan; Cysteine)
Bi4f7 (Bi2S3; Bi2O3)

Oxygen Peak

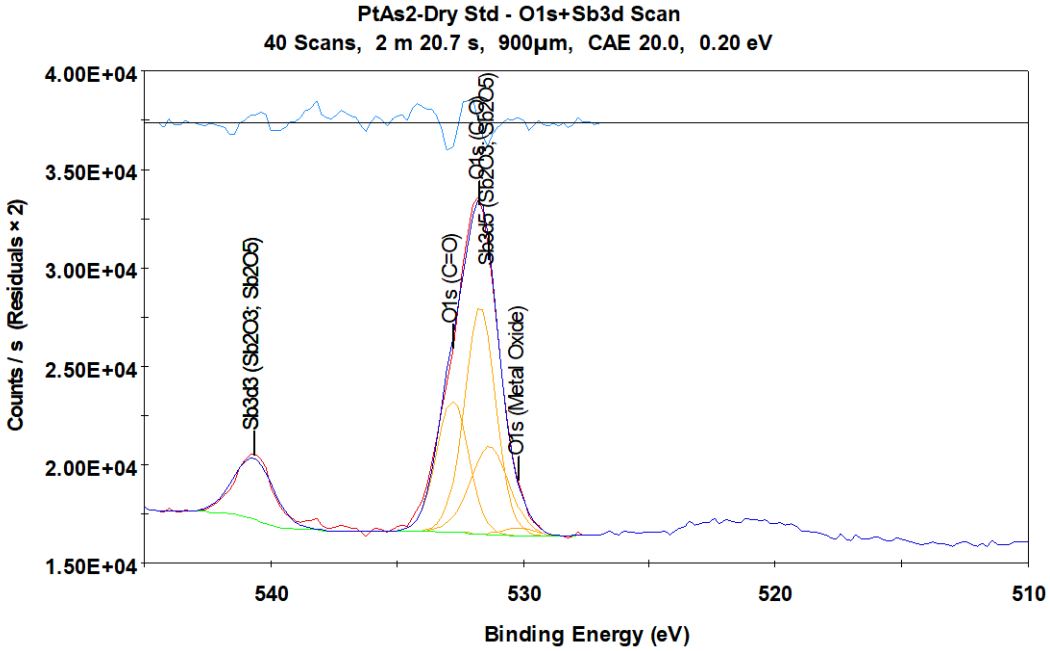
PtAs2-Dry Std - O1s+Sb3d Scan
40 Scans, 2 m 20.7 s, 900µm, CAE 20.0, 0.20 eV
Counts / s (Residuals × 2)
Binding Energy (eV)
Sb3d3 (Sb2O3; Sb2O5)
O1s (C=O)
Sb3d5 (Sb2O3; Sb2O5)
O1s (Sb2O3; Sb2O5)
O1s (Metal Oxide)

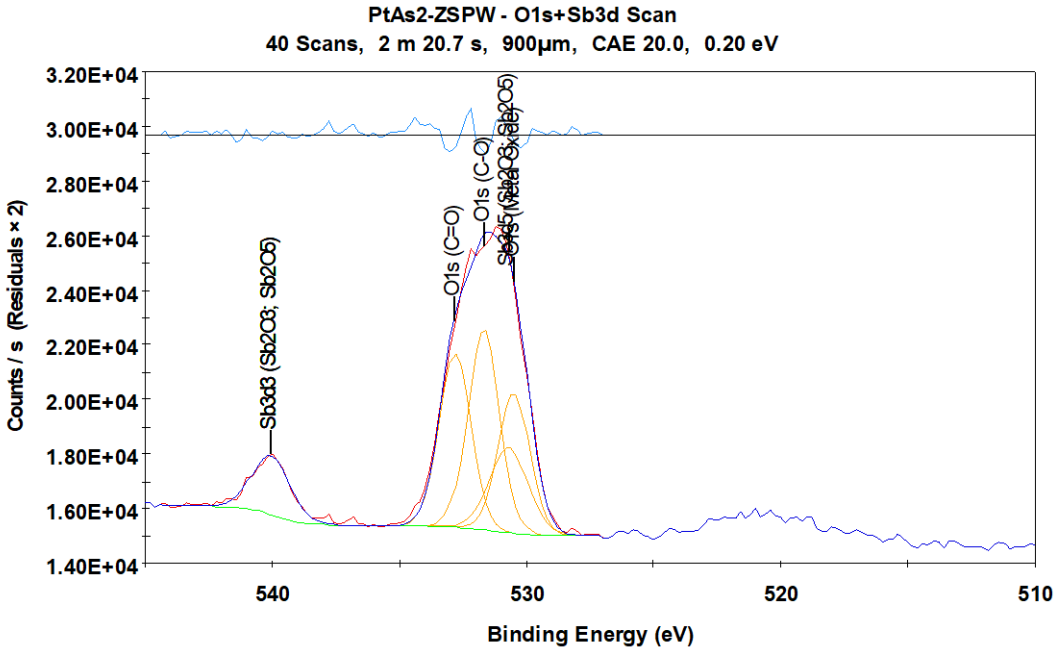
PtAs2-ZSPW - O1s+Sb3d Scan
40 Scans, 2 m 20.7 s, 900µm, CAE 20.0, 0.20 eV
Counts / s (Residuals × 2)
3.20E+04
3.00E+04
2.80E+04
2.60E+04
2.40E+04
2.20E+04
2.00E+04
1.80E+04
1.60E+04
1.40E+04
Sb3d3 (Sb2O3; Sb2O5)
O1s (C=O)
O1s (C-O)
Sb3d5 (Sb2O3; Sb2O5)
O1s (Meta Oxide)
540
530
520
510
Binding Energy (eV)

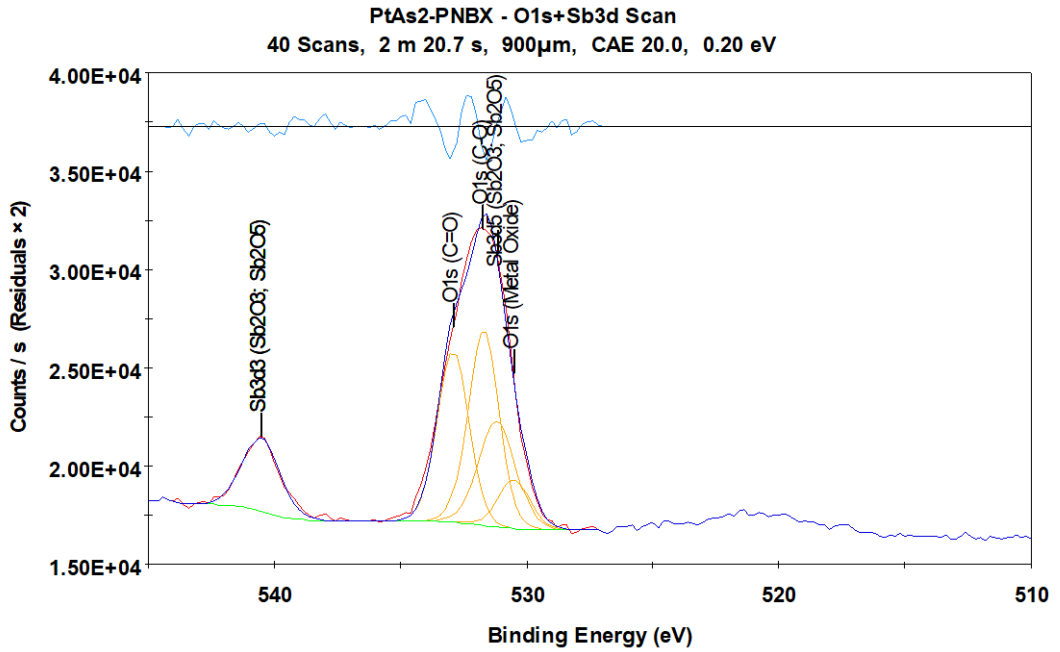
PtAs2-PNBX - O1s+Sb3d Scan
40 Scans, 2 m 20.7 s, 900µm, CAE 20.0, 0.20 eV
Counts / s (Residuals × 2)
4.00E+04
3.50E+04
3.00E+04
2.50E+04
2.00E+04
1.50E+04
Sb3d3 (Sb2O3; Sb2O5)
O1s (C=O)
O1s (C-O)
Sb3d5 (Sb2O3; Sb2O5)
O1s (Meta Oxide)
540
530
520
510
Binding Energy (eV)

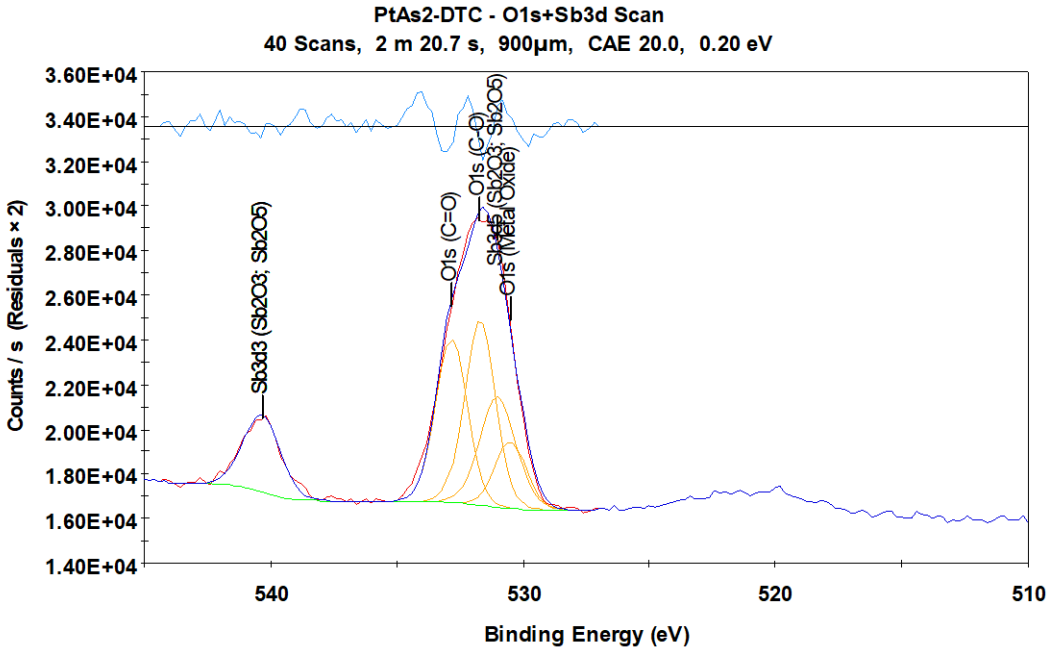
PtAs2-DTC - O1s+Sb3d Scan
40 Scans, 2 m 20.7 s, 900µm, CAE 20.0, 0.20 eV
Counts / s (Residuals × 2)
Binding Energy (eV)
Sb3d3 (Sb2O3; Sb2O5)
O1s (C=O)
O1s (C-O)
Sb3d5 (Sb2O3; Sb2O5)
O1s (Metal Oxide)

Arsenolite

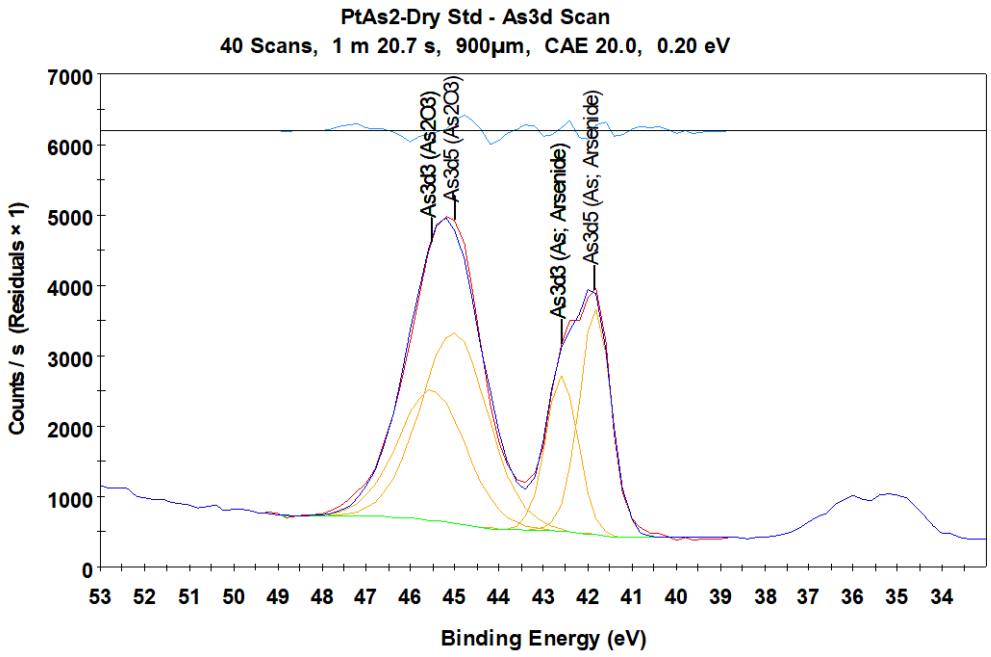
PtAs2-Dry Std - As3d Scan
40 Scans, 1 m 20.7 s, 900µm, CAE 20.0, 0.20 eV
Counts / s (Residuals × 1)
Binding Energy (eV)
As3d3 (As2O3)
As3d5 (As2O3)
As3d3 (As; Arsenide)
As3d5 (As; Arsenide)

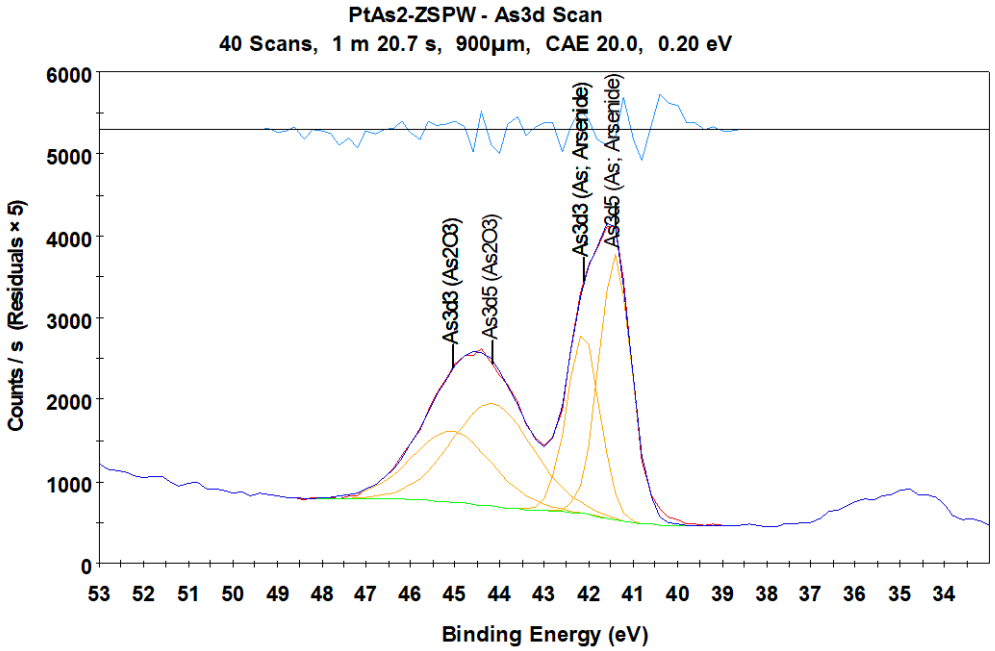
PtAs2-ZSPW - As3d Scan
40 Scans, 1 m 20.7 s, 900µm, CAE 20.0, 0.20 eV
Counts / s (Residuals × 5)
Binding Energy (eV)
As3d3 (As2O3)
As3d5 (As2O3)
As3d3 (As; Arsenide)
As3d5 (As; Arsenide)

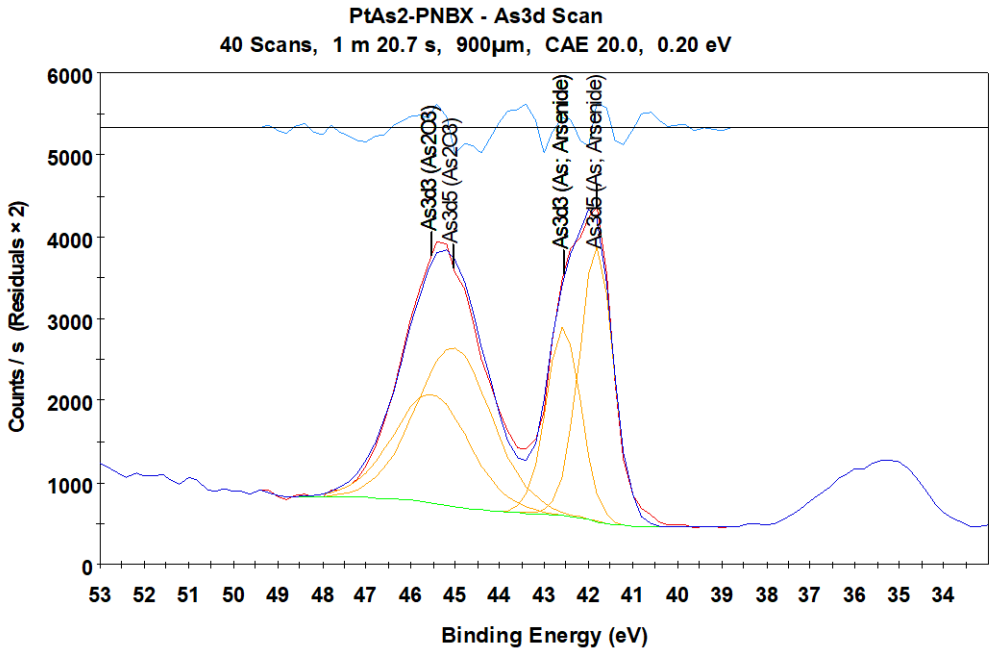
PtAs2-PNBX - As3d Scan
40 Scans, 1 m 20.7 s, 900µm, CAE 20.0, 0.20 eV
Counts / s (Residuals × 2)
Binding Energy (eV)
As3d3 (As2O3)
As3d5 (As2O3)
As3d3 (As; Arsenide)
As3d5 (As; Arsenide)

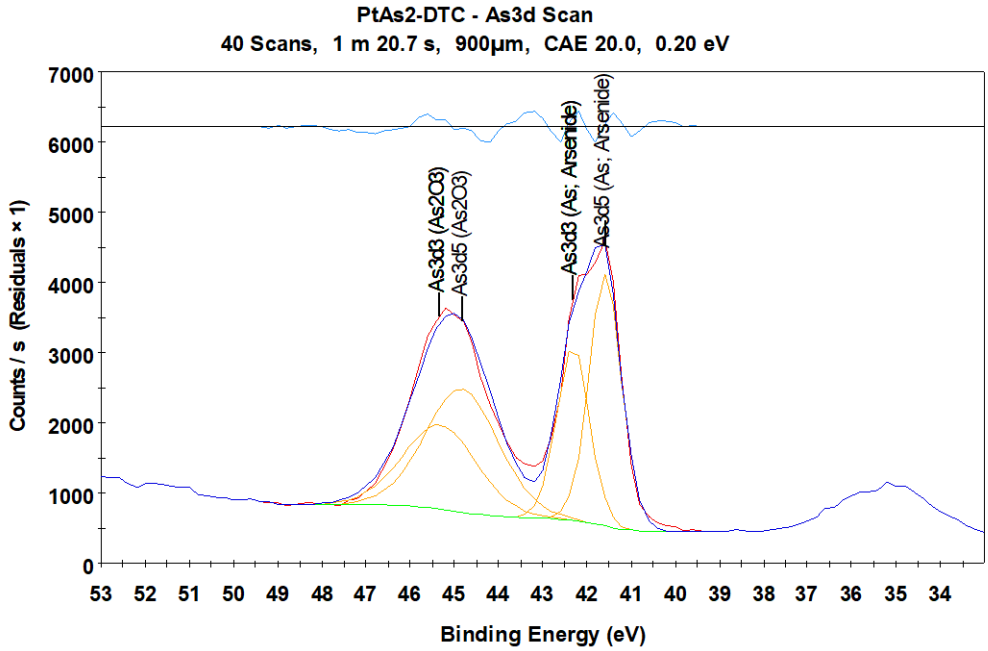

Plant Water Ions

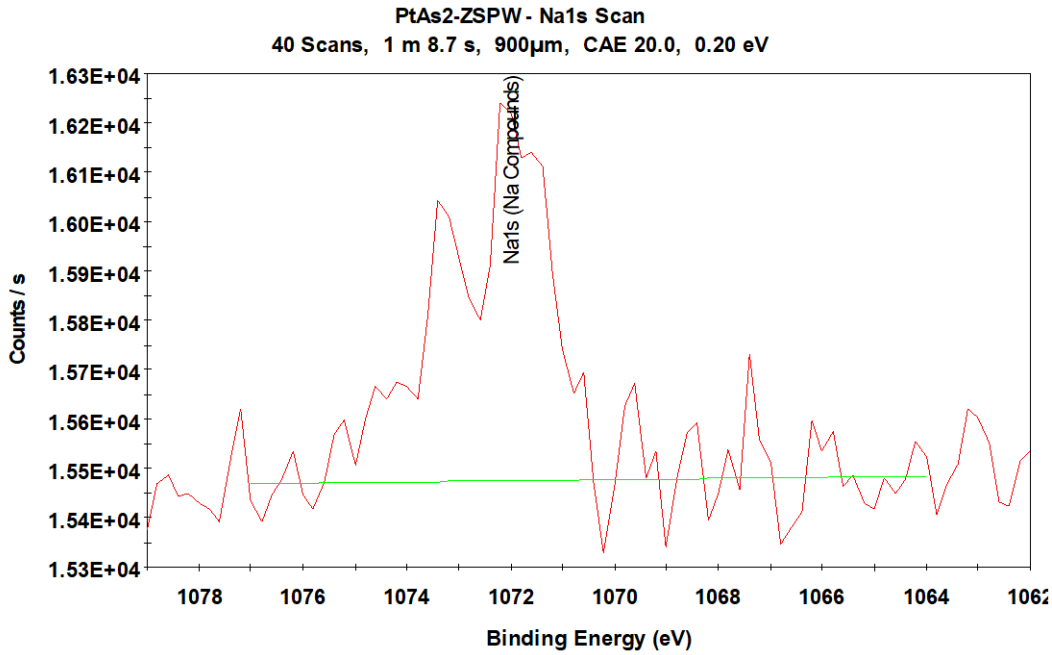

APPENDIX D: ARSENOPYRITE XPS RESULTS

C-C Peaks

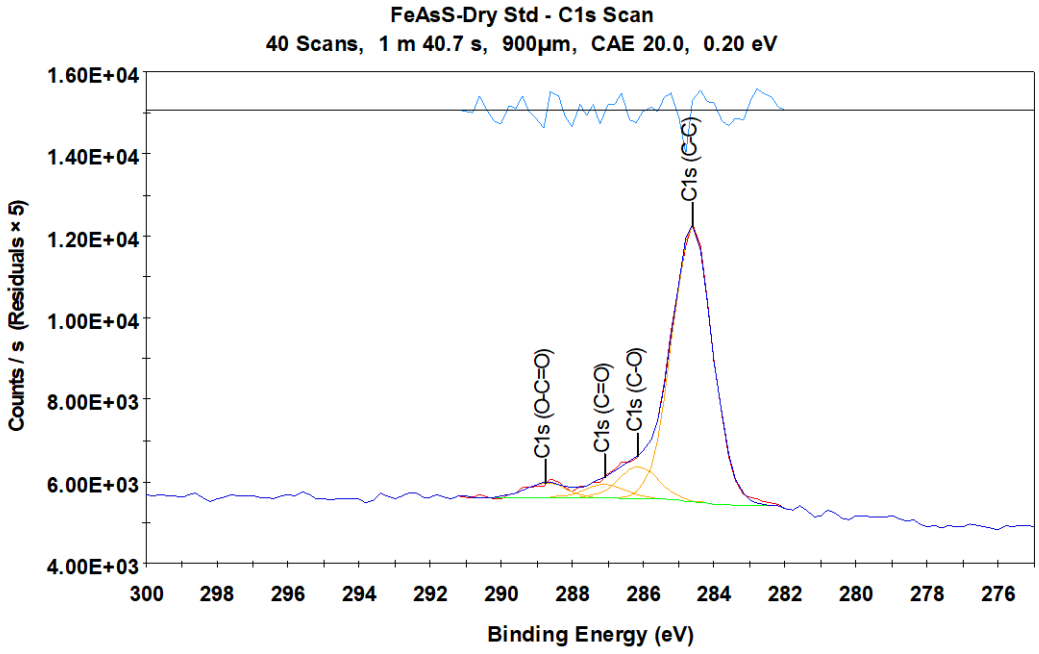

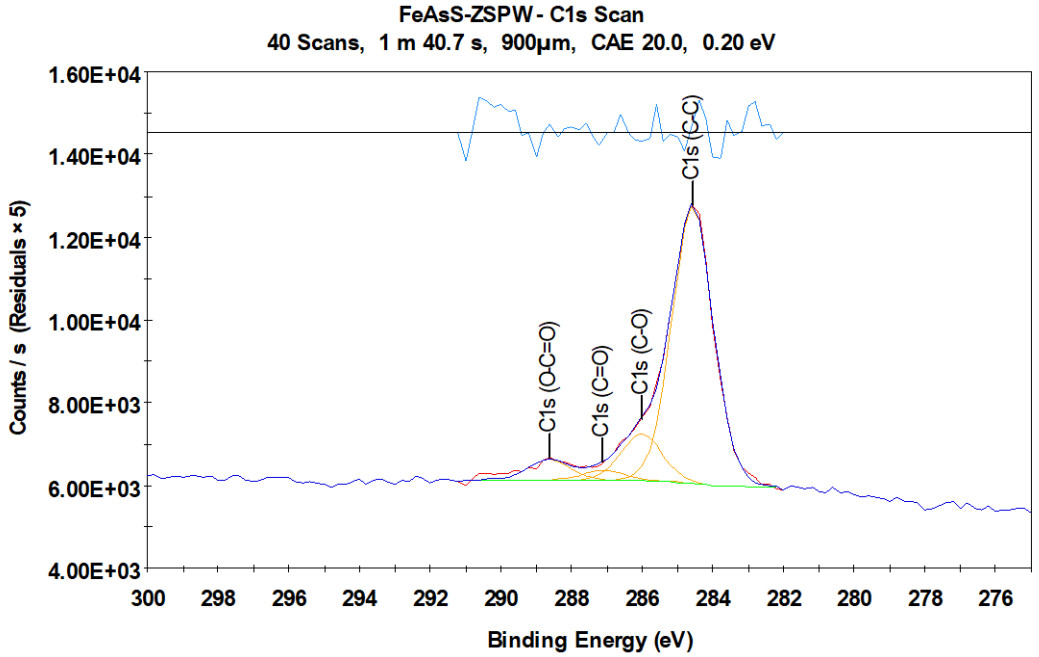

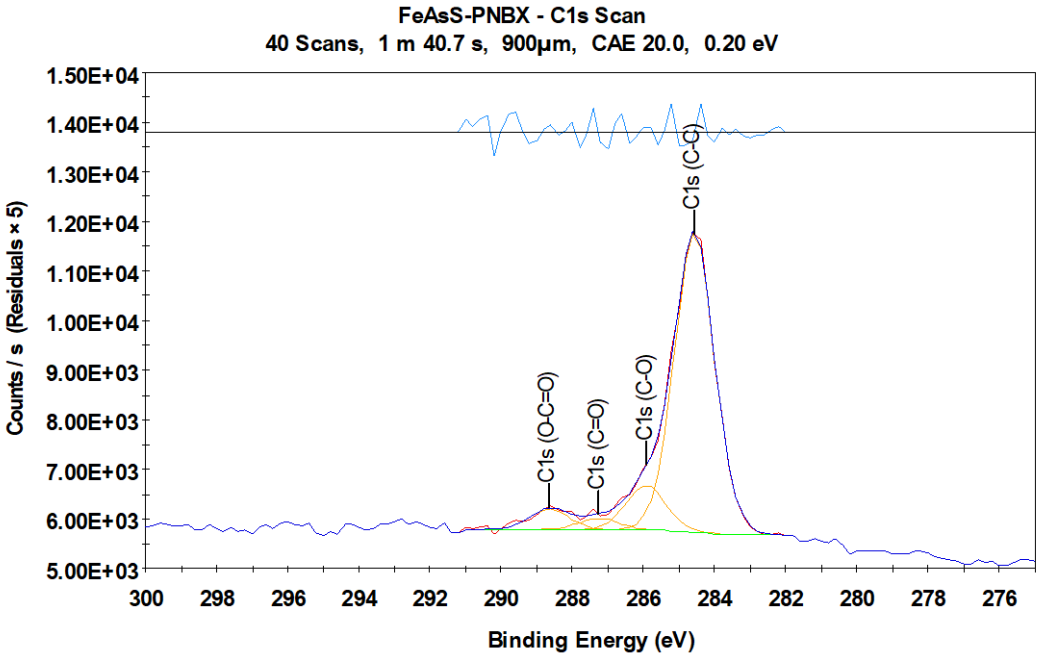

Sulphide Peaks

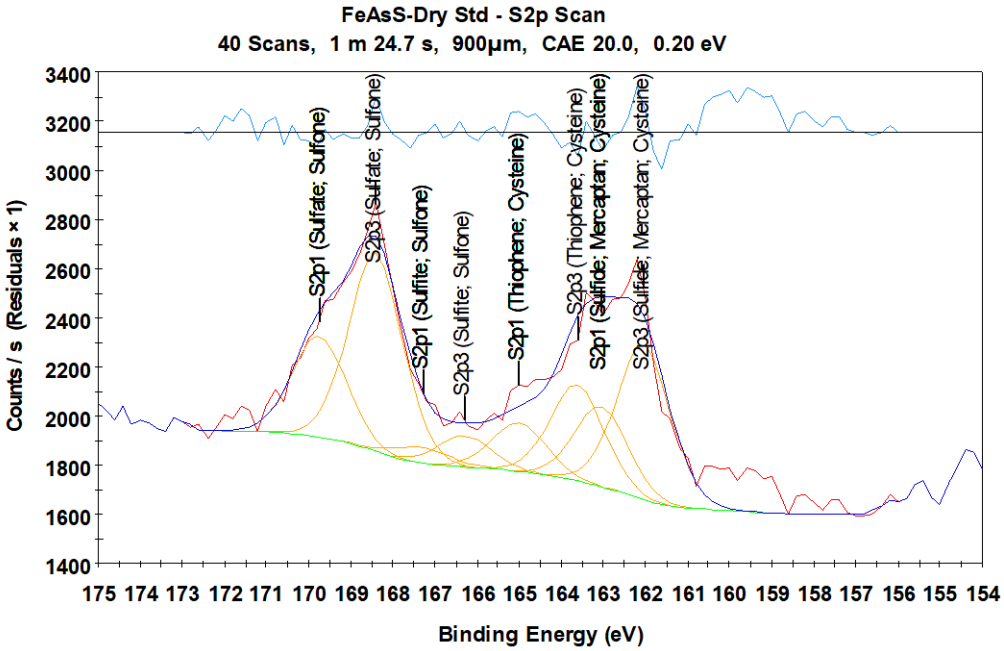

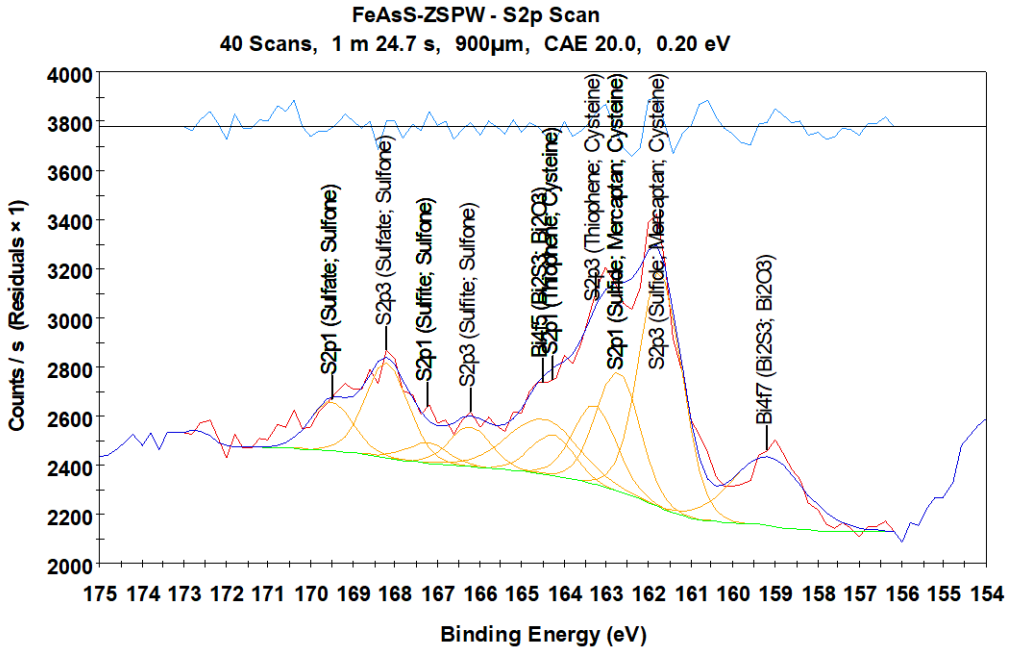
FeAsS-ZSPW - S2p Scan
40 Scans, 1 m 24.7 s, 900µm, CAE 20.0, 0.20 eV
Counts / s (Residuals × 1)
Binding Energy (eV)
S2p1 (Sulfate; Sulfone)
S2p3 (Sulfate; Sulfone)
S2p1 (Sulfite; Sulfone)
S2p3 (Sulfite; Sulfone)
S2p3 (Thiophene; Cysteine)
S2p1 (Sulfide; Mercaptan; Cysteine)
S2p3 (Sulfide; Mercaptan; Cysteine)
Bi4f7 (Bi2S3; Bi2O3)

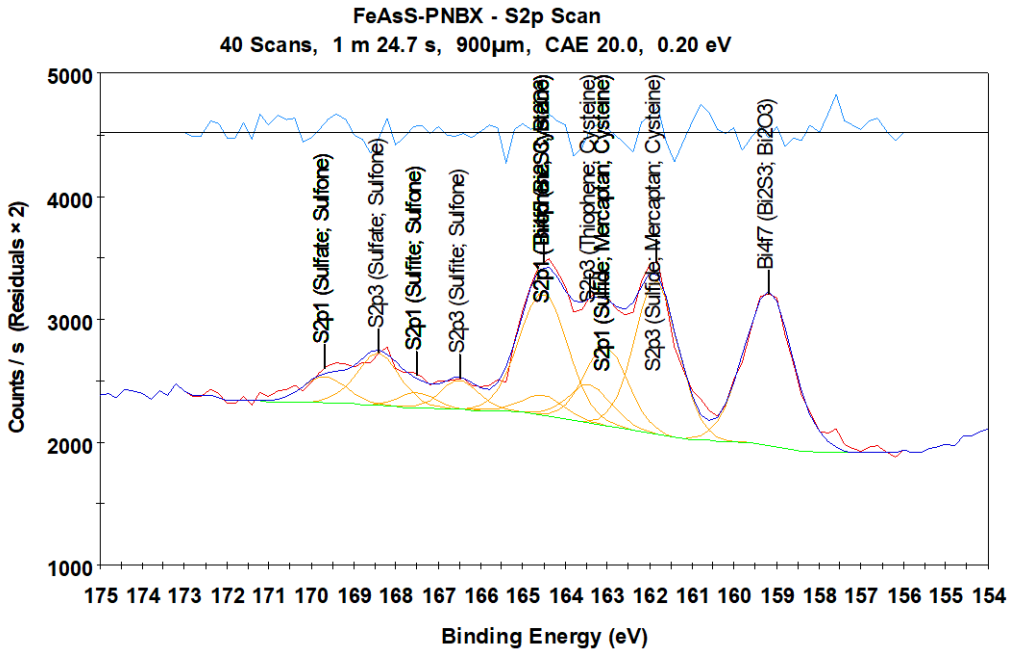
FeAsS-PNBX - S2p Scan
40 Scans, 1 m 24.7 s, 900µm, CAE 20.0, 0.20 eV
Counts / s (Residuals × 2)
Binding Energy (eV)
S2p1 (Sulfate; Sulfone)
S2p3 (Sulfate; Sulfone)
S2p1 (Sulfite; Sulfone)
S2p3 (Sulfite; Sulfone)
S2p3 (Thiophene; Cysteine)
S2p1 (Sulfide; Mercaptan; Cysteine)
S2p3 (Sulfide; Mercaptan; Cysteine)
Bi4f7 (Bi2S3; Bi2O3)

Oxygen

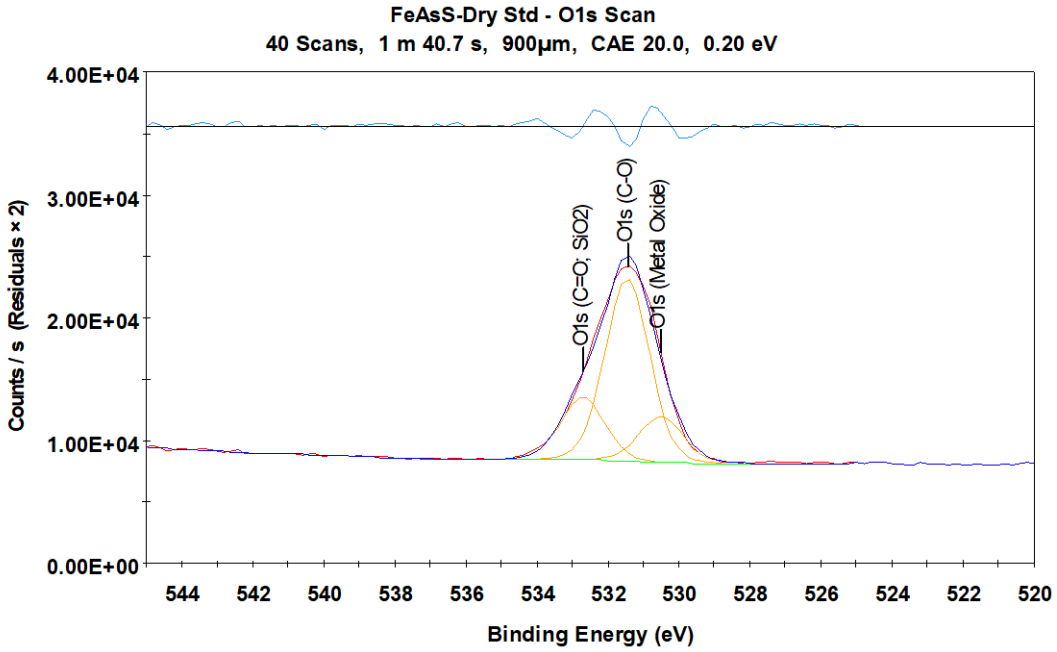
FeAsS-Dry Std - O1s Scan
40 Scans, 1 m 40.7 s, 900µm, CAE 20.0, 0.20 eV
4.00E+04
3.00E+04
2.00E+04
1.00E+04
0.00E+00
Counts / s (Residuals × 2)
O1s (C=O; SiO2)
O1s (C-O)
O1s (Metal Oxide)
544 542 540 538 536 534 532 530 528 526 524 522 520
Binding Energy (eV)

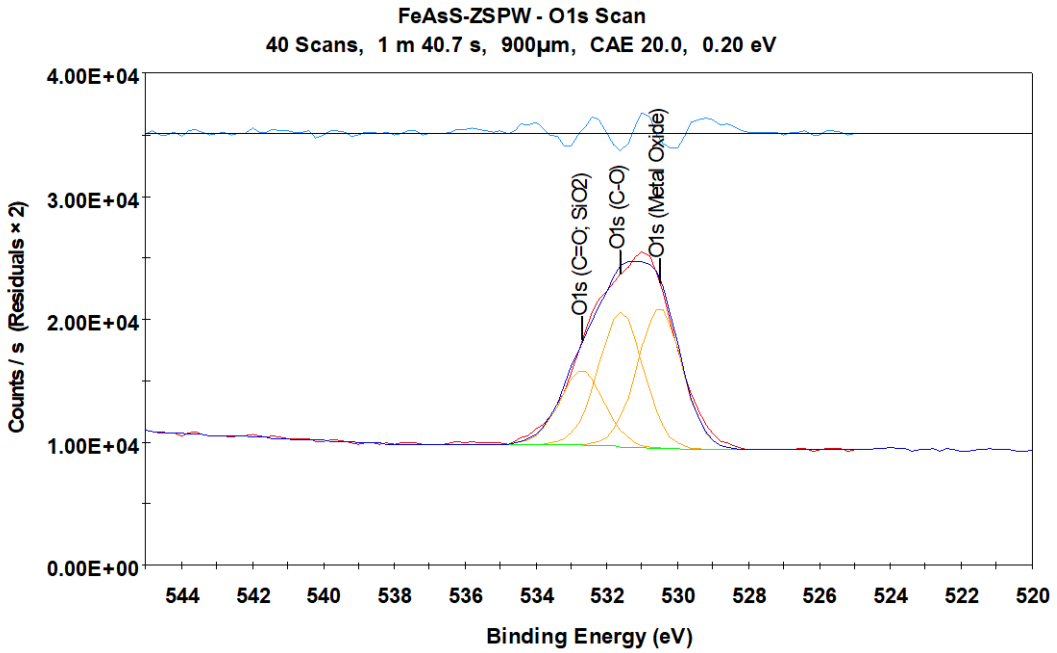
FeAsS-ZSPW - O1s Scan
40 Scans, 1 m 40.7 s, 900µm, CAE 20.0, 0.20 eV
4.00E+04
3.00E+04
2.00E+04
1.00E+04
0.00E+00
Counts / s (Residuals × 2)
O1s (C=O; SiO2)
O1s (C-O)
O1s (Metal Oxide)
544 542 540 538 536 534 532 530 528 526 524 522 520
Binding Energy (eV)

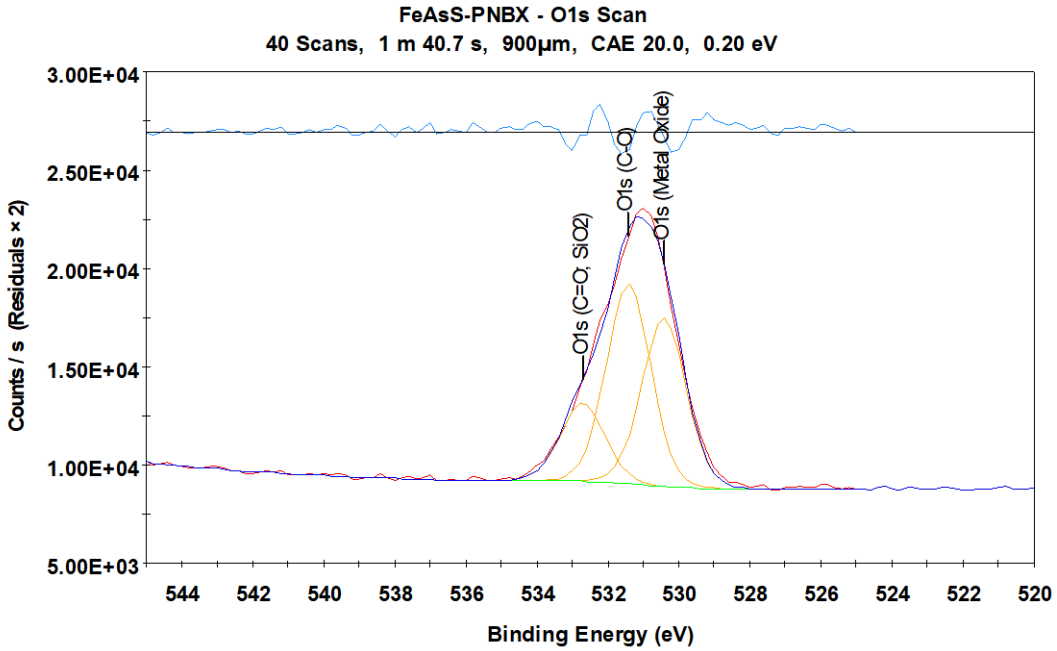
FeAsS-PNBX - O1s Scan
40 Scans, 1 m 40.7 s, 900µm, CAE 20.0, 0.20 eV
Counts / s (Residuals × 2)
3.00E+04
2.50E+04
2.00E+04
1.50E+04
1.00E+04
5.00E+03
O1s (C=O, SiO2)
O1s (C-O)
O1s (Metal Oxide)
544 542 540 538 536 534 532 530 528 526 524 522 520
Binding Energy (eV)

Arsenolite

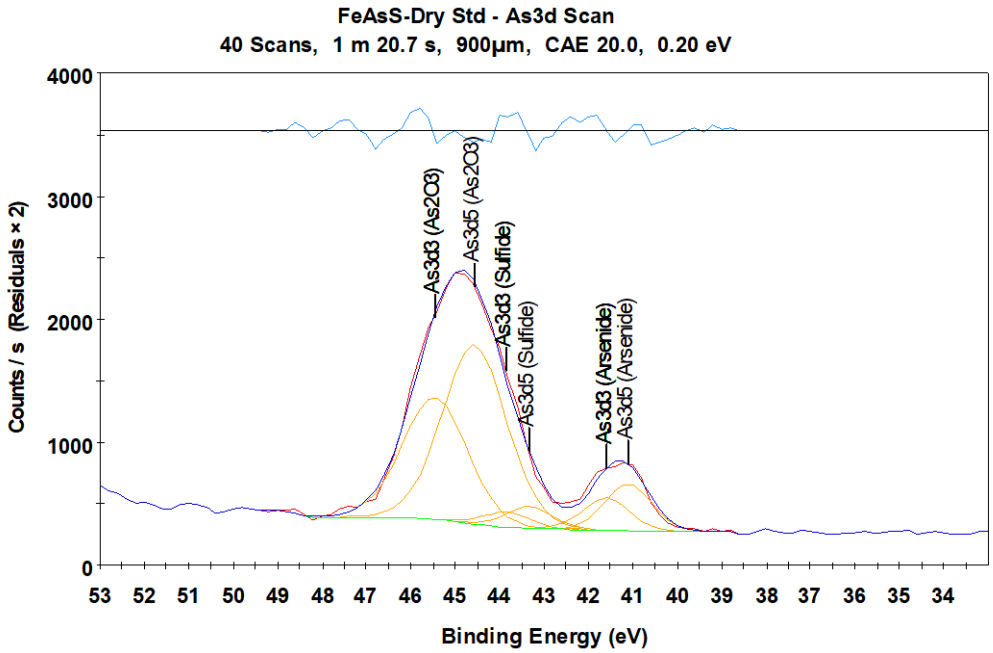
FeAsS-Dry Std - As3d Scan
40 Scans, 1 m 20.7 s, 900µm, CAE 20.0, 0.20 eV
Counts / s (Residuals × 2)
4000
3000
2000
1000
0
As3d3 (As2O3)
As3d5 (As2O3)
As3d3 (Sulfide)
As3d5 (Sulfide)
As3d3 (Arsenide)
As3d5 (Arsenide)
53 52 51 50 49 48 47 46 45 44 43 42 41 40 39 38 37 36 35 34
Binding Energy (eV)

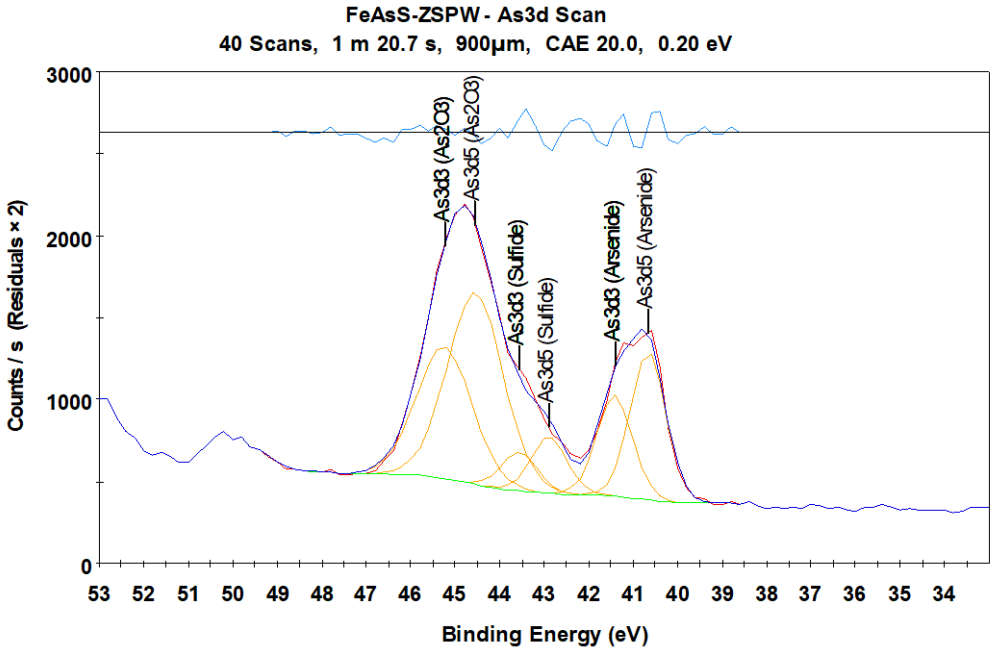
FeAsS-ZSPW - As3d Scan
40 Scans, 1 m 20.7 s, 900µm, CAE 20.0, 0.20 eV
Counts / s (Residuals × 2)
3000
2000
1000
0
As3d3 (As2O3)
As3d5 (As2O3)
As3d3 (Sulfide)
As3d5 (Sulfide)
As3d3 (Arsenide)
As3d5 (Arsenide)
53 52 51 50 49 48 47 46 45 44 43 42 41 40 39 38 37 36 35 34
Binding Energy (eV)

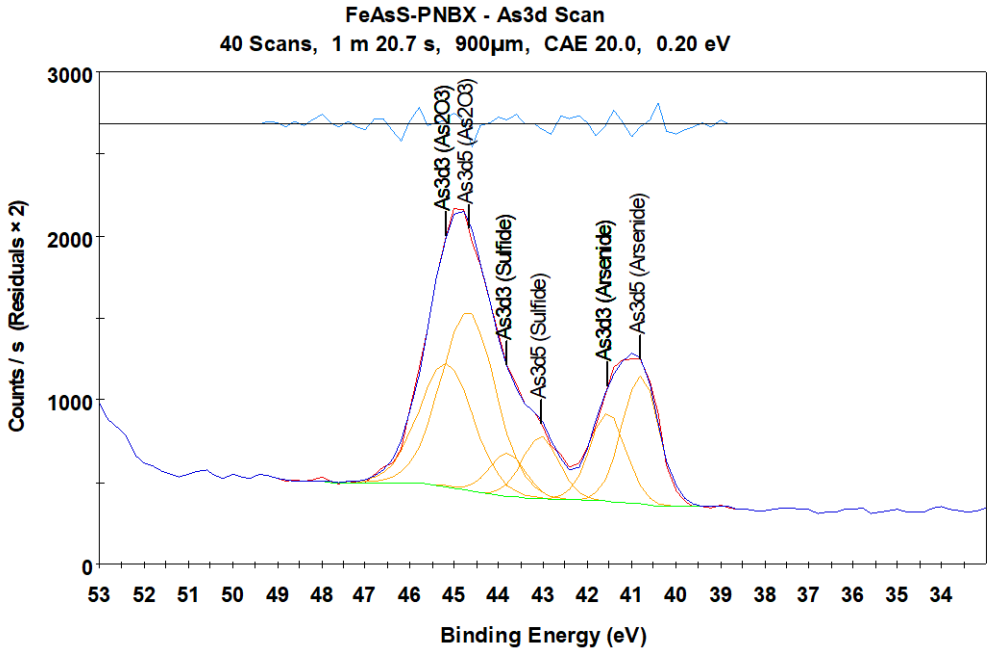
FeAsS-PNBX - As3d Scan
40 Scans, 1 m 20.7 s, 900µm, CAE 20.0, 0.20 eV
Counts / s (Residuals × 2)
3000
2000
1000
0
As3d3 (As2O3)
As3d5 (As2O3)
As3d3 (Sulfide)
As3d5 (Sulfide)
As3d3 (Arsenide)
As3d5 (Arsenide)
53 52 51 50 49 48 47 46 45 44 43 42 41 40 39 38 37 36 35 34
Binding Energy (eV)

APPENDIX E: ARSENOPYRITE TOF-SIMS IMAGES

FeAsS-Dry Std

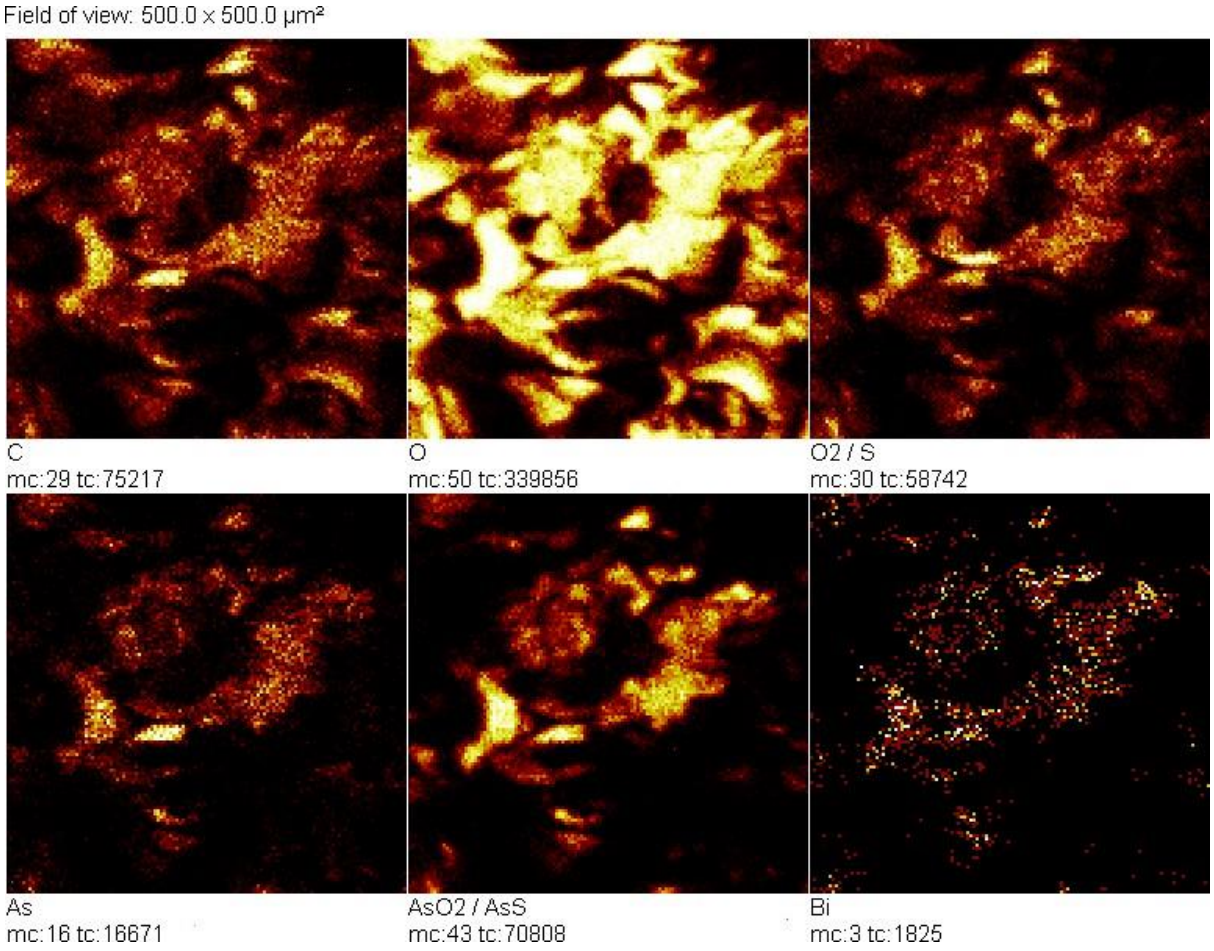

Field of view: 500.0 x 500.0 µm²

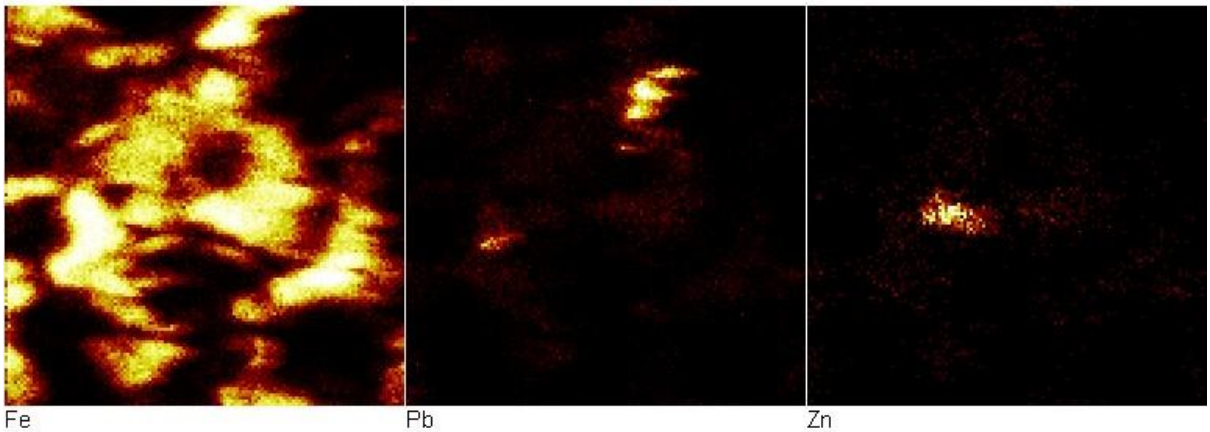

Fe
mc:50 tc:258920

Pb
mc:35 tc:15285

Zn
mc:10 tc:2126

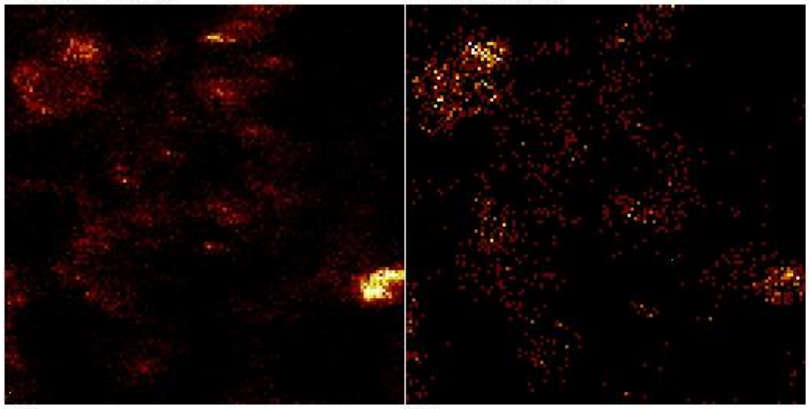

Mg
mc:16 tc:9174

Sn
mc:4 tc:1364

FeAsS-PNBX

Field of view: 500.0 x 500.0 µm²

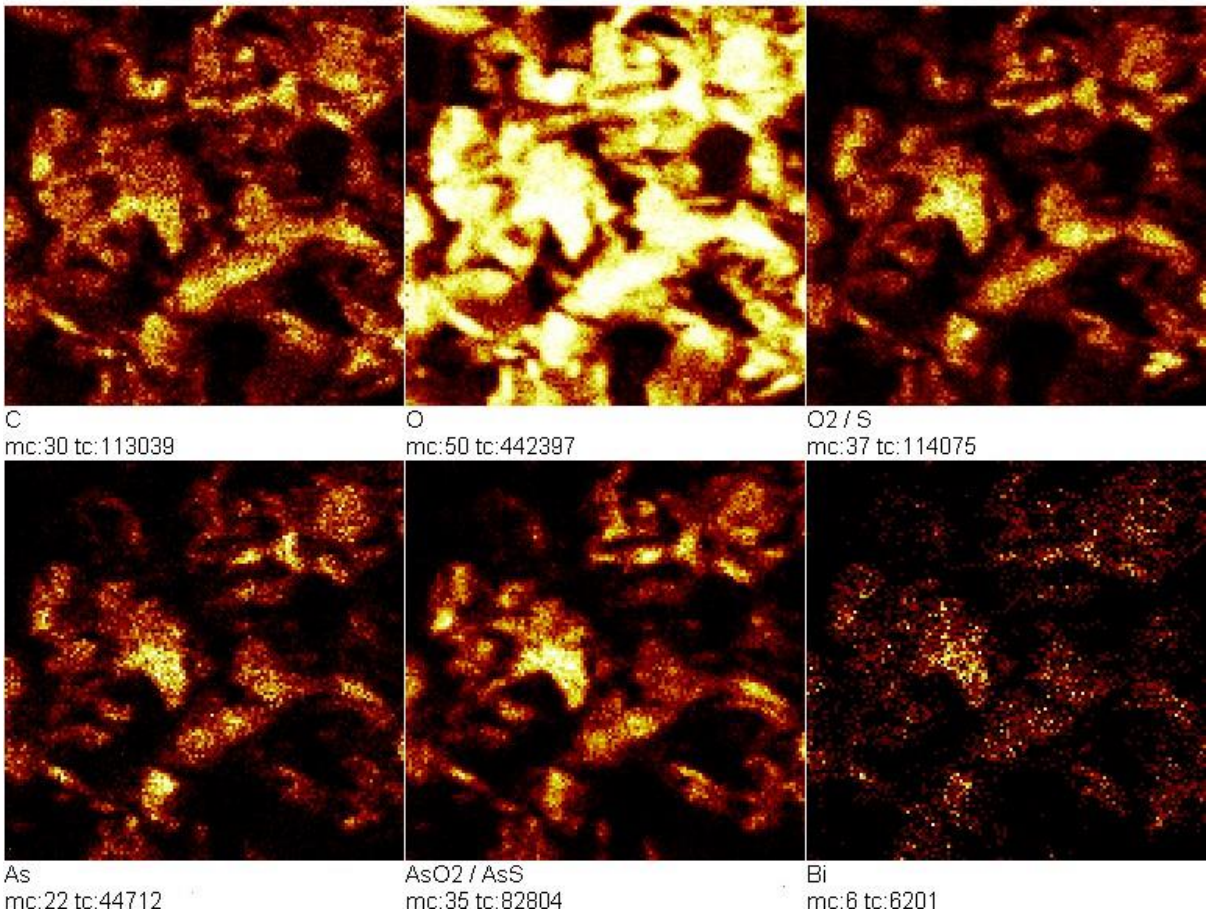

C
mc:30 tc:113039

O
mc:50 tc:442397

O2 / S
mc:37 tc:114075

As
mc:22 tc:44712

AsO2 / AsS
mc:35 tc:82804

Bi
mc:6 tc:6201

Field of view: 500.0 x 500.0 µm²

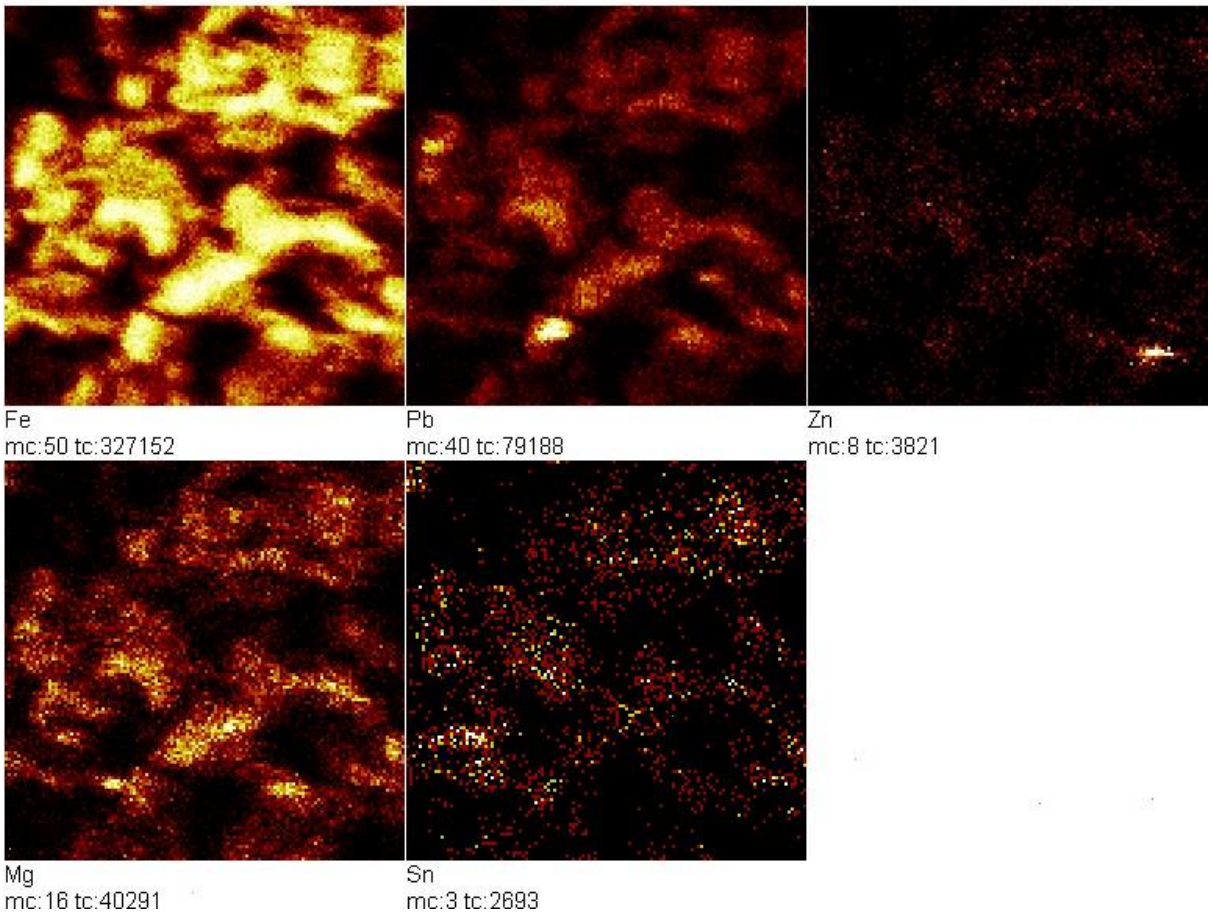

Fe
mc:50 tc:327152

Pb
mc:40 tc:79188

Zn
mc:8 tc:3821

Mg
mc:16 tc:40291

Sn
mc:3 tc:2693

FeAsS-2SPW (Synthetic Plant Water)

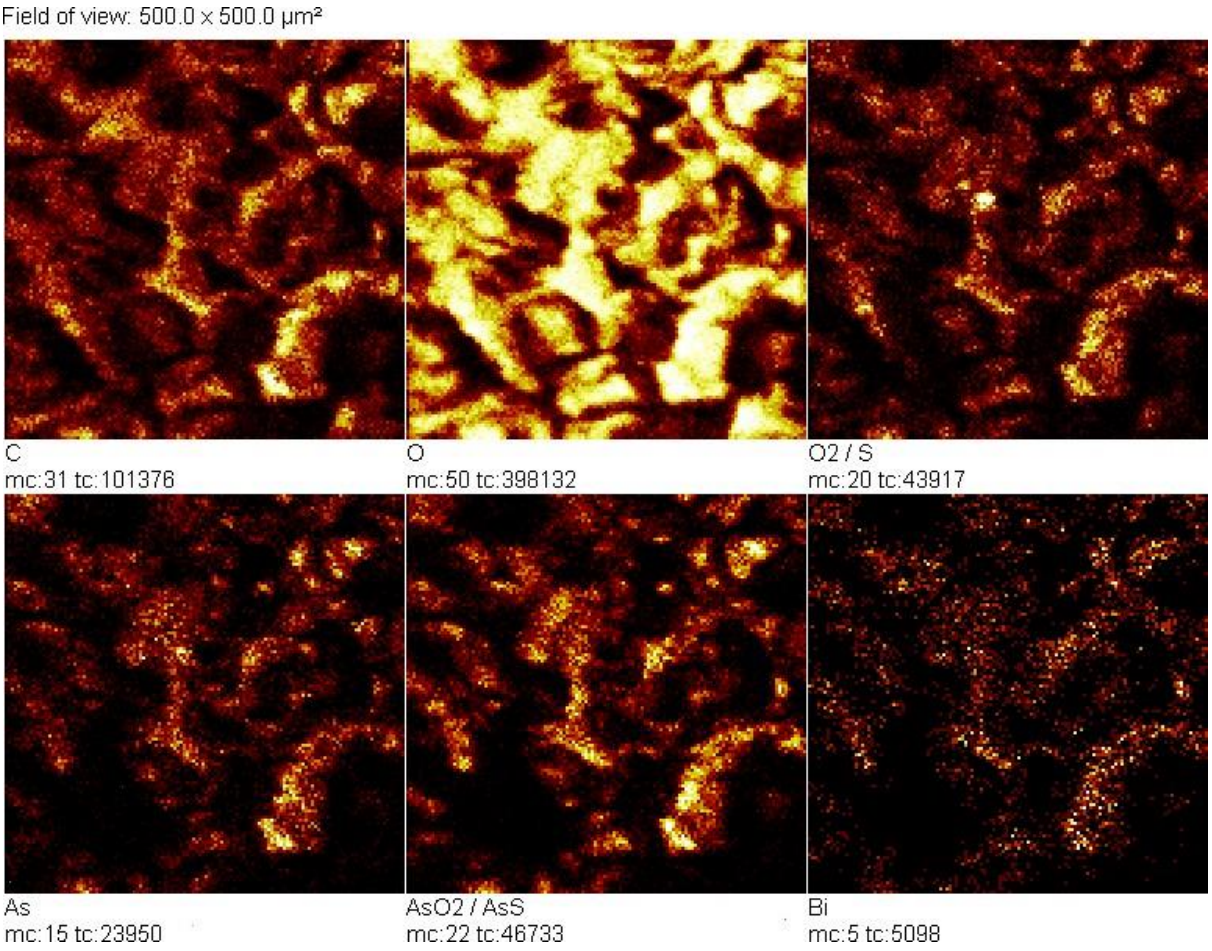

Field of view: 500.0 x 500.0 µm²

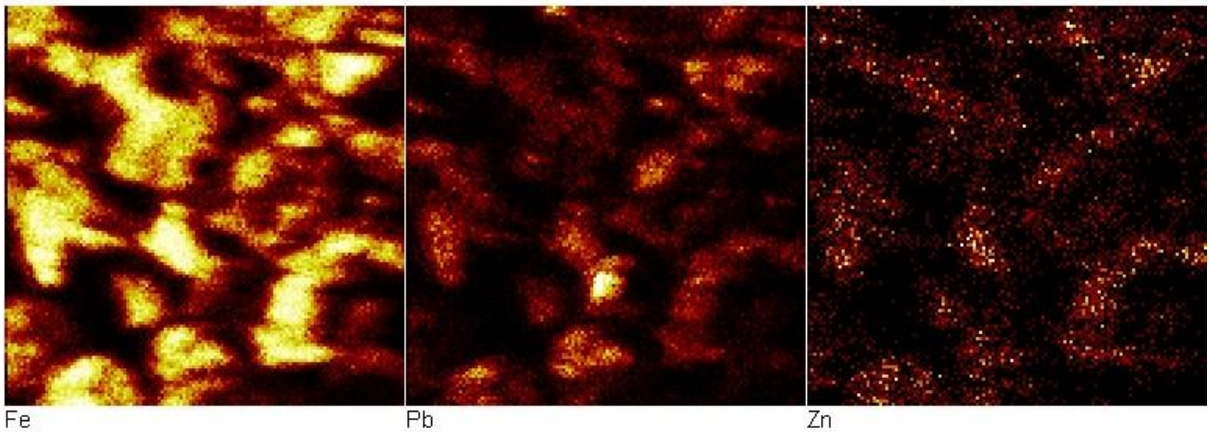

Fe
mc:49 tc:281699

Pb
mc:34 tc:61424

Zn
mc:6 tc:6968

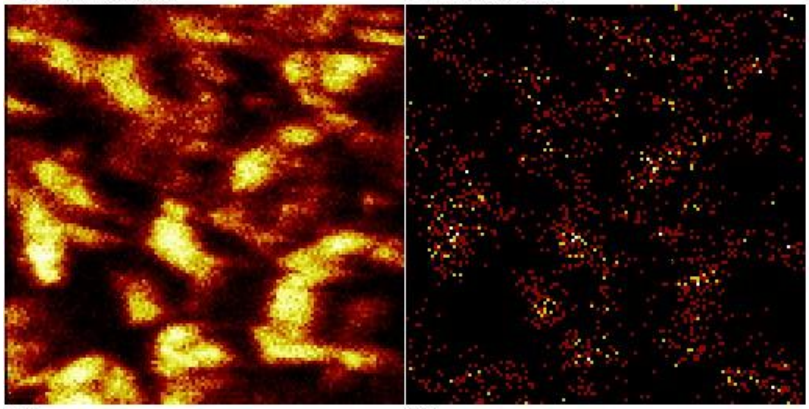

Mg
mc:46 tc:213339

Sn
mc:3 tc:1851

APPENDIX F: SPERRYLITE TOF-SIMS IMAGES

$PtAs_2$-Dry Std

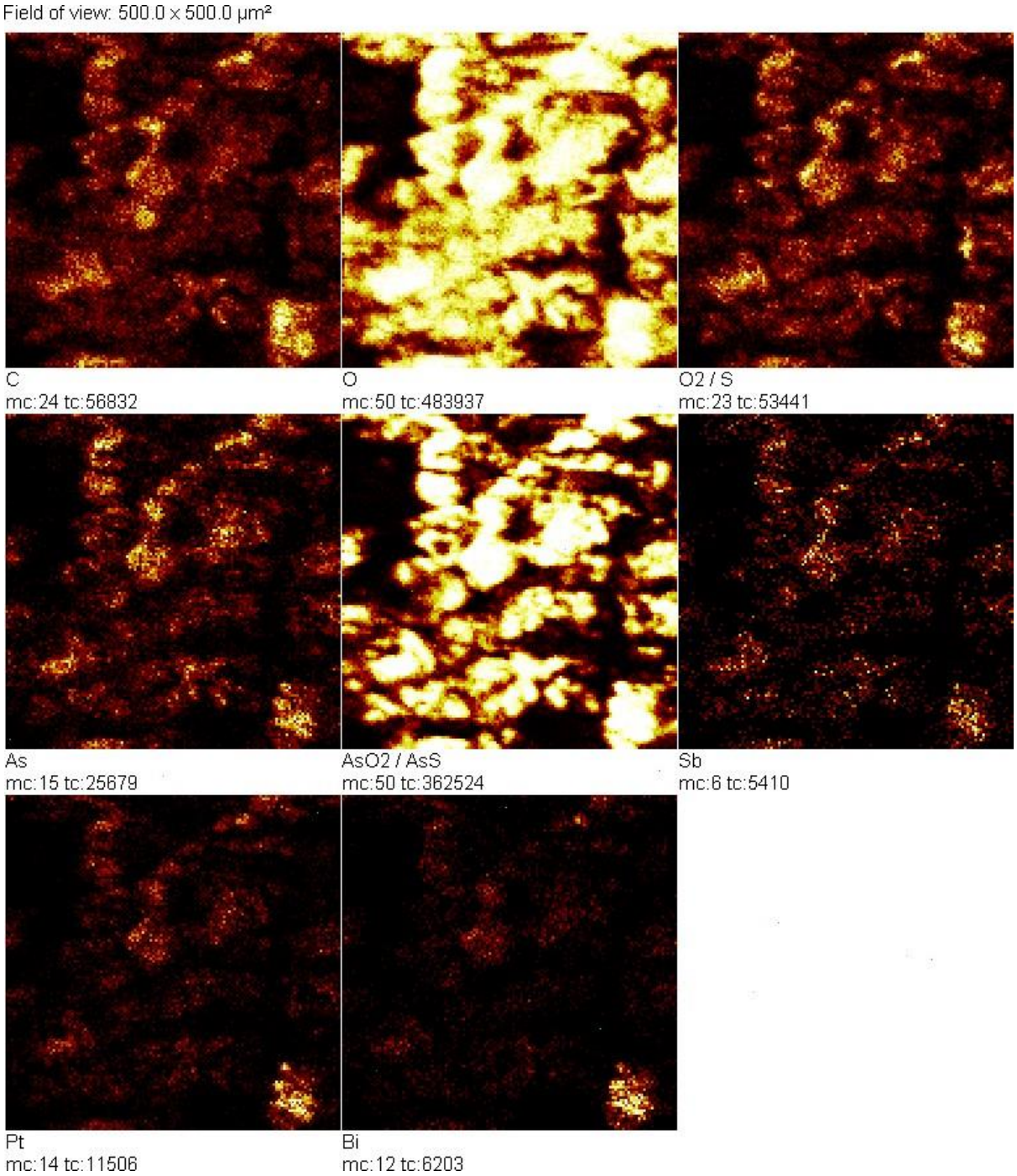

$PtAs_2$-SNBDTC

Field of view: 500.0 × 500.0 µm²

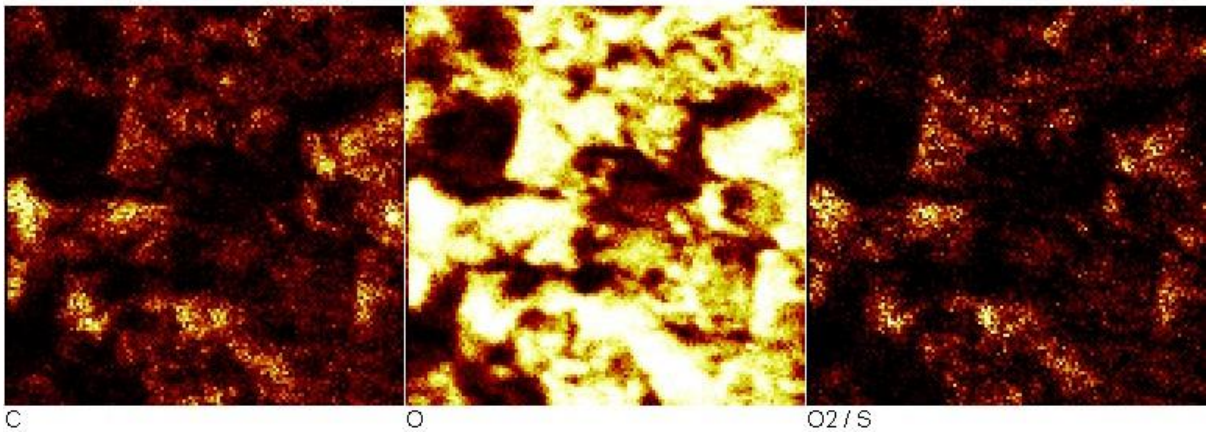

C
mc:20 tc:50521

O
mc:50 tc:496553

O2 / S
mc:13 tc:24126

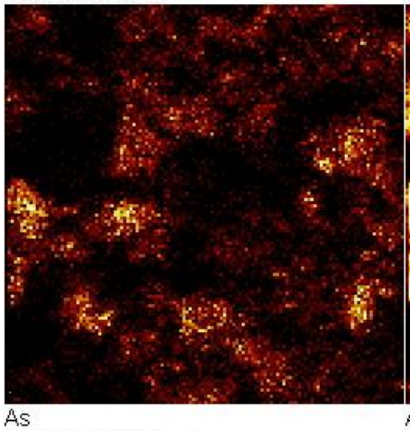

As
mc:11 tc:18331

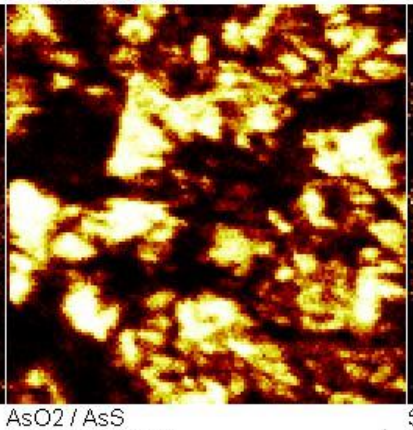

AsO2 / AsS
mc:50 tc:314681

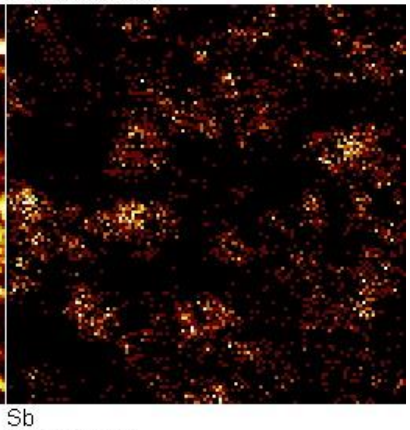

Sb
mc:4 tc:3610

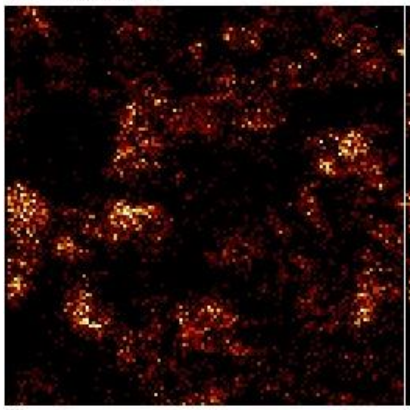

Pt
mc:7 tc:7298

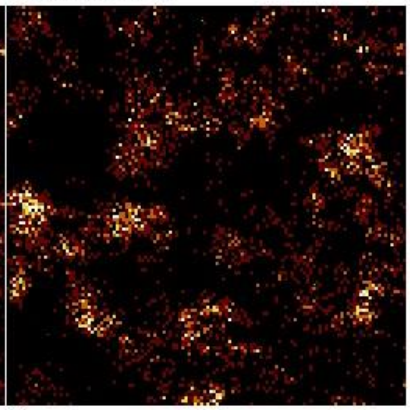

Bi
mc:4 tc:4031

$PtAs_2$-PNBX

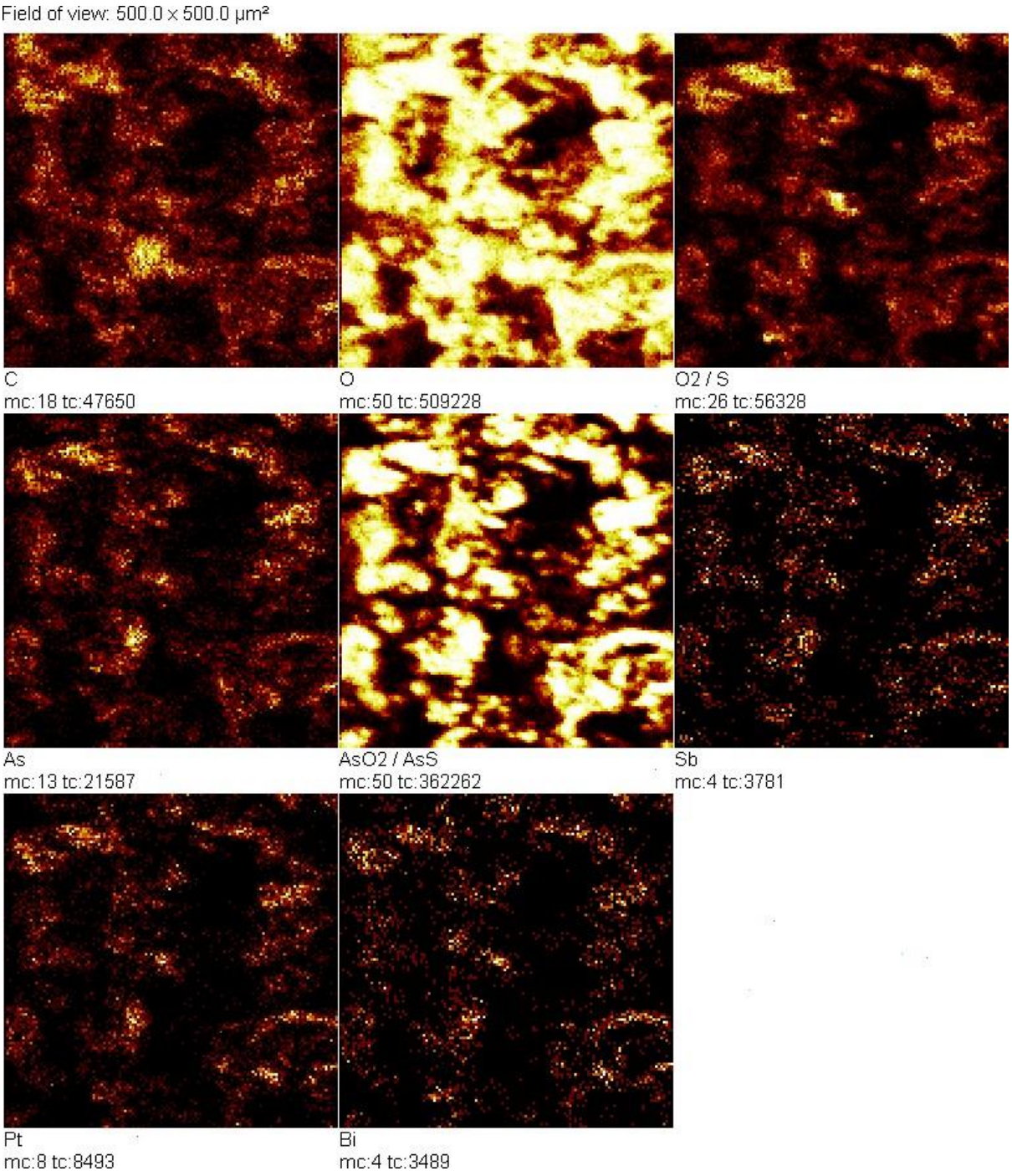
Field of view: 500.0 × 500.0 µm²
C
mc:18 tc:47650
O
mc:50 tc:509228
O2 / S
mc:26 tc:56328
As
mc:13 tc:21587
AsO2 / AsS
mc:50 tc:362262
Sb
mc:4 tc:3781
Pt
mc:8 tc:8493
Bi
mc:4 tc:3489

$PtAs_2$-2SPW (Synthetic Plant Water)